A THERMODYNAMIC AND KINETIC STUDY OF THE VAPOUR TRANSPORT OF SOME SEMICONDUCTORS

A thesis submitted for the degree of
Doctor of Philosophy in the
University of London

by

MICHAEL HAMILTON LYONS M.A.

Department of Chemistry
Royal Holloway College
Egham
Surrey TW20 0EX

December 1981

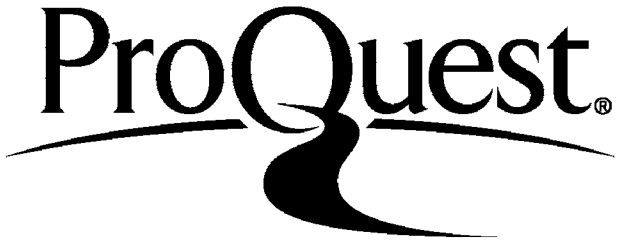

ABSTRACT

Detailed models of crystal growth have, for the most part, been limited to simple sublimation systems. These systems have little relevance to the complex chemical vapour transport systems used to produce modern semiconductors such as the III-V compounds, and the development of these systems has frequently been by trial and error. The work described in this thesis has attempted to bridge the gap between the crystal growth theories and technologically important growth systems.

Crystal growth is a sequential process in which reactants are first transported to the surface of the growing crystal and then undergo a series of surface reactions. A major difficulty in investigating heterogeneous reaction kinetics is separating the two processes. In chapter 2 a formalism is developed which enables transport and surface kinetics to be uncoupled. The practical application of this is demonstrated in chapters 3 and 4 in which the sublimation of red phosphorus and the GaAs/HBr reaction are investigated using the modified entrainment method (MEM).

The choice of experimental systems, and the depth to which they could be studied, was dictated largely by the interests of British Telecom. Consequently, the experimental work could only demonstrate the potential of MEM as a kinetic probe. More detailed examination of the dependence of the GaAs/HCl and GaAs/HBr reactions on reactant pressures has still to be carried out.

The later chapters are concerned with the growth of the mixed semiconductor systems GaInAs and GaInAsP. These materials are required for the new generation of optical communications systems currently under development.

Not only were the surface kinetics for these systems unknown, but even the transport equations for these systems had not been developed. Chapters 5-7 describe the development of a vapour phase system for the growth of these ternary and quaternary compounds. The basic principles are discussed for InP growth in chapter 5. Chapter 6 then developes thermodynamic and transport models for the mixed compounds and chapter 7 discusses the results obtained with practical growth system. Although many features of growth can be explained by the models developed in chapter 6, it is clear that a complete understanding of growth requires close study of the various processes occurring on the surface.

To Young Ja

"I wonder, by my troth, what thou and I did, till we lov'd?"

ACKNOWLEDGEMENTS

It is with great pleasure that I acknowledge the help and guidance of Dr P J Gardner (university supervisor) and Dr M M Faktor (external supervisor) during both the course of this work, and the preparation of this thesis. I also thank Dr E A D White for his advice on the preparation of this thesis.

Many colleagues at the British Telecom Research Laboratories were responsible for the assessment of the materials produced in this work and I thank them for their help. I am also grateful for the many useful discussions I had with my colleagues on various aspects of the work.

I acknowledge the Director of Research at BTRL for the provision of a collaborative award and thank his staff in typing and photographic for their assistance in the preparation of this thesis.

Finally, I am grateful to my parents for their encouragement and support over many years.

CONTENTS

LIST OF FIGURES

CHAPTER 1: INTRODUCTION

CHAPTER 2: METHODS OF STUDYING HETEROGENEOUS REACTIONS: THEORETICAL DISCUSSION

CHAPTER 3: THE SUBLIMATION OF RED PHOSPHORUS

CHAPTER 4: THE CHEMICAL VAPOUR TRANSPORT OF GaAs

CHAPTER 5: GROWTH OF InP

CHAPTER 6: GROWTH OF MIXED III-V COMPOUNDS: THEORY

CHAPTER 7: GROWTH OF MIXED III-V COMPOUNDS: EXPERIMENTAL

LIST OF TABLES

CHAPTER 3: THE SUBLIMATION OF RED PHOSPHORUS

CHAPTER 4: THE CHEMICAL VAPOUR TRANSPORT OF GaAs

CHAPTER 5: GROWTH OF InP

CHAPTER 7: GROWTH OF MIXED III-V COMPOUNDS: EXPERIMENTAL

CHAPTER 1: INTRODUCTION

The ever-increasing interest and importance of semiconductor materials in the last thirty years had led to a similar increase in the development of crystal growth research. It has long been known that the presence of defects and impurities in the crystal structure of a semiconductor can give rise to a variety of electrical effects [1].

Consequently, much effort has gone into the development of techniques for producing single crystal, high purity materials. Most semiconductor devices have several regions in which the electrical properties are markedly different. In the earliest devices this was achieved by diffusion of various dopants into the bulk of the crystal [2]. However, the need for closer control of device geometries and the introduction of integrated circuits have resulted in epitaxial deposition techniques in which layers of semiconductor, with controlled electrical properties, are deposited sequentially. In epitaxial growth systems, a fluid phase containing the various components of the semiconductor (together with any dopant species) is brought into contact with a suitable substrate. By control of reactant concentrations and substrate temperature, a condition is created in which the fluid phase is supersaturated. Solid will thus be deposited from the fluid and a layer of material form on the substrate. Providing the growth conditions have been chosen correctly, this layer will be crystalline and have a unique crystal orientation with respect to the substrate. The material is said to be epitaxially oriented.

In practice, epitaxial growth systems are divided into liquid phase and vapour phase systems. This thesis is concerned with the growth of crystals in vapour-phase systems, although many of the ideas discussed may be applied

to liquid phase systems. Despite the large numbers working on crystal growth, the actual processes involved are still not understood for most systems. The bulk of the research effort has been aimed at the production of material for commercial device applications. The result is that research is limited to finding, by trial and error, suitable growth conditions for a particular material, without seeking any understanding of the processes involved.

A further problem is the complexity of heterogeneous reactions. Growth of a crystal involves many different processes, for which there are few theoretical descriptions and little experimental data. Before proceeding further a review is presented of some of the most important processes occurring during crystal growth.

1.1 Growth Processes

Most theoretical discussions of crystal growth are limited to systems in which no chemical changes occur: only vapourisation and condensation reactions are considered. Despite this limitation the theories are of some importance since many of the concepts discussed apply equally to chemical vapour transport systems in which heterogeneous chemical reactions do occur.

A typical growth system might contain a source which may be heated and so be vapourised. The vapour species will then be transported to a seed crystal, at which point condensation or crystallization will occur. The growth sequence thus consists of three processes:

i. vapourisation of the source
ii. transport through the gas-phase
and iii. nucleation and growth of the seed

All aspects will be discussed, starting with the vapourisation and condensation processes. Where there is a seed crystal present, the surface processes involved in condensation and vapourisation are closely related and will be discussed together. However, in the absence of a seed crystal, nucleation must occur. This will be discussed first.

1.1.1 Nucleation Theories

The classical theories of nucleation [3,4] were based on the Thomson equation [5] which showed that very small particles of a substance have an increased vapour pressure given by

$$kT \ln (p_r^o/p_\infty^o) = 2\sigma V_o/r \qquad \ldots\ldots 1$$

where σ is the specific surface energy, V_o the atomic volume and r the radius of the particle. The vapour pressure of the particle is p_r^o, while p_∞^o is the vapour pressure over a flat surface (infinite radius). The effect of this equation, together with consideration of the total surface energy of the particles, is to show that the free energy of formation of a particle is a function of the size of that particle. For systems in which the pressure (p) of the substance is greater than the vapour pressure (p_∞^o), the plot of free energy of particle formation vs particle size (radius) passes through a maximum. The particle corresponding to the maximum free energy of formation is termed the critical nucleus. Particles, or nuclei, smaller than this will tend to dissociate since this will involve a reduction in free energy. However, for particles larger than the critical nucleus it is the addition of another atom to this nucleus which reduces the free energy of the nucleus. Such nuclei will therefore tend to grow spontaneously. It is clear that the initial stage is the formation of the critical nucleus, for which the free energy of formation (ΔG^*) is given by

$$\Delta G^* = \frac{16 \pi V_o^2 \sigma^3}{3(kT \ln (p/p_\infty^o))^2} \qquad \ldots\ldots 2$$

Note that p/p_∞^o is the supersaturation.

The classical nucleation theory aimedto determine the rate of formation of critical nuclei and showed

$$R \propto \exp\left(\frac{\Delta G^*}{kT}\right) \qquad \ldots\ldots 3$$

where R is the rate of formation of critical nuclei (or nucleation rate). From equations 2 and 3 it is clear that the nucleation rate is a strong function of the supersaturation (p/p_∞^o) and the dependence is such that it is possible to determine a critical supersaturation. Below this critical value the nucleation rate is negligible whereas at supersaturations larger than the critical value the rate is very large.

Equation 2 refers to spherical nuclei. When heterogeneous nucleation occurs (eg on the walls of a container) the shape of the nucleus will, in general, not be a sphere, and the free energy of formation of the critical nucleus will not be given by 2. Hirth and Pound [6] examined the case where the nucleus is assumed to have a spherical cap. They found

$$\Delta G^* = \frac{16\,\pi\,V_o^{\,2}\,\sigma^3}{3\,(kT\,\ell n\,(p/p_\infty^o))^2}\,f(\theta) \qquad \ldots\ldots 4$$

where σ now refers to the specific free energy of the cluster-vapour interface and $f(\theta)$ is defined by

$$f(\theta) = \tfrac{1}{4}\,(2-3\cos\theta+\cos^3\theta) \qquad \ldots\ldots 5$$

where θ is the contact angle (the angle subtended by the cap at the substrate surface). For complete unwetting ($\theta = 180^o$), $f(\theta) = 1$ and ΔG^* takes the value for homogeneous nucleation. For very small angles ($\theta = 5^o$) $f(\theta)$ approaches zero. Under these conditions the model is no longer an adequate description of the physical processes and the equations lose their validity [5].

The classical theory of nucleation is of importance for the concepts of critical nuclei and critical supersaturation. These concepts are used qualitatively in the discussion of very much more complicated systems than single component condensation. For example, the chemical vapour transport of III-V compounds (eg GaAs) is carried out in silica apparatus. Growth conditions are chosen such that growth occurs only on the prepared substrate, not on the surrounding silica. The fact that this is possible is explained by postulating that the critical supersaturation for nucleation on the silica has not been exceeded.

The qualitative aspects of the theory are open to criticism, particularly the use of bulk properties (notably the surface free energy) to describe what may be very smaller clusters of atoms. This is not justified [7] and modern treatments of nucleation [8,9,10] examine the interactions between the individual atoms of the cluster. These treatments dispense with the idea of a critical nucleus [11].

1.1.2 Growth and Vapourisation Models

The rate of vapourisation of a single component system (J_e) is given by the Hertz-Knudsen equation [12,13]:-

$$J_e = \alpha_e (2\pi mkT)^{-\frac{1}{2}} (p^o - p) \qquad \ldots\ldots 6$$

where p^o is the saturated vapour pressure and p the pressure above the surface of the solid. The term $(2\pi mkT)^{-\frac{1}{2}}$ - where m is the molecular weight - arises from the kinetic theory of gases from which it can be shown that if the gas has a Maxwellian velocity distribution then $(2\pi mkT)^{-\frac{1}{2}} p^o$ is the number of vapour

species striking unit surface area in unit time at the saturated vapour pressure.

An equation similar to 6 may be written for the condensation rate (J_c):

$$J_c = \alpha_c (2\pi mkT)^{-\frac{1}{2}} (p-p^o) \qquad \ldots\ldots 7$$

The terms α_e and α_c are the vapourisation and condensation coefficients. The condensation coefficient, α_c, takes into account the fact that not all collisions with the surface result in the incorporation of additional molecules into the lattice. The evaporation coefficient compensates for the fact that the number of atoms leaving the surface is not necessarily equal to the equilibrium bombardment rate. Both coefficients may have any value between 0 and 1.

The values of α_e and α_c depend on the importance of the various processes which may occur on the surface. These have been discussed in a qualitative way using the Kossel-Stranski surface [14,15]. This envisages the crystal surface of a close-packed lattice as composed of monomolecular layers separated by steps, which in turn have kinks in them (half-crystal position) (Fig 1). Various positions are identified (surface, ledge, kink etc) and an energy is assigned to an atom at each position by simply adding the number of contiguous atoms. Thus, an atom in the bulk of the crystal has an energy of -6ϕ (where ϕ is the bond energy between adjacent atoms); an atom in the surface has an energy of -5ϕ while the energy of a kink or half-crystal position is -3ϕ. The vapourisation process can be described in three

Fig 1

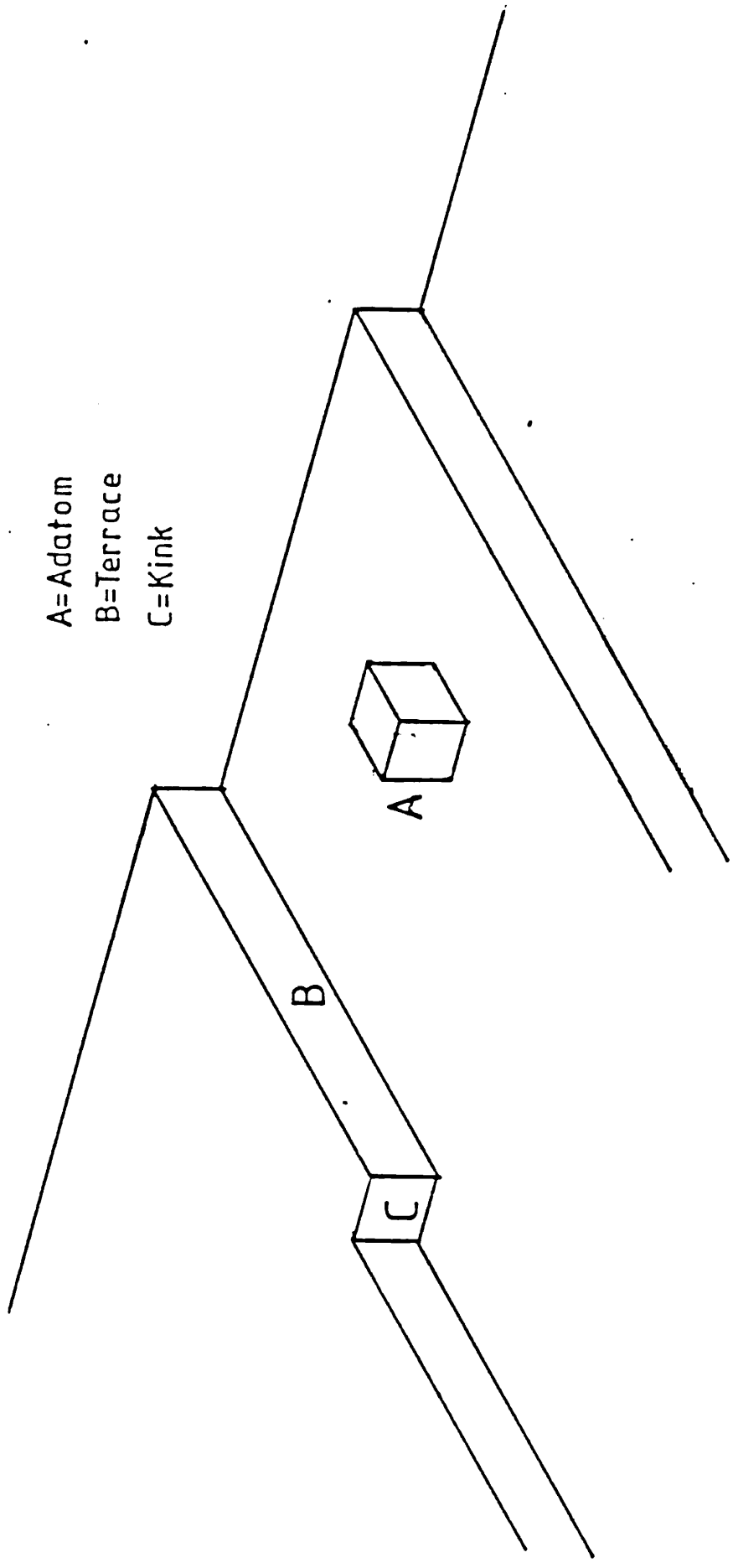

Kössel Surface

stages [6,16,17]: (1) An atom or molecule dissociates from a kink position; (2) the free atom is adsorbed on the surface and diffuses across this until (3) it is evaporated. If process (2) or (3) is rate limiting it is possible to calculate numerical values for α_e. Thus the evaporation coefficient α_e has values $\frac{1}{3} \leqslant \alpha_e \leqslant 1$ is the desorption process (step 3) is rate limiting and $\alpha_e \approx \frac{1}{3}$ if the rate limiting step is the surface diffusion [6]. Other processes, such as direct vapourisation from a kink do not contribute greatly to the overall rate [18]. Values of α_e close to unity are found when the vapourisation process involves no change of molecular structure. Thus, the evaporation coefficient for monatomic solids such as metals is given by [6]

$$\alpha_e = \frac{2}{3}\left(\frac{p}{p_o}\right) + \frac{1}{3} \qquad \ldots\ldots 8$$

However, when the phase transition involves a change of molecular structure, as in the case of red phosphorus or arsenic, the value of α_e is much lower (8.3×10^{-5} for arsenic at 550K [19]). Since vapourisation is an activated process, it is more properly described by an Arrhenious-type rate law [6]

$$\alpha_e = B \exp(-E/RT)$$

The activation barrier, E, may be reduced by illumination at a suitable wavelength [17] or by covering the crystal with a suitable metal [20].

Condensation on a Kossel-Stranski surface proceeds by the reverse processes of evaporation: atoms are adsorbed on the surface and migrate till they re-evaporate or join the kink-

position of a ledge. Growth of the crystal proceeds by the spreading of layers across this surface. The most important stage of this process is the formation of a layer bounded by ledges. Formation of this layer has been explained in several different ways. Thus, the growth of a perfect crystal is described by a 2-D nucleation mechanism [4]. This envisages growth as a sequence in which a two-dimensional nucleus forms on a singular surface. The new layer spreads across the face, at which point nucleation must occur once more. If the growth of the nuclei is sufficiently rapid then the crystal growth rate is proportional to the nucleation rate. The concepts of critical nucleus and critical supersaturation apply equally to two-dimensional nucleation. However the dependence of nucleation rate on supersaturation is somewhat different. For 2-D nucleation,

$$\text{Rate} \propto \exp \frac{1}{\ell n\ (p/p^{o})} \qquad \ldots\ldots\ 9$$

(cf equations 2 and 3).

A real crystal does not grow perfectly, but will contain dislocations which may eliminate the need for nucleation. Frank [21] showed that a screw dislocation acts as a continuous source of a ledge during growth, this ledge wrapping into a spiral. This requires much less supersaturation than 2-D nucleation [22]. The growth rate depends on the rate at which atoms are incorporated at the ledges caused by successive winding about the dislocation. The details were described by Burton, Cabrera and Frank (BCF) who found that in general

$$J \propto (p-p^{o}) \qquad \ldots\ldots 10$$

that is, growth obeyed a linear growth law (cf equation 7). However, when the distance between successive ledges was small compared to the diffusion length of adsorbed species, and at low supersaturations ($p/p^{o} \approx 1$), then a parabolic growth law was found:

$$J \propto (p-p^{o})^{2} \qquad \ldots\ldots 11$$

The conditions under which a perfectly flat surface could occur were examined by Jackson [23,24]. He found that at high temperatures the surface consisted of smooth planes with additional atoms bound randomly on this surface. Such surfaces were termed rough. The transition from a smooth to rough surface was described by a parameter

$$\beta = \frac{L}{kT}\,\phi \qquad \ldots\ldots 12$$

where L is the heat of phase transition and ϕ is a geometrical factor which depends on the geometry of the crystal surface. Values of $\beta \lesssim 2$ correspond to a rough interface [24]; larger values correspond to a smooth surface. A critical surface roughening temperature may be defined, at which temperature the surface undergoes a transition from smooth to rough. Clearly, growth by the spread of ledges is only important on atomically smooth surfaces. When the surface is rough atoms may be incorporated anywhere on the surface.

This brief discussion of the various growth models for single component solids is sufficient to show the complexity of the

process. Many of the concepts are carried over into discussions of the more complex chemical vapour transport systems; however, a description of the growth processes in these systems must also consider adsorbed reactants, products and reaction intermediates and consider whether the various reaction steps are homogeneous or heterogeneous. The gap between the theoretical condensation models based on the idealised Kossel surface, and the systems of practical importance is enormous. The first part of this thesis describes one approach to bridging this gap by providing basic kinetic information for the growth reactions in chemical vapour transport systems.

In all kinetic studies it is necessary to distinguish between the effect of surface kinetics, and rate variations arising from gas transport. Consequently, it is necessary to discuss mass transport.

1.1.3 Mass Transport

A full description of transport in a growth system requires consideration of both mass and heat transport. In general these processes are coupled and a complete description of even very simple systems is complex, requiring numerical solutions of the various conservation equations. However, when the thermal properties depend only weakly on composition or when the temperature differences are small, then the independent solution of the temperature and concentration profiles is a good approximation [25]. This section presents a single one-dimensional treatment of mass transport developed originally by Faktor et al [26,27,28,29]. The model will be discussed in some detail as it

underlines an important experimental tool - the modified entrainment method (MEM) - and is used in the discussion of several practical growth systems later in this thesis.

Consideration of mass conservation results in a continuity or diffusion equation for each species i:

$$\frac{\partial}{\partial t} \rho_i = -\nabla . (\rho_i \underline{u} + \underline{j}_i) \qquad \ldots\ldots 13$$

or, in one-dimension

$$\frac{\partial}{\partial t} \rho_i = -\rho_i \frac{du}{dx} + \frac{dj_i}{dx} \qquad \ldots\ldots 14$$

where ρ_i is the mass density of component i, $\underline{j}_i$ represents the diffusive flux with respect to the mass average velocity $\underline{u}$ and $\underline{u}$ is defined by

$$\underline{u} = \frac{1}{\rho} \Sigma \rho_i \underline{u}_i \qquad \ldots\ldots 15$$

The first term in equations 13 and 14 is termed the convective flux; the second, the diffusive flux. The term convective flux is misleading since this represents a motion of the bulk of the gas which may have nothing to do with bouyancy driven convection. To illustrate this, consider a closed capsule containing a source material A which may be transport as a vapour species to a seed crystal (Fig 2). The capsule also contains an inert gas Z. Transport occurs by heating the seed so that it sublimes. The sublimed atoms then pass along the capsule to the seed end, where condensation takes place. Another way of looking at this

Fig 2

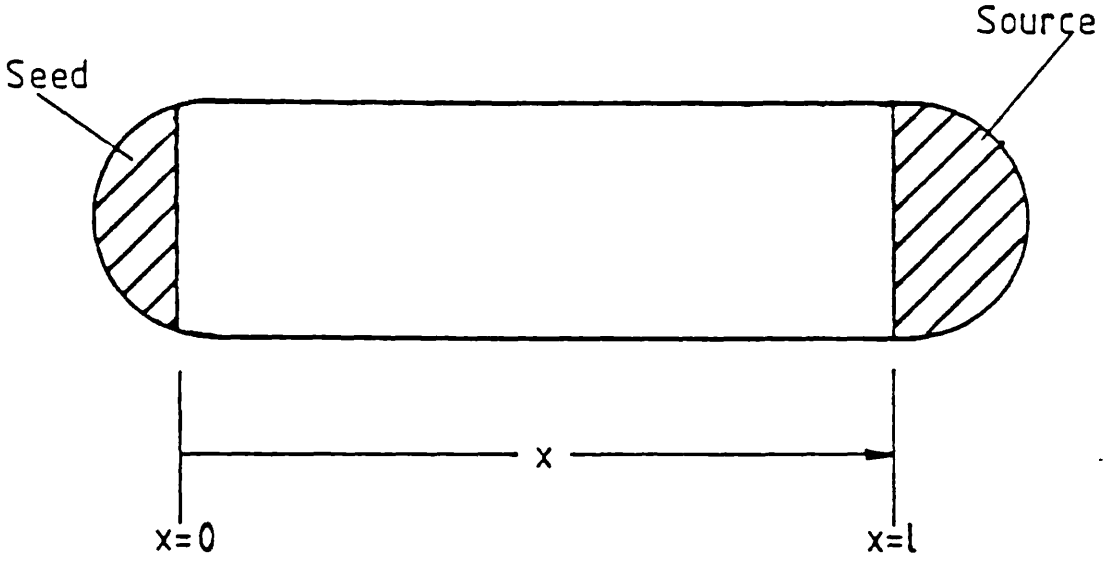

Closed Capsule Transport System

is to consider the seed as a generator of gas species and the source as a scavenger of these species. The source and seed act together as a gas pump and hence impart a bulk flow of velocity U to the gas-phase. In addition there will be a lower pressure of A at the seed end than at the source so that there will also be a diffusive flux of A.

The fluxes of A and Z may be written

$$J_A = \frac{Up_A}{RT} - \frac{D}{RT}\frac{dp_A}{dx} = J \qquad \ldots\ldots 16$$

$$J_Z = \frac{Up_Z}{RT} - \frac{D}{RT}\frac{dp_Z}{dx} = 0 \qquad \ldots\ldots 17$$

U is called the Stefan velocity since this bulk gas flow was originally reported by Stefan in 1890 [30,31]. Equation 17 merely reflects that since Z is neither sublimed nor condensed, the net flow of Z is opposed by the diffusive flux. Adding 16 and 17 enables U to be eliminated:

$$J = \frac{UP}{RT} \quad \text{or} \quad U = \frac{JRT}{P} \qquad \ldots\ldots 18$$

where P is the total pressure. Note that this elimination assumes P is independent of the distance from the seed (x) - a reasonable assumption if the capsule has a radius of ~1 cm or more [27].

Substituting for U in 16 and 17 gives

$$J = \frac{J}{P}\,p_A - \frac{D}{RT}\frac{dp_A}{dx} \qquad \ldots\ldots 19$$

and $$J = \frac{J}{P} p_Z - \frac{D}{RT} \frac{dp_Z}{dx} \quad \ldots\ldots 20$$

Rearrangement of 19 gives

$$\frac{dp_A}{P-p_A} = \frac{JRT}{DP} dx \quad \ldots\ldots 21$$

which on integration from x = 0 to x = ℓ yields

$$\ell n \frac{[p_A(\ell) - P]}{[p_A(o) - P]} = \frac{JRT\ell}{DP} \quad \ldots\ldots 22$$

or

$$J = \frac{DP}{RT\ell} \ell n \frac{[p_A(\ell) - P]}{[p_A(o) - P]} \quad \ldots\ldots 23$$

When the inert gas is the majority component (ie $P >> p_A(\ell) > p_A(o)$) the argument of the logarithm in equation 23 will be close to unity, and on expansion of this term equation 23 may be simplified:

$$J = \frac{DP}{RT\ell} \left[\frac{p_A(\ell) - P}{p_A(o) - P} - 1 \right]$$

$$\simeq \frac{D}{RT} \left[\frac{p_A(\ell) - p_A(o)}{\ell} \right] \quad \ldots\ldots 24$$

Equation 24 is the equation obtained if the Stefan flow was ignored and only diffusion considered. The diffusion-only calculation is valid only when the transporting species are minority components.

This model of gas transport may readily be extended to deal with more complex systems such as dissociative sublimation and chemical vapour transport [26]. Discussion of these systems

will be left till later, when describing practical growth systems. For the present, this section has considered a single sublimation system in some detail in order to emphasise the origin and importance of the Stefan flow in transport systems.

1.2 The Modified Entrainment Method (MEM)

This experimental technique may be used to study both the thermodynamics and the kinetics of a transport reaction. Most studies have concentrated on the thermodynamic investigations and the early chapters of this thesis are concerned with the extension of the method (and underlying theory) to the study of heterogeneous reaction kinetics. In this section, the technique will be described, together with its use in thermodynamic studies.

1.2.1 Experimental

The most important part of the apparatus for MEM is the sample bottle (Fig 3), in which the only opening is a long, narrow capilliary. The design is such that changes in gas composition due to transport are confined to the channel. The transport of material through this channel is effectively one-dimensional and may be represented by equations similar to 16 and 17. In use, the sample bottle is suspended from an electrobalance which monitors the weight continuously. The bottle is placed so that gas is swept past the opening of the channel and at this point (ℓ) the gas composition is taken to be that of the bulk gas flow.

The measured rate of weight loss enables the flux through the channel of each gas-phase species to be calculated; provided the stoichiometry of the transport reaction (or reactions) is known. This information, together with the bulk gas pressures, enables the pressure of each species inside the bottle to be calculated. It is important to note that all that is measured is the flux of material through the channel and that no assumption is made about the achievement of equilibrium within the bottle. By

Fig 3

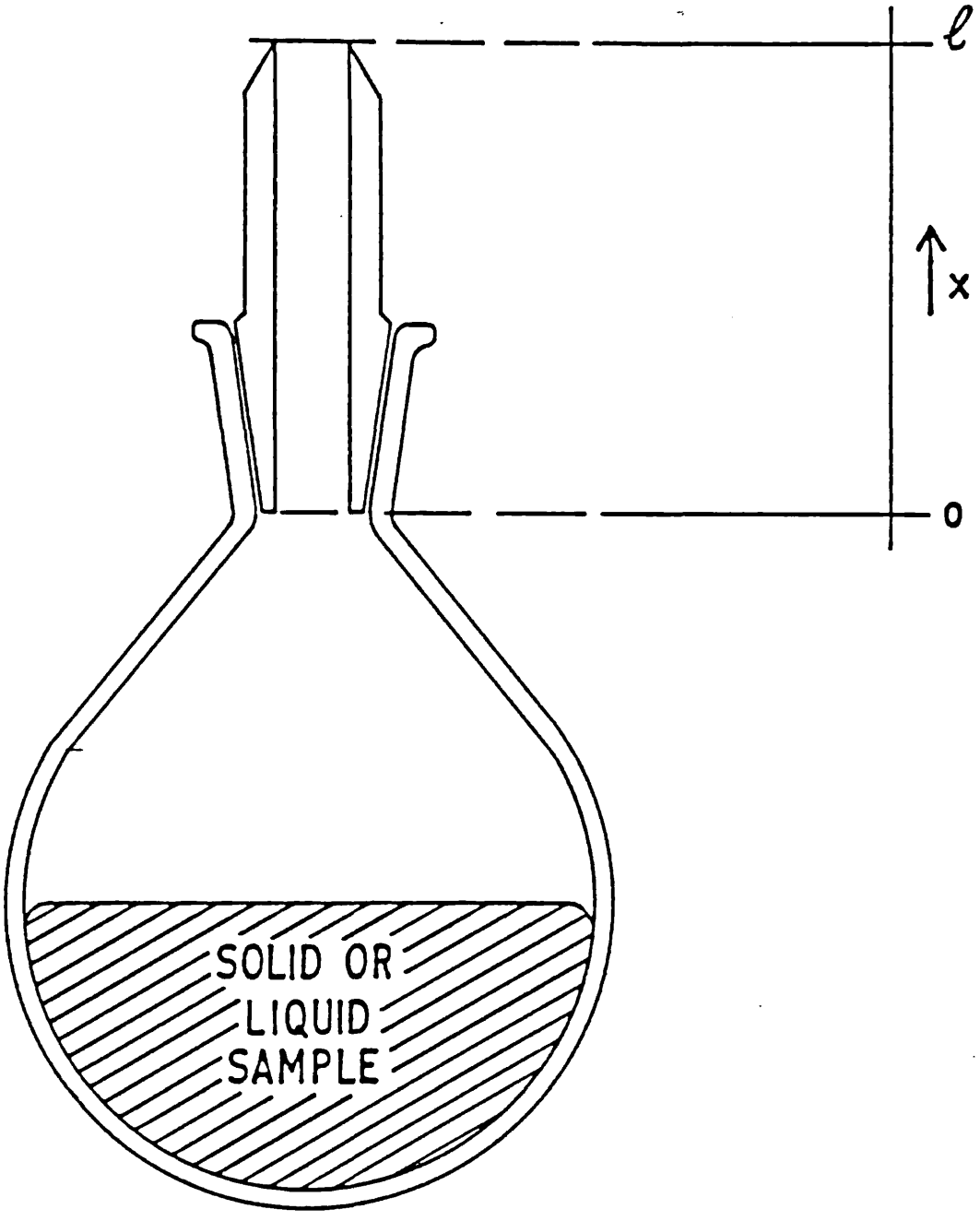

MEM Sample Bottle

confining all pressure gradients within the channel it is possible to obtain values for the interfacial pressures of the various reactants. This is of particular value in kinetic investigations.

The early part of this thesis is concerned primarily with the use of MEM in surface kinetic investigations; consequently this aspect will not be discussed here. However, if the channel is sufficiently long and narrow then the departure from equilibrium will be insignificant and the technique may be used to obtain thermodynamic values for the reaction.

Here, some model systems will be discussed in order to demonstrate the scope of the method as a source of thermodynamic data.

1.2.2 Model Systems

1.2.2.1 Simple Sublimation

This is the simplest system to be investigated; the sample is placed in the bottle and the inert gas flowed past. Examples of this are lead [32] and zinc [33] in hydrogen. The rate of loss of sample is governed by equation 23. By flowing the inert gas past the channel opening the pressure of vapourised sample at this point (ℓ) may be taken to be zero, so equation 23 becomes [32]:

$$J = \frac{\dot{W}}{Mc} = \frac{DP}{RT\ell} \ell n \frac{P}{[P - p_A(o)]}$$

or $$p_A(o) = P [1 - \exp(-\xi)] \qquad \ldots\ldots 25$$

where $\xi = \frac{JRT\ell}{DP} = \frac{\dot{W}RT\ell}{DPMc}$

where $\dot{W}$ is the rate of weight loss, M is the molecular weight of A and c is the cross-sectional area of the channel. For systems in which the rate of weight loss is small ($\xi << 1$) then equation 25 may be simplified:

$$p_A(x) \approx \xi p = \frac{\dot{W}RT\ell}{DMc} \qquad \ldots\ldots 26$$

When there is little departure from equilibrium within the bottle, $p_A(o)$ is the saturated vapour pressure (p_A^o) which is expressed as a function of temperature:

$$-RT \ln p_A^o = \Delta H_v - T\Delta S_v \qquad \ldots\ldots 27$$

where ΔH_v and ΔS_v are the enthalpy and entropy of vapourisation respectively. Combining equations 26 and 27 gives

$$\ln \dot{W} = - \frac{\Delta H_v}{RT} + \left(\frac{\Delta S_v}{R} - \ln \frac{RT\ell}{DMc} \right) \qquad \ldots\ldots 28$$

so a plot of $\ln \dot{W}$ vs $^1/_T$ will be a straight line of gradient $- {}^{\Delta H}/_R$. In practice a small correction has to be made for the temperature dependence of the diffusion constant [34]:

$$D = D_o \left(\frac{T}{T_o} \right)^{1+s} \qquad \ldots\ldots 29$$

where D_o is the diffusion constant at a reference temperature T_o, and s is a constant, usually between 0.5 and 1 and frequently close to 0.8.

1.2.2.2 Simple CVT Reaction [32]

Consider a simple heterogeneous reaction of the type

$$M_{(s)} + HX_{(g)} \gtrless MX_{(g)} + \tfrac{1}{2}H_2 \qquad \ldots\ldots 30$$

The equilibrium constant is given by

$$K_p = \frac{p^o_{MX} \, (p^o_{H_2})^{\frac{1}{2}}}{p^o_{HX}} = \exp\left[-\frac{\Delta H}{RT} + \frac{\Delta S}{R}\right] \qquad \ldots\ldots 31$$

Equation 30 involves a change in the number of vapour species, hence there will be bulk (Stefan) gas flow in the channel. The transport equations are then

$$J_M = \frac{U p_{MX}}{RT} - \frac{D}{RT}\frac{dp_{MX}}{dx} = \frac{W}{M_M c} \qquad \ldots\ldots 32$$

$$J_H = \frac{U}{RT}(p_{HX} + 2p_{H_2}) - \frac{D}{RT}\frac{d}{dx}(p_{HX} + 2p_{H_2}) = 0 \qquad \ldots 33$$

$$J_X = \frac{U}{RT}(p_{MX} + p_{HX}) - \frac{D}{RT}\frac{d}{dx}(p_{MX} + p_{HX}) = 0 \qquad \ldots 34$$

An average diffusion constant has been assumed for all species. Addition of equations 32-34 gives

$$J_M = 2UP/RT \qquad \ldots\ldots 35$$

U may now be eliminated from equations 32-34, and the equations integrated from x = 0 to x = ℓ. Since $p_{MX}(\ell) \sim 0$, equation 32 yields

$$p^o_{MX} = 2P\,(1 - e^{-\xi}) \qquad \ldots\ldots 36$$

where in this case $\xi = \frac{J_M RT\ell}{2DP} = \frac{\dot{W}RT\ell}{2DPM_M c}$

Similarly,

$$p^o_{HX} = (p_{HX}(\ell) + 2P)\, e^{-\xi} - 2P \qquad \ldots\ldots 37$$

$$p^o_{H_2} = (p_{H_2}(\ell) - P)\, e^{-\xi} + P \qquad \ldots\ldots 38$$

where $P = p_{H_2}(x) + p_{HX}(x) + p_{MX}(x)$ and is constant for all x. It is clear that measurement of the rate of weight loss of M enables the equilibrium partial pressures to be calculated, and hence the equilibrium constant. Equations 36-38 may be simplified when $\xi << 1$. This may occur if the reactant partial pressure is small ($p_{HX}/P = \varepsilon << 1$) or if the equilibrium constant is small ($K_p << 1$). Three cases may be considered:

1. $\varepsilon << 1$, $\xi \simeq \varepsilon$

The simplified equations are

$$p^o_{MX} \approx 2P\xi$$

$$p^o_{HX} \approx P(\varepsilon - 2\xi)$$

$$p^o_{H_2} \approx P(1 - \varepsilon)$$

and the equilibrium constant is

$$K_p \approx \frac{2\xi\sqrt{P}}{\varepsilon - 2\xi} \qquad \ldots\ldots 39$$

The situation is unrevealing since if $\xi \sim \varepsilon$, the reaction has essentially gone to completion and K_p is large. Under these conditions large changes in K_p may not significantly alter the rate of weight loss W, which is determined by the rate at which HX reaches the sample. These conditions may be used to determine the diffusion constant of HX in hydrogen. For example, the reaction of liquid gallium with HCl is extreme at temperatures around 1000K. By studying this reaction in the range 700-1300K, a value for diffusion constant of HCl in hydrogen was obtained [35].

2. $\xi << 1$, $\varepsilon \sim 1$

When the equilibrium constant is small, then the rate of weight loss is a strong function of K_p and thermodynamic information may be obtained. For the case where $\xi << 1$ and $\varepsilon \sim 1$, the simplified equations are

$$p^o_{MX} = 2P\xi$$

$$p^o_{HX} = P(\varepsilon - \varepsilon\xi - 2\xi) = P\varepsilon$$

and $$p^o_{H_2} = P(1 - \varepsilon + \varepsilon\xi) = P(1 - \varepsilon)$$

so, $$K_p \approx 2\xi P^{\frac{1}{2}} \frac{(1-\varepsilon)^{\frac{1}{2}}}{\varepsilon} \qquad \ldots\ldots 40$$

and as for simple sublimation, a plot of $\ln \dot{W}$ vs $^1/_T$ gives a straight line of slope $-\frac{\Delta H}{R}$.

Case 3, $\xi << \varepsilon << 1$

When $\varepsilon << 1$, equation 40 simplifies further, to

$$K_p \sim \frac{2\xi\sqrt{P}}{\varepsilon} \qquad \ldots\ldots 41$$

and ΔH may again be obtained from a plot of $\ell n\ \dot{W}$ vs $^1/T$.

In most practical applications the reactant partial pressure is small (ie $\varepsilon << 1$). Over a large enough temperature range both case (1) and case (3) will apply, and the plot of $\ell n\ \dot{W}$ vs $^1/T$ will have the form shown in fig 4.

This discussion is sufficient to demonstrate the general features of an MEM experiment to obtain thermodynamic information. The more complex systems used in CVT of III-V compounds may be analysed in a similar way. The detailed treatment of these systems will be left till the appropriate point in the text.

1.2.3 Original Work

To end this introduction to the modified entrainment method two brief discussions by the author are included. These complete the description of MEM as a thermodynamic tool.

1.2.3.1 Determination of Enthalpy of Reaction

In the examples of section 1.2.2, it was found that a plot of $\ell n\ \xi$ vs $^1/T$ gave a straight line with a slope $-\frac{\Delta H}{R}$. It would be a mistake, however, to assume that a

Fig 4

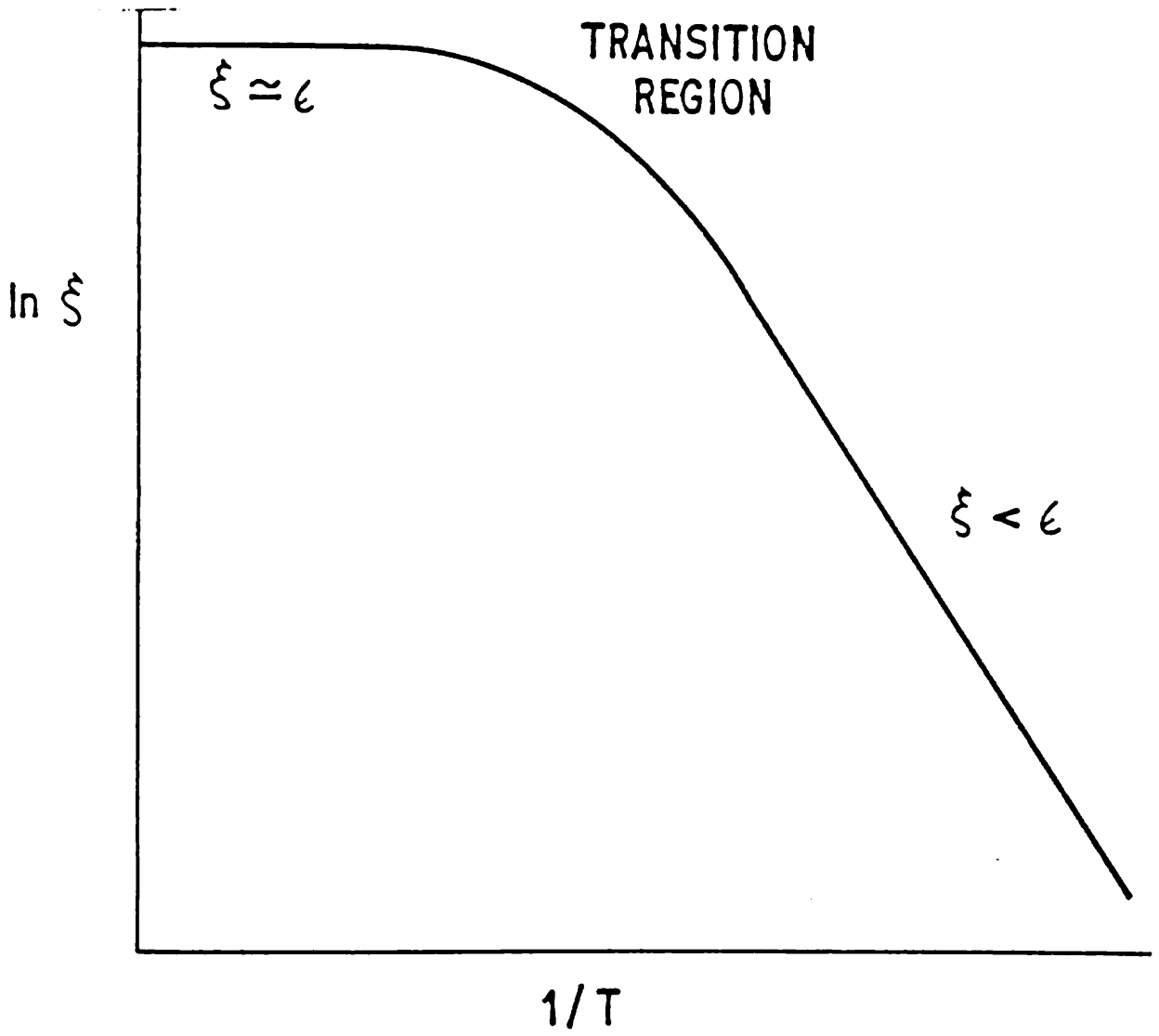

Schematic Diagram of MEM Plot

straight line plot always has a slope $-\frac{\Delta H}{R}$. Apart from the perturbations which arise when several transport reactions are occurring simultaneously [36], certain types of reaction will always give an apparent enthalpy which differs markedly from the true value.

Consider the reaction

$$InP_{(s)} \rightleftharpoons In_{(\ell)} + \frac{1}{n} P_{n(g)} \qquad \ldots\ldots 42$$

For this system, it is the loss of phosphorus from the bottle which is measured. It is possible to define a notional pressure of P atoms (cf equation 26)

$$p_p = \xi \qquad \ldots\ldots 43$$

$\therefore$ The pressure of P_n molecules is

$$p_{P_n} = \xi/n \qquad \ldots\ldots 44$$

The equilibrium constant for reaction 42 is given by

$$K = (p_{P_n})^{1/n}$$

Then

$$\ell nK = \frac{1}{n} \ell n\ (p_{P_n}) = \left(-\frac{\Delta H}{R}\right)\frac{1}{T} + \frac{\Delta S}{R} \qquad \ldots\ldots 45$$

substituting from 3 gives

$$\frac{1}{n} \ell n \left(\frac{\xi}{n}\right) = \left(-\frac{\Delta H}{R}\right)\frac{1}{T} + \frac{\Delta S}{R}$$

$$\text{or} \quad \ell n \left(\frac{\xi}{n}\right) = \left(- \frac{n\Delta H}{R}\right) \frac{1}{T} + \frac{n\Delta S}{R} \qquad \ldots\ldots 46$$

whence it is clear that the slope of the $\ell n\ \xi$ vs $\frac{1}{T}$ plot is $- \frac{n\Delta H}{R}$. When n = 2, the apparent enthalpy of reaction is thus double its true value.

This result occurs whenever the rate of loss is measured of a species which changes its stoichiometry on passing from the solid to the vapour phase.

In a general case, the reaction might be

$$AX_{m(s)} \rightleftharpoons A_{(s \text{ or } 1)} + \frac{m}{n} X_n$$

in which the weight loss is a measure of the amount of X leaving the bottle. Using the same arguments as above it can be shown

$$\ell n\ \dot{W} \propto \ell n\ (p_{x_n}) = \left(- \frac{n}{m} \frac{\Delta H}{R}\right). \frac{1}{T} + \left(\frac{n}{m} \frac{\Delta S}{R}\right) \qquad \ldots\ldots 47$$

A similar equation will be found for all reactions in which it is possible to make the approximation

$$K \propto \xi \text{ or } \dot{W}$$

Equation (6) demonstrates that the slope of the plot $\ell n\ \dot{W}$ (or $\ell n\ \xi$) vs $\frac{1}{T}$ will equal $- \frac{\Delta H}{R}$ only when m = n.

1.2.3.2 The Determination of the Stoichiometry of Gas-Phase Species

The interpretation of the results of an MEM experiment requires knowledge of the reactions which are occurring.

In some cases this information is uncertain and in favourable circumstances the results of MEM studies may help the identification of transport reactions. For example, consider the transport of germanium by HCl. The reaction may be written

$$Ge + nHCl \rightleftharpoons GeCl_n + {}^{n}/_{2}H_2 \qquad \ldots\ldots 48$$

where n may take the values n = 1, 2, 3, 4. On chemical grounds the most likely values are 2 or 4 but it is not possible to eliminate one of these. By controlling the conditions of the MEM experiment carefully it is possible to determine the stoichiometry of the chloride.

The transport equations for the various vapour species are:

$$J_{Ge} = J = J_{GeCl_n} = \frac{UP_{GeCln}}{RT} - \frac{D}{RT}\frac{dP_{GeCln}}{dx} \qquad \ldots\ldots 49$$

$$J_{H_2} = \frac{nJ}{2} = \frac{UP_{H_2}}{RT} - \frac{D}{RT}\frac{dP_{H_2}}{dx} \qquad \ldots\ldots 50$$

$$J_{HCl} = -nJ = \frac{UP_{HCl}}{RT} - \frac{D}{RT}\frac{dP_{HCl}}{dx} \qquad \ldots\ldots 51$$

For simplicity the same diffusion constant is assumed for all species.

Summing these equations, gives

$$sJ = UP/RT \qquad \ldots\ldots 52$$

where $s = 1 - {}^{n}/_{2}$

Then, on substituting for U in equations 2-4;

$$J = \frac{sJ\,p_{GeCl_n}}{P} - \frac{D}{RT}\frac{dp_{GeCl_n}}{dx} \qquad \ldots\ldots 53$$

$$\frac{nJ}{2} = \frac{sJ\,p_{H_2}}{P} - \frac{D}{RT}\frac{dp_{H_2}}{dx} \qquad \ldots\ldots 54$$

$$-nJ = \frac{sJ\,p_{HCl}}{P} - \frac{D}{RT}\frac{dp_{HCl}}{dx} \qquad \ldots\ldots 55$$

These equations may be integrated between the limits $0 \leqslant x \leqslant \ell$ and $p_i(o) \leqslant p_i(x) \leqslant p_i(\ell)$. [NB. In an MEM system $p_{GeCl_n}(\ell) = 0$]

Thus:

$$p_{GeCl_n}(o) = \frac{P}{s}[1 - \exp(-s\xi)] \qquad \ldots\ldots 56$$

$$p_{H_2}(o) = \frac{P}{s}\left[\frac{n}{2} - \left(\frac{n}{2} - \frac{sp_{H_2}(\ell)}{P}\right)\exp(-s\xi)\right] \ldots\ldots 57$$

and $$p_{HCl}(o) = \frac{P}{s}\left[\left(n + \frac{sp_{HCl}(\ell)}{P}\right)\exp(-s\xi) - n\right] \ldots 58$$

where $\xi = \frac{JRT\ell}{DPc}$

When $p_{HCl} \ll 1$ (hence $\xi \ll 1$), these equations may be simplified:

$$P_{GeCl_n}(o) = P\xi \qquad \ldots\ldots 59$$

$$P_{HCl} = P\,[\varepsilon - n\xi] \qquad \ldots\ldots 60$$

$$\left(\text{where } \varepsilon = \frac{P_{HCl}(\ell)}{P}\right)$$

Finally, taking $p_{H_2} \simeq 1$ - a valid approximation for most practical systems-the general equation for the equilibrium constant is obtained:

$$K_n = \frac{P\xi}{[\varepsilon - n\xi]^n} \qquad \ldots\ldots 61$$

When $K_n << 1$ (and hence $\xi << \varepsilon$) 61 may be simplified further

$$K_n \simeq \frac{P\xi}{\varepsilon^n} \qquad \ldots\ldots 62$$

Substituting for K_n and taking logarithms

$$\left(\frac{\Delta H}{R}\right)\frac{1}{T} = \ell n\, P\xi - \left[n\, \ell n\, \varepsilon - \frac{\Delta S}{R}\right] \qquad \ldots\ldots 63$$

Similarly when $K_n >> 1$

$$P_{GeBr_n}(o) \simeq \frac{\varepsilon}{n}$$

$$\therefore \quad P\xi \simeq \varepsilon/n \qquad \ldots\ldots 64$$

$$\text{or } \ell n\, P\xi = \ell n\, \varepsilon - \ell n\, n \qquad \ldots\ldots 65$$

In theory the value of n could be obtained directly from equation 64. Two difficulties lie in this approach: (1) it may not be possible to reach a temperature where equation 64 is applicable, and (2) any errors in the physical constants (eg diffusion constants) will give wrong information. A better approach is to alter the pressure of HCl in the system. Suppose the HCl pressure is doubled (to 2ε). When $K \gg 1$, it can be seen from 65 that the effect will be to displace the $\ell n\ W$ vs $^1/_T$ plot by $\ell n\ 2$. However, when $K \ll 1$ the displacement is (from 63) $n\ \ell n\ 2$. Thus, at temperatures where $K \ll 1$ it is possible to establish the value of n by the extent to which the curve is displaced by increasing ε. Fig 5 shows the effect for an endothermic reaction.

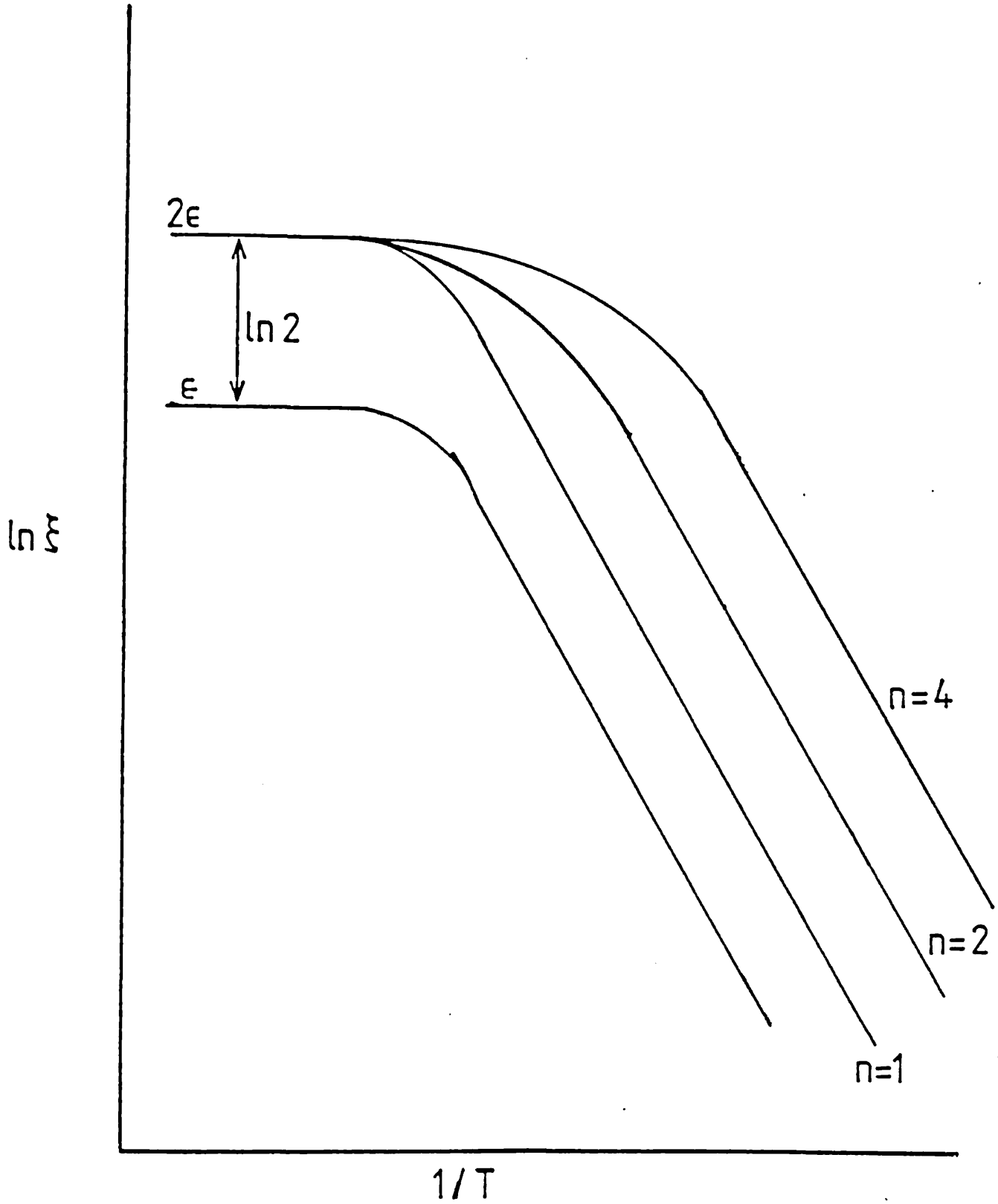

Schematic MEM Plot for $Ge+nHCl \rightleftharpoons GeCl_n + \frac{1}{2}H_2$

showing effect of doubling external HCl pressure.

REFERENCES

1 see eg R A Smith : 'Semiconductors' 2nd Edition, Cambridge University Press, 1978.

2 C A West, R M Thomson : 'Physics of Solids', McGraw-Hill, New York, 1964.

3 J Lothe, G M Pound : J. Chem. Phys. 36, 2080, 1962.

4 M Volmer, A Weber : Z. phys. Chem. 119, 277, 1926.

5 E Schonherr : Chap. 2 of 'Crystals' Vol 2, Springer-Verlag, Berlin, 1980.

6 J P Hirth, G M Pound : J. Chem. Phys. 26, 1216, 1957.

7 S Stoyanov : Chap. 4 of 'Current Topics in Materials Science' 3, 423, Ed. E Kaldis, North-Holland, Amsterdam, 1979.

8 C L Briant, J J Burton : J. Chem. Phys. 63, 2045, 1975.

9 T N Rhodin, D Walton : Metal Surfaces, ASM-AIME monograph, ASM, Ohio, 1963.

10 B Lewis, D S Campbell : J. Vac. Sci. Tech. 4, 209, 1967.

11 B K Chakraverty : Chap. 2 of 'Crystal Growth' Ed. P Hartman, North-Holland/Elsevier, Amsterdam, 1973.

12 H Hertz : Annalen Phys. Chem, Neue Folge 17, 177, 1882.

13 M Knudsen : Annalen Phys. 47, 4 Folge, 697, 1915.

14 W Kossel : Naturwissenschaften 18, 901, 1930.

15 I N Stranski : Z. Phys. Chem. 136, 259, 1928.

16 O Knacke, I N Stranski : Progress in Metal Physics 6, 181, 1956.

17 G A Somorjai : Surface Sci. 2, 298, 1964.

18 W Hirschwald, I N Stranski : "Condensation and Evaporation of Solids" p.59, Ed. E Rutner, P Goldfinger, J P Hirth, Gordon and Breach, New York, 1964.

19 P K Lee, G M Rosenblatt : J. Chem. Phys. 49, 2995, 1968.

20 L Brewer, J S Kane : J. Phys. Chem. 59, 105, 1955.

21 F C Frank : Disc. Far. Soc. 5, 48, 1949.

22 W K Burton, N Cabrera, F C Frank : Phil. Trans. Roy. Soc. 243A, 299, 1951.

23 K A Jackson : 'Growth and Perfection of Crystals' p.319, Eds. R H Doremus, B W Roberts, D Turnball, Wiley, New York, 1958.

24 K A Jackson : in 'Treatise of Solid State Chemistry' 5, 233, Ed. N B Hannay, Plenum, New York, 1975.

25 F Rosenberger : 'Fundamentals of Crystal Growth I' Springer-Verlag, Berlin, 1979.

26 M M Faktor, I Garrett : 'Growth of Crystals from the Vapour Phase', Chapman and Hall, London, 1974.

27 M M Faktor, R Heckingbottom, I Garrett : J. Chem. Soc. A, 2657, 1970.

28 M M Faktor, R Heckingbottom, I Garrett : J. Chem. Soc. A, 1, 1971.

29 M M Faktor, R Heckingbottom, I Garrett : J. Chem. Soc. A, 934, 1971.

30 J Stefan : Annalen Phys. Chem. 17, 550, 1890.

31 J Stefan : Annalen Phys. 41, 725.

32 D Battat, M M Faktor, I Garrett, R H Moss : J. Chem. Soc. Faraday Trans. I, 70, 2267, 1974 .

33 A Finch, P J Gardner, E Tarbox, S Yardley : J. Chem. Soc. Faraday Trans I, 75, 545, 1979 .

34 S Chapman, T G Cowling : 'The Mathematical Theory of Non-Uniform Gases' Cambridge, 1960.

35 D Battat, M M Faktor, I Garrett, R H Moss : J. Chem. Soc. Faraday Trans I, 70, 2293, 1974 .

36 D Battat, M M Faktor, I Garrett, R H Moss : J. Chem. Soc. Faraday Trans I, 70, 2302, 1974 .

CHAPTER 2: METHODS FOR STUDYING HETEROGENEOUS REACTIONS: THEORETICAL DISCUSSION

The experimental investigation of a heterogeneous reaction between a solid and a gas is straightforward since the rate of weight change of the solid is a direct measure of the rate of the reaction. However, although raw kinetic data can be readily generated, the interpretation of that data in mechanistic terms is very difficult. The observed rate of reaction will be the result of a large number of different processes eg transport of reactants to the surface, absorption of one or more reactants at the surface (either by physisorption or chemisorption), the formation of reaction intermediates, reaction between adsorbed species, desorption of products and transport of products away from surface. In addition, the rate may depend on the crystal orientation and on the number of defects in the sample. Clearly simple gravimetric techniques could not be used to identify all the reaction stages and the species involved; but measurement of overall reaction rates may give some clues to the detailed mechanism, and provide an important check on proposed reaction models.

In this chapter, three gravimetric techniques - the Langmuir, Knudsen and modified entrainment methods - are discussed in relation to the kinetic investigation of increasingly complex reaction systems. Equations are derived relating the rate of weight loss to surface kinetic parameters.

2.1 Simple Sublimation

The simplest heterogeneous reaction is the sublimation of an element (N) for which the reaction might be written

$$N_{(solid)} \rightleftharpoons N_{(vap)} \qquad \ldots\ldots 1$$

and the equilibrium constant is

$$K_N^o = p_N^o \qquad \ldots\ldots 2$$

The forward and reverse reaction rates may be written $k_f A$ and $k_r A p_N^o$ respectively; where k_f and k_r are the rate constants per unit area of the forward and reverse reactions and A is the surface area of the solid. The rate constants are functions of temperature and surface orientation. In the most general case they may be functions of pressure of N above the solid (p_N^*), but for the present k_f and k_r will be assumed to be independent of p_N^*.

At equilibrium, the rates of the forward and reverse reactions are equal:

$$k_f A = k_r A p_N^o \qquad \ldots\ldots 3$$

When the system departs from equilibrium, the net (measurable) rate is given by

$$J = k_f A - k_r A p_N^* \qquad \ldots\ldots 4$$

so J (the total flux) is negative for growth and positive for etching. If the departure from equilibrium does not cause a change in reaction

mechanism (a reasonable assumption in systems close to equilibrium), then equations 4 and 5 may be combined:

$$J = \frac{\dot{W}^*}{M} = k_r A (p^o - p_N^*) \qquad \ldots\ldots 5$$

$$\text{or} \quad \frac{W^*}{M} = k_r A p^o \left(1 - \frac{p^*}{p_N^o}\right) = k_f A \left(1 - \frac{p^*}{p_N^o}\right)$$

$$= J^o A \left[1 - \frac{p_N^*}{p_N^o}\right] \qquad \ldots\ldots 6$$

where J^o is, by analogy with electrochemistry, called the exchange current.

The term p_N^*/p_N^o is a measure of the driving force of the reaction and is henceforth termed the supersaturation (s). A thermodynamic driving force may also be defined, called here the overpotential (ω):

$$\omega = RT \ln \frac{p^*}{p^o} \qquad \ldots\ldots 7$$

The kinetic theory of gases may be used to calculate the bombardment rate (ν) of the solid:

$$\nu = \frac{A}{(2\pi MRT)^{\frac{1}{2}}} p_N^o = AZp_N^o \qquad \ldots\ldots 8$$

If only a fraction, α, of the collisions result in a reaction then equation 5 becomes

$$\frac{\dot{W}^*}{MA} = \frac{\alpha}{(2\pi MRT)^{\frac{1}{2}}} (p_N^o - p_N^*) \qquad \ldots\ldots 9$$

This is the Hertz-Knudsen equation [1,2] quoted in chapter 1. The coefficient α is called the evaporation coefficient (α_e) if $p_N^* < p_N^o$ and the condensation coefficient (α_c) if $p_N^* > p_N^o$. Since the experimental techniques described below all involve sublimation of the solid, use of equation 9 will enable the vapourisation coefficient to be studied.

2.1.1 Langmuir Technique

In this technique [3] the solid sample is simply suspended in vacuo from a balance, and the rate of weight loss measured. In an efficiently pumped apparatus, the pressure above the sample (p_N^*) is effectively zero and the rate of weight loss (W^*) is given by (from 9):

$$\frac{\dot{W}^*}{MA} = \alpha Z\, p_N^o \qquad \ldots\ldots 10$$

where $Z = \frac{1}{(2\pi MRT)^{\frac{1}{2}}}$

Originally presented as a means of determining vapour pressures, the Langmuir method made two assumptions (i) the forward rate is independent of the reverse rate (and hence, independent of the extent of departure from equilibrium) and (ii) there was no barrier to vapourisation at the surface. Under these conditions $\alpha = 1$ and the vapour pressure of the sample given by:

$$p_N^o = \frac{\dot{W}^*}{M} \frac{1}{AZ} \qquad \ldots\ldots 11$$

For many substances, especially metals, equation 11 has been found to hold [4]. However, comparison of Langmuir pressures with near-equilibrium techniques (such as Knudsen) sometimes shows the Langmuir results to be lower than the equilibrium value. This is most marked for substances such as arsenic and phosphorus which involve a rearrangement of bonding during vapourisation [5] and hence have a considerable barrier to vapourisation. The vapourisation coefficient allows results of Langmuir experiments to be correlated with the equilibrium vapour pressures.

As well as single component systems, equation 11 has been applied to more complex system such as III-V compounds where the vapourisation is incongruent and only the group V element contributes significantly to the vapour pressure [6]. In all kinetic studies involving the Langmuir method the main disadvantage is that only one (extreme) condition can be investigated. The system is far from equilibrium and rates obtained by this technique may not represent the vapourisation rates close to equilibrium. Of more interest, particularly for crystal growth systems, are those techniques in which the solid is at, or close to, equilibrium with the vapour and which enable the pressure dependence of the vapourisation coefficient to be investigated.

2.1.2 The Knudsen Technique

In this technique the sample (N) is placed in a small cell [2,7], in which there is a small hole of known dimensions. The cell is suspended in vacuo and the rate of weight loss measured. It is

assumed that the rate of loss of material is equal to the bombardment rate of a portion of the cell wall equal in area to that of the hole, which at low pressures may be calculated from the kinetic theory of gases. In effect the Knudsen cell acts as an ideal Langmuir source since there is no barrier to the passage of atoms from the interior of the cell to its surroundings.

The rate of loss of atoms from the cell is given by

$$\frac{\dot{W}^*}{M} = aZ\, p_N^* \qquad \ldots\ldots 12$$

where a is the area of the hole and p_N^* the pressure of N inside the cell. Equation 12 allows the pressure inside the cell to be obtained from a measured rate of weight loss.

The Knudsen method is frequently used to determine equilibrium vapour pressures: if the hole is sufficiently small the sample may be assumed to be in equilibrium with the vapour in the cell. The vapour pressure may then be found directly from the weight loss measurement using equation 11. By increasing the size of the hole, a significant departure from equilibrium is caused and the system may then be used in kinetic studies.

Since equation 12 is central to both kinetic and thermodynamic studies, the conditions for which it is valid will be discussed first, before continuing with the kinetic studies using the Knudsen method. Two assumptions were made in the derivation of equation 12:

1. It was assumed that the rate of loss of material was equal to the bombardment rate of the hole area. This is equivalent to assuming the hole is infinitely thin. In practice this can never be true and equation 12 should have the form [8]:

$$\frac{\dot{W}}{M} = aZ \quad K \, p_N^* \qquad \ldots\ldots 13$$

where K is the Clausing correction factor which allows for atomic back reflections which introduce a resistance to molecular flow through the hole [8,9]. The value of K depends on the ratio ℓ/r where ℓ is the thickness and r the radius of the hole. The calculation of K is complex; tables have been produced by Clausing [8,9] and others [10]. For many applications an empirical relation obtained by Kennard [11] is adequate (accurate to within ~1% in specified range):

$$K = \frac{1}{1 + 0.5 \, \ell/r} \qquad \left(0 < \frac{\ell}{r} < 1.5\right) \qquad \ldots\ldots 14$$

For most sizes of hole it is easy to arrange $\frac{\ell}{r} \lesssim 0.02$ so that equation 12 may be used with little error. However, a limit is reached with very small holes due to the low mechanical strength of any material only a few μm thick. This limitation, together with a requirement that K be close to unity, imposes a minimum value on the size of the hole. Typically, the holes in a Knudsen cell are 0.4-0.5 mm diameter (~10^{-3} cm^2 area) [12,13,14].

2. The second implicit assumption of equation 11 is that flow through the hole is molecular (as opposed to hydrodynamic flow). The change from molecular to hydrodynamic flow is generally taken as a characteristic of the length of the mean free path relative to the diameter of the hole. Knudsen [15] found equation 12 to be valid for $\lambda/2r > 10$, where λ is the mean free path length and 2r the diameter of the hole. Other workers have found that for mercury vapour the transition from molecular to hydrodynamic flow begins at [14]

$$\frac{\lambda}{2r} \approx 1$$

Since the mean free path is inversely proportional to pressure, the condition $\lambda/2r > 10$ imposes a maximum value on the pressures which might be determined using equation 12. For a hole 0.4 mm diameter ($\sim 10^{-3}$ cm^2) the maximum pressure is of the order 10^{-6} - 10^{-5} atm [16], although other workers report a maximum operating pressure of $\sim 10^{-3}$ atm [17].

In conclusion, the two assumptions implicit in the derivation of equation 12 result in a limit to the pressures which may be studied. For most practical cells, this maximum pressure is of the order of 10^{-5} atm, although operating pressures as high as 10^{-3} atm may be possible.

Having discussed the limits of validity of equation 12 it is now possible to consider systems in which there is a significant departure from equilibrium within the bottle. In a steady-state

system the rate at which material leaves the bottle must equal the rate at which the solid vapourises. This later rate is given by equation 5:

$$\frac{\dot{W}^*}{M} = k_r (p_N^o - p_N^*) \qquad \ldots\ldots 5$$

If the system is in a steady-state, equation 12 may be used to substitute for either p_N^* or p_N^o, yielding respectively:

$$\frac{\dot{W}^*}{M} = \frac{aZ\, k_r A}{aZ + k_r A}\, p_N^o \qquad \ldots\ldots 15$$

or $$\frac{p_N^*}{p_N^o} = \frac{k_r A}{aZ + k_r A} \qquad \ldots\ldots 16$$

It is clear from equation 16 that the Knudsen method gives equilibrium vapour pressures when the vapourisation rate of the solid is much greater than the rate of loss of material from the cell (ie $k_r A >> aZ$). Using equation 9, k_r may be rewritten $k_r = \alpha Z$ and equations 15 and 16 become

$$\frac{\dot{W}^*}{M} = \frac{aZ\alpha}{\left(\frac{a}{A} + \alpha\right)} p_N^o \qquad \ldots\ldots 17$$

and $$\frac{p_N^*}{p_N^o} = \frac{\alpha}{\left(\frac{a}{A} + \alpha\right)} \qquad \ldots\ldots 18$$

The equations are plotted in figs 1 and 2 for several different values of α. The diagrams show that as the area of the hole increases, the rate of weight loss ($\dot{W}^*$) reaches a constant value, while in contrast the pressure inside the cell (p_N^*) falls

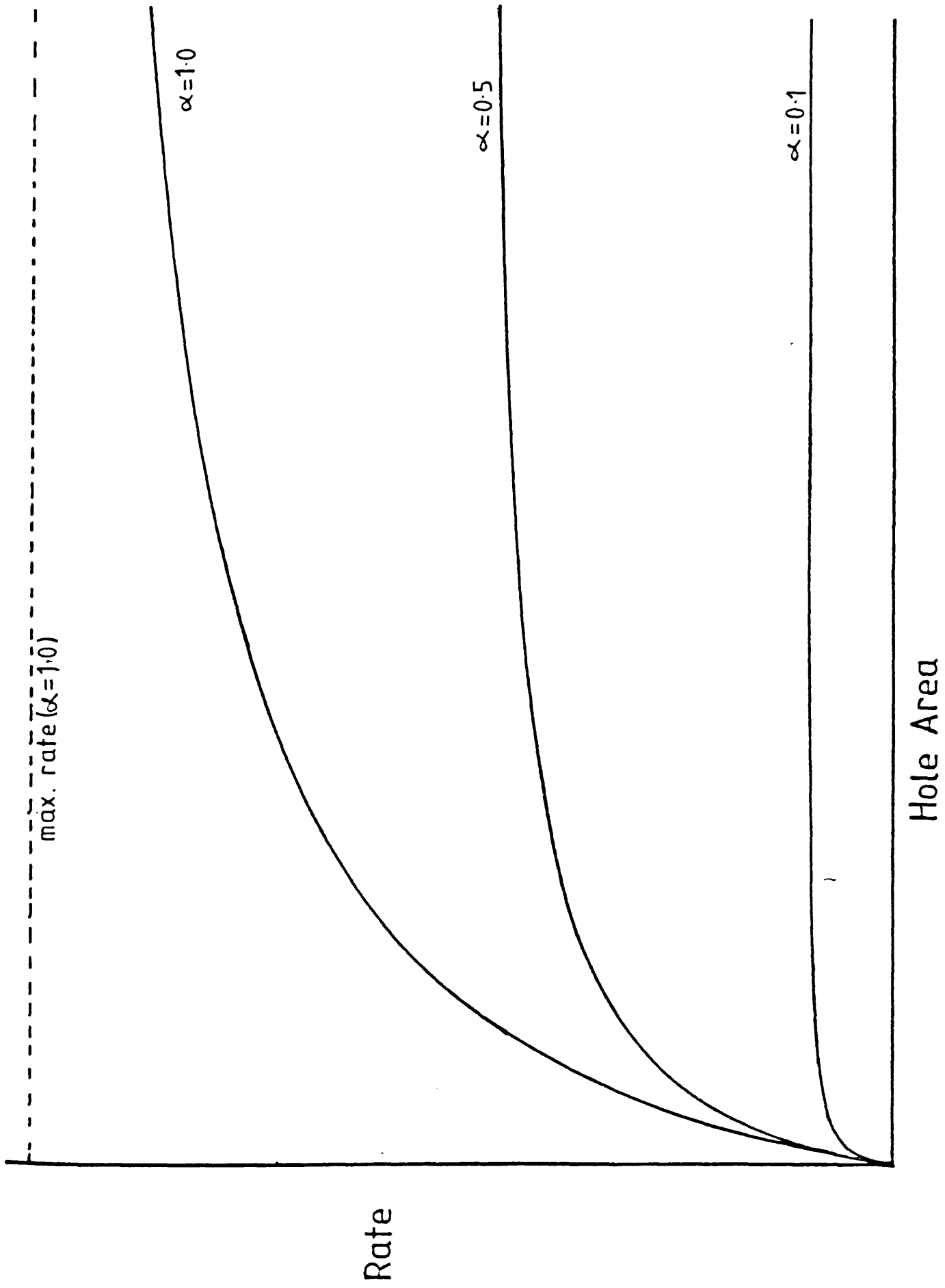

Effusion Rate vs. Knudsen Cell Hole Area

Fig 2-2

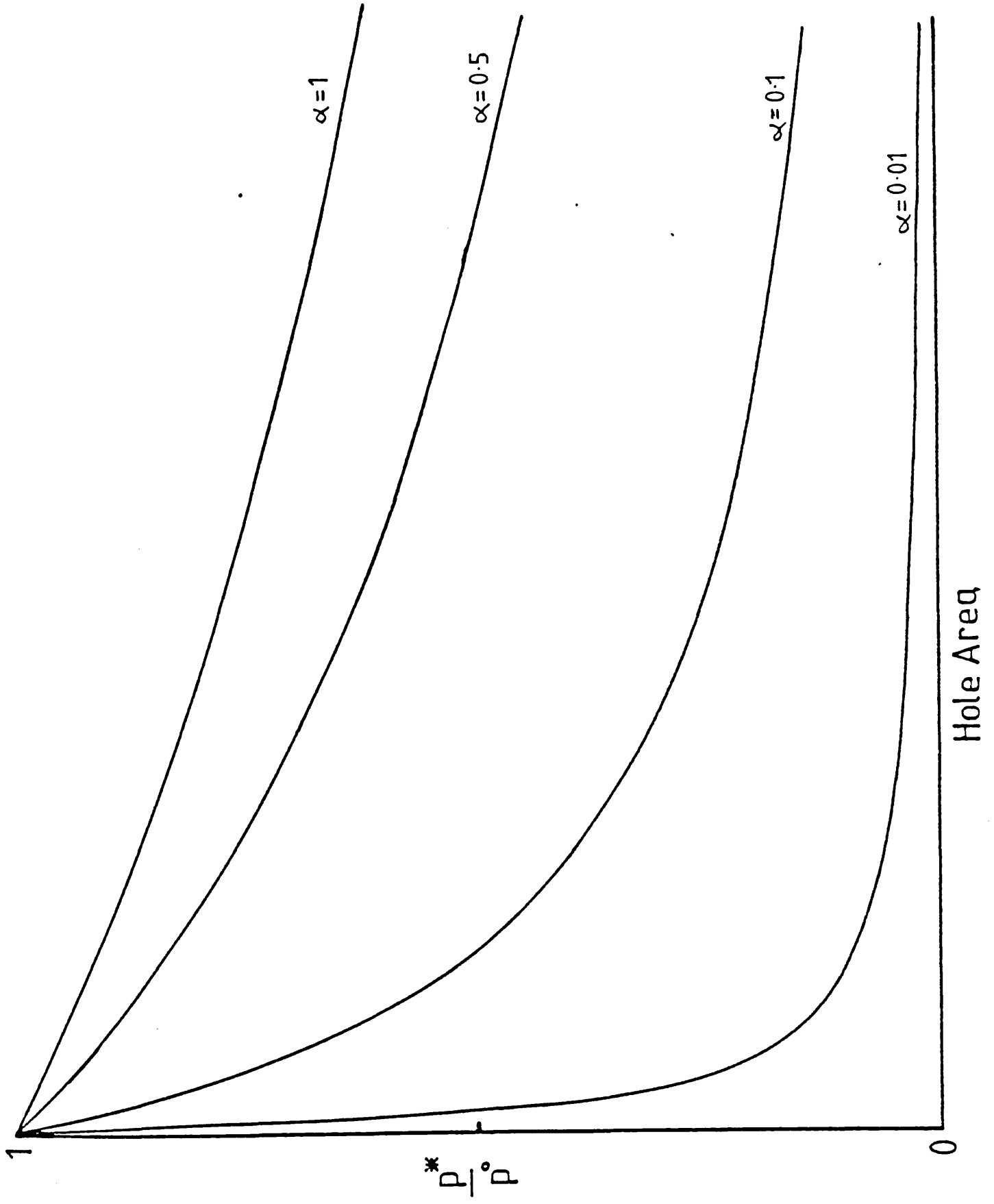

Pressure in Knudsen Cell vs. Hole Area

to zero. The limiting rate of weight loss is found by letting $\frac{a}{A} >> \alpha$, so that 17 simplifies to

$$\frac{\dot{W}^*}{M} = AZ\alpha\, p_N^o$$

which is identical to equation 10 for the Langmuir experiment.

If k_r (or α) is not a function of p_N^*, equation 15 may be linearised by taking reciprocals:

$$M\left(\frac{1}{\dot{W}^*}\right) = \frac{1}{Zp_N^o}\left(\frac{1}{a}\right) + \frac{1}{k_r\, Ap_N^o} \qquad \ldots\ldots 19$$

Clearly, a plot of $\frac{1}{\dot{W}^*}$ vs $\frac{1}{a}$ will give a straight line with an intercept $\frac{1}{k_r A}$. Curvature in the plot indicates a pressure dependence in k_r.

The Knudsen method is a very much more flexible method for investigating the kinetics of vapourisation than the Langmuir technique. By changing the size of the hole measurements may be made in a variety of different conditions. However the main equation used in interpretation of the results (equation 12) has a limited range of validity and the technique may only be used to study systems in which the experimental pressures are not greater than 10^{-3} - 10^{-4} atm. To study systems at higher pressures, the modified entrainment method may be used.

2.1.3 The Modified Entrainment Method

The experimental system described above and the equations governing their results are well established. A detailed

discussion was necessary in order to place in context the contribution a well-designed MEM experiment may make to kinetic investigations. The basic features of the MEM system, and the application to equilibrium systems were described in chapter 1. Here, the theory is for the first time extended to non-equilibrium systems using the same procedure as that used for the Langmuir and Knudsen techniques. This treatment emphasises the conceptual similarities between the Knudsen and MEM techniques.

If the apparatus is arranged so that the pressure of N at the open end of the channel is zero, then the pressure inside the bottle is given by equation 23 of chapter 1:

$$p_N^* = P\,(1 - \exp(-\xi)) \qquad \ldots\ldots 20$$

where $\xi = \frac{RT\ell}{DPc} \cdot \frac{\dot{W}^*}{M}$

and P is the total pressure in the system, D the binary diffusion coefficient of N in the gas and ℓ and c are the length and cross-sectional area of the channel in the MEM bottle. Equation 22 may be used to calculate the pressure inside the bottle provided that two conditions are fulfilled. These conditions limit both the size of the channel (ℓ/c) and the total pressure in the system:

1. It is essential that any pressure gradients be confined to the channel. This is achieved by ensuring the transport resistance if the channel is much higher than that of the main body of the bottle. This resistance is proportional to $\int \frac{dx}{A}$ (where A is the area at position x).

For a cylindrical channel (or bottle) $\int \frac{dx}{A} = \frac{\ell}{c}$. A typical bottle used for thermodynamic investigations is cylindrical in shape, about 1 cm in diameter and 1-1.5 cm long. The corresponding channel has a similar length, but a diameter of ~1 mm, so that the channel resistance is approximately one hundred times that of the bottle. Other common shapes for bottles are spherical or conical: the formulae for transport resistance are given in the appendix. The ratio of channel and bottle resistances may become important in kinetic investigations where it is necessary to use wider channels. Misleading results may be obtained if the transport resistance of the channel falls to a value similar to that of the bottle.

2. The second condition limiting the validity of equation 20 is the underlying assumption of hydrodynamic flow in the channel. The changeover from molecular to hydrodynamic flow was discussed in section 2.1.2 where it was shown that the critical parameter was $\frac{\lambda}{d}$ where λ is the mean free path length and d the diameter of the opening. Taking the critical value for hydrodynamic flow as unity, the condition $\lambda/d < 1$ is obtained, which imposes a minimum value on the total pressure in the system. With a channel ~1 mm diameter, this minimum pressure is $\sim 10^{-4}$ atm. In practice, experiments are carried out at atmospheric pressure under which condition equation 20 is valid.

It is now possible to derive the equation linking the measured rate of weight loss with the kinetic processes occurring at the

surface. The equations produced represent a completely new extension to the theory of the modified entrainment method and show that by using this technique it is possible to uncouple the sequential processes of transport and surface reaction, a problem normally overcome by assuming the system is either transport-limited or surface-limited.

Equation 20 may be rearranged to give

$$\frac{\dot{W}^*}{M} = \frac{DP}{RT} \cdot \frac{c}{\ell} \ln \frac{P}{P-P_N^*} \qquad \ldots\ldots 21$$

It is clear that a decrease in ℓ/c (the channel resistance) will increase the rate of weight loss, at constant p_N^*. If the surface processes are too slow to maintain a constant pressure in the bottle, as would be the case when investigating kinetics, then the pressure in the bottle will decrease with decreasing channel resistance.

The effect of pressure is less obvious since the diffusion constant is also pressure dependent. In general,the diffusion constant may be represented by an equation [30]

$$D = D'/P \qquad \ldots\ldots 22$$

where D' is the binary diffusion coefficient of N in the inert gas at 1 atm. Substituting for D in 21 gives

$$\frac{\dot{W}^*}{M} = \frac{D'}{RT} \cdot \frac{c}{\ell} \cdot \ln \frac{P}{P-p_r^*} \qquad \ldots\ldots 23$$

from which it can be seen that increasing the total pressure reduces the measured rate of weight loss. Increasing the

amount of inert gas in the system effectively increases the transport resistance of the channel. This is shown schematically in fig 3.

Substituting for $\dot{W}^*/M$ from 5, and using $k_r = \alpha Z$ yields

$$\frac{DP}{RT} \cdot \frac{c}{\ell} \cdot \frac{1}{\alpha Z A p_N^o} \cdot \ell n \frac{P}{P-p_N^*} = 1 - \frac{p_N^*}{p_N^o} \qquad \ldots\ldots 24$$

The right-hand side of this equation is a measure of the departure from equilibrium; this can be seen to increase with decreasing channel resistance, as shown in fig 4. By substituting for p_N^* instead of W^*/M, the following equation can be obtained:

$$\frac{\dot{W}^*}{M} = \frac{DP}{RT} \cdot \frac{c}{\ell} \ell n \frac{P}{P-p^o + \frac{\dot{W}^*}{M\alpha Z}} \qquad \ldots\ldots 25$$

Although more complex, the qualitative relations described by equations 24 and 25 are similar to those of equations 16 and 15 respectively. This can be seen more clearly by examining the limiting case where $\xi << 1$. This occurs when there is a large excess of the inert gas, and is a common situation in experiments. When $\xi << 1$, equation 20 simplifies to

$$p^* = P\xi = \frac{RT\ell}{Dc} \cdot \frac{\dot{W}^*}{M} \qquad \ldots\ldots 26$$

This may be compared with equation 12 for the Knudsen cell: in both cases the rate of weight loss is directly proportional to the pressure inside the bottle (or cell). Using equation 26 to substitute for p_N^* in 5 gives:

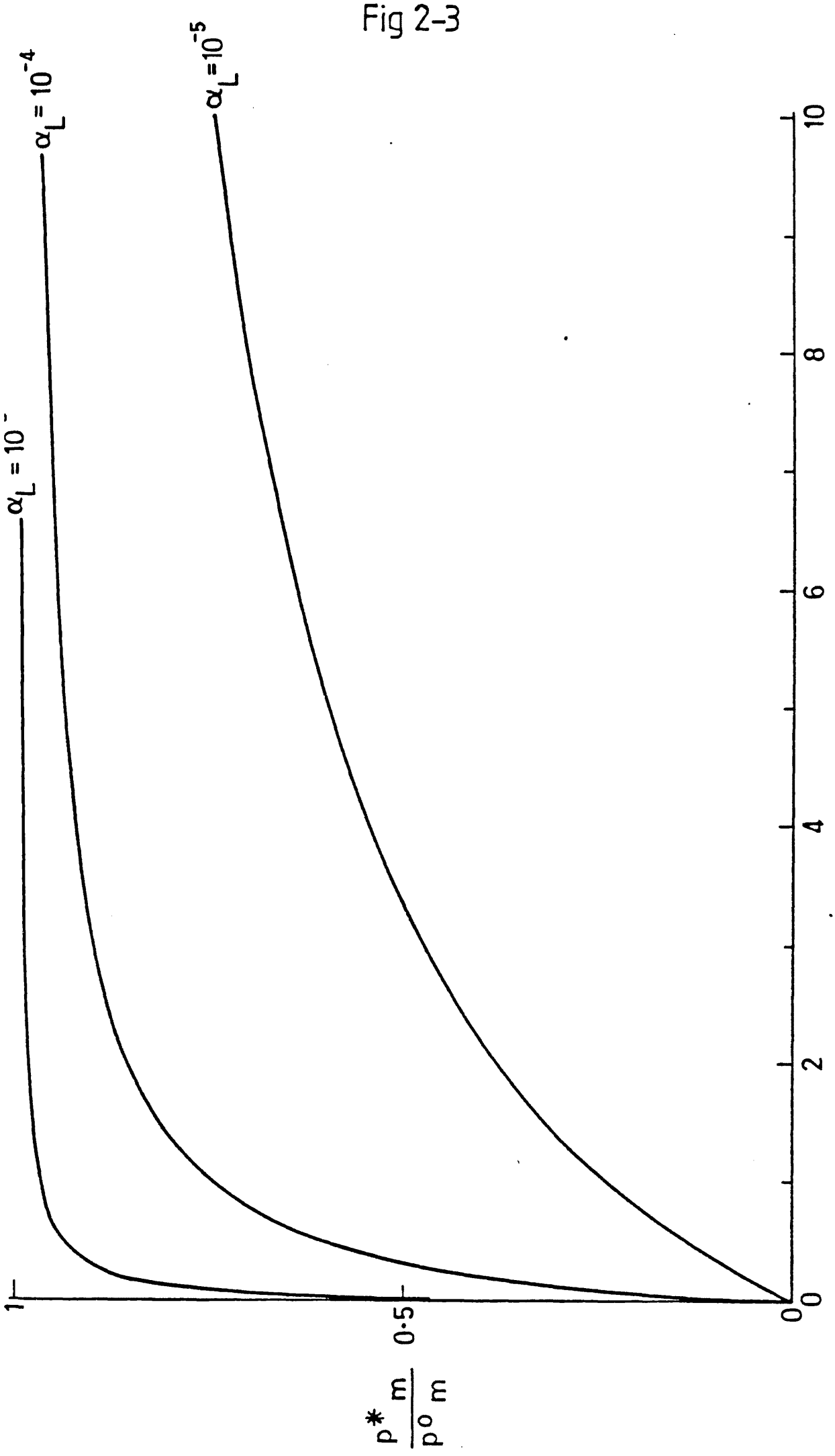

Effect of total pressure on MEM Plot

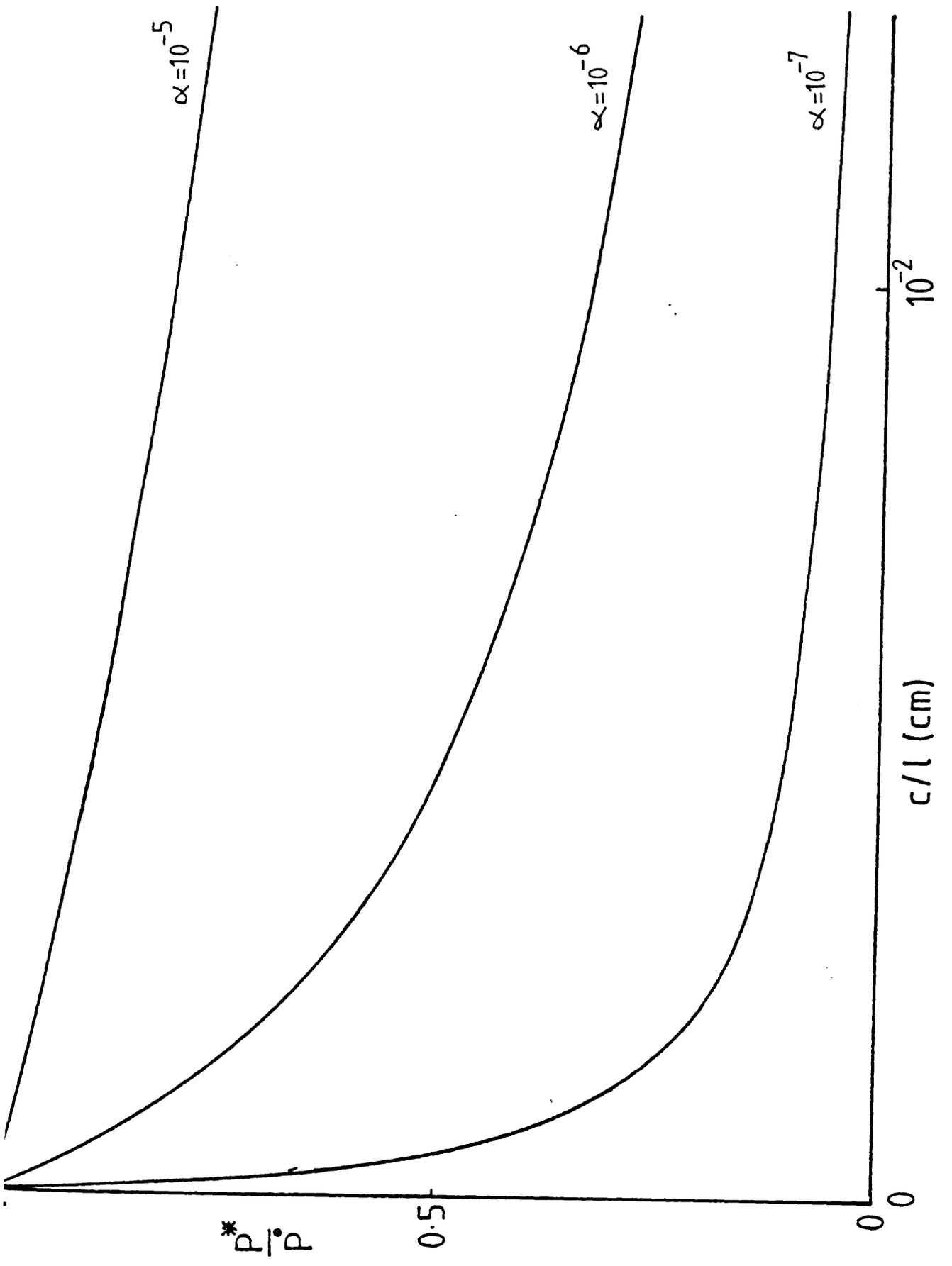

Pressure in MEM Bottle vs. Channel Size

(calculated for red phosphorus at 400°C - p*=0·624)

$$\frac{\dot{W}^*}{M} = \frac{\frac{Dc}{RT\ell} \cdot k_r A}{\frac{Dc}{RT\ell} + k_r A} p_N^o \qquad \ldots\ldots 27$$

This has the same form as equation 15, and may be linearized to give an equation similar to equation 19:

$$M\left(\frac{1}{\dot{W}^*}\right) = \frac{RT}{Dp_N^o} \cdot \left(\frac{\ell}{c}\right) + \frac{1}{k_r A p_N^o} \qquad \ldots\ldots 28$$

So far, the pressure of N at the outlet of the channel has been fixed at zero. However, the great advantage of the MEM system is that it is possible to introduce N into the external gas-stream and thus to fix the pressure at the outlet at any value. When there is a large excess of inert gas in the system ($\xi << 1$), then the weight loss rate is given by equation 24 of chapter 1 :

$$\frac{\dot{W}^*}{M} = \frac{Dc}{RT\ell}\left[p_N^* - p_N^\ell\right] \qquad \ldots\ldots 29$$

where p_N^ℓ is the pressure of N at the outlet of the channel and p_N^* the pressure inside the bottle.

Rearrangement of 29 gives

$$p_N^* = p_N^\ell + \frac{RT\ell}{Dc} \cdot \frac{\dot{W}^*}{M} \qquad \ldots\ldots 30$$

Substituting in 5:-

$$\frac{\dot{W}^*}{M} = k_r A \left[p_N^o - p^\ell - \frac{RT\ell}{Dc} \cdot \frac{\dot{W}^*}{M}\right] \qquad \ldots\ldots 31$$

which gives, on rearrangement:

$$\frac{\dot{W}^*}{M} = \frac{k_r A}{1 - \frac{k_r A.RT\ell}{Dc}} [p^o - p^\ell] \qquad \ldots\ldots 32$$

If the rate constant k_r is independent of pressure (as originally assumed) then $\dot{W}^*$ will be a linear function of p^ℓ: any non-linearity is indicative of a pressure-dependence in k_r, the nature of which can be investigated. The introduction of gaseous species into the external gas-stream is both simpler and quicker than varying channel-size (as in the use of equation 28) or hole-sizes (Knudsen - equation 19). Furthermore, the MEM allows the introduction of other gaseous species which may have a catalytic effect on the vapourisation rate. This is discussed more fully in chapter 3.

2.1.4 Summary

The three gravimetric techniques: Langmuir, Knudsen and modified entrainment (MEM), were discussed as a methods of carrying out kinetic investigations of a simple sublimation system. Using procedures well-established for the Langmuir and Knudsen techniques, the theory underlying MEM was extended to deal with sublimation systems in which the surface reaction rate has a major influence on the overall rate of weight loss. The modified entrainment method was shown to be a powerful tool in kinetic investigations, allowing reaction rates to be investigated under a wide range of experimental conditions which could be changed rapidly and easily.

2.2 Dissociative Sublimation

In this section, the more complex system of dissociative sublimation is considered:

$$BC_{(s)} \rightleftharpoons B_{(vap)} + \frac{1}{m} C_{m(vap)} \qquad \ldots\ldots 33$$

This type of reaction is an important means of growing II-VI compound semiconductors such as CdS [18,19,20]. In this system the forward and reverse currents are unlikely to be independent and consequently, the results of a Langmuir experiment are unlikely to give a good indication of reaction rates close to equilibrium. Depending on the efficiency of the pumping system, pressures of B and C_m above the solid will be of the order 10^{-14} - 10^{-9} atm. If the substance under investigation has vapour pressures of the order of, say, 10^{-5} atm then the Langmuir conditions represent a highly specialized case in which the reverse current is negligible compared to the forward (vapourisation current). Although these conditions may be of theoretical interest [20,21,22] they contrast strongly with those found in practical growth systems. Here, the solids are close to equilibrium, and the magnitudes of forward and reverse currents are comparable.

The Knudsen and modified entrainment (MEM) methods may both be used to study the surface kinetics of dissociative sublimation. As was shown in section 2.1, both methods allow measurements to be made over a range of conditions close to equilibrium, and allow the dependence of rate on the reactant pressures to be investigated. Both methods will be discussed, after a formalism is derived for relating growth rate to overpotential. The method is that of Faktor and Garrett [23].

2.2.1 Theory

The procedure is similar to that in section 2.1 (derivation of equation 5). For reaction 31:

$$BC_{(s)} \rightleftharpoons B_{(v)} + \frac{1}{m} C_{m(v)}$$

a forward and reverse reaction rate is defined. In this case both forward and reverse reactions are considered to be functions of the reactant procedures. In general, the exact nature of this dependence is unknown. Nevertheless, the forward current may be represented by the equation

$$J_f = k_f A p_B^x p_C^y \qquad \ldots\ldots 34$$

where A is the area of the sample and k_f the specific rate constant for the forward reaction. Since the pressure dependence of J_f has been stated explicitly, k_f is a function of temperature and surface orientation only. A similar expression may be used to represent the reverse current (J_r):

$$J_r = k_r A p_B^{x+1} p_C^{y+\frac{1}{m}} \qquad \ldots\ldots 35$$

where k_r is the specific rate constant for the reverse reaction and like k_f a function of temperature and surface orientation only.

At equilibrium, the forward and reverse currents are equal:

$$k_f A p_B^x p_C^y = k_r A p_B^{x+1} p_C^{y+\frac{1}{m}}$$

$$\therefore \quad \frac{k_f}{k_r} = p_B^o p_C^{o\frac{1}{m}} = K^o \qquad \ldots\ldots 36$$

where p_B^o, p_C^o are equilibrium pressures and K^o the equilibrium constant for reaction 31.

The indices x and y will be functions of surface orientation and also, in the most general case, functions of temperature and reactant pressures. However, for small departures from equilibrium these indices may be taken to be constants. The rate of weight loss ($\dot{W}$) is then given by

$$\frac{\dot{W}}{M} = k_f A p_B^x p_C^y - k_r A p_B^{x+1} p_C^{y+\frac{1}{m}} \quad \ldots\ldots 37$$

where M is the molecular weight of BC.

From 36, k_r/k_f may be substituted:-

$$\frac{\dot{W}}{M} = k_f A p_B^x p_C^y [1 - K^*/K^o] \quad \ldots\ldots 38$$

where $K^* = p_B p_C^{\frac{1}{m}}$

An alternative formulation is

$$-J = J_f (1 - K^*/K^o) \quad \ldots\ldots 39$$

where J is the growth rate, and J_f, the forward current defined by equation 35.

In some applications, a different formulation is more useful. Two new variables are defined: β and P such that

$$\beta = \frac{p_B}{p_C} \quad \text{and} \quad P = p_B + p_C$$

Then

$$p_B = \frac{\beta}{1+\beta} P \qquad \text{and} \qquad p_C = \frac{1}{1+\beta} P \qquad \ldots\ldots 40$$

Substituting for p_B and p_C in 36 gives

$$\frac{\dot{W}}{M} = k_f A \beta^x \left(\frac{P}{1+\beta}\right)^{x+y} [1 - K^*/K^o] \qquad \ldots\ldots 41$$

where K^* is now given by

$$K^* = \beta \left(\frac{P}{1+P}\right)^{1+\frac{1}{m}} \qquad \ldots\ldots 42$$

Clearly the ratio of the pressures of B and C_m over the solid (β) can have considerable influence over both the rate of weight loss (J) and the value of K^*. Equation 42 may be rearranged to give

$$K^{*m} (1+\beta)^{1+m} - \beta^m P^{m+1} = 0 \qquad \ldots\ldots 43$$

from which it can be seen that if the total pressure (P) is kept constant, a given value of K^* may correspond to several different values of β [24]. Equation 43 will have m+1 roots, although those which are negative or imaginary have no physical significance.

If x and y are positive it can be seen from equation 41 that extreme values of β lead to very low rates of weight loss. Thus, if $\beta << 1$, then

$$\frac{\dot{W}}{M} \approx k_f A \beta^x P^{x+y} [1 - K^*/K^o]$$

and if $\beta >> 1$

$$\frac{\dot{W}}{M} \approx k_f A \frac{P^{x+y}}{\beta^y} [1 - K^*/K^o]$$

To some extent this effect is opposed by a similar change in K^*, which will tend to increase the term $[1 - K^*/K^o]$. However, the effect of this is limited. The fact that K^* is a function of β indicates that experiments carried out with a large excess of B or C_m should be interpreted with caution. For these systems K^* may be much less than K^o and the system very far from equilibrium, so that equations 36 and 39(which were derived for small departures from equilibrium) may no longer apply.

Having obtained a suitable formalism for discussing kinetic results, it is possible to discuss in turn the use of Knudsen and modified entrainment methods in the investigation of dissociative sublimation systems.

2.2.2 Knudsen Method

In section 2.1.2 it was shown that the rate of loss of material from a Knudsen cell is given by:

$$J = \frac{\dot{W}}{M} = aZp \qquad \ldots\ldots 12$$

where $Z = (2\pi MRT)^{-\frac{1}{2}}$

Equations identical to 12 may be written for the loss both B and C_m:

$$J_B = aZ_B p_B \qquad \ldots\ldots 44$$

and $$J_C = aZ_C p_C \qquad \ldots\ldots 45$$

where $Z_i = (2\pi M_i RT)$, and J_i is the rate of loss of species i. It is important to note that neither J_B nor J_C may be obtained directly from gravimetric measurements. One way to overcome this difficulty is to simply use the Knudsen cell as a molecular beam source, which may be examined using mass spectrometric techniques [6,25,26]; although it may be difficult in some cases to distinguish between the effusion flux and the background signal [26]. Such techniques are only necessary if the vapourisation is incongruent - as in the case of III-V compounds such as InP. When the compound vapourizes congruently, and providing it has a narrow stoichiometry range, then B and C_m will enter the gas-phase in the stoichiometric ratio given by equation 33. This is the case with II-VI compound semiconductors such as CdS [20]. For these systems the rates of loss of the gas species may readily be obtained from a measured rate of weight loss. Since the system inside the Knudsen cell is in a steady-state it follows that the species must be lost from the cell in the same ratio as they have when entering the gas-phase, that is, in the stoichiometric ratio. Thus, if $J = \dot{W}/M$ where $\dot{W}$ is the measured rate of weight loss of BC and M the gram-formula weight, then

$$J = J_B \qquad \ldots\ldots 46$$

and $$J_C = \frac{1}{m} J_B = \frac{1}{m} J \qquad \ldots\ldots 47$$

Thus, from 44, 45, 46 and 47

$$p_B = \frac{J}{aZ_B} = \frac{\dot{W}}{M} \cdot \frac{1}{aZ_B} \qquad \ldots\ldots 48$$

$$\text{and } P_C = \frac{J}{aZ_C} = \frac{W}{mM} \cdot \frac{1}{aZ_c} \qquad \ldots\ldots 49$$

In section 2.1.2 it was shown that by altering the size of the Knudsen orifice the kinetics of simple sublimation could be investigated. A similar method may be used to investigate dissociative sublimation, subject to the limitations on total pressure discussed earlier. However, in using a Knudsen cell a certain amount of kinetic information will be lost. This is most clearly seen from equation 39:

$$J = k_f A \frac{\beta^x}{(1+\beta)^{x+y}} p^{x+y} [1 - K^*/K^o] \qquad \ldots\ldots 41$$

From 48 and 49, β is given by

$$\beta = \frac{P_B}{P_C} = m \sqrt{\frac{M_B}{M_C}} = \text{a constant} \qquad \ldots\ldots 50$$

Thus, equation 41 may be written

$$J = C.\ p^{x+y} [1 - K^*/K^o] \qquad \ldots\ldots 51$$

where $C = k_f A.\ \beta^x\ (\beta+1)^{-(x+y)}$ = a constant

A study of dissociative sublimation by means of a Knudsen cell will yield some kinetic information. However, because the gas pressure ratio in the cell is fixed (equation 50) it is not possible to investigate the pressure dependence of the reaction rate. This problem is overcome in the modified entrainment method.

2.2.3 Modified Entrainment Method

The transport equations for a dissociative sublimation system such as CdS have been discussed in considerable detail by Faktor et al [24,27,28] for a typical growth system in which equilibrium was assumed at the surface. In the discussion of simple sublimation the bottle was assumed to be suspended in a stream of inert gas, to which could be added other gas species including the subliming substance itself. For dissociative sublimation the same experimental arrangement may be used; it is thus possible to envisage a situation in which the gas-stream is composed wholly of one of the reactive species (B or C_m). This feature indicates the extreme range of conditions which may be investigated with MEM.

As with the Knudsen method only the weight loss of the sample is measured and the pressures inside the bottle may only be calculated if the solid sublimes congruently. An exception to this rule is a substance such as InP where at high temperatures the only significant gas species is phosphorus vapour. The system may then be treated as a simple sublimation system (see chap 1). The incongruent sublimation of InP has, indeed, been investigated using MEM [29]..

For the purpose of this discussion, however, the sublimation will be assumed to be congruent so that the pressures inside the bottle will then be given by [27]

$$p_B = \frac{P_T}{s}\left[1 - \exp\left(-\xi_B\right)\right] + p_B(\ell)\exp\left(-\xi_B\right) \qquad \ldots\ldots 52$$

and

$$p_C = \frac{P_T}{ms}\left[1 - \exp(-\xi_C)\right] + p_C(\ell)\exp(-\xi_C) \qquad \ldots\ldots 53$$

where $s = 1 + \frac{1}{m}$; $\xi_i = \frac{RT\ell s}{D_i P_T c} \cdot \frac{\dot{W}}{M}$; D_i is the diffusion constant of species i, P_T the total pressure in the system, and $\dot{W}$ the measured rate of weight loss of the sample.

Equation 52 and 53 may be combined with equation 41 to give:

$$\frac{\dot{W}}{M} = k_f A\left[\frac{P_T}{s} - \left(\frac{P_T}{s} - p_B(\ell)\right)e^{-\xi_B}\right]^x \left[\frac{P_T}{ms} - \left(\frac{P_T}{ms} - p_C(\ell)\right) e^{-\xi_C}\right]^y \left[1 - K^*/K^o\right] \qquad \ldots\ldots 54$$

where K^* is given by:

$$K^* = \left[\frac{P_T}{s} - \left(\frac{P_T}{s} - p_B(\ell)\right)e^{-\xi_B}\right]\left[\frac{P_T}{ms} - \left(\frac{P_T}{ms} - p_C(\ell)\right) e^{-\xi_C}\right]^{\frac{1}{m}}$$

Equation 52 is very complex, but it is apparent from this equation and the definition of ξ_i that p_B and p_C may be altered by changing the channel size $(\frac{\ell}{c})$, the total pressure (P_T) or the individual reactant pressures ($p_B(\ell)$ and $p_C(\ell)$) in the external gas-stream.

The effect of changing channel size was discussed in connection with simple sublimation (section 2.1.3): an increase in channel resistance (increased ℓ/c) will increase the pressures of B and C_m inside the bottle and consequently, K^*. An increase in channel resistance is thus equivalent to a reduction in the undersaturation of the vapour in the bottle.

An increase in total pressure, and increases in the pressures of $p_B(\ell)$ and $p_C(\ell)$ are closely related. However if the pressure increase is due solely to an increase in the amount of inert gas in the system then the effects may be separated. It was shown in section 2.1.3 (simple sublimation) that increasing the total pressure in the system was equivalent to an increase in the transport resistance. A similar effect is found in dissociative sublimation systems [28]. Consequently, an increase in the total pressure in the system will have the same effect as an increase in (ℓ/c) and the vapour in the bottle will come closer to equilibrium. Although both methods offer some measure of control over conditions inside the bottle the range is limited. Only by introducing reactive species into the gas-phase (ie altering $p_B(\ell)$ or $p_C(\ell)$) can a large measure of control over conditions inside the bottle be achieved. Although the detailed consequences of a change in, say, $p_B(\ell)$ are difficult to establish from equation 54, the general behaviour of the system may be understood. For there to be a net loss of material from the system there is the condition

$$K^*(\ell) < K^* < K^o \qquad \ldots\ldots 55$$

where $K^*(\ell) = p_B(\ell)\, p_C(\ell)^{\frac{1}{m}}$

Furthermore, if the system is in steady-state, the following conditions apply:-

$$p_B(\ell) < p_B \qquad \ldots\ldots 56$$

$$p_C(\ell) < p_C \qquad \ldots\ldots 57$$

Clearly, an increase in the pressure of one of the reactants in the external gas-stream is reflected by a similar increase inside the bottle.

Equation 54 may be simplified under certain circumstances: for example, by setting one or both of the reactant pressures ($p_B(\ell)$ and $p_C(\ell)$) to zero. When there is a large excess of inert gas a simplification similar to that used to obtain equation 32 is possible.

Thus, if p_B, $p_C \ll P_T$ then ξ_B and $\xi_C \ll 1$ and equations 52 and 53 become:

$$p_B = p_B(\ell) + \xi'_B \qquad \ldots\ldots 58$$

$$p_C = p_C(\ell) + \frac{1}{m}\xi'_C \qquad \ldots\ldots 59$$

where $\xi'_i = \frac{RT\ell}{D_i c} \cdot \frac{\dot{W}}{M}$. Taking the diffusion constants to be equal, and letting

$$k_f A \cdot \frac{RT\ell}{Dc} = \xi_E \qquad \ldots\ldots 60$$

equation 54 may be written:

$$\xi' = \xi_E \left[p_B(\ell) + \xi\right]^x \left[p_C(\ell) + \frac{\xi}{m}\right]^y \left[1 - \frac{\left[p_B(\ell) + \xi\right]\left[p_C(\ell) + \frac{\xi}{m}\right]}{K^o}\right]^{\frac{1}{m}} \qquad \ldots\ldots 61$$

Even in this simplified form, the overall rate equation is very complex. Nevertheless it is clear that careful measurement of

the rate of weight loss as a function of external gas pressures would enable the various kinetic parameters to be determined. As with the simple sublimation system, the modified entrainment method is a much more flexible technique than the Knudsen cell and allows more detailed kinetic investigations to be carried out. As well as studying the effects of the reactants on overall rate, catalytic effects may be investigated.

2.3 Chemical Vapour Transport

No new concepts are introduced when considering chemical vapour transport. However, the requirement of a vapour phase transporting agent means that the modified entrainment method is the only gravimetric technique which may be used with these systems. Although results from open flow entrainment experiments have been reported [31,32] the failure to uncouple the surface kinetic and transport processes limits their usefulness.

In this section a general, though approximate, form of the weight loss equation is derived [33] which may be used to interpret results from an MEM experiment. A transporting equation may be written

$$M + aA + bB + ... \rightleftharpoons qQ + rR + ... \qquad ..... 62$$

where M is the solid compound and all other species are gaseous. Simple and dissociative sublimation are then special cases of equation 62. For each species i, the equation for transport through the channel in the MEM bottle is

$$\frac{p_i(o)}{P} - \frac{\nu_i}{N} = \left[\frac{p_i(\ell)}{P} - \frac{\nu_i}{N}\right] e^{-\xi_i} \qquad ..... 63$$

where $p_i(o)$ and $p_i(\ell)$ are the pressures of i inside the bottle and at the channel outlet respectively, ν_i is the stoichiometric coefficient of species i and $N = \Sigma\nu_i$. The transport function of species i is defined by:

$$\xi_i = \frac{RT\ell N}{D_i P_c} J = \frac{RT\ell N\dot{W}}{D_i P_c M} \qquad ..... 64$$

[cf. equations 26, 52 and 53]

When the partial pressures of the reactant species are small so that $\xi_i << 1$ equation 63 may be simplified in the same way as 52 and 53:

$$\frac{p_i(o)}{P} = \frac{\nu_i}{N}\xi_i + \varepsilon_i \qquad \ldots\ldots 65$$

where $\varepsilon_i = p_i(\ell)/P$

This situation is found in many practical systems.

In order to obtain a simple weight loss expression it is convenient to divide the gas species into three groups:

1. all reactants

2. all products which are not included in the external gas-stream (for which $\varepsilon_i = 0$)

3. all other products.

For species in group 2, let $\nu_i = N'$. If the reaction is not extreme, so that $\xi << \varepsilon_i$ for all non zero ε_i then the products K^* or K^o may be written

$$K = \prod_i p_i^{\nu_i} = p^N \prod_i \left\{ \frac{\nu_i}{N}\xi + \varepsilon_i \right\}^{\nu_i}$$

and

$$\frac{K}{p^N} = \prod_1 \varepsilon_i^{\nu_i} \prod_2 \left\{ \frac{\nu_i}{N}\xi \right\}^{\nu_i} \prod_3 \varepsilon_i^{\nu_i} \qquad \ldots\ldots 66$$

where the product is split into the three groups described above. Equation 66 may then be rearranged to give:

$$\frac{K}{p^N} = (\xi)^{N'} \left(\prod_{1,3} \varepsilon_i^{\nu_i} \right) \left(\prod_2 \left\{ \frac{\nu_i}{N} \right\}^{\nu_i} \right) \qquad \ldots\ldots 67$$

The third term is a number; the second contains the dependence on the feed components and the first is the dependence of ξ or W. Equation 67 may be more simply written as

$$K = p^{N} \xi^{N'} a(\epsilon_i) \qquad \ldots\ldots 68$$

To obtain an expression for the rate of weight loss, equation 39 is used:

$$\frac{\dot{W}}{M} = J_f [1 - K^*/K^o] \qquad \ldots\ldots 39$$

Although this equation was originally obtained for a dissociative sublimation system, the derivation may easily be extended to any transport system [23].

Equations 68 may be used to substitute for both K^* and K^o:

$$\dot{W} = \dot{W}_f \left[1 - \left(\frac{\dot{W}}{\dot{W}^o} \right)^{N'} \right] \qquad \ldots\ldots 69$$

where $\dot{W}_f = MJ_f$ and $\dot{W}^o$ is the rate of weight loss expected if equilibrium obtains in the bottle.

The advantage of equation 69 is that by changing the size of the channel in the bottle both $\dot{W}$ and $\dot{W}^o$ may be found. It is therefore possible to determine the forward current (J_f) without having use thermodynamic data to estimate the equilibrium constant K^o. A major source of error is thus eliminated. The procedure is discussed in more detail in chapter 4.

2.4 Appendix: Calculation of Channel Resistance

In the gas transport equations there is a term which represents the resistance of the channel to transport. For cylindrical channels this term is ℓ/c where ℓ is the length and c the cross-sectional area. However, the general equation for this resistance term:-

$$\int_0^{\ell} \frac{dx}{A(x)}$$

where A(x) is the area of the channel at the point x along the channel axis.

The resistance can now be calculated for two types of non-cylindrical channel of particular interest: conical channels, and channels which form part of a sphere (found in the main body of the bottle).

i. Conical Channels

For a conical channel $A(x) = \Pi\, r(x)$

Let $r = r(\ell)$

and $R = r(0)$

Then $r(x) = r + \frac{(R-r)}{\ell} x$

and the resistance is given by

$$\int_0^{\ell} \frac{dx}{\Pi\left[r + \frac{(R-r)}{\ell} x\right]^2} = \frac{\ell^2}{\Pi} \int_0^{\ell} \frac{dx}{\left[r\ell + (R-r)x\right]^2}$$

$$\therefore \quad \text{resistance} = \frac{\ell^2}{\Pi} \left[\frac{-1}{(R-r)\left[r\ell + (R-r)x\right]} \right]_0^{\ell}$$

$$= \frac{\ell^2}{\Pi} \left[\frac{1}{(R-r)r\ell} - \frac{1}{(R-r)R\ell} \right]$$

$$= \frac{\ell^2}{\Pi}\left[\frac{(R-r)\ell}{(R-r)rR\ell^2}\right]$$

$$= \underline{\underline{\frac{\ell}{\Pi rR}}}$$

FOR SPHERICAL CHANNELS

Assuming that at x = 0 the radius is that of the sphere ie if R = radius of sphere then

$$r(o) = R$$

Then $r^2(x) = R^2 - x^2$

and $A(x) = \Pi[R^2 - x^2]$

$$\text{Resistance} = \frac{1}{\Pi}\int_o^{\ell} \frac{dx}{R^2 - x^2}$$

$$= \frac{1}{2\Pi R}\left[\ell n \frac{R + x}{R - x}\right]_o^{\ell}$$

$$= \underline{\underline{\frac{1}{2\Pi R}\left[\ell n \frac{R + \ell}{R - \ell}\right]}}$$

REFERENCES

1 Hertz H : Ann. Phys. Chem, Neue Folge 17, 177 (1982).

2 Knudsen M : Ann. Phys. 47, 697 (1915).

3 Langmuir I : Physik Z. 14, 1273 (1913).

4 G M Pound : J. Phys. Chem. Ref. Data 1, 135 (1972).

5 Brewer L, Kane J S : J. Phys. Chem, 59, 105 (1955).

6 Foxon C T, Joyce B A, Furrow R F C, Griffiths R M : J. Phys. D : Appl. Phys. 7, 2436 (1974).

7 Knudsen M : Ann. Phys. 29, 179 (1909).

8 Clausing P : Z. Phys. 66, 471 (1930).

9 Clausing P : Ann. Phys. 12, 961 (1932).

10 Seary A W, Freeman R D : J. Chem. Phys. 22, 762 (1954).

11 Kennard E H : Kinetic Theory of Gases, McGraw-Hill, New York (1938).

12 Murray J J, Pupp C, Pottie R F : J. Chem. Phys. 58, 2569 (1973).

13 Macur G J, Edwards R E, Wahlbeck P G : J. Phys. Chem. 70, 2956 (1966).

14 Carlsen K D, Gilles P W, Thorn R J : J. Chem. Phys. 38, 2725 (1963).

15 Knudsen M : Ann. Phys. 28, 999 (1909).

16 Paule R C, Margrave J L : in 'The Characterization of High Temperature Vapours' Ed. J L Margrave, John Wiley & Sons, New York (1967).

17 Kubaschewski O, Alcock C B : 'Metallurgical Thermochemistry' 5th Edition, Pergamon, Oxford (1979).

18 Bishop M E, Libson S H : J. Appl. Phys. 5, 24 (1954).

19 Goldfinger P, Jeunehomme M : Trans. Faraday Soc. 59, 2851 (1963).

20 Caveney R J : J. Cryst. Growth 7, 102 (1970).

21 Somorjai G A : in 'Condensation and Evaporation of Solids' Eds. P Goldfinger, J P Hirth, Gordon and Breach, New York (1964).

22 Somorjai G A : Surface Science 2, 298 (1964).

23 Faktor M M, Garrett I : 'Growth of Crystals from the Vapour', Chapman and Hall, London, (1974).

24 Faktor M M, Garrett I : J. Cryst. Growth 9, 3 (1971).

25 Gingerich K A, Cocke D L, Kordis J : J. Phys. Chem. 78, 603 (1974).

26 Farrow R F C : J. Phys. D : Appl. Phys. 7, 2436 (1974).

27 Faktor M M, Garrett I, Heckingbottom R : J. Chem. Soc (A), 2657 (1970).

28 Faktor M M, Heckingbottom R, Garrett I : J. Chem. Soc (A), 1, (1971).

29 B de Largy : Private Communication.

30 Schafer H :"Chemical Transport Reactions" Academic Press (1964).

31 Shaw D W : J. Electrochem. Soc. 115, 405 (1968).

32 Mizuno O, Watanabe H : J. Crys. Growth 30, 240 (1975).

33 Faktor M M, Garrett I, Lyons M H : J. Cryst. Growth 46, 21 (1979).

CHAPTER 3: THE SUBLIMATION OF RED PHOSPHORUS

The vapourisation of red phosphorus was undertaken as a means of demonstrating some of the concepts discussed in the previous chapter. Although the substance was known to have a highly hindered vapourisation reaction, detailed information was scarce. Figures of 10^{-7} [1] or 10^{-6} [2,3] have been reported, but the temperature of the measurements were not given. Veprek [4] measured the rate of loss of red phosphorus in a vacuum and by comparing with literature data [5] obtained vapourisation coefficients of 3×10^{-8} and 1×10^{-7} at 300°C and 400°C respectively corresponding to an activation energy of 26 kcal mol^{-1}. Elsewhere [6], Veprek quotes a vapourisation energy of 52 kcal mol^{-1} which, using the equilibrium data in reference 5, gives an activation energy of 21 kcal mol^{-1}. The very low vapourisation coefficient of red phosphorus (which contrasts strongly with the value of approximately one found for white phosphorus [3]) is associated with changes in the bonding of phosphorus atoms during evaporation [3,6]. Brewer and Kane showed that the evaporation rate could be increased by the addition of a non-volatile and chemically inert liquid, such as thallium or lead [2]. A similar increase in evaporation rate was observed by Schafer and Trenkel [7] when iodine was added to red phosphorus in a sealed capsule.

These workers showed that the iodine did not react chemically with red phosphorus at the experimental temperatures (350-400°C), but acted as a catalyst on the vapourisation. It was hoped to study the catalytic effect of iodine using the modified entrainment method.

An additional reason for studying the sublimation of red phosphorus was the possibility that red phosphorus might be used as a source of phosphorus

vapour in vapour phase growth systems for the compound semiconductors InP and (Ga,In)(As,P).

3.1 Theory

The theory outlined in chapter 2 only considered explicitly the situation at a constant temperature. Modified entrainment experiments are carried out over a range of temperatures and in this section the variation of rate of weight loss with temperature is discussed. In order to simplify the argument it is assumed that the pressure of phosphorus vapour in the bottle is much less than the total pressure, so that the rate of weight loss is given by

$$p^* = P\xi = \frac{RT\ell}{Dc} \cdot \frac{\dot{W}^*}{M} \qquad \ldots\ldots 1$$

$$\therefore \quad \frac{\dot{W}^*}{M} = p^* \frac{Dc}{RT\ell} \qquad \ldots\ldots 2$$

The rate of weight loss for simple sublimation is given by

$$\frac{\dot{W}^*}{M} = k_r A \, (p^o - p^*) \qquad \ldots\ldots 3$$

Combining equations 1 and 3 gives

$$\frac{\dot{W}^*}{M} = \frac{p^o}{\frac{1}{k_r A} + \frac{RT\ell}{Dc}} \qquad \ldots\ldots 4$$

Two extreme cases can be considered.

1. $\frac{RT\ell}{Dc} >> \frac{1}{k_r A}$

   Here the resistance to transport through the channel is very high and inside the bottle the system is close to equilibrium. Equation 4 simplifies to

$$\frac{\dot{W}^o}{M} = \frac{Dc}{RT\ell} p^o \qquad \ldots\ldots 5$$

where $\dot{W}$ is the rate of weight loss expected for an equilibrium system. This is the situation which is assumed to exist when thermodynamic investigations are carried out by MEM. A plot of the logarithm of the rate of weight loss as a function of reciprocal temperature will be a straight line with a slope of $-\frac{\Delta H_s}{R}$ where ΔH_s is the enthalpy of sublimation.

2. $\frac{1}{k_r A} >> \frac{RT\ell}{Dc}$

In this region the rate of weight loss is dominated by the surface reaction kinetics. Equation 4 becomes

$$\frac{\dot{W}^*}{M} = k_r A\, p^o = k_f A \qquad \ldots\ldots 6$$

To see the effect of temperature in this region it is assumed that k_f follows an Arrhenious rate law, so that

$$k_f = B \exp(-E_f/RT) \qquad \ldots\ldots 7$$

where B is a constant and E_f is the activation energy of the sublimation reaction. It can be shown that

$$E_r = E + \Delta H_s \qquad \ldots\ldots 8$$

where E is the activation energy of condensation.

Clearly, when the weight loss is controlled by surface kinetics, a plot of ℓn W as a function of reciprocal temperature will again be a straight line. This slope of this line will be $-(E + \Delta H_s)/R$. Consideration of equations 6, 7 and 8 show that the surface kinetic region will be found at low temperatures.

In Fig 1 a schematic plot of the results for a simple sublimation system is shown. The transport and kinetic limited regions are clearly seen. To analyse results from the intermediate region the full equation (equation 4) must be used.

Fig 3-1

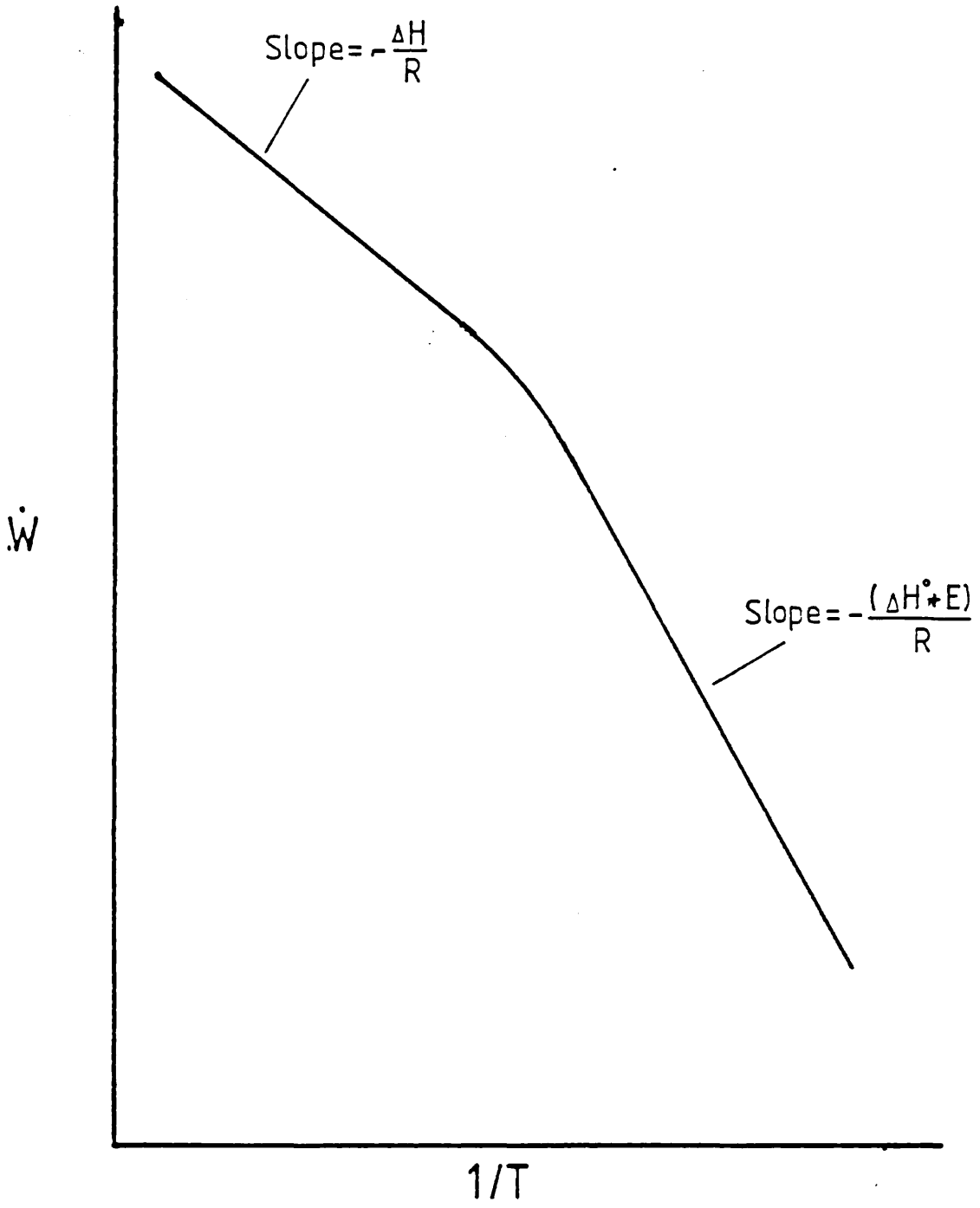

Schematic MEM Plot for Simple Sublimation System showing kinetic-limited region

3.2 Materials

Red phosphorus was obtained from MCP Electronics Ltd with a nominal 6N purity. Two different forms were supplied, known simply as Form I and Form II. These were prepared by heating white phosphorus for two to three days at 270°C and 480°C respectively. Densities, sublimation temperatures and heats were all quoted with slightly different values. Although the various crystalline forms of red phosphorus have been studied extensively [8,9], the resultant literature is confusing. Samples of red phosphorus are contaminated by varying amounts of the amorphous form giving different physical properties. This was demonstrated by Bachmann and Buehler [10] who studied the vapour pressures of commercial samples of red phosphorus using a static method. A wide range of values were obtained at temperatures below 430°C. These workers obtained a pure monoclinic form of red P by prolonged heating at 575°C.

The heat capacities of the various forms of phosphorus were studied by Stephenson et al [9] who identified two reproducible crystalline forms of red phosphorus. These forms were labelled IV and V. Type V corresponds to Bachmann and Buehler's pure monoclinic form. Type IV was prepared at slightly lower temperatures and corresponds to the Form II red phosphorus supplied by MCP. The form I material supplied was contaminated with amorphous phosphorus which tends to form at lower temperatures. The presence of this amorphous material would lead to irreproducible results. Consequently, most of the experimental work was carried out with the crystalline form II material.

Iodine was resublimed analar grade, supplied by BDH.

The experiments were carried out in a nitrogen atmosphere. Nitrogen was supplied from a BOC "white spot" grade cylinder and dried by passing through 4Å molecular sieves.

3.3 Experimental

In order to remove any oxide film on the surface of the phosphorus, the material was cleaned by refluxing in aqueous NaOH. The MEM bottle was loaded under nitrogen. However, some oxide formation was possible during the short period of time the bottle was exposed to the atmosphere whilst setting up the apparatus.

Two bottles were used for experiments. Initial work used a small bottle with a capacity of about 2 cm^3 (~1g of red phosphorus). Later experiments involved a much larger bottle containing approximately 8g of phosphorus. The reasons for the larger bottle are discussed below. In both cases the channel was nominally 1 mm diameter (ℓ = 2.55 cm, c = 1.033×10^{-2} cm^2). The large bottle had a total length of 10 cms including the channel (see fig 2). This meant there was a large temperature gradient across the sample. The bottle was carefully positioned to give the smallest gradient compatible with the condition that the capillary should have a temperature equal to, or greater than the hottest part of the solid (thus preventing blockage of the channel by condensed phosphorus vapour). However there was still a large temperature difference between the top and bottom of the sample (23° when the temperature controller was set to $420^\circ C$).

Rates of weight loss were studied in the temperature range $350^\circ C$-$420^\circ C$ ($470^\circ C$ with the small sample bottle). The temperature inside the furnace tube was measured with a thermocouple positioned immediately below the sample bottle. Because the observed rate was an aggregate over the whole sample, which covered a temperature range of over $20^\circ C$, it was not clear how the results could be interpreted.

Fig 3-2

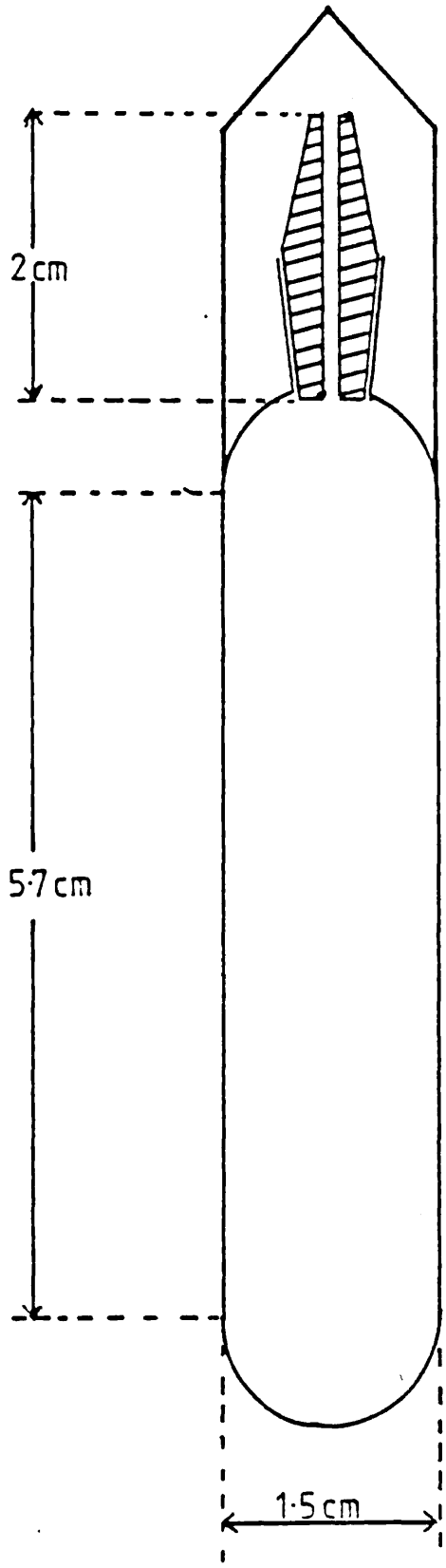

Sample Bottle for Red Phosphorus Experiments.

A simple mathematical model of the system is described in the appendix. This suggested that by plotting the logarithm of the rate of weight loss as a function of the reciprocal temperature of a particular point in the sample, a reasonable estimate of activation energy could be made. The most accurate results would be obtained by choosing the mid-point of the temperature range. However, little error was introduced in the activation energy by plotting against the lowest temperature of the sample - which was measured directly by the thermocouple. Consequently, this temperature was used in the compilation of the results table (table 2) and in fig 3.

Iodine was introduced by passing the gas through a U-tube filled with solid iodine. The U-tube was placed in a temperature controlled oil-bath. The iodine pressure was estimated from data given by Nesmeyanov [11].

3.4 Results and Discussion

3.4.1 Qualitative Experiments

Initial experiments were carried out with a small bottle containing approximately 1g of sample. Attempts to obtain quantitative information were unsuccessful. At any given temperature the observed rate of weight loss was found to decrease with time, thus making it impossible to obtain reproducible plots of rate of weight loss as a function of temperature. As a consequence, the experiments with the small bottle were restricted to a qualitative study of the effect of iodine on the vapourisation reaction. Consecutive experiments were carried out in which was studied the effect of introducing iodine (at constant pressure but decreasing sample temperatures). Upon introducing iodine into the system, the rate of weight loss increased slowly, but appeared eventually to reach a constant value. At a nominal sample temperature of 470^{o}C this effect was minimal, but as the sample temperature was decreased the influence of iodine became more pronounced. The change in rate of weight loss was shown to be due to the presence of iodine by examining the effect of closing the iodine line. At each temperature studied the rate of weight loss decreased, although the change was slower than that observed when iodine entered the system.

A second set of experiments was carried out at a constant nominal sample temperature of 430^{o}C. The effects of increasing concentrations of iodine were studied. Iodine pressure was increased by changing the temperature of the iodine source. On allowing iodine to enter the system, the rate was seen to increase. Eventually the rate of weight loss appeared to reach

a constant value. This could be compared with the rate in the absence of iodine, which was measured after each iodine experiment. The results for consecutive runs are shown in table 1.

Two points emerged from these experiments.

1. The rate of weight loss in the absence of iodine increased after each exposure to iodine. This trend was the exact opposite of the normally observed decrease of rate with time.

2. The maximum rate of weight loss increased with iodine pressure.

Both observations are consistent with a mechanism in which the catalytic effect of iodine on phosphorus vapourisation is the result of adsorption of iodine onto the phosphorus surface. The amount of phosphorus adsorbed will be proportional to the pressure of iodine. With the iodine source closed, the adsorbed iodine is lost slowly from the surface giving rise to the observed decay in rate. The apparent increase in the iodine-absent rate may simply indicate that the system was not left long enough for all the iodine to be desorbed.

The qualitative experiments demonstrated clearly the catalytic effect of iodine vapour on the sublimation of red phosphorus, particularly at lower temperatures. The effect appeared to be related to the pressure of iodine in the system.

TABLE 3.1

Run	Temp (^{o}C)	Iodine Temp (^{o}C)	Rate of Wt Loss ($x10^{9}$ kg s^{-1})
1	450	-	2.78
2	450	59.5	3.74
3	450	-	3.56
4	430	-	1.07
5	430	59.5	2.13
6	430	-	1.49
7	430	79	3.10
8	430	-	1.80
9	430	98.5	3.97
10	430	-	1.96

Successive experiments showing effect of Iodine on the sublimation rate of red phosphorus.

3.4.2 Quantitative Experiments

To obtain reproducible qualitative information it was necessary to eliminate the steady decrease in weight loss rate with time. Several explanations were possible, mainly related to the surface of the sample. These were:

i. the amount of material lost from the sample bottle during the experiments represented a significant fraction of the initial sample. The effect on surface area, and hence on rate is obvious.

ii. Regrowth could occur within the bottle with larger particles growing at the expense of the smallest particles. Since the surface to volume ratio decreases with increasing particle size there would again be an overall loss of surface area.

iii. A third explanation was not based on changes of surface area, but on changes in reactivity. A crushed, polycrystalline sample had many different faces exposed; some of which were more reactive than others. Over a period of time the more reactive faces would decrease in area and eventually disappear, thus leading to a decrease in sublimation rate. A similar argument could be applied to surface defects [2].

In order to overcome the first problem the sample bottle was redesigned to hold large amounts of material (~8-10g). This ensured that the material lost during a normal set of experiments (a few hundred milligrams at most) would not significantly alter the surface area. The sample was also crushed less finely than

in the initial experiments so that changes in surface area due to regrowth would be of less significance.

Initial experiments were aimed at finding out whether a steady change in rate of weight loss could be observed. For this purpose the furnace was heated to 420°C and the system left overnight. The weight was plotted on a 10mg range. Although slight variations in rate of weight loss were observed, there was no general trend. The steady decrease in rate which had bedevilled earlier experiments had clearly been eliminated. Rates were usually measured using the 10mg range of the balance. This was because the measurements made using the 1mg scale were more sensitive to fluctuations in rate.

Figure 3 shows the logarithm of rate of weight loss as a function of reciprocal temperature. It can be seen that the rate is very dependent on temperature. The slope of the plot indicated an activation energy of 52 kcal mol^{-1} for the sublimation reaction - a value also given by Veprek [6]. The sublimation energy of the sample (given by the suppliers) is 25 kcal mol^{-1}, giving a barrier to sublimation of 27 kcal.

The strong dependence of rate on temperature explains changes in rate observed when the furnace setting was 380°C. Initially, the rate was 1.06×10^{-9} kg S^{-1}. Measurements were made using the 1mg range of the balance, and the rate was found to decrease with time to a constant value of 8.7×10^{-10} kg S^{-1}. Although this represents a change of almost 20% in the rate, examination of figure 3 shows that this change is equivalent to an error of

Fig 3-3

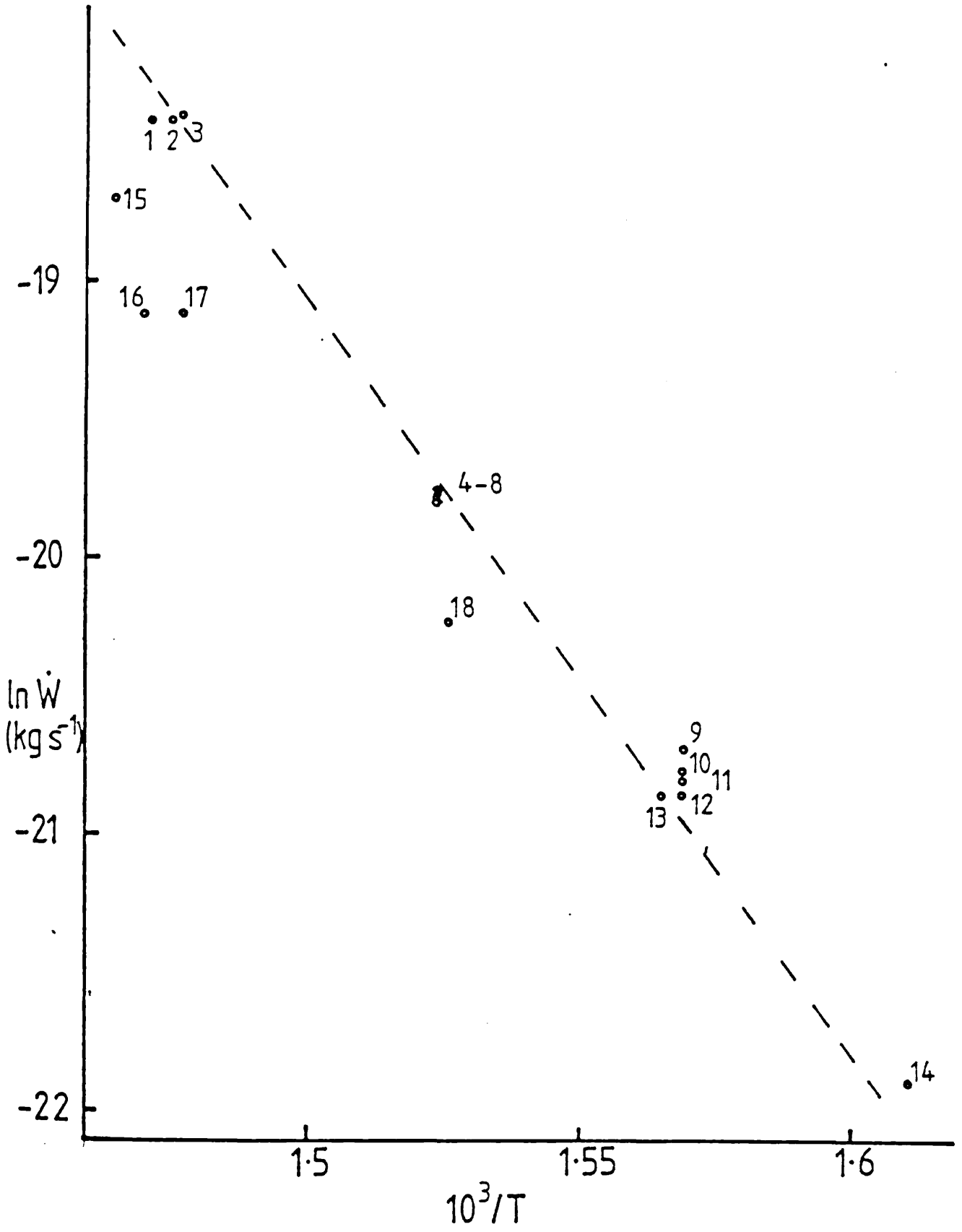

Experimental Results

Points are numbered in chronological order

TABLE 3.2

Run No	Furnace Setting	Temp (K)	$W(kg\ s^{-1})x10^{9}$
1	420	679.5	10.04
2	420	677.7	10.04
3	420	677.6	10.22
4	400	656.1	2.616
5	400	656.1	2.611
6	400	656.0	2.56
7	400	656.0	2.59
8	400	656.0	2.53
9	380	637.4	1.055
10	380	637.5	0.958
11	380	637.5	0.916
12	380	637.5	0.877
13	380	639.0	0.868
14	360	621.0	0.306
15	420	682.3	7.64
16	420	679.7	4.99
17	420	676.7	4.99
18	380	655.4	1.645

Experimental results for sublimation of red phosphorus

only 2°C in temperature. The results indicate that insufficient time was allowed for the sample to come to equilibrium before making the measurements.

An attempt was made to test the reproducibility of the results by measuring rates in order of decreasing temperature and then going back to the highest temperature. Only one point was obtained on returning to the highest temperature, and this had a value approximately 25% lower than the original results. Before any more measurements could be made the wires of the controlling thermocouple short-circuited leading to massive overheating of the furnace. Over 2g of material were lost and subsequent rate measurements were found to be less than half the original values. This reflects both the smaller surface area of the depleted sample, and the lower average temperature. Similar factors may have been the reason for the 25% change in rate described above. However, a firm conclusion cannot be made on the evidence of one point.

The work was continued by B de Largy and N Kell of Royal Holloway College. Their results are shown in Fig 4, for two experiments. The points shown as circles are for the sublimation of phosphorus in the absence of iodine, the numbers indicating the order in which the points were measured. The slope of this line is 49 kcal mol^{-1} (a barrier to sublimation of 24 kcal mol^{-1}), giving reasonable agreement with the value of 52 kcal mol^{-1} found in the work described above. The points marked as triangles were obtained in the presence of 5 mm of Iodine vapour. At temperatures above ~395°C, the plots (with and

Fig 3-4

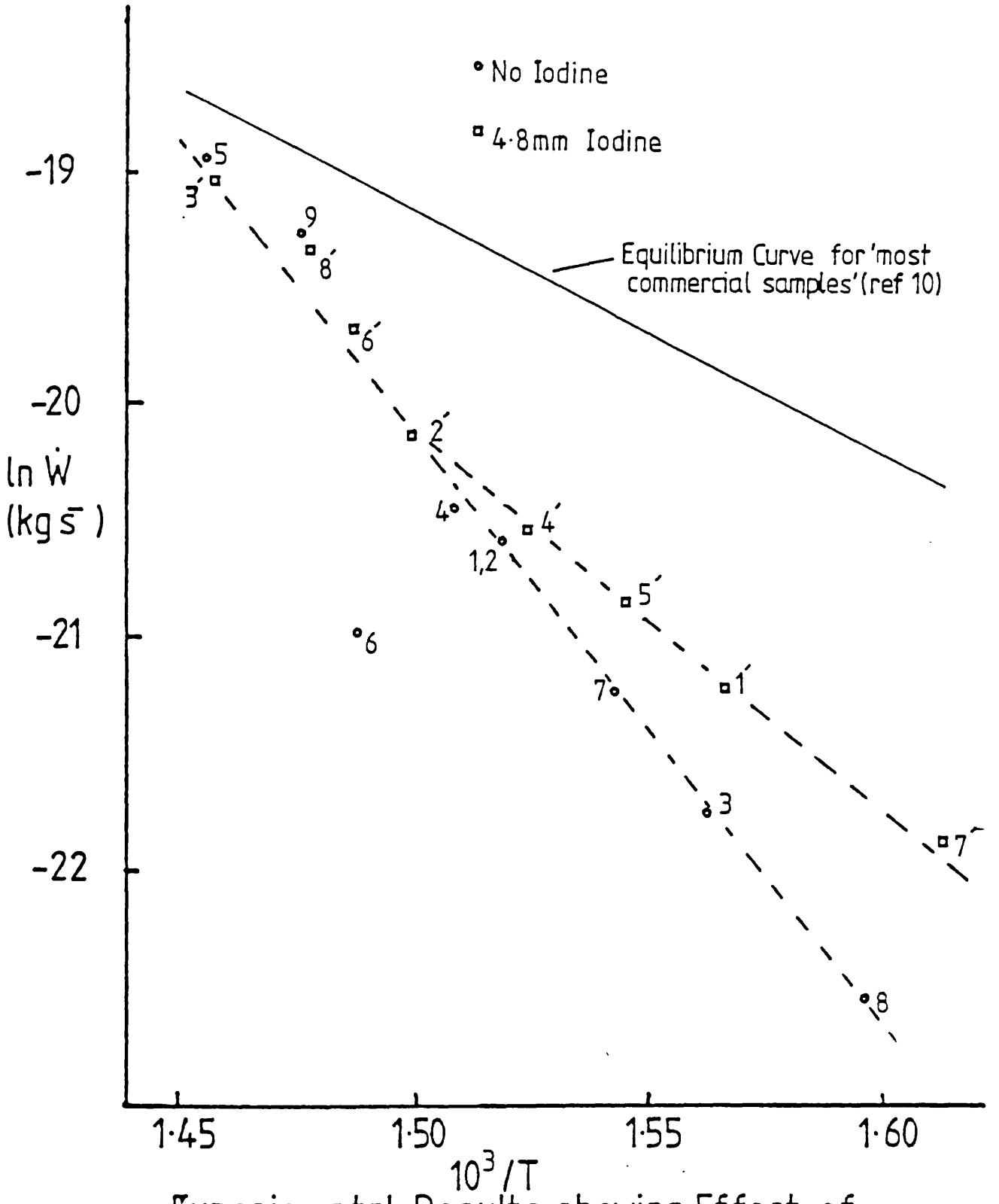

Experimental Results showing Effect of Iodine on Red Phosphorus Sublimation

without iodine) merge, but at temperatures below 395°C, the rate of weight loss is higher in the presence of iodine. The slope of this lower portion is equivalent to an energy of 35 kcal mol^{-1}. It is clear that the catalytic action of iodine is due to a reduction of about 15 kcal mol^{-1} in the activation energy for sublimation.

Also plotted in Fig 4 is the equilibrium line for "most commercial samples". At high temperatures the experimental points approach this line and some curvature in the experimental lines are apparent. At higher temperatures the experimental points would be expected to merge with the equilibrium line, as shown schematically in fig 1.

3.5 Conclusion

The value of the modified entrainment method in kinetic investigations was clearly demonstrated. The barrier to the sublimation of red phosphorus was shown to be about 25 kcal mol^{-1}, agreeing well with the value of 26 kcal mol^{-1} obtained by Veprek [4]. The catalytic effect of iodine on red phosphorus sublimation was shown to be due to a reduction in the activation energy. In the presence of 5 mm of iodine vapour, the energy barrier to sublimation was lowered to about 10 kcal mol^{-1}.

Plainly much work remains to be done. In particular, the way in which the sublimation rate depends on iodine pressure needs to be investigated further. The early experiments showed the rate to increase with increasing iodine pressure, but this effect needs to be quantified.

3.6 Appendix

The presence of a temperature gradient across the sample will obviously perturb the results. In order to see how important this perturbation is, a simple model was set up. It is assumed that the rate of sublimation is described by an Arrhenious law:

$$r = a\, e^{-E/RT} \qquad \ldots\ldots 9$$

where a is a constant which includes the area of the sample. Normally temperature is a continuous function; however for the purposes of calculation we assume the temperature across a sample to rise in discrete steps. By choosing small enough steps the model will approximate to a continuous temperature distribution. At each temperature the rate is given by an equation similar to 1. Thus, the total rate is given by:-

$$\text{rate} = a_1 e^{-E/RT_1} + a_2 e^{-E/RT_2} + a_3 e^{-E/RT_3} \qquad \ldots\ldots 10$$

A further simplification is possible if it is assumed that all the pre-exponential constants are equal. Then, rate is given by

$$\text{rate} = a\,[e^{-E/RT_1} + e^{-E/RT_2} + e^{-E/RT_3} ..] \qquad \ldots\ldots 11$$

This situation will be found if a single crystallographic plane is placed in a linear temperature gradient and is also a good approximation for an evenly distributed powder in a linear temperature gradient.

To see how the presence of a temperature gradient could affect the results of the experiments with phosphorus, equation 3 was calculated for a system in which the difference between the highest and lowest

temperature was 22°C. The activation energy was taken to be 55 kcal mol^{-1} - estimated from the apparent slope of the experimental plots.

The results are listed in table 3. T_L and T_H correspond to temperatures at the bottom and top of the gradient respectively. T_M is the temperature at which the sample would give the same rate as that obtained in the temperature gradient. It can be seen that this is very close to the arithmetic mean of T_L and T_H.

Figure 5 is a graph of ℓn (rate) vs 1/T, the two plots are for (a) ℓn (rate) vs $1/T_H$, and (b) ℓn (rate) vs $1/T_L$. Both plots are approximately linear (some slight curvature is visible in plot b), and both plots give apparent activation energies very close to the true value (55 kcal mol^{-1}). When ℓn (rate) is plotted as a function of $1/T_H$ the apparent activation energy is low (52.44 kcal mol^{-1}) whereas when plotted against $1/T_L$ the apparent activation energy is slightly high (55.82 kcal mol^{-1}).

Two conclusions can be drawn from this study.

i. The existence of a temperature gradient does not prevent the estimation of activation energies from a plot of ℓn (rate) vs 1/T. However, it is not possible to obtain an accurate value for the pre-exponential factor of an Arrhenious type rate law.

ii. In plotting rate as a function of temperature little error is introduced whether the temperature chosen is that at the top of the gradient (T_H) or at the bottom (T_L). The best value temperature seems to be the arithmetic mean.

TABLE 3.3

T_L(K)	T_H(K)	T_M(K)	$\frac{T_L + T_H}{2}$(K)	rate (arbitrary units)
679	701	691.2	690	1.21×10^{-16}
659	681	671.3	670	3.71×10^{-17}
639	661	651.3	650	1.06×10^{-17}
619	641	631.4	630	2.80×10^{-18}

Theoretical rates of weight loss for idealised sample in a temperature gradient.

Fig 3-5

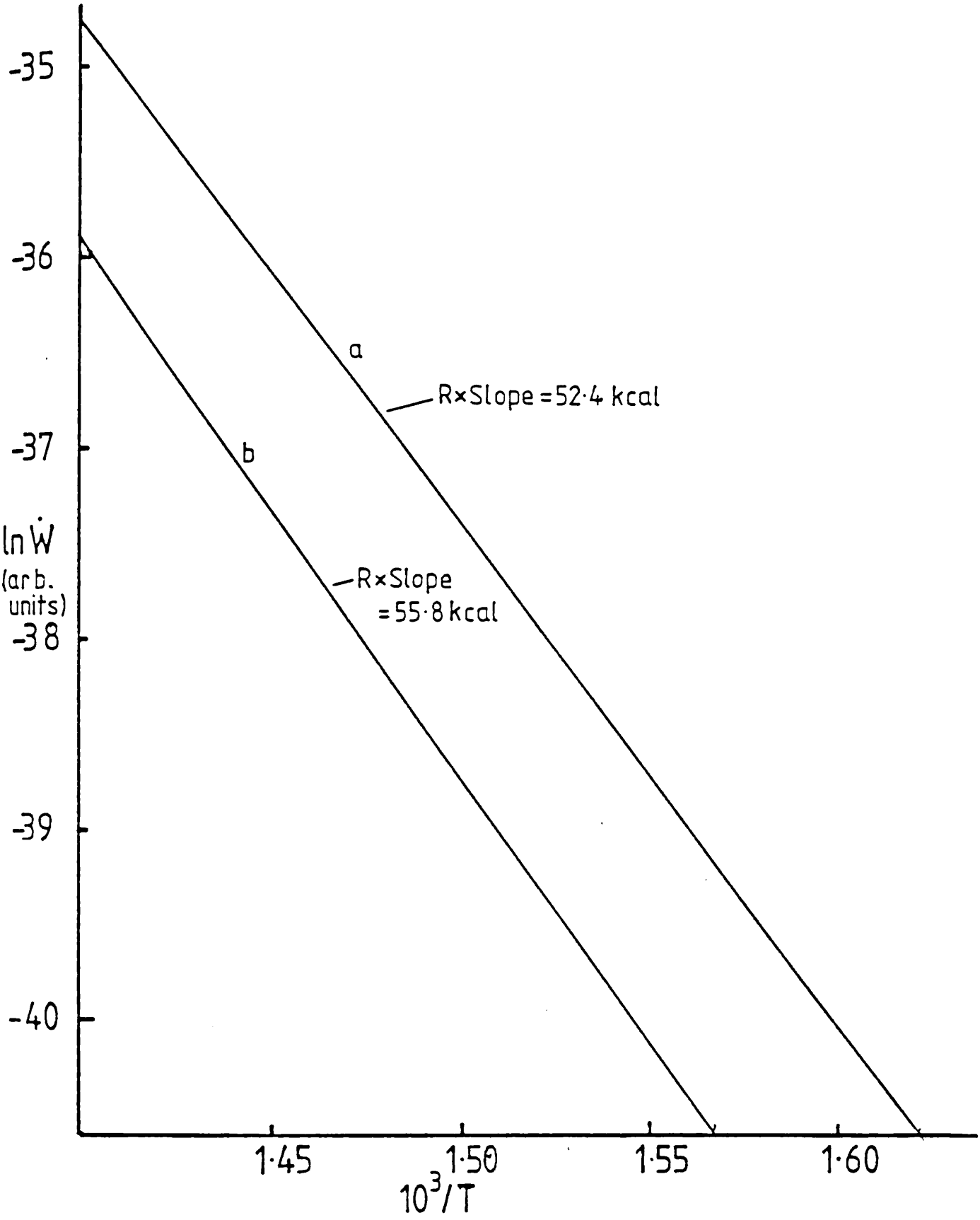

Theoretical Plot of ln(sublimation rate) vs.
a) $1/T_H$ & b) $1/T_L$

It should be noted that these arguments only apply in systems in which no regrowth occurs. If T_L is so far below T_H that at the lowest temperatures deposition of the vapour occurs, then rate can no longer be estimated on the basis of a simple addition such as equation 11.

REFERENCES

1 Melville H W, Gray S C : Trans. Faraday Soc. 32, 1026 (1936).

2 Brewer L, Kane J S : J. Phys. Chem. 59, 105 (1955).

3 Somorjai G A, Lester J E in 'Progress in Solid-State Chemistry' Vol 4, Ed. H Reiss, Pergamon, Oxford.

4 S Veprek : Habilitationsschrift, University of Zurich 1977.

5 JANAF, Thermochemical Tables US NBS 2nd ed NSRDS-NBS 37 (1971).

6 S Veprek : Chap 4 of 'Current Topics in Materials Science' Vol 4, Ed. E Kaldis, North-Holland, Amsterdam 1980.

7 Schafer H, Trenkel M : Z. anorg. allg. Chem 391, 11 (1972).

8 Roth W L, De Witt T W, Smith A J : J. Amer. Chem. Soc. 69, 2881 (1947).

9 Stephenson C C, Potter R L, Maple T G, Morrow J C : J. Chem. Thermodynamics 1, 59 (1969).

10 Bachmann K J, Buehler E : J. Electrochem. Soc. 121, 835 (1974).

11 Nesmeyanov An N : 'Vapour Pressure of the Elements', Infosearch Ltd, London 1963.

CHAPTER 4: THE CHEMICAL VAPOUR TRANSPORT OF GaAs

The III-V compound semiconductors (eg GaAs, InP etc) are of great technological importance because of their use in a wide variety of electronic devices (field effect transistors, photodiodes, lasers, etc) [1,2]. Chemical vapour transport reactions involving the hydrogen halides as the transporting agent have been widely used to produce the epitaxial layers of the III-V compounds which are required for device fabrication [3]. Despite the importance of reactions such as that of HCl with GaAs, the mechanisms are not well understood. In this chapter the work carried out by various workers on the GaAs/HCl reaction is reviewed. This is followed by a discussion of the results of a modified entrainment experiment carried out by Miss E J Tarbox [4] on the GaAs/HBr reaction, which demonstrates the use of MEM to investigate the kinetics of chemical vapour transport reactions.

4.1 Studies on the Kinetics of Vapour Phase Growth of Gallium Arsenide

4.1.1 Introduction

This section surveys the various studies which have been made of the vapour phase growth of GaAs via the reaction

$$GaAs + HCl \rightleftharpoons GaCl + \tfrac{1}{4}As_4 + HCl \qquad \ldots\ldots 1$$

Before embarking on the project the various factors which can influence growth rate, and their inter-relationships are examined. The starting point is the general equation for growth of a solid phase from the vapour [1].

$$J = J^o \left\{ \frac{K^*}{K^o} - 1 \right\} \qquad \ldots\ldots 2$$

In this equation J is the observed growth rate, J^o is the exchange current - a generalised term containing the various kinetic factors, and the term in brackets describes the overpotential driving the reaction. K^o is the equilibrium constant for reaction 1 at the growth temperature, and K^* is the pressure product for the gas-phase immediately above the solid. It can be seen that equation 2 provides a simple means of separating the effect of changing overpotential from that of a change in the exchange current. It is tempting to assume that K^* is the same as the pressure product of the input gases (K_s). In practice, however, $K^* < K_s$ since the system will have a finite resistance to transport of material to the reacting surface. In favourable cases, where the resistance to growth at the surface is much greater than the resistance to transport, the difference between K^* and K_s is negligible and equation 1 may be rewritten as:

$$J = J^{o}\left\{\frac{K_s}{K^{o}} - 1\right\} \qquad \ldots\ldots 3$$

It will be shown that all recorded kinetic investigations have made the assumption that the reaction is surface limited so that $K^{*} = K_s$.

Having discussed the overpotential term, the factors influencing the exchange current J^{o} may be considered.

This may be rewritten in an expanded form

$$J^{o} = k.A.\ f(P_i) \qquad \ldots\ldots 4$$

in which A is the area of the sample and $f(P_i)$ is a function describing the pressure dependence of J^{o}. This may be derived theoretically; alternatively, the experimental results could be fitted to a function of the form

$$f(P_i) = P_{GaCl}^{w}\ P_{As_4}^{x}\ P_{HCl}^{y}\ P_{H_2}^{z} \qquad \ldots\ldots 5$$

where P_i is the pressure of species i, and w, x, y, z are indices, the values of which are chosen to fit the available data. It should be noted that equation 5 gives no indication of the actual mechanism of growth, and that the values of the indices may well change if the range of pressures studied is extended. Nevertheless, the fitting of experimental results to equations of this form is of great importance in checking the validity of theoretical mechanisms.

The term k in equation 4 is a function describing the temperature dependence of J^o, and the effect of substrate orientation. It may be assumed that k is described by an Arrhenious type equation:

$$k = C\, e^{-E/RT} \qquad \ldots\ldots 6$$

where C is a constant, and E is the activation energy. Both C and E depend on the nature of the surface.

To summarize, then, the results of a kinetic investigation of reaction (1), may be interpreted by assuming that J^o has the form

$$J^o = A.C\, e^{-E/RT} \cdot P_{GaCl}^{w} P_{As_4}^{x} P_{HCl}^{y} P_{H_2}^{z} \qquad \ldots\ldots 7$$

Already there are six unknowns to be determined experimentally, and yet even this expression doesn't adequately describe the growth process. Not only may w, x, y, z be slowly varying functions of the pressures, but the 'constants' C and E may themselves depend on the pressures. Furthermore, equation 6 really applies to a single type of surface, with no defects. A real surface will contain defects and have several exposed faces, so that J^o should be denoted by:

$$J^o = a_1 C_1 e^{-E_1/RT} P_{GaCl}^{w_1} P_{As_4}^{x_1} P_{HCl}^{y_1} P_{H_2}^{z_1}$$
$$+ a_2 c_2 e^{-E_2/RT} P_{GaCl}^{w_2} P_{As_4}^{x_2} P_{HCl}^{y_2} P_{H_2}^{z_2}$$
$$+ a_3 C_3 e^{-E_3/RT} P_{GaCl}^{w_3} P_{As_4}^{x_3} P_{HCl}^{y_3} P_{H_2}^{z_3}$$
$$+ \ldots\ldots$$

where $\Sigma a_i = A$ - the total surface area of the sample.

Fortunately, flat, polished slices can be obtained, for which the surface kinetics are dominated by one face only.

The purpose of this discussion has been to show the complex nature of heterogeneous kinetics, and the immense amount of information needed to give a complete account of the growth of a given compound. It is now possible to discuss actual investigations which have been carried out on the growth of GaAs. These investigations fall into three groups:

i. the variation of growth rate with temperature

ii. the variation of growth rate with surface orientation

and iii. the dependence of growth rate on reactant pressures.

Each aspect will be discussed in turn.

4.1.2 The Effect of Temperature on Growth Rate

In early experiments [6,7,8] the effect of decreasing substrate temperature given constant input pressures of the reactants was studied. Before describing the results from these experiments, it is necessary to consider the behaviour to be expected if the growth rate was determined by the rate of transport of the various gas-phase species.

In Chapter 2 it was shown that the rate of transport of a gaseous species was given by the equation

$$\frac{p_i(o)}{P} - \frac{\nu_i}{N}\left[\frac{p_i(\ell)}{P} - \frac{\nu_i}{N}\right] e^{-\xi_i} \qquad \ldots\ldots 8$$

where $p_i(o)$ and $p_i(\ell)$ are the interfacial and bulk pressures respectively of species i, ν_i is the stoichiometric coefficient of species i in the transport equation under consideration and $N = \sum_i \nu_i$. The transport function ξ_i is a measure of the transport rate. In a typical experimental system, the total pressure - P - is 1 atm and, with the exception of hydrogen, the reactant pressures are all << 1. Consequently the transport function is << 1 and it is possible to simplify 8:

$$p_i(o) = p_i(\ell) + \frac{\nu_i}{N} \xi_i \qquad \ldots\ldots 9$$

(NB The definition of ξ_i is such that it has a negative value in a growth system).

Equation 9 applies to any system; but if the rate of reaction is assumed to be controlled by the transport then equilibrium obtains at the surface. Thus, if the transport reaction is

$$GaAs_{(s)} + HCl_{(g)} \rightleftharpoons GaCl_{(g)} + \tfrac{1}{4}As_{4(g)} + \tfrac{1}{2}H_{2(g)} \qquad \ldots\ldots 10$$

then the interfacial pressures of the reactants are given by (see also Chapter 5)

$$p^{(o)}_{GaCl} = p^{(\ell)}_{GaCl} + \frac{4}{3} \xi_{GaCl} \qquad \ldots\ldots 11$$

$$p^{(o)}_{As_4} = p^{(\ell)}_{As_4} + \frac{1}{3} \xi_{As_4} \qquad \ldots\ldots 12$$

$$p^{(o)}_{HCl} = p^{(\ell)}_{HCl} - \frac{4}{3} \xi_{HCl} \qquad \ldots\ldots 13$$

$$p^{(o)}_{H_2} = p^{(\ell)}_{H_2} = 1 \qquad \ldots\ldots 14$$

For simplicity, all the diffusion constants are assumed to be equal, so $\xi_{GaCl} = 4\xi_{As_4} = \xi_{HCl} = \xi$. In the transport limited case, the interfacial pressures must satisfy the equilibrium constant ie

$$K^{o} = \frac{(p_{GaCl} + \frac{4}{3}\xi)(p_{As_4} + \frac{1}{3}\xi)^{\frac{1}{4}}}{(p_{HCl} - \frac{4}{3}\xi)} \qquad \ldots\ldots 15$$

For a given set of input pressures, equation 15 may be solved for any growth temperature providing the thermodynamics of the reaction are known. This is shown for a typical growth system [9] in fig 1 in which growth rate is plotted as a function of deposition temperature using thermodynamic data for the GaAs/HCl reaction [26].

At high temperatures the rate increases with decreasing temperature, reflecting the steady increases in supersaturation. However, as the temperature decreases further the rate eventually reaches a limiting value. This arises when the substrate temperature is such that the corresponding equilibrium constant is very small. Under these conditions the equilibrium pressures of the reactants (GaCl or As_4) became very small compared with the bulk pressures and a further decrease in the equilibrium constant does not alter the amount of GaAs transported to the surface.

Having considered the transport limited system, it is now possible to discuss a system in which surface kinetics are also important. Equations 11 to 14 merely showed a relationship

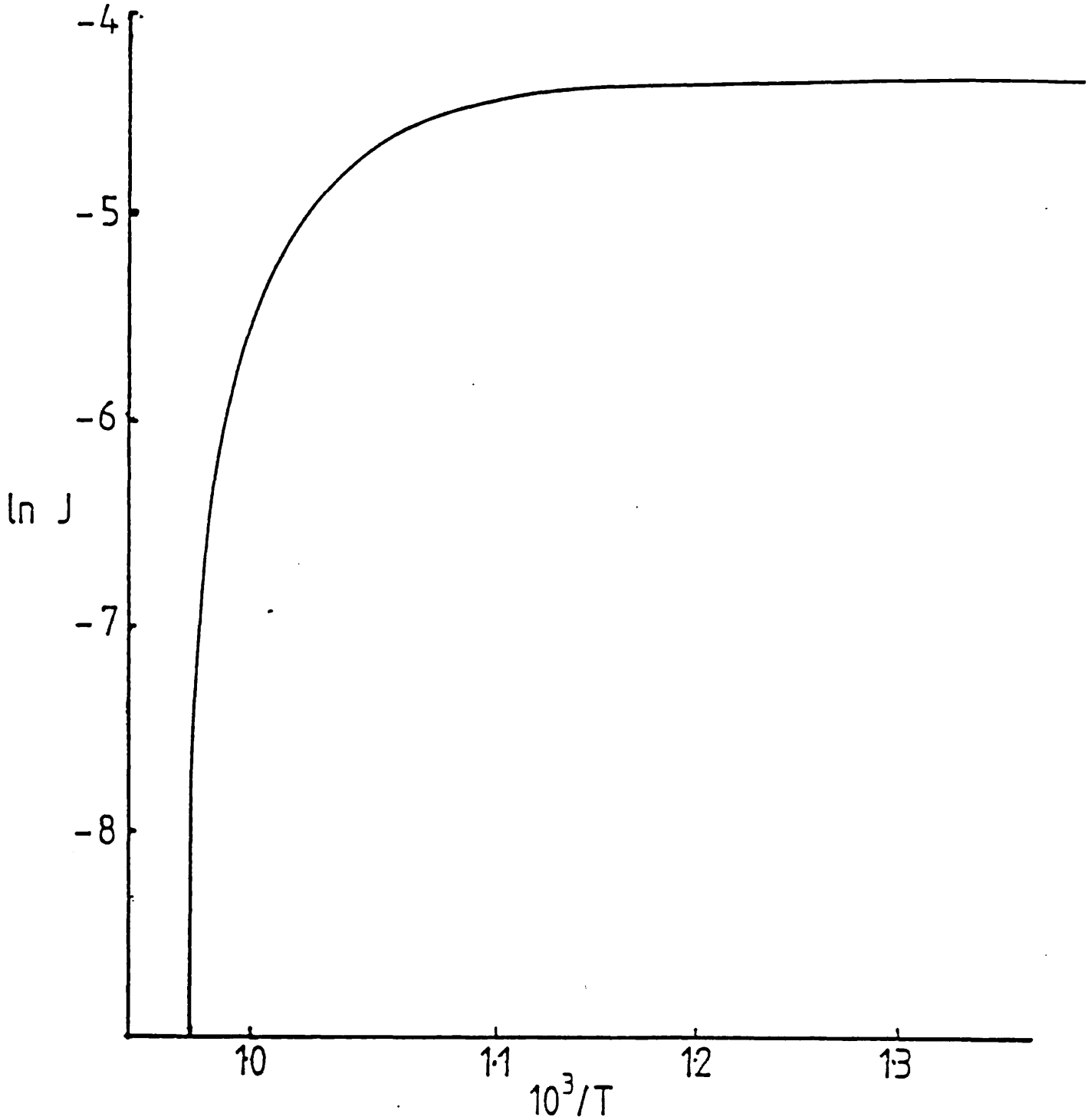

Growth Rate as a function of Growth Temperature

Transport-Limited Case

Calculated for GaAs/HCl: input pressures - $p_{GaCl} = 0{\cdot}0136$, $p_{As_4} = 6{\cdot}26\times10^{-3}$, $p_{HCl} = 0{\cdot}0209$

between transport rate and interfacial and bulk pressures. The equations are valid for any system. To model a system in which surface kinetics are important, the transport equations are substituted in K_s in equation 3:

$$J = J^o \left[\frac{(p_{GaCl} + \frac{4}{3}\xi)(p_{As_4} + \frac{1}{3}\xi)^{\frac{1}{4}}}{K^o (p_{HCl} - \frac{4}{3}\xi)} - 1 \right] \quad \ldots\ldots 16$$

Since $\xi = \frac{3RT\ell}{4D}(-J)$, equation 16 may be written

$$-\xi = \xi^o \left[\frac{(p_{GaCl} + \frac{4}{3}\xi)(p_{As_4} + \frac{1}{3}\xi)^{\frac{1}{4}}}{K^o (p_{HCl} - \frac{4}{3}\xi)} - 1 \right] \quad \ldots\ldots 17$$

Equation 16 is a polynomial in ξ, which may be readily solved using iterative techniques. This calculation was carried out by the author for the GaAs/HCl reaction using an Arrhenius rate expression for J^o:

$$J^o = \alpha \exp(-(E + \Delta H)/RT) \quad \ldots\ldots 18$$

where ΔH is the heat of reaction. Figs 2 and 3 show the results of the calculation. In fig 2 several curves are plotted for different values of the activation energy; in fig 3, it is the pre-exponential factor α which is varied. In both cases the transport limited curves are shown for comparison. All the curves pass through a maximum and at the highest temperatures merge with the transport limited curve. As the temperature is decreased, the surface kinetics become more important and the

Fig 4-2

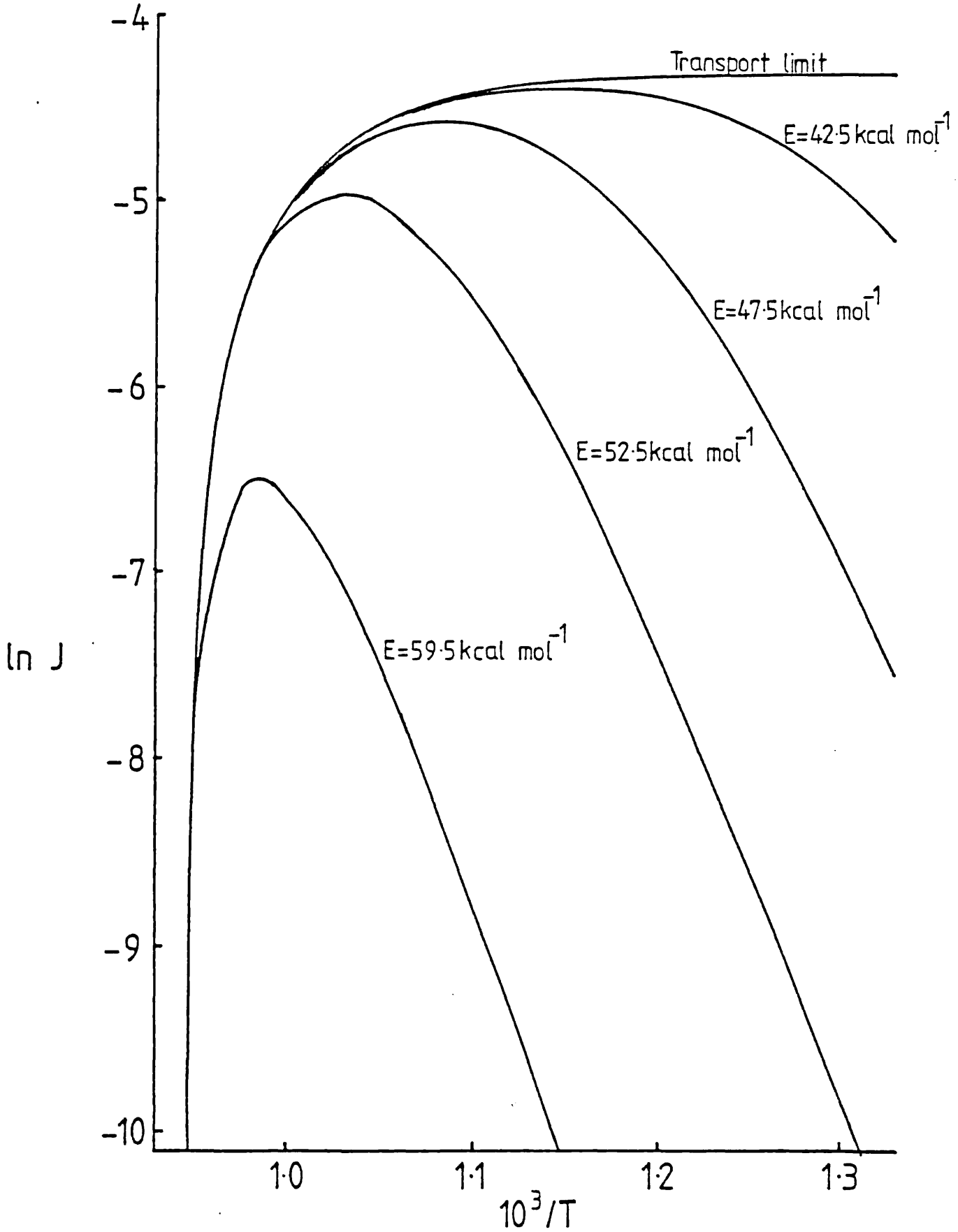

Growth rate vs. reciprocal temperature

Curves plotted for four activation energies. Pre-exponential factor (α) = $4{\cdot}75 \times 10^{13}$ mol s^{-1}. Calculated for same conditions as fig 4-1

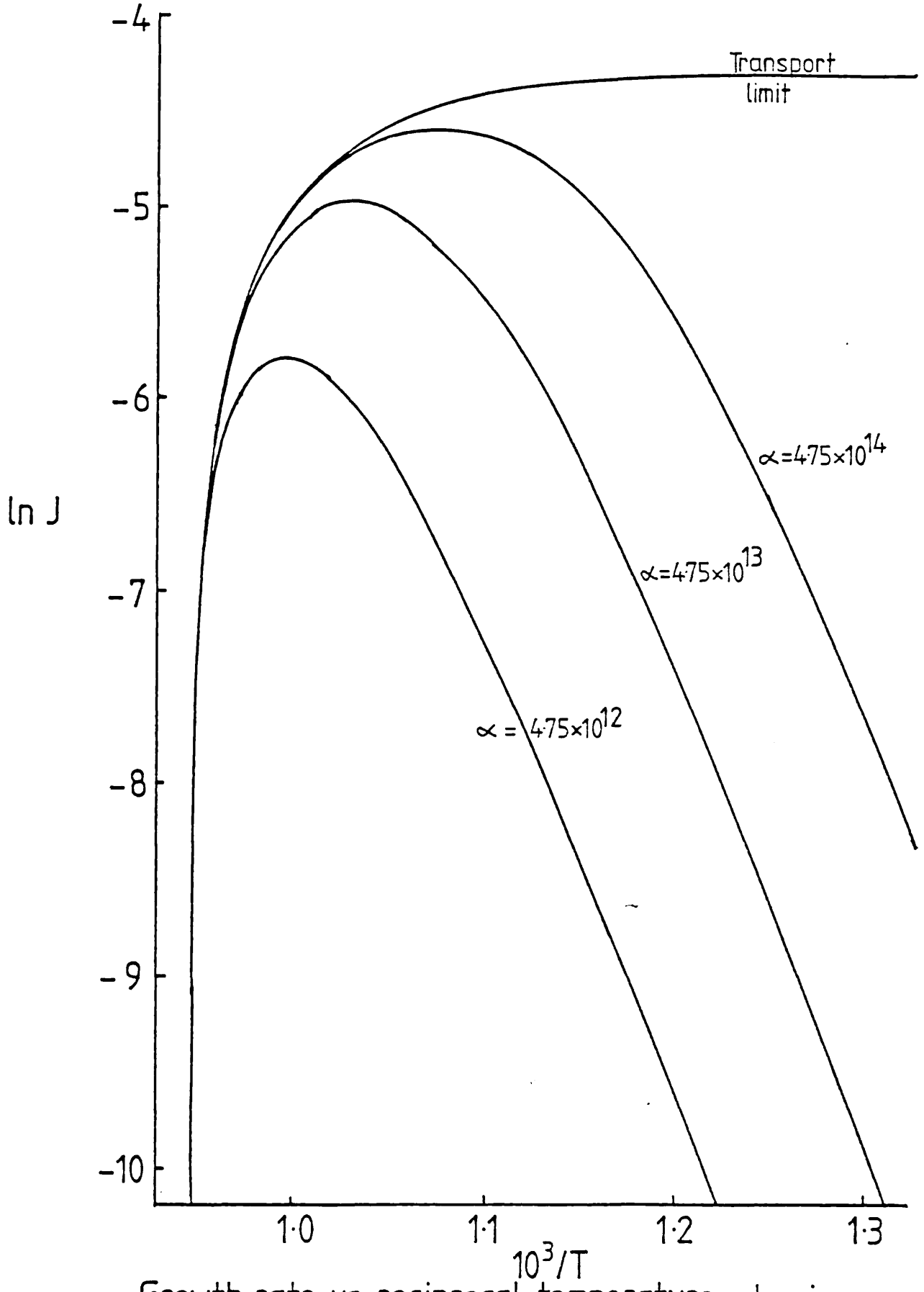

Growth rate vs. reciprocal temperature showing effect of pre-exponential factor. Calculated for same conditions as fig 4-1. E = 47·5 kcal m^{-1}

growth rate falls below the transport limit. At low temperatures, growth rate is controlled completely by the surface kinetics. A plot of the logarithm of growth rate vs reciprocal temperature will have a slope of $-E/R$.

Experimental curves of growth rate as a function of temperature were found to show the variations predicted by equations 16 and 17. Thus, over a limited temperature range, the growth rate was found to increase with decreasing growth temperature [10]. However when the temperature range was extended, the growth rate passed through a maximum [6,7,8] so that at low temperatures it decreased with decreasing temperature (fig 4). This low temperature region arose, as seen above, from surface kinetic effects which dominate the growth rate at low temperatures. This view was confirmed by the fact that changing the orientation of the substrates only altered the growth rates in the low temperature region [6,7,8,11].

As can be seen in figs 2 and 3, the growth rate at highest temperatures is controlled by the gas transport rates and is unaffected by variations in the surface reactions rates as the surface orientation is changed.

When results were plotted as $\ell n\ \tau$ (where τ is the growth rate in $\mu m\ min^{-1}$) vs reciprocal temperature, it was possible to obtain values of the activation energy.

Boucher and Hollan [8] obtained a value of 40 kcal mol^{-1} for the (100) plane. For the same plane Shaw estimated an activation

Fig 4-4

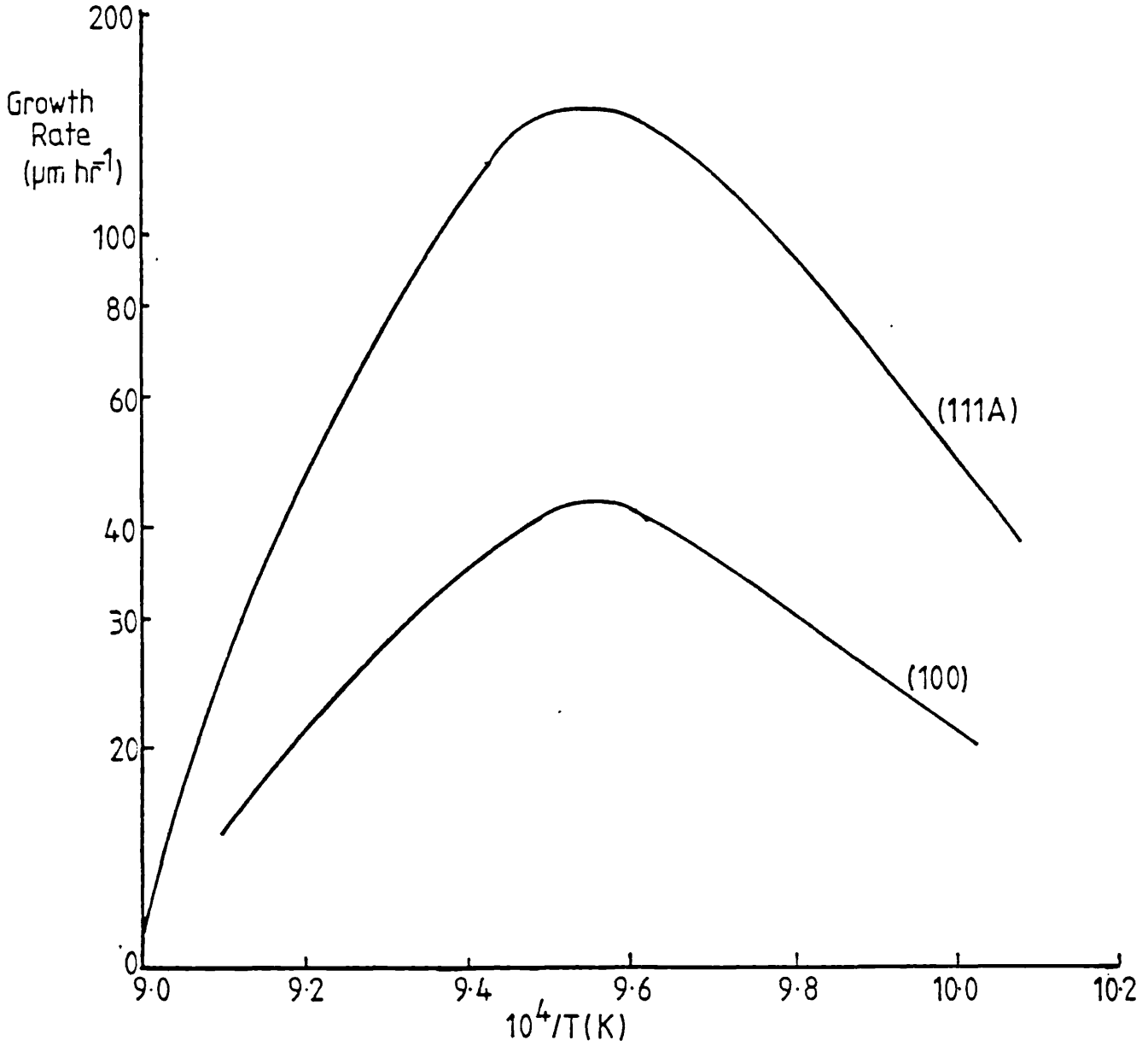

Experimental growth rate as a function of substrate temperature: from the results of Shaw (ref 6)

energy of 48.7 ± 3.5 kcal mol^{-1} [7] a value rather larger than his earlier work suggested [6]. In this he had reported values of 15-40 kcal mol^{-1} depending on surface orientation.

Recent work by Hollan et al [12] did not show a linear dependence at low temperatures. However, the available data were limited and the apparent curvature could be due to experimental error. An additional problem with this work is that the authors maintained a constant temperature difference between source and substrate. This procedure can itself lead to erroneous values of activation energy if the results are incorrectly interpreted by unwary workers. (See Appendix - section 4.1.6).

4.1.3 Experiments to Investigate the Effect of Substrate Orientation on Growth

The effect of substrate orientation on growth rate has been studied by several workers [6, 11, 13-17]. The most detailed work was carried out by Loyau et al [16,17] who used hemispherical substrates to obtain values of the relative growth rates in all directions in the range [(110)B - 100 - (110)A]. A typical experimental plot is shown in fig 5. All the plots obtained had certain qualitative features in common, although the actual values of the growth rates varied considerably from run to run. The most striking feature is the anisotropy in the growth rates on either side of the (100) direction. This anisotropy becomes more marked as the faces become more polar, becoming extreme in the (111)A and (111)B directions. (Exposed Ga or As face respectively). The (111)A direction shows by far the largest growth rate observed, whereas the (111)B direction shows one of the slowest growth rates.

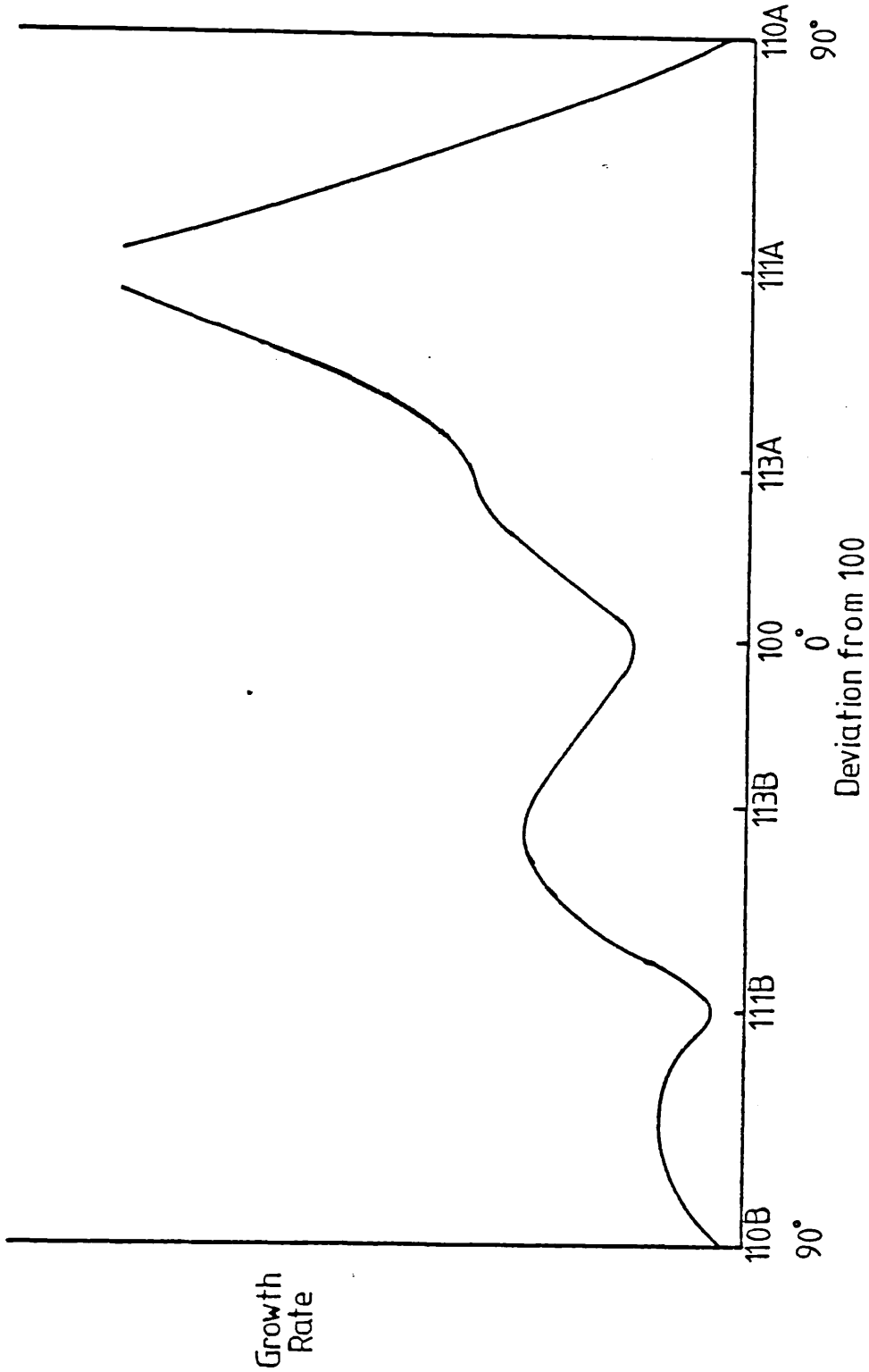

Growth rate vs. substrate orientation
(from refs 6,16 & 19)

These results are consistent with earlier work by Shaw [6,11] who studied orientation effects using substrates oriented in eight directions: (111)A, (112)A, (113)A, (115), (001), (113)B, (112)B, (111)B, he too found the highest growth rate with the (111)A face, and the slowest rate with the (111)B. Similarly both the French workers and Shaw found a small maximum in the (113)B direction. On the other hand the small minimum in the (113)A direction found by Loyau et al is not apparent in Shaw's work.

To some extent the qualitative agreement between these workers is fortuitous, reflecting the fact that both sets of workers were growing from an As-rich vapour phase. Earlier studies had given confused and sometimes contradictory results [18]. This probably arose from the different growth regimes studied. Ewing and Green [13] showed that growth rates of the $\{111\}$A, $\{111\}$B and $\{100\}$ faces were strongly dependent on the Ga:As ratio in the gas-phase. This dependence varies for different surfaces and can result in changes in the relative rates of the surfaces. Thus, at high Ga:As ratios the $\{111\}$B face may in fact react more rapidly than the $\{111\}$A face. This is the reverse of the situation found by Shaw and Loyau et al.

Dilorenzo [14], using a liquid gallium source and $AsCl_3$, studied growth rates on several faces and obtained an order for growth rates of $\{111\}A > \{211\}A > \{211\}B > \{311\}B \simeq \{311\}A > \{100\}$. This order was independent of the pressure of $AsCl_3$. A similar study was carried out by Lavrentyeva et al [19] on a closely related system: growth of GaAs using iodine in hydrogen (ie HI) as the transporting agent. These workers also found a growth

rate anisotropy about the (100) direction (cf fig 5). As with the work on GaAs/HCl, minima were observed in the (100) and (111)B directions, with a broad maximum in the (113)B direction. However, although the highest rates of growth were observed close to the (111)A direction, the growth rate was found to drop very sharply to give a minimum in the growth rate curve precisely in the (111)A direction. This minimum in the (111)A direction may also arise in the GaAs/HCl system. Loyau et al [16] were unable to measure growth rates in the (111)A direction itself due to facetting and the growth of small islands in this direction. However, neither Shaw [8] nor Dilorenzo [14] observed facetting on $\{111\}$A faces.

An attempt to explain the growth anisotropy of GaAs was made by Lavrentyeva et al [19] in terms of the BCF-theory. They obtained an expression involving the angular deviation from a plane surface and the parameter $\left(\frac{\lambda_s}{y_o}\right)$, where λ_s is the average diffusion distance of adatoms and y_o distance between steps. It was found that experimental results in directions (100)-(111)A could be fitted to the theoretical curve. That surface steps are important in determining the overall growth rate was made clear by Hollan & Schiller [15]. They studied the growth of GaAs on the (100) facet and vicinal faces. A plot of growth rate vs angular deviation from the (100) direction showed a steady increase in growth rate with increases angular deviation. However, the rate obtained for the singular face was always smaller than that expected from extrapolation of the rates of the vicinal faces.

The observed rate was found to be between 50% and 90% of the expected value. The lower values were associated with high purity conditions and a dislocation free substrate.

4.1.4 The Dependence of Growth Rate on the Pressures of the Reactants

Studies on the effect of the pressures of the various gas-phase species on the rate of reaction were reported by Shaw [7], Hollan et al [12,20] and Mizuno and Watanabe [24]. These investigations were carried out on the (100) face of GaAs. Unfortunately the investigations are not entirely satisfactory. Although the experimental systems are very different, in each case the sample is open to the gas-stream so that transport of the reactants occurs in an undefined region above the substrate. It follows then that the pressures of the reactants immediately above the sample are not known. Thus, although the results may give qualitative indications of the behaviour of the system they cannot be used quantitatively.

Shaw [7] used a microbalance system in which the sample was placed in an open crucible with the gas-stream passing over it. There were separate sources for GaCl, arsenic and HCl thus allowing the pressures of these to be varied independently. The most important results reported by Shaw were obtained by keeping the sample at a constant temperature and increasing either the GaCl pressure or the arsenic pressure, (in both cases keeping the pressure of the other species constant). The results are shown in figs 6 and 7. By combining these results with growth rate vs temperature data Shaw was able to identify which points occurred in the thermodynamically controlled regime, and which belonged to

Fig 4-6

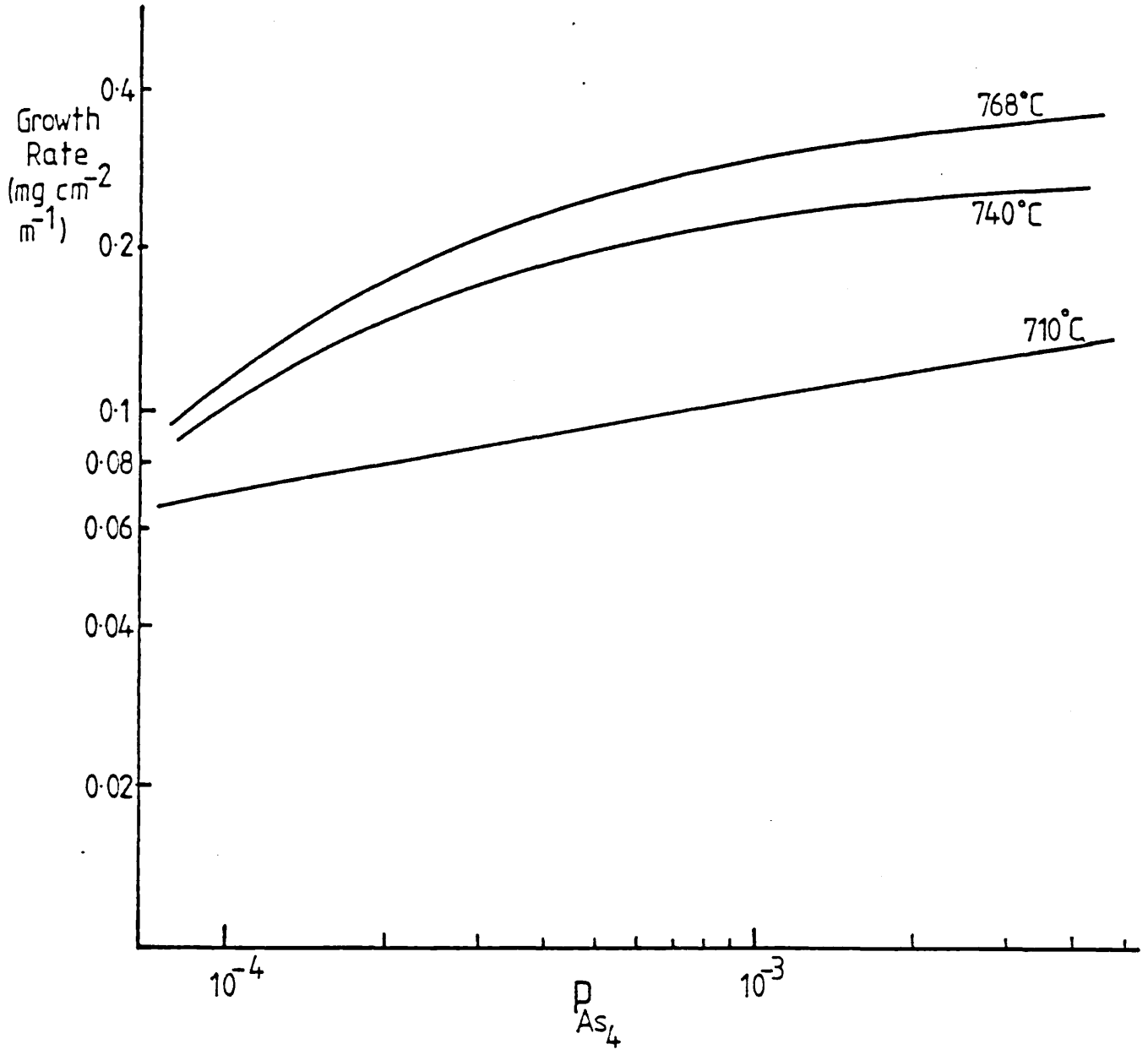

Growth rate vs. arsenic pressure (from Shaw[7])

Curves plotted for three substrate temperatures

Fig 4-7

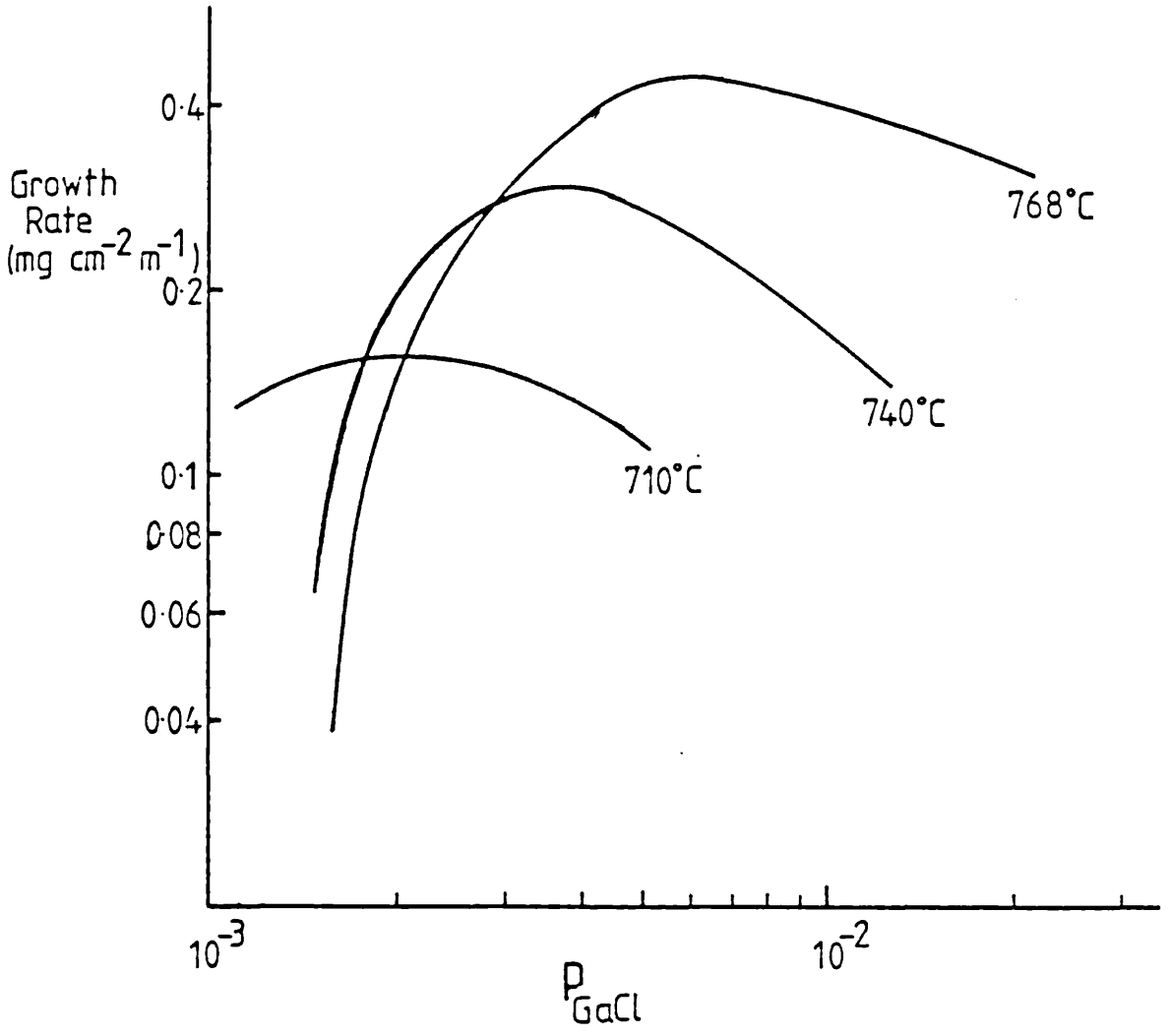

Growth rate vs. gallium chloride pressure (from Shaw[7])

Curves plotted for three substrate temperatures

the kinetic regime (see Section 4.1.2). However, he failed to recognise that even in the kinetically controlled region transport effects can cause the gas pressures above the solid to depart significantly from the values in the bulk gas-stream. Despite these shortcomings, some information can be gained from Shaw's results.

The variation of growth rate with arsenic pressure (fig 6) is unrevealing, even for the lowest substrate temperatures where kinetic effects dominate. The results show an increase in rate with increasing arsenic pressure; but since increasing the arsenic pressure is equivalent to increasing the over-potential for growth this result is not unexpected. Since the results have not taken into account the transport of material to the surface, any attempt to derive a mathematical expression to describe the pressure dependence could be very misleading. The variation of growth rate with gallium chloride pressure (fig 7) gives far more revealing results. Like arsenic, an increase in GaCl pressure increases the overpotential for the reaction and plots might be expected which are similar to fig 6 and show a steady increase in rate with arsenic pressure. In fact there is a tendency for the growth rate to drop at higher GaCl pressures. Such a result cannot be explained in thermodynamic terms, nor can gas transport be invoked to explain the results. It appears then that the growth of GaAs is hindered by excess GaCl. The only doubt regarding this conclusion lies in Shaw's method of introducing GaCl into the system. This is achieved by passing HCl over liquid Ga at 900^{o}C. At this temperature the reaction

is extreme and it is assumed that all the HCl reacts. In practice, however it is possible that some HCl passes into the system, thus reducing the growth potential. If the unreacted HCl was a significant fraction of the initial concentration this could easily account for the observed results.

In contrast, to Shaw, Hollan et al [12,20] used an open flow epitaxial kit with a GaAs source. The system is thus far less flexible, but more closely defined. Overpotential is determined by the values of the source and substrate temperature. Only one parameter, the input pressure of $AsCl_3$, controls pressures of all gas-phase species. This method immediately overcomes one of the difficulties of Shaw's method, namely the problem of altering reactant pressures without changing the supersaturation. In this system supersaturation is defined solely by the source and substrate temperatures; once these are fixed then changes in $AsCl_3$ pressure cannot affect the supersaturation. Typical results are shown in fig 8. The growth rate increases with mole fraction of $AsCl_3$ at first, but at higher $AsCl_3$ pressures the rate becomes constant or even decreases [12,20]. Similar results were obtained by Mizuno and Watanabe [24]. In the range of $AsCl_3$ pressures considered it can be shown that the GaCl pressure is roughly proportional to the $AsCl_3$ pressure (fig 9). The results shown in fig 8 are, therefore, consistent with Shaw's observation that high GaCl pressures reduce the growth rate. However, at very high $AsCl_3$ mole-fractions ($>10^{-2}$) a different behaviour was found. In this region growth rate rose sharply with increasing $AsCl_3$ reaching growth rates as high as 100 $\mu m\ h^{-1}$.

Fig 4-8

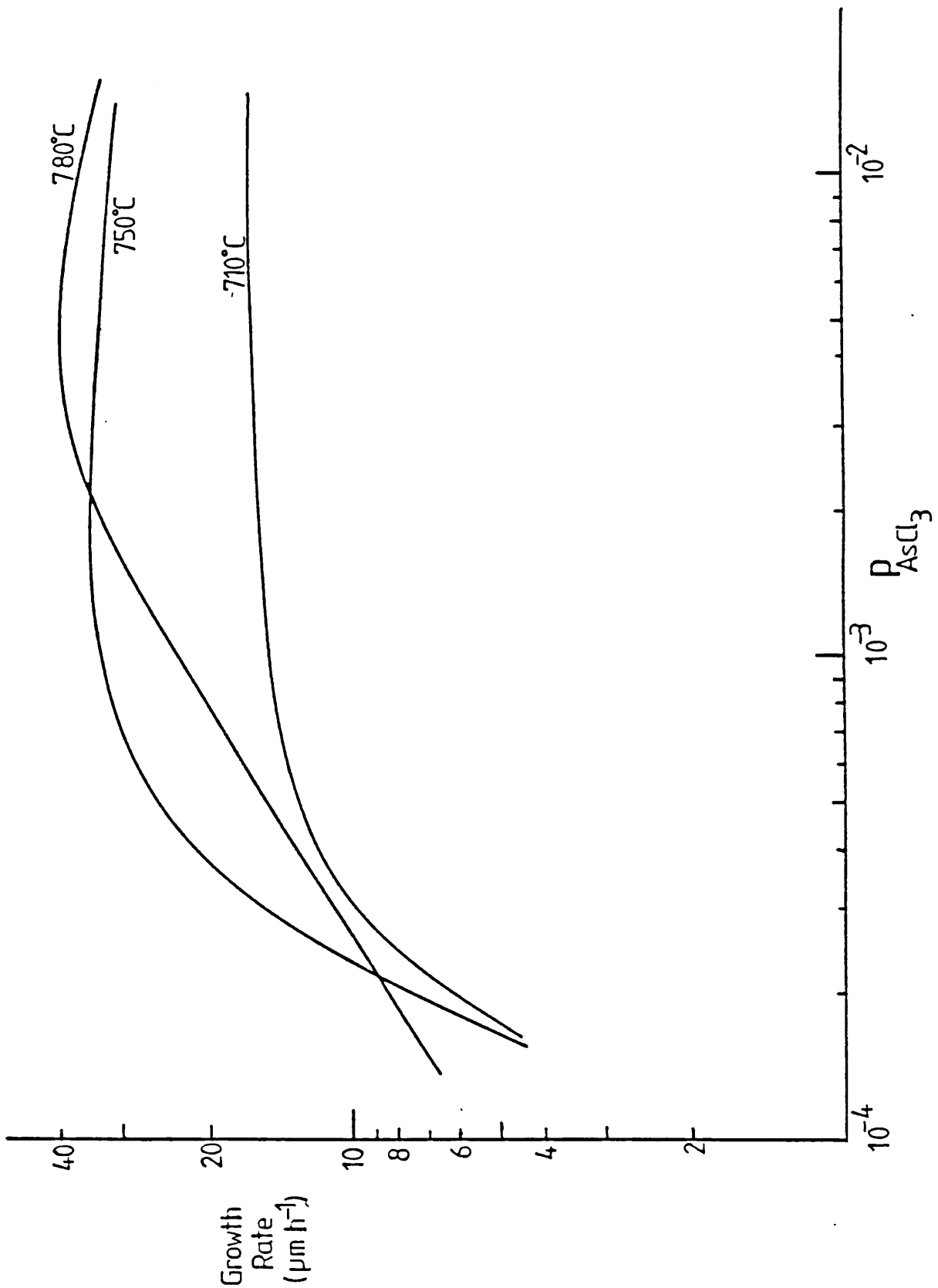

Growth rate vs. $AsCl_3$ pressure (from Hollan et al. [12])

Curves plotted for three substrate temperatures - temperature difference between source and substrate = 80°C

Fig. 4-9

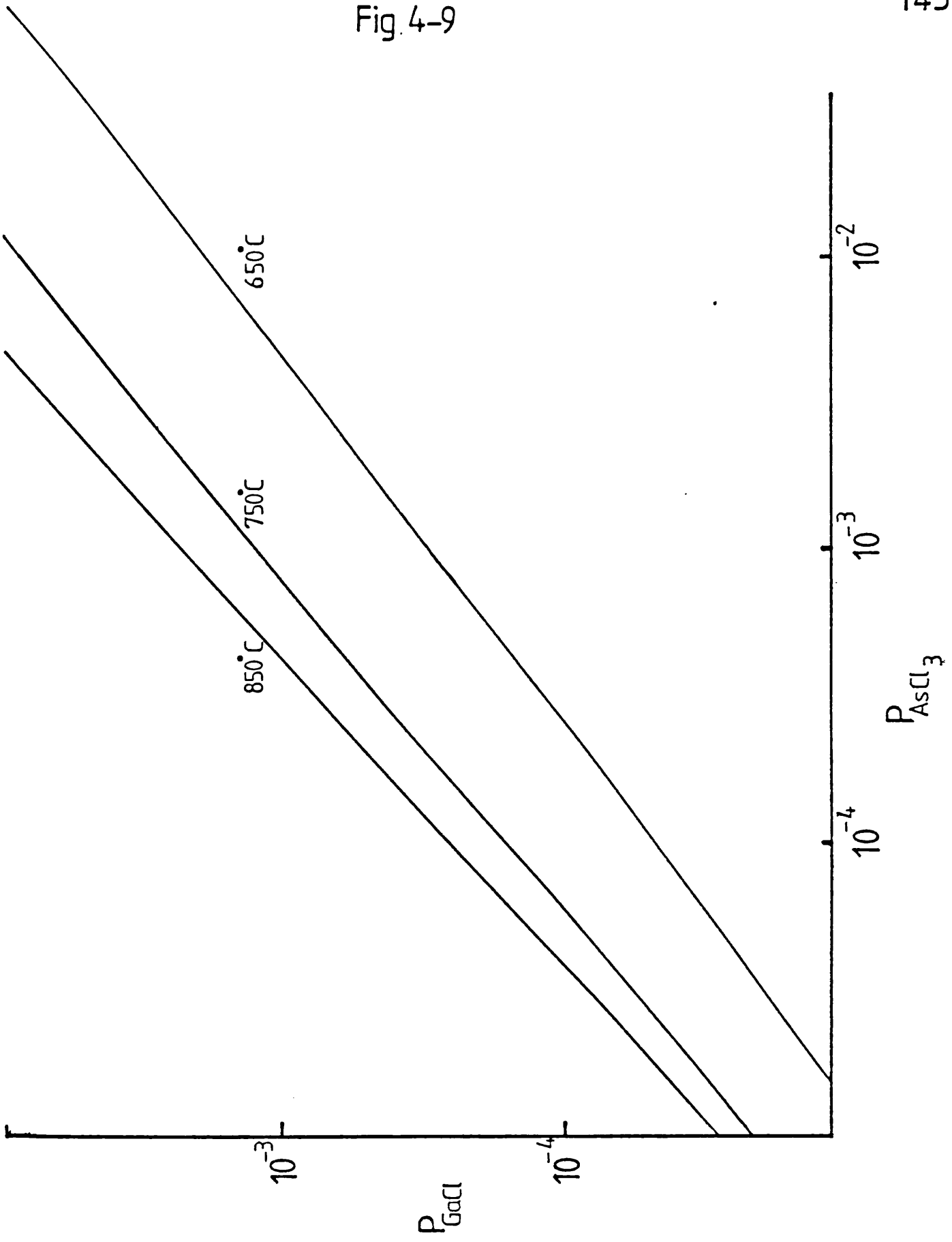

P_{GaCl} as a function of input P_{AsCl_3}
(calcuted for three source temperatures)

The dependence of growth rate with lower mole-fractions of $AsCl_3$ ($<10^{-2}$) (and the corresponding dependences on As_4 and GaCl pressures) has been interpreted by Cadoret [21,22] in terms of a growth model involving As-Ga-Cl complexes. At high GaCl pressures, adsorbed GaCl molecules prevent the formation of the triatomic complexes, leading to a reduction of growth rate under these conditions. However, the very rapid increase in rate when the $AsCl_3$ mole fraction was greater than $\sim 10^{-2}$ cannot be explained by this model.

Although most growth systems are operated with a vast excess of hydrogen (so that its pressure may always be taken to be approx 1 atm), some Japanese workers [23] found that high purity GaAs could be obtained by growing GaAs in a nitrogen atmosphere. Mizuno and Watanabe [24] studied the GaAs/HCl reaction in a variety of inert gases and were able to examine the dependence of growth rate on hydrogen pressure. These workers found a linear dependence of growth rate with hydrogen pressure (fig 10). Identical results were obtained when He, N_2 or Ar were used as the inert gas. This linear dependence was interpreted as due to a rate-limiting process involving the formation of an adsorbed GaH_2Cl complex. However, Cadoret claims the result is also consistent with his model [22].

4.1.5 Summary

In this section, attention is confined to results obtained for the growth of GaAs on (100) oriented substrates. At present, there are clearly shortcomings in the available experimental evidence. However, some general conclusions can be made. Thus,

Fig 4-10

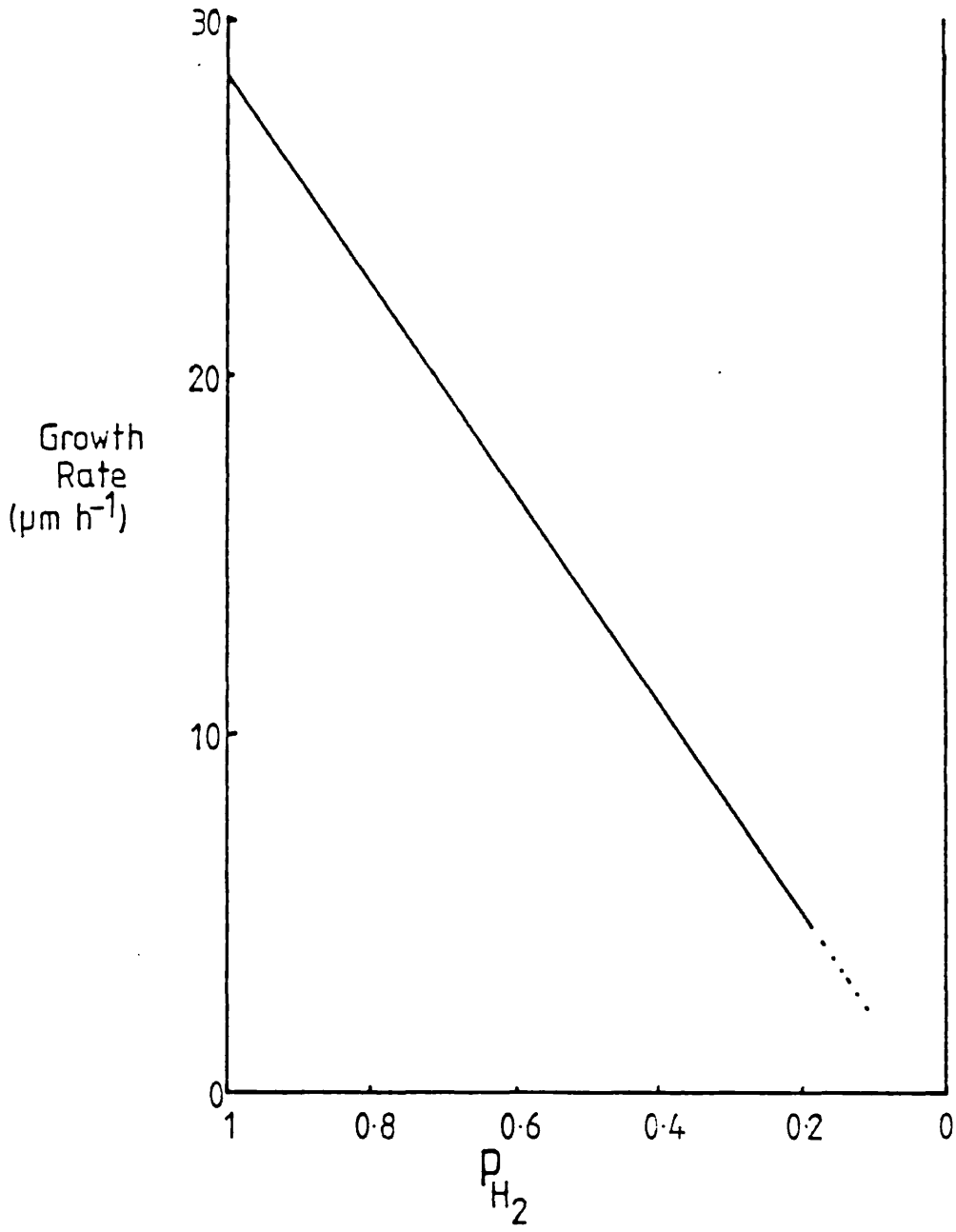

Growth rate vs. hydrogen pressure (from ref 24)

the activation energy of the reaction appears to be in the range 40-50 kcal mol^{-1} (section 4.1.2) and the evidence of both Shaw [7] and Hollan [12,20] indicates that increasing the GaCl pressure can reduce the growth rate. Although in most systems hydrogen is in vast excess (so that minor pressure variations can be neglected) the dependence of growth rate on hydrogen pressure is important when considering a particular growth mechanism. The work of Mizuno and Watanabe [24] clearly demonstrated that growth rate was directly proportional to hydrogen pressure.

Both Cadoret [21,22] and Mizuno and Watanabe [24] have presented growth models for the GaAs/HCl system. That of Cadoret is the more detailed. Both models have as a rate-limiting step the formation of a surface complex, although the nature of this complex differs in the two models. Despite this, both models give good qualitative agreement with the experimental results, reflecting the difficulty in interpreting kinetic results unambiguously. Cadoret claims good quantitative agreements with the experimental data. However, this claim must be treated with caution as much of the data is not corrected for transport effects in the vapour phase.

4.1.6 Appendix

Hollan et al [12] studied the variation of growth rate with substrate temperature. Instead of keeping input pressures constant and simply reducing the substrate temperature - a procedure which inevitably results in an increasing overpotential - these workers attempted to maintain a constant overpotential by keeping a constant temperature difference between source and substrate. Although the French workers did not attempt to derive activation energies from their data, it would obviously be

possible to do so. It is therefore, of interest to see how the apparent activation energy derived from a $\ell n\ \tau$ vs $1/T$ plot compares with the real activation energy. Consider a growth rate given by

$$r = e^{-E/RT}\left[\frac{K^*}{K^o} - 1\right] \qquad \ldots\ldots 1$$

Examining first the supersaturation term

$$\gamma = K^*/K^o - 1 \qquad \ldots\ldots 2$$

If ΔT is the temperature difference between source and substrate, and T is the substrate temperature then

$$K^* = e^{-\Delta G/R(T+\Delta T)} = e^{-\Delta H/R(T+\Delta T)} \cdot e^{\Delta S/R} \qquad \ldots\ldots 3$$

Similarly at the substrate

$$K^o = e^{-\Delta G/RT} = e^{-\Delta H/RT} \cdot e^{\Delta S/R}$$

$$\text{Thus } K^*/K^o = \frac{e^{-\Delta H/R(T+\Delta T)}}{e^{-\Delta H/RT}} = \exp\left[\frac{\Delta H}{R}\left(\frac{1}{T} - \frac{1}{T+\Delta T}\right)\right]$$

$$= \exp\left[\frac{\Delta H}{RT}\left(\frac{\Delta T}{T+\Delta T}\right)\right] \qquad \ldots\ldots 4$$

$$\text{Hence, } \gamma = \left\{\exp\left[\frac{\Delta H}{RT}\left(\frac{\Delta T}{T+\Delta T}\right)\right]\right\} - 1 \qquad \ldots\ldots 5$$

The value of this function has been calculated for the GaAs/HCl system. The reaction is assumed to be

$$GaAs + HCl \rightleftharpoons GaCl + \tfrac{1}{4}As_4 + \tfrac{1}{2}H_2 \qquad \ldots\ldots 6$$

ΔH = 34.4 kcal mol^{-1}. Table 1 shows the values of γ for $\Delta T = 80^{o}C$ and $\Delta T = 20^{o}C$. It can be seen that maintaining a constant temperature difference between source and substrate is not equivalent to constant overpotential, especially with high values of ΔT.

The question arises as to how this variation in γ will affect the shape of the growth rate vs reciprocal temperature plot. This can be seen by plotting $\ell n\ \gamma$ vs 1/T (fig 11). It can be seen that for $\Delta T = 80^{o}C$, the plot is linear over the temperature range of interest; for $\Delta T = 20^{o}C$ some slight curvature is detectable. The important thing to note is that the temperature dependence of γ could lead to a serious underestimate of the activation energy. The slope of the $\Delta T = 80^{o}$ plot is equivalent to -7.1kcal mol^{-1} whilst that for ΔT = 20 is $\simeq$ -4.5kcal kJ mol^{-1}.

Thus a plot of ℓn r vs 1/T where E = 50 kcal mol^{-1} and a $\Delta T = 80^{o}C$ has a slope equivalent to an activation energy of 43 kcal mol^{-1} (fig 12).

In contrast to this situation, the results obtained by the traditional method of effectively maintaining a constant source temperature and decreasing the substrate temperature are found, after an initial rate increase, to give roughly linear plots of ℓn r vs 1/T with a slope approximately equal to the activation energy (figs 2 and 3).

To summarise, it appears that although maintaining a constant temperature difference between source and substrate does indeed

TABLE 4.1

Substrate Temp-T (^{o}C)	$\gamma(\Delta T = 20^{o}C)$	$\gamma(\Delta T = 80^{o}C)$
750	0.814	8.12
800	0.689	6.06
850	0.592	4.70
900	0.515	3.76
950	0.452	3.08
1000	0.401	2.57
1050	0.358	2.19
1100	0.322	1.89

Variation of the function γ with substrate temperature for two values of the temperature difference between source and substrate (ΔT). Calculated for the GaAs/HCl reaction.

Fig 4-11

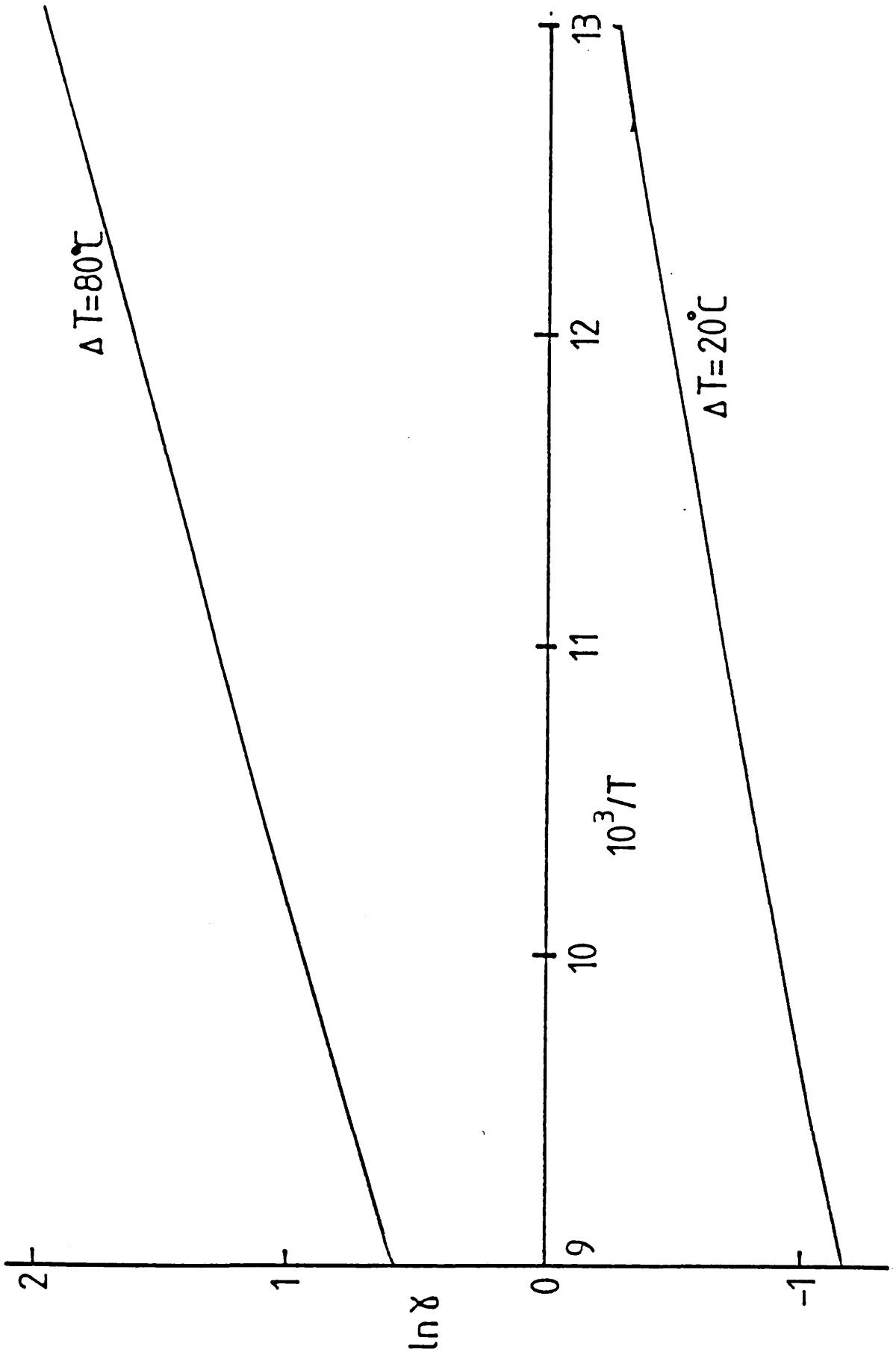

Effect of substrate temperature on supersaturation for system with constant temperature difference between source and substrate

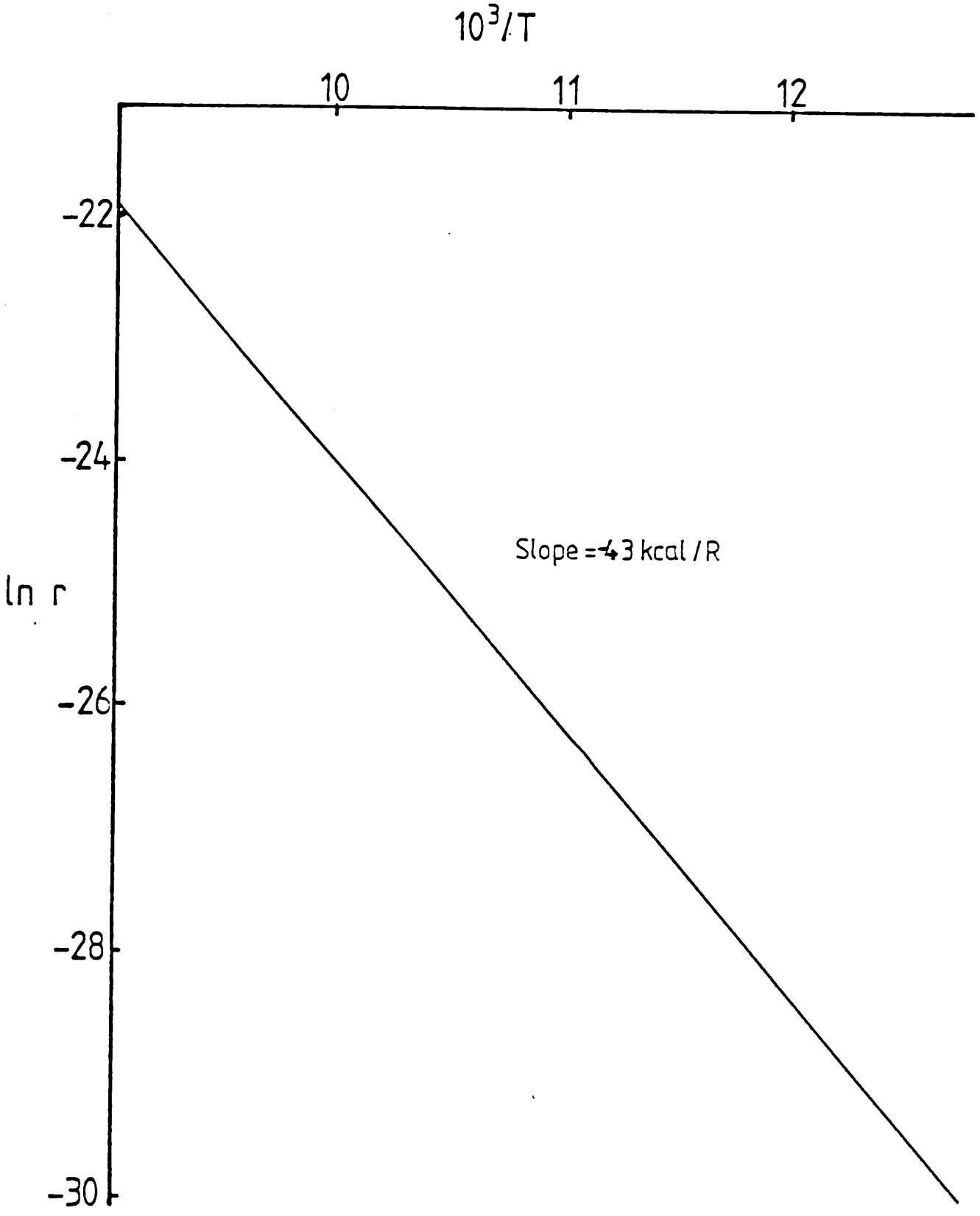

Log (rate) as function of substrate temperature

(calculated for E = 50 kcal mol^{-1})

reduce the variation in the term γ, the results obtained from such a procedure are more misleading than those obtained using constant source temperature.

4.2 A Study of the GaAs/HBr Reaction using the Modified Entrainment Method

Most of the results discussed in the previous section were obtained in growth systems. However, for small departures from equilibrium the same reaction mechanism will apply to both growth and etching situations. Consequently, it is possible to obtain information about the surface reactions by studying the rates of weight loss in a MEM experiment. The basic principles of kinetic investigations were discussed in Chapter 2 (section 2.3): the key feature of the modified entrainment method is that the effects of transport are limited to the narrow channel in the sample bottle and may thus be calculated. Hence it is possible to determine the gas-phase pressure immediately above the sample. This is not possible in the open flow systems used in the kinetic investigations described in section 4.1: it was simply assumed that transport effects are negligible, and that there were no pressure gradients in the gas-phase.

In order to demonstrate the study of a chemical vapour transport reaction, the results obtained for the GaAs/HBr reaction by Miss E J Tarbox [4] were re-examined using the equations developed in Chapter 2. This system had originally been studied by the author and co-workers [25] who found it similar to the GaAs/HCl system [26]. Thermodynamic values were obtained for the reactions

$$GaAs_{(s)} + HBr_{(g)} \rightleftharpoons GaBr_{(g)} + \tfrac{1}{2}As_{2(g)} + \tfrac{1}{2}H_{2(g)} \qquad \ldots\ldots 19$$

and $$GaAs_{(s)} + 2HBr_{(g)} \rightleftharpoons GaBr_{2(g)} + \tfrac{1}{2}As_{2(g)} + H_{2(g)} \qquad \ldots\ldots 20$$

The work was continued by Miss Tarbox. Her results were examined by the author and, as discussed below, found to demonstrate a kinetic

limitation in the observed rate of weight loss at low temperatures. Unfortunately, the aim of the investigation had been to obtain thermodynamic information and thus the sample used was crushed polycrystalline material. This clearly limits the usefulness of the results as the observed rate will be an aggregate of all the various exposed surfaces, and may differ considerably from the rate of any single surface orientation. Furthermore, as the reaction proceeds the most reactive faces will disappear. Thus the observed rates do not represent accurate steady-state values. However, the discussion below will demonstrate the main features of a kinetic investigation by MEM and show the sort of information which can be obtained. Future investigations will clearly involve the use of single crystal substrates in which effectively only one face, of known orientation and area, is exposed.

4.2.1 Experimental

The experimental apparatus was described in ref 25 and in chapter one (section 1.2). Fig 13 is a schematic diagram of the apparatus. HBr was formed by passing Br_2 into the furnace tube where it reacted with the hydrogen carrier gas before passing to the sample bottle. The rate at which Br_2 passed into the system was a function of the geometry of the four tubes connecting the reservoir to the main apparatus, the flow rate of hydrogen passing over the tubes (in practice, kept constant using flow controllers) and the temperature of the bromine. The last was controlled by placing the bromine reservoir in a water bottle which maintained the temperature to within $\pm$ 0.1°C. The rate of weight loss ($\dot{W}$) was studied as a function of temperature at two different HBr partial pressures: ε = 0.0354 and 0.0591.

Fig 4-13

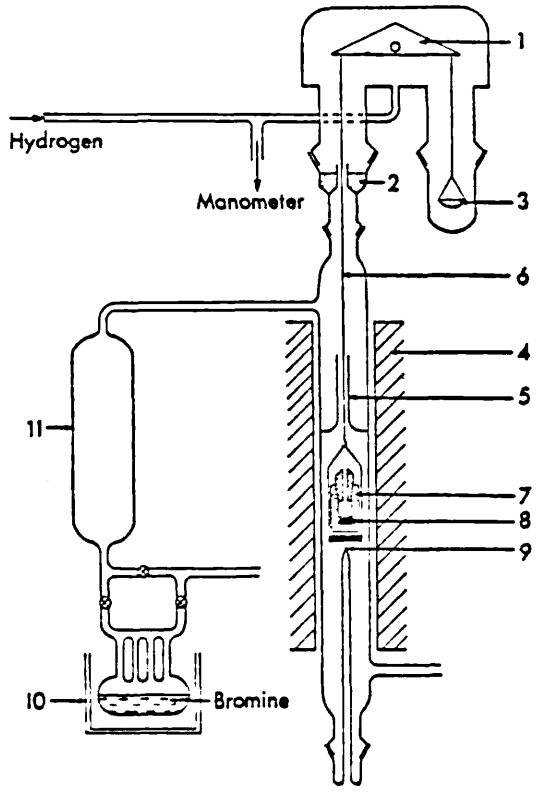

—Schematic diagram of the entrainment apparatus. 1. Recording microbalance, 2. calcium oxide, 3. counter-weight, 4. furnace, 5. jet tube, 6. silica fibre, 7. alumina reaction bottle, 8. sample, 9. thermocouple sheath, 10. thermostatic bath, 11. ballast chamber.

The experiment was carried out using three different sized channels. These were all the same length, but had nominal diameters of 1 mm, 2 mm and 3 mm.

4.2.2 Results and Discussion

The results of the experiments are shown in figs 14 and 15 (for HBr pressure of 0.0354 and 0.0591 respectively) as plots of $\ell n\ \dot{W}$ vs reciprocal temperature.

It can be seen that the results for the 2 mm and 3 mm channels show a rapid decrease of rate of weight loss with temperature over most of the temperature range, with a slight inflexion in the weight loss curves at about 900K ($10^4/T = 1.1$). The shapes of the weight loss curves are similar to those obtained in ref 25. In contrast, the plots for the 1 mm channel show a shallower slope in the low temperature region, similar to those obtained for GaAs/HCl [26]. If equilibrium obtained in the sample bottle for every channel size, then the shapes of the curves would be identical. The curves for the 2 and 3 mm channels would simply be vertical transpositions of the 1 mm curve; the vertical difference between the curves being the logarithm of the ratio of the channel resistances. This was not the case at low temperatures - surface kinetics were clearly limiting the rate of weight loss when the 2 mm and 3 mm were used, and may possibly have been of importance with the 1 mm channel.

Further evidence that surface kinetic effects were being detected at low temperatures was obtained by studying two samples under

Fig 4-14

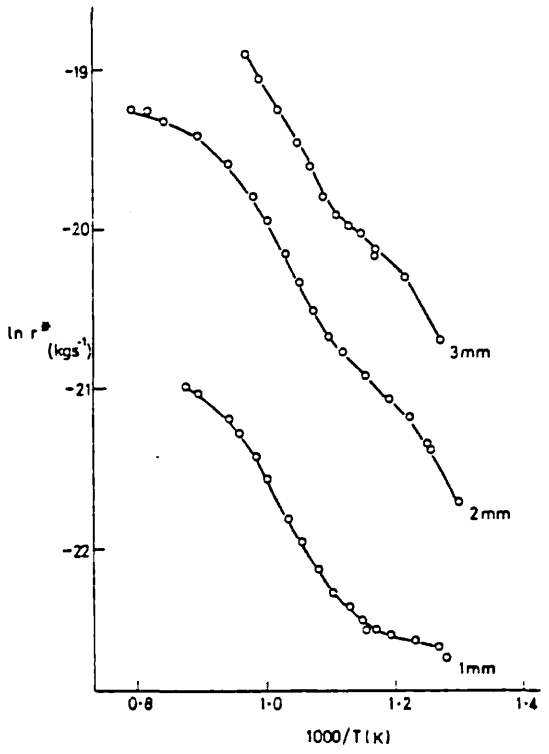

$\epsilon = 0{\cdot}0354$

Fig 4-15

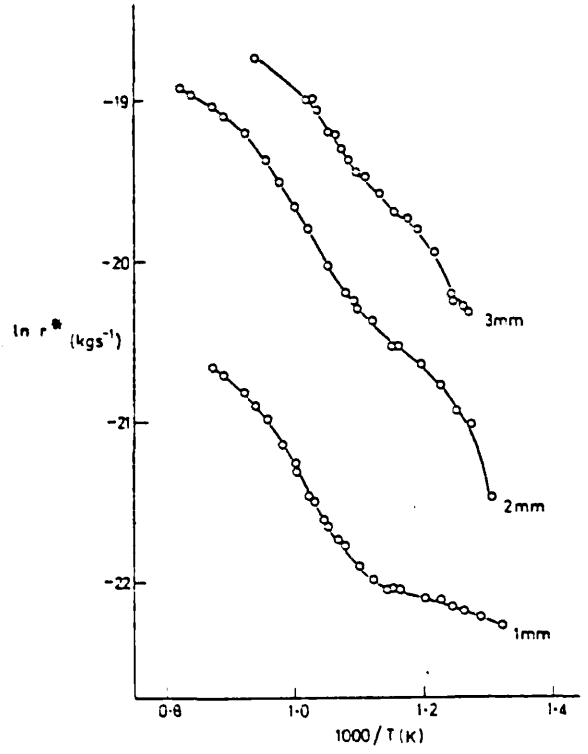

$\epsilon = 0{\cdot}0591$

Plots of $\ln \dot{W}$ vs $1/T$ for GaAs/HBr system. Results are shown for three channels and two HBr pressures(ϵ).

the same conditions (3 mm channel, $\varepsilon = 0.0354$). One of the samples was more finely ground than the other and hence had a larger surface area. If surface kinetics were influencing the observed rate of weight loss, then the finer sample should give the larger rate. The results are shown in fig 16 and it can be seen that at temperatures below about 1000K the more finely ground sample gave a higher rate of weight loss and that the difference between the samples increased at lower temperatures.

The results were interpreted using equation 69 of Chapter 2:

$$\dot{W}_f = \frac{\dot{W}}{\left[1 - \left(\frac{\dot{W}}{\dot{W}^o}\right)^{N'}\right]} \qquad \ldots\ldots 21$$

where $\dot{W}_f = MJ_f$ is the forward (exchange) reaction current, W is the observed rate of weight loss and $\dot{W}^o$ the rate of weight loss which would be observed if equilibrium obtained in the sample bottle. To estimate values of $\dot{W}^o$ it was assumed that the experiments carried out using the 1 mm channel corresponded to equilibrium conditions inside the bottle. The results in figs 14 and 15 showed very clearly that the slopes of the weight loss curves obtained with the 2 mm and 3 mm channels increased very markedly with decreasing temperature in the low temperature region. This sudden increase in slope was taken to be due to the change from gas-transport (and equilibrium) limitations on rate of weight loss to surface kinetic limits and was not observed with the 1 mm channel. This showed that over the experimental temperature range, surface kinetics had little (if

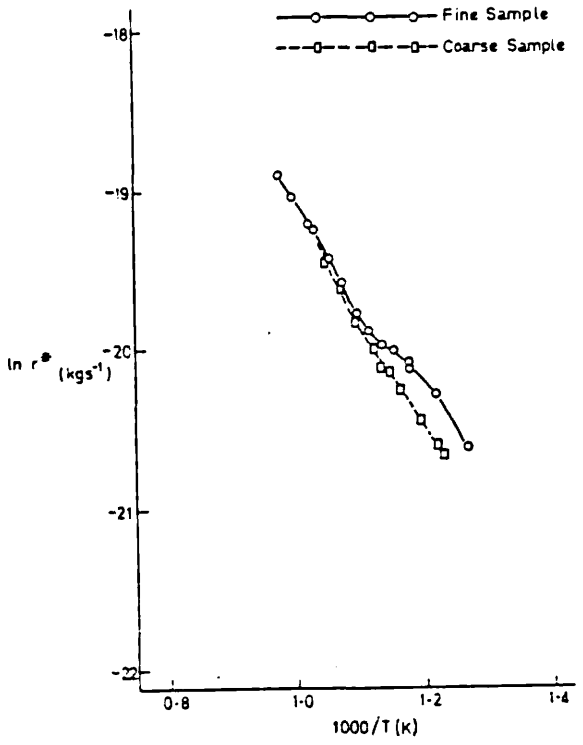

Experimental results showing effect of altering sample area
Results obtained with 3mm channel and $\epsilon = 0{\cdot}0354$

any) effect on the overall rate of weight loss from a sample bottle with the 1 mm channel.

To estimate the equilibrium curves for the 2 and 3 mm channels, the result from the 1 mm channel was transposed vertically until the high temperature parts of the curve coincided. The lower temperature portions of the 2 and 3 mm curves were found to lie beneath the theoretical plot, indicating the effect of surface kinetics. This approach eliminated the need to estimate an equilibrium curve using literature values of the thermodynamic data and diffusion constants. An important source of error in the method was thus removed. To confirm that the procedure was valid, it was noted that the extent by which the curve for the 1 mm channel was moved vertically should reflect the ratios of the channel resistances. A comparison of calculated and experimental ratios (ie obtained from the distance by which the 1 mm curve is transposed) was possible. The results are shown in table 2. It will be seen that the experimental ratios obtained for two different HBr pressures were similar, although they were somewhat higher than those calculated from the channel dimensions. To use equation 21 to calculate the exchange current it was necessary to identify the reaction so that N' could be determined. The shape of the equilibrium weight loss curves was interpreted in the same way as the curves obtained for the GaAs/HCl reaction [25,26]. Thus, at high temperatures gallium was transported as the monohalide, whereas at lower temperatures the main gallium species was the dihalide ($GaBr_2$). At the temperatures where the surface kinetics were dominant, the main

TABLE 4.2

Table showing the relative sizes of the transport conductances of the channels; theoretical values obtained from the channel dimensions; for experimental values, see text.

	Channel size (mm)		
	1	2	3
Ratio of channel conductance (R)			
Theoretical	1	4.25	10.20
Experimental			
$\epsilon = 0.0354$	1	4.95	12.18
$\epsilon = 0.0591$	1	5.16	11.47
ℓn R			
Theoretical	0	1.45	2.32
Experimental			
$\epsilon = 0.0354$	0	1.60	2.50
$\epsilon = 0.0591$	0	1.64	2.44

arsenic species is As_2 [27] so that the surface reaction was taken to be reaction 20

$$GaAs + 2HBr \rightleftharpoons GaBr_2 + \tfrac{1}{2}As_2 + H_2 \qquad \ldots\ldots 20$$

and $N' = {}^3/_2$.

The exchange currents in the temperature range 909K-769K were calculated for both channel sizes and two HBr pressures (ε). The results are shown in figs 17 and 18 in the form of $\ell n\, W_f$ vs reciprocal temperature plots. The results may be seen to lie approximately along straight lines from which the activation energy of the reaction could be estimated. Table 3 lists the activation energy found from each plot. The arithmetical mean value of the results was $49\ \text{kcal mol}^{-1}$. The spread in values reflected both inaccuracies in the data used and possibly the pressure dependence of the exchange rate:

$$r_{ex} = k_f.S.M.\ p_{GaBr_2}^{(x_1)} \cdot p_{As_2}^{(x_2)} \cdot p_{H_2}^{(x_3)} \cdot p_{HBr}^{(x_4)} \qquad \ldots 23$$

In order to obtain values of the activation energy (included in the Arrhenious rate constant k_f) it was assumed that the exchange current had only a small dependence on the pressures of the various species when compared with the changes brought about by the temperature dependence of k_f. Although this was an assumption, some idea of the effect of pressure changes on the exchange rates could be gauged by comparing the results of runs (1) and (2) (2 mm channel) and runs (3) and (4) (3 mm channel). In both sets of results the only difference between the two runs was in the pressure of HBr used, and hence the pressures of all

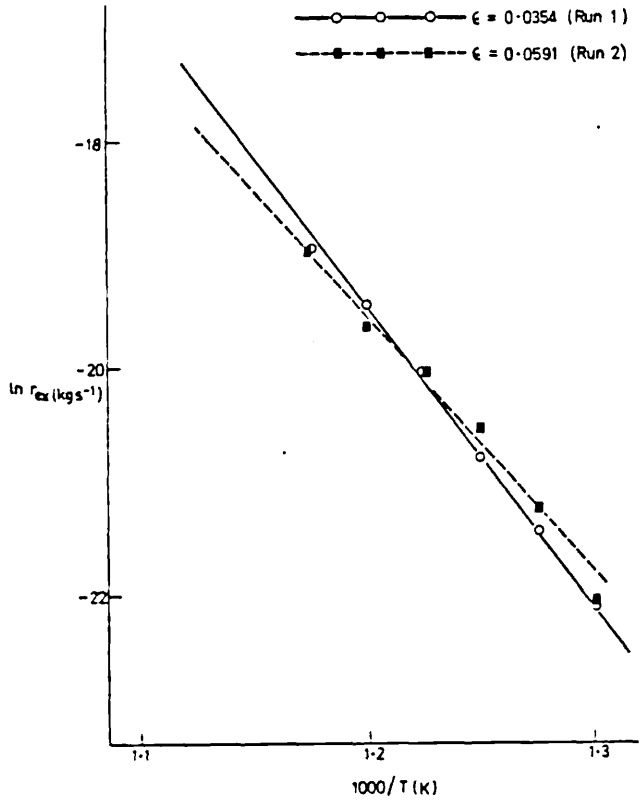

Exchange current vs 1/T-results for 2mm channel

Fig 4-18

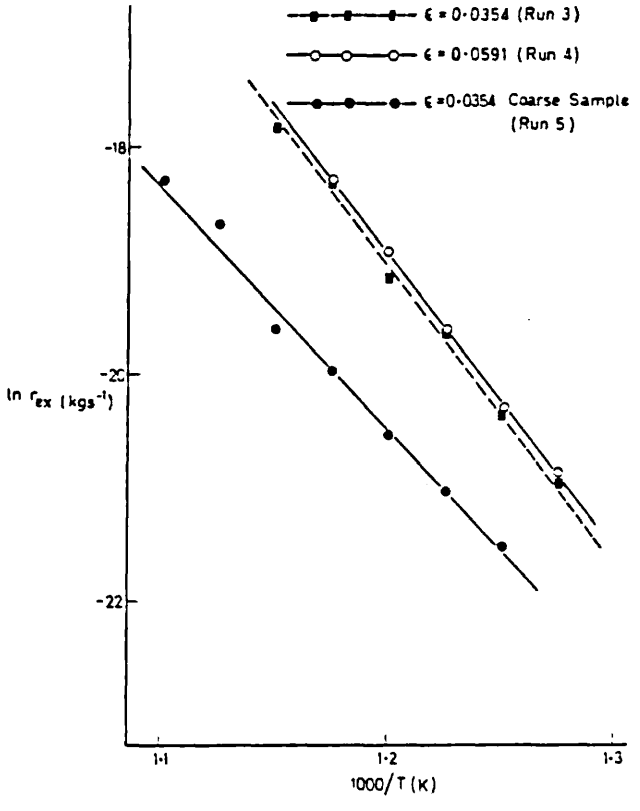

Exchange current vs 1/T-results for 3mm channel

TABLE 4.3

Experimental values of the activation energy, calculated from figs 17 and 18.

Run	Channel size (mm)	ε	E (k cal mol^{-1})
1	2	0.0354	53.1
2	2	0.0591	45.2
3	3	0.0354	52.9
4	3	0.0591	51.2
5	3 a)	0.0354	42.9

a) Coarse sample.

the other gas-phase species. Examination of figs 17 and 18 show that for the 3 mm channel the results for the lower HBr pressure lie on a line below that obtained for the higher pressure. With the 2 mm channel, the results for $\varepsilon = 0.0591$ are scattered about the line for $\varepsilon = 0.0354$. These results could easily arise from experimental scatter and it is clear that the overall dependence of the exchange current on the pressures of the gas-phase species was small when compared with the temperature dependence.

However, the ratio of HBr pressures is only about 1.7 and the effect of any change in HBr pressure may be offset by similar changes in the pressures of the other reactants. To detect pressure dependences it may be necessary to vary the HBr pressure by an order of magnitude or more.

By assuming the exchange current had the form

$$r_{ex} = \beta e^{-E/RT}$$

where β was constant, it was possible to calculate values of β for each of the experiments listed in table 3. These values are shown in table 4, and were calculated using the value of 49 kcal mol^{-1} (found above) for the activation energy. It is clear that the values of β are very similar. The differences between the values of β from different samples are due to the samples having different areas. This is most clearly seen in comparing runs (5) (coarse sample) and (3) (fine sample) in Table III. The value of β for the fine ground sample is approximately four times that of the coarse sample.

TABLE 4.4

Experimental values of the pre-exponential factor (β).

Run	Channel size (mm)	ε	β (kg s^{-1})
1	2	0.0354	2.64×10^4
2	2	0.0591	2.79×10^4
3	3	0.0354	4.24×10^4
4	3	0.0591	4.62×10^4
5	3 a)	0.0354	0.98×10^4

a) Coarse sample.

It should be noted that although table 4 gives a good indication of the relative sizes of β, there may be considerable error in the absolute values. The value of the activation energy could be in error by $\pm$ 5 kcal mol^{-1} and the corresponding range of values of β covers two orders of magnitude in the experimental temperature range.

4.2.3 Conclusion

Using results obtained for the GaAs/HBr reaction it was possible to obtain a mean activation energy for a polycrystalline sample. The value of 49 kcal mol^{-1} is of the same order as the activation energies obtained for the GaAs/HCl reaction. Using MEM it was also possible to obtain numerical values of the pre-exponential term β in the rate expression

$$J^{o} = \beta \exp (^{-E}/RT)$$

The importance of this lies in the fact that β contains the information about the dependence of the rate on the various reactant pressures. Future experiments, using single crystal substrates in which the exposed surface orientation and area are well-defined, should concentrate on the study of β as a function of the various input parameters. Such studies may involve the addition of GaCl or arsenic to the external gas-stream.

REFERENCES

1 L Hollan, J P Hallais, J C Brice : Chap 1 of 'Current Topics in Materials Science' Vol 5 Ed. E Kaldis, North Holland, Amsterdam 1980.

2 H C Casey, M B Panish : 'Heterostructure Lasers' Academic Press, New York, 1978.

3 R W Brander, M M Faktor : Inst Phys. Conf. Ser 57, 187, 1981.

4 E J Tarbox : Ph.D Thesis, London University, 1977

5 M M Faktor, I Garrett : "Growth of Crystals from the Vapour Phase" Chapman and Hall, London, 1974.

6 D W Shaw : J. Electrochem. Soc, 115, 405, 1968.

7 D W Shaw : J. Electrochem. Soc, 117, 683, 1970.

8 A Boucher, L Hollan : J. Electrochem. Soc, 117, 932, 1970.

9 A K Chatterjee: Private Communication.

10 H Seki, K Morjama, S Matumato, M Uranoto : Jap. J. Appl. Phys, 6, 784, 1967.

11 D W Shaw : J. Cryst. Growth, 31, 130, 1975.

12 L Hollan, J M Durand, R Cadoret : J. Electrochem Soc 124, 135 1977.

13 R E Ewing, P E Greene : J. Electrochem. Soc, 111, 1266, 1964.

14 J V Di Lorenzo : J. Cryst. Growth 17, 189, 1972.

15 L Hollan, C Schiller : J. Cryst. Growth 22, 175, 1974.

16 J B Loyan, M Oberlin, A Oberlin, L Hollan, R Cadoret : J. Cryst. Growth 29, 176, 1975.

17 R Cadoret, L Hollan, J B Loyau, M Oberlin, A Oberlin : J. Cryst. Growth 29, 187, 1975.

18 B Joyce : J. Cryst. Growth : 3,4, 43, 1968.

19 L G Lavrentyeva, Yu G Kataer, V A Moskovkin, M P Yakubenya : Kristall und Technik, 6, 607, 1971.

20 L Hollan : 5th Intern. Symp on GaAs and Related Compounds, Deauville, 1974.

21 R Cadoret, M Cadoret : J. Cryst. Growth 31, 142, 1975.

22 R Cadoret : Chap 2 in 'Current Topics in Materials Science' Volume 5, Ed. E Kaldis, North-Holland, Amsterdam, 1980.

23 M Ihara, K Dayai, D Ryuzan : J. Appl. Phys. 45, 528, 1974.

24 O Mizuno, H Watanabe : J. Crystal Growth 30, 240, 1975.

25 M M Faktor, I Garrett, M H Lyons, R H Moss : J. Chem. Soc. Far. Trans. I, 73, 1446, 1977.

26 D Battat, M M Faktor, I Garrett, R H Moss : J. Chem. Soc. Far. Trans. I, 70, 2302, 1974.

27 J J Murray, C Pupp, R F Pottie : J. Chem. Phys. 58, 2569, 1973.

CHAPTER 5: GROWTH OF InP

The growth of InP was investigated as the first stage of a project designed to develop a vapour phase system for the growth of the quaternary $Ga_xIn_{1-x}As_yP_{1-y}$. Thermodynamic calculations [1-8] showed that at typical growth temps the reaction of HCl with InP had a larger equilibrium constant than GaAs, InAs or GaP. Consequently, InP was the most difficult of the species to deposit, requiring higher reactant pressures. Once a suitable growth regime for InP was established, extension of the method to the ternary compounds and the quaternary was readily achieved.

The most common system for the vapour phase growth of InP involves the use of a liquid indium source over which PCl_3 vapour is passed [9,10]. The system is similar to the Effer-Minden process for GaAs [11] and has been shown to give good epitaxial layers [12]. However, this method cannot easily be extended to produce ternary and quaternary layers. In order to control fully the composition of the quaternary it is essential that the Ga:In and As:P ratios in the vapour phase can be varied independently. The simplest way to do this is to introduce the group III and group V elements separately.

The choice of transporting agent for the group III elements was straightforward. The reactions of HCl with both In and Ga are known to be extreme at 800°C and higher [13]; thus the pressure of the metal chlorides could be easily controlled by varying the input pressure of HCl. However, there were several possible ways to introduce the As and P: vapourisation of the elements, thermal decomposition of the hybrids (AsH_3 or PH_3) and reduction of the trichlorides. The use of the elemental forms was rejected because of the slow and irreversible kinetics of vapourisation [14,15]. Thermal

decomposition of the hydrides is used by several groups to produce both ternary and quaternary compounds [16,17]: Although the reported results have been encouraging this method was also rejected because of the slowness of the decomposition reactions [18] which could lead to irreproducibility and inhomogeneity in the grown layers. In contrast the reduction by hydrogen of both PCl_3 and $AsCl_3$ is very rapid at growth temperatures, allowing close control of the arsenic and phosphorus pressures in the growth zone.

5.1 Model Systems

In this section, the proposed growth system is discussed using firstly a thermodynamic model, and then a transport-limited growth model. Although the treatments use standard equations, their application to this system is novel. The calculations are discussed in some detail as they form the foundation for later calculations on the more complex ternary and quaternary systems and some of the findings are equally valid for these systems.

5.1.1 Thermodynamic Model

A consideration of the equilibrium conditions showed that growth of InP could only occur in a very narrow range of input pressures. For simplicity only one deposition reaction was considered:

$$InP_{(s)} + HCl_{(g)} \rightleftharpoons InCl_{(g)} + \tfrac{1}{4}P_{4(g)} + \tfrac{1}{2}H_{2(g)} \qquad \ldots\ldots (1)$$

[Other species, particularly $InCl_2$ [19] and P_2 [18] are important minority species at the growth temperature ($\sim 650^{\circ}C$). However, the argument is not altered by the exclusion of these species]. The equilibrium constant for this reaction is:

$$K^{o}_{InP} = \frac{P^{o}_{InCl}\, P^{o\frac{1}{4}}_{P_4}\, P^{o\frac{1}{2}}_{H_2}}{P^{o}_{HCl}} \qquad \ldots\ldots (2)$$

where p_i^o is an equilibrium pressure of species i. For a growth system with input pressures p_i, a partial pressure product K^*_{InP} may be defined:

$$K^*_{InP} = \frac{P_{InCl}\ P_{P_4}^{\frac{1}{4}}\ P_{H_2}^{\frac{1}{2}}}{P_{HCl}} \qquad \ldots\ldots 3$$

Growth occurs where $K^*_{InP} > K^o_{InP}$.

Let the pressure of HCl passing over the metal boat be ε. Since the reaction is extreme, the pressure of InCl passing into the reaction chamber will also be ε and allowing for the dilution effects of other gas flows into the reaction chamber, this gives

$$P_{InCl} = \frac{f_1}{F}\ \varepsilon$$

where f_1 is the gas flow over the source boat, and F the total flow of gas into the reaction chamber. Similarly, let the input pressure of PCl_3 be η. In the reaction chamber the PCl_3 is reduced to P_4 and HCl:

$$PCl_3 \rightleftharpoons \tfrac{1}{4}\ P_4 + 3\ HCl \qquad \ldots\ldots 4$$

Hence

$$P_{P_4} = \eta/4 \qquad \ldots\ldots 5$$

and

$$P_{HCl} = 3\eta \qquad \ldots\ldots 6$$

Substituting in equation 3 gives

$$K^{*}_{InP} = \frac{f_1}{F}\,\frac{\varepsilon}{3\eta}\cdot\frac{\eta^{\frac{1}{4}}}{\sqrt{2}}\;P^{\frac{1}{2}}_{H_2} \qquad \ldots\ldots 7$$

In most practical systems $p^{\frac{1}{2}}_{H_2} \simeq 1$, so the condition for growth becomes

$$\frac{f_1}{3\sqrt{2}F}\,\frac{\varepsilon}{\eta^{\frac{1}{4}}} > K^{o}_{InP} \qquad \ldots\ldots 8$$

Equation 8 showed that, as might be expected, increasing the pressure of HCl(ε) over the metal source (and hence the pressure of InCl) increased the supersaturation for growth. However, an increase in PCl_3 pressure (η) caused a decrease in supersaturation due to the large amount of HCl produced in reaction 4. Clearly, there was a critical value of η, above which etching would occur, and conversely, decreasing the PCl_3 pressure caused an increase in the supersaturation, with the result that as η tended to zero, so K^{*} became infinite. This result emphasises the inadequacy of growth rate theories in which the growth rate is assumed to be proportional to the supersaturation since for this system the assumption would lead to the prediction of huge growth rates in the absence of one of the reactants!

A minor refinement to the thermodynamic model ensured that the supersaturation tended to zero as the pressure of PCl_3 approached zero. However, to obtain more realistic estimates of the growth condition for maximum growth rate, the thermodynamic model was

abandoned in favour of a growth model which included the gas transport processes. This model is described in the next section, after a brief description of the refined thermodynamic model.

In deriving equations 7 and 8 it was assumed that all the HCl passing over the metal source was converted to InCl. In reality, a small amount of HCl will always remain unconverted. This may be estimated from the equilibrium constant for the reaction

$$In_{(\ell)} + HCl_{(g)} \rightleftharpoons InCl_{(g)} + \tfrac{1}{2} H_{2(g)} \qquad \ldots\ldots 9$$

$$K^{o}_{In} = \frac{P_{InCl}\, P^{\frac{1}{2}}_{H_2}}{P_{HCl}} \qquad \ldots\ldots 10$$

Under typical experimental conditions, $K^{o}_{In} >> 1$ and the pressure of InCl (p_{InCl}) may be taken to be ε (the input pressure of HCl) with negligible error. The equilibrium pressure of HCl is then:

$$P_{HCl} = \frac{\varepsilon(1-\varepsilon)^{\frac{1}{2}}}{K^{o}_{In}} \qquad \ldots\ldots 11$$

Using thermodynamic data from a variety of sources [1-8], K^{o}_{In} was estimated to be ~ 210 at 800°C. An input pressure of 0.1 atm HCl gave $p_{HCl} \approx 4.5 \times 10^{-4}$ atm at equilibrium.

Inclusion of this unconverted HCl in the equation for K^* gave

$$K^*_{InP} = \frac{f_1}{\sqrt{2}F} \frac{\epsilon\eta^{\frac{1}{4}}}{3\eta + \frac{f_1}{F} p_{HCl}} \quad \ldots\ldots 12$$

where, as before, $p_{H_2}^{\frac{1}{2}} \sim 1$. When $3\eta >> \frac{f_1}{F} p_{HCl}$, equation 12 simplifies to equation 7. However, if the input pressure of PCl_3 is very small, then equation 12 becomes

$$K^*_{InP} \sim \frac{\epsilon\eta^{\frac{1}{4}}}{p_{HCl}} \quad \ldots\ldots 13$$

The variation of K^*_{InP} with PCl_3 pressure is shown in fig 1. A horizontal line drawn on this curve and representing the value of the equilibrium constant at a particular temperature, will cross the curve at two points. There is clearly a range of PCl_3 pressures in which growth is possible. Outside this range the substrate will be etched by the passing gas. However, unless the value of the equilibrium constant is very close to the maximum value of K^*, only the upper PCl_3 pressure limit is of practical importance.

5.1.2 A Growth Model derived from the Theory of Gas Transport.

Thermodynamic calculations can only indicate the conditions under which growth is possible. To estimate growth rates it is necessary to consider both the rates of reactions on the substrate surface (surface kinetics) and the rate of transport of the reactants through the gas phase. These are sequential processes

Fig 5-1

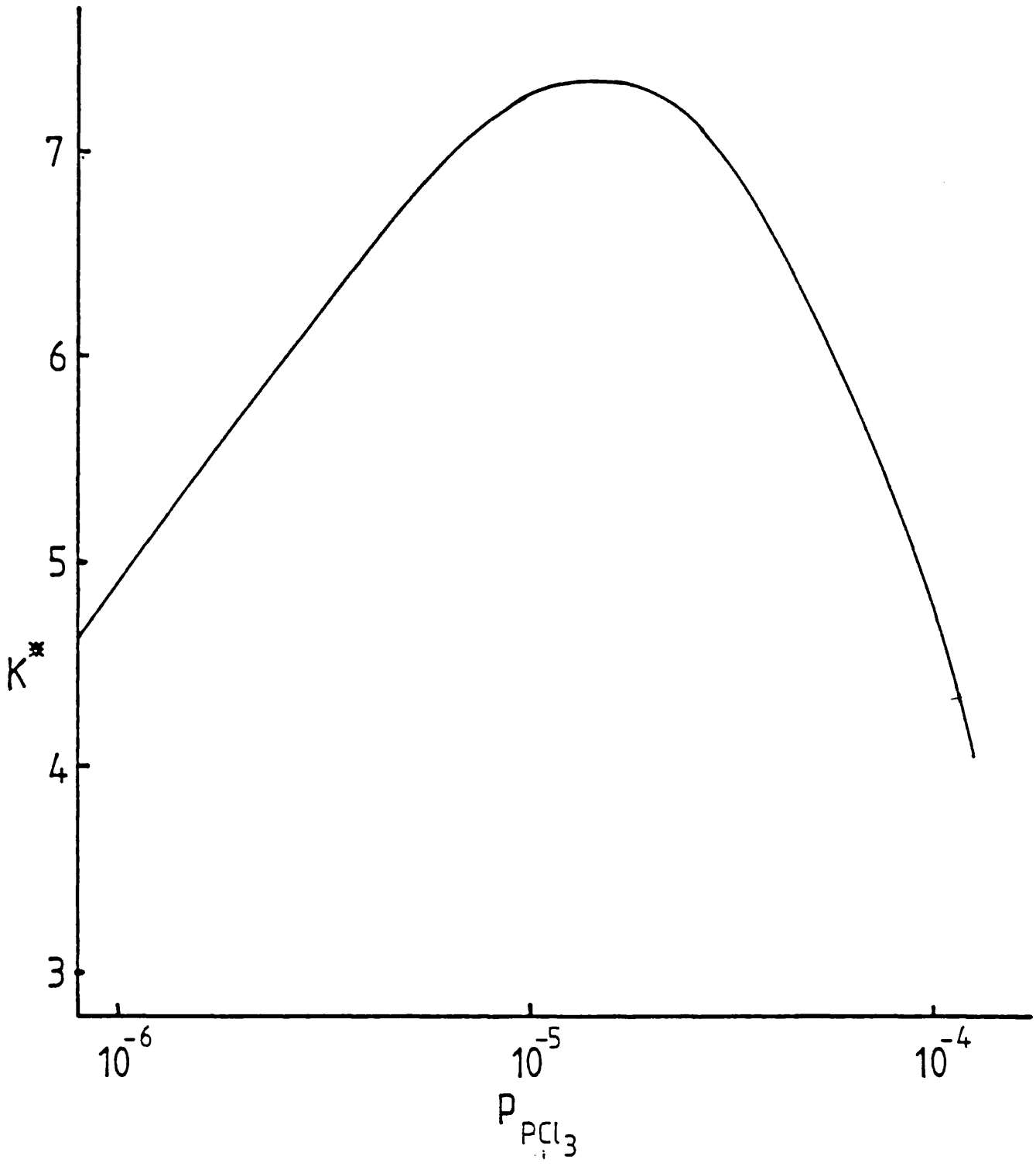

Variation of K^* with pressure of PCl_3

and disentangling the two for a real system is difficult. In this section equations are derived describing the gas-transport processes. By making assumptions about the rate of the surface processes, it is possible to calculate growth rates.

The equation for growth is taken to be that given by equation 1

$$InP_{(s)} + HCl_{(g)} \rightleftharpoons InCl_{(g)} + \tfrac{1}{4}P_{4(g)} + \tfrac{1}{2}H_{2(g)} \qquad \ldots\ldots 1$$

For each gas species an equation for the flux of that species can be written in terms of the transport rate (J) of InP [20]. Thus

$$J_{InCl} = J = \frac{U P_{InCl}}{RT} - \frac{D}{RT}\frac{dp_{InCl}}{dx} \qquad \ldots\ldots 14$$

$$J_{P_4} = \tfrac{1}{4}J = \frac{U p_{P_4}}{RT} - \frac{D}{RT}\frac{dp_{P_4}}{dx} \qquad \ldots\ldots 15$$

$$J_{HCl} = -J = \frac{U P_{HCl}}{RT} - \frac{D}{RT}\frac{dp_{HCl}}{dx} \qquad \ldots\ldots 16$$

$$J_{H_2} = \tfrac{1}{2}J = \frac{U p_{H_2}}{RT} - \frac{D}{RT}\frac{dp_{H_2}}{dx} \qquad \ldots\ldots 17$$

For simplicity, the same diffusion constant - D - has been assumed for all species. Also, since hydrogen is present in excess its pressure may be assumed to be $\simeq 1$ at all points. Nevertheless the transport of hydrogen (equation 17) must be included at this stage in order to obtain a correct value for the Stefan flow velocity (U). Summing equations 14-17 and rearranging gives:

$$U = \tfrac{3}{2}\frac{JRT}{DP} \qquad \ldots\ldots 18$$

where P = total pressure (= 1 atm in the growth apparatus).

Substituting for U in each of equations (14-16):-

$$J = \frac{3}{4} J \frac{P_{InCl}}{P} - \frac{D}{RT} \frac{dp_{InCl}}{dx} \qquad \ldots\ldots 19$$

$$\tfrac{1}{4}J = \tfrac{3}{4}J \frac{P_{P_4}}{P} - \frac{D}{RT} \frac{dp_{P_4}}{dx} \qquad \ldots\ldots 20$$

$$-J = \tfrac{3}{4}J \frac{P_{JCl}}{P} - \frac{D}{RT} \frac{dp_{HCl}}{dx} \qquad \ldots\ldots 21$$

Each of these equations may be solved by rearranging and integrating between the limits x = 0, the surface of the growing solid, and x = ℓ, a point in space which is considered to be the source of the transporting species. Physically, this latter point may represent an actual source or an equivalent point such as the edge of a boundary layer. The calculation is carried out in detail for InCl, but the results for the other species are merely quoted.

Rearranging 19:-

$$-JRT \left[P - \tfrac{3}{4} p_{InCl}\right] = -DP \frac{dp_{InCl}}{dx}$$

Integrating:-

$$\int_0^{\ell} -\frac{JRT}{DP}\, dx = \int_{p_{InCl}^{(o)}}^{p_{InCl}^{(\ell)}} \frac{dp_{InCl}}{(P - \frac{3}{4}p_{InCl})}$$

$$\therefore \; -\frac{JRT\ell}{DP} = \left[-\frac{4}{3} \ln (P - \tfrac{3}{4}p_{InCl}(x))\right]_{p_{InCl}^{(o)}}^{p_{InCl}^{(\ell)}}$$

Let $\xi = \frac{3}{4} \frac{JRT\ell}{DP}$ 22

Then

$$-\xi = \ln \frac{[P - \frac{3}{4} p_{InCl}(o)]}{[P - \frac{3}{4} p_{InCl}(\ell)]}$$

$$p_{InCl}(o) = \frac{4}{3} P - [\frac{4}{3} P - p_{InCl}(\ell)] \exp(-\xi) \quad \ldots\ldots 23$$

Equation 22 provides a relationship between the bulk and interfacial pressures of InCl, and the growth rate. Similar relationships can be obtained for the other gas-phase species. In systems of experimental interest, in which P = 1, and the input pressures of the reactants ($\frac{f_1}{F}\varepsilon$, and η) are $\ll 1$, then $\xi \ll 1$ and equation 22 may be simplified by the approximation $\exp(-\xi) \simeq 1 - \xi$.

Substituting the bulk pressure of InCl ($\frac{f_1}{F}\varepsilon$) for $p_{InCl}(\ell)$ gives

$$p_{InCl}(o) = \frac{f_1}{F}\varepsilon + \frac{4}{3}\xi \quad \ldots\ldots 24$$

Note that the way the fluxes in equations (14-17) were defined means that for growth, ξ will be negative.

Similar calculations for P_4 and HCl give

$$p_{P_4}(o) = {}^{P}/_{3} - [{}^{P}/_{3} - p_{P_4}(\ell)] \exp(-\xi) \quad \ldots\ldots 25$$

and

$$p_{HCl}(o) = \frac{4}{3} P - [\frac{4}{3} P - p_{HCl}(\ell)] \exp \xi \quad \ldots\ldots 26$$

Simplifying as above and using the same notation as in the discussion of the thermodynamic model, the equations become:

$$p_{P_4}(o) = \frac{\eta}{4} + \frac{\xi}{3} \quad \ldots\ldots 27$$

and

$$p_{HCl}(o) = 3\eta - \frac{4}{3} \xi \quad \ldots\ldots 28$$

(or, if the HCl introduced with the InCl is included,

$$p_{HCl}(o) = 3\eta + p'_{HCl} - \frac{4}{3} \xi \quad \ldots\ldots 28a$$

where p'_{HCl} is defined by equation 11).

It is important to note that so far, no assumption has been made concerning the relationship of the interfacial pressures to the equilibrium constant. Equations (23-28) apply both to equilibrium and non-equilibrium systems. It has already been shown in Chapter 4 how the surface kinetics may be combined with this transport model. The surface processes of the InP/HCl system are even less understood than those of the GaAs/HCl system. In the

absence of any reliable kinetic data, the limiting case was calculated in which the interfacial pressures are assumed to satisfy the equilibrium constant. This is equivalent to the assumption that the growth rate (J) is very small compared to the rate of the surface reactions (the exchange current $-J^{o}$). Substitution of equations 24, 27 and 28 in the expression for the equilibrium constant gives

$$K^{o}_{InP} = \frac{P_{InCl}\, P_{P_4}^{\frac{1}{4}}\, P_{H_2}^{\frac{1}{2}}}{P_{HCl}} = \frac{(\frac{f_1}{F}\varepsilon + \frac{4}{3}\xi)(\frac{\eta}{4} + \frac{\xi}{3})^{\frac{1}{4}}}{(3\eta - \frac{4}{3}\xi)} \quad \ldots\ldots 29$$

This is a polynomial in ξ which may readily solved by iterative methods.

In theory it is possible to convert the dimensionless transport function (ξ) into a measureable growth rate (mg h^{-1} cm^{-2} or $\mu m\ h^{-1}\ cm^{-2}$) using the definition (equation 22):

$$\xi = \frac{3}{4}\ \frac{JRT\ell}{DP}$$

The main difficulty arises in the choice of a suitable value of ℓ - the distance over which transport occurs. For a substrate lying horizontally, a value of about 1 cm has been used [21]. In the present system substrates are supported vertically so that the original hydrodynamic argument no longer applies. However, the change from a horizontal to vertical substrate was not found to cause significant change in growth rate [22], showing that the boundary layer thickness was not significantly different. Using, therefore, a value of 1 cm for ℓ growth rates were calculated from 29 and are plotted in fig 2 as a function of PCl_3 pressure (η).

Fig 5-2

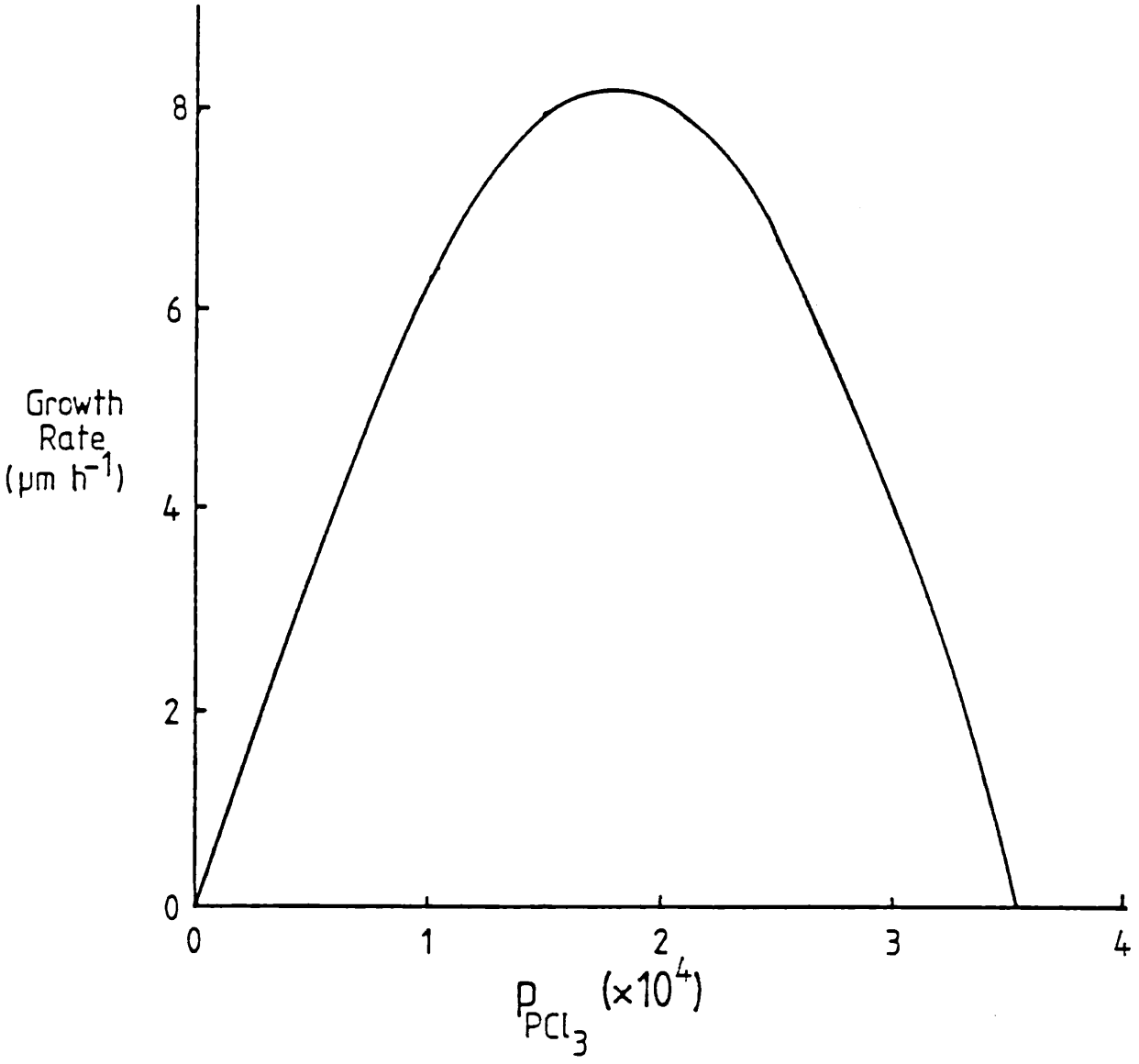

Calculated growth rate vs. pressure of PCl_3

Although the calculated growth rates are unlikely to be precise, they do indicate the likely order of magnitude. The curve was calculated for a system with $p_{InCl} = 2.46 \times 10^{-2}$ (typical of the early growth experiments) and $K^{o}_{InP} = 2.03$ at 600°C (estimated from thermodynamic data [1-8]). Inclusion of the small amount of HCl introduced with the InCl did not alter the curve shown in fig 2. Two regions may be distinguished;at high PCl_3 pressures, growth rate decreases with increasing values of η. This was predicted from the thermodynamics and is a consequence of the reduction in supersaturation. However, at low PCl_3 pressures, growth rate is proportional to η. Maximum growth rate occurred with the pressure of PCl_3 about 1.8×10^{-4} atom. The contrast between transport and thermodynamics is shown in fig 3 in which both growth rate and supersaturation are shown as functions of PCl_3 pressure. It can be seen that the maximum supersaturation is obtained with a PCl_3 pressure of 1.3×10^{-5} atm - over an order of magnitude lower than the PCl_3 pressure corresponding to maximum growth rate.

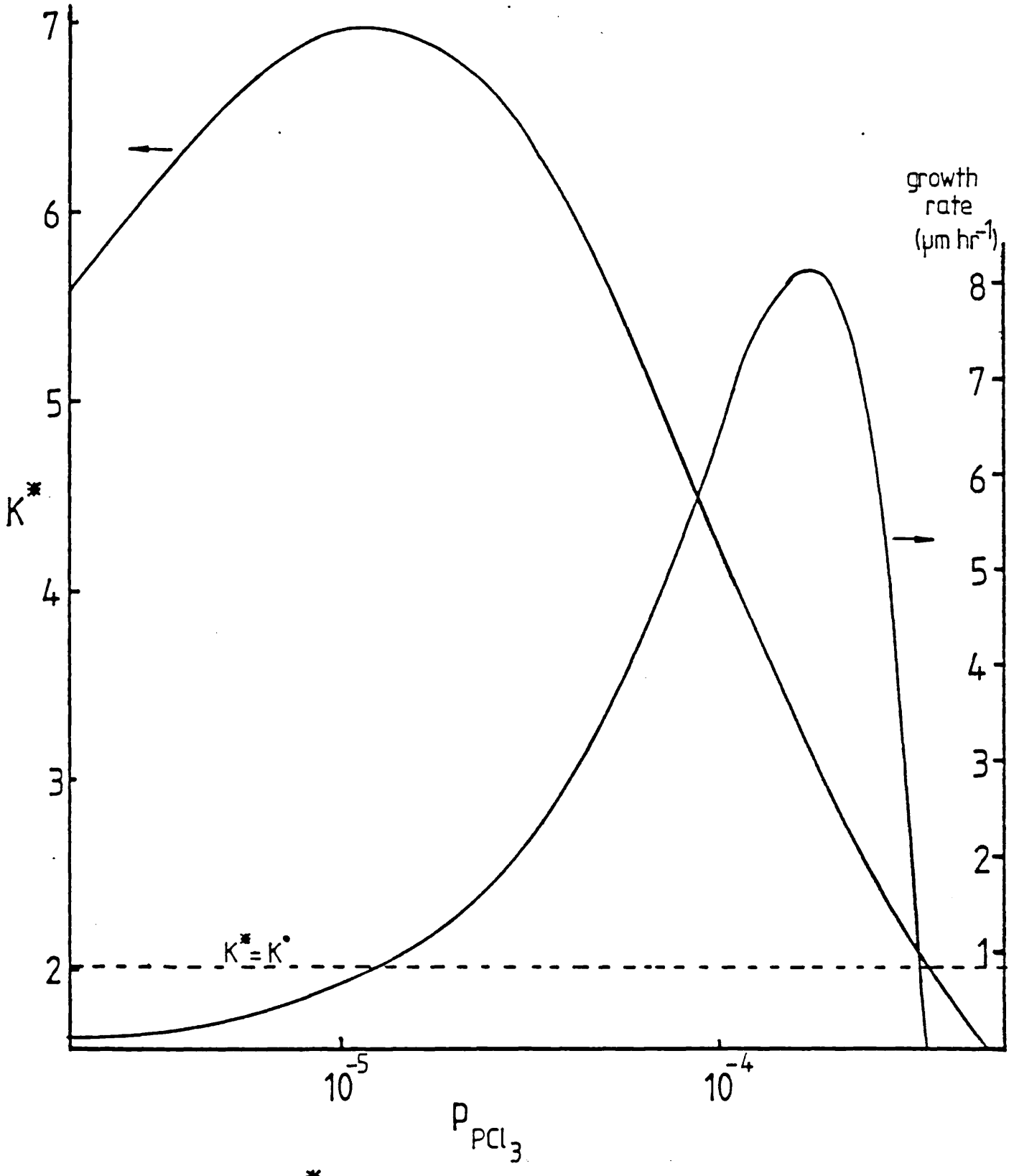

Comparison of K^* & Growth Rate as functions of P_{PCl_3}

5.2 Experimental

5.2.1 Materials

Hydrogen chloride gas was obtained from a cylinder supplied by BOC. Early experiments used a mixture of 10% HCl in hydrogen; later work involved 100% HCl.

Phosphorus trichloride was supplied by MCP (electronic grade - 99.99% nominal purity). The vapour was introduced into the system by bubbling hydrogen through the liquid. The bubbler arrangement is shown in fig 4. This was immersed in a water/ antifreeze bath, the temperature of which could be controlled at temperatures between -11^{o} and $80^{o}C$ using a Grant Instruments water cooler. Input pressure of PCl_3 was controlled by varying the flow rate of hydrogen through the bubbler, or by changing the temperature of the water bath.

Hydrogen was supplied from cylinders (BOC) and purified using a Johnson-Matthey hydrogen purifier.

Indium phosphide substrates were supplied by Metals Research Ltd. All substrates used in this work were Sn-doped ($n^{+} \approx 10^{18}$ cm^{-3}) and supplied ready polished. The surface orientation was 2^{o} off - orientation (100)→ (111). Substrates were prepared by a free etch in 1% bromine-methanol solution immediately prior to use.

Indium metal was obtained from MCP (99.9999% purity).

Fig 5-4

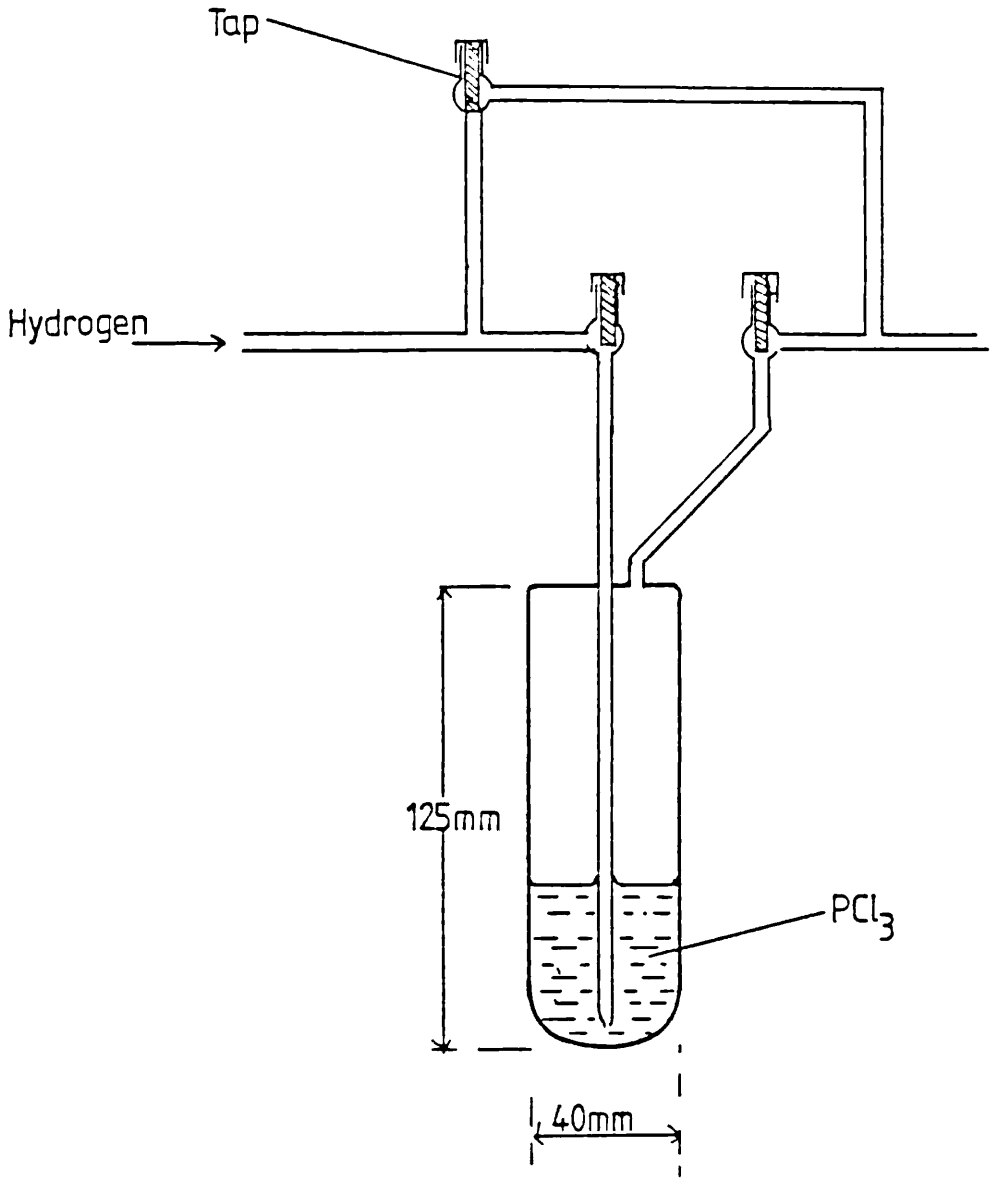

PCl_3 Bubbler showing by-pass arrangement

5.2.2 Apparatus

The final form of the apparatus is shown in fig 5. The furnace tube was made of high purity silica while input lines were stainless steel or pyrex. Gas flows through the input lines were controlled by needle valves and monitored by 'Brooks' flow meters.

The two main input lines carried HCl (in hydrogen) and PCl_3 into the reaction zone. A third line allowed hydrogen to be passed through the annular space between the furnace tube and a removeable dump tube, thus keeping this region free from deposit. In order to maximise the efficiency of the InCl source, the HCl flow was split before passing over two separate vitreous carbon boats containing In metal at 800°C. After the reaction, the InCl vapour passed through a series of baffles where it was thoroughly mixed with the PCl_3. The gas then passed over the InP substrates which were supported vertically, at 1 cm intervals, by a silica rack. This rack was placed in a silica dump tube and positioned in a region where the temperature profile decreased at about $3Kcm^{-1}$. The temperature of the hottest substrate was, in most experiments, $\sim$ 660°C although in some early experiments it was $\sim$ 60°C cooler. At these temperatures, incongruent evaporation of phosphorus can occur with damage to the surface and poor growth morphology. To minimise this, it was standard practice to allow the furnace to reach temperature in a position clear of the substrates, and to roll it into the final position just prior to growth.

Fig 5-5

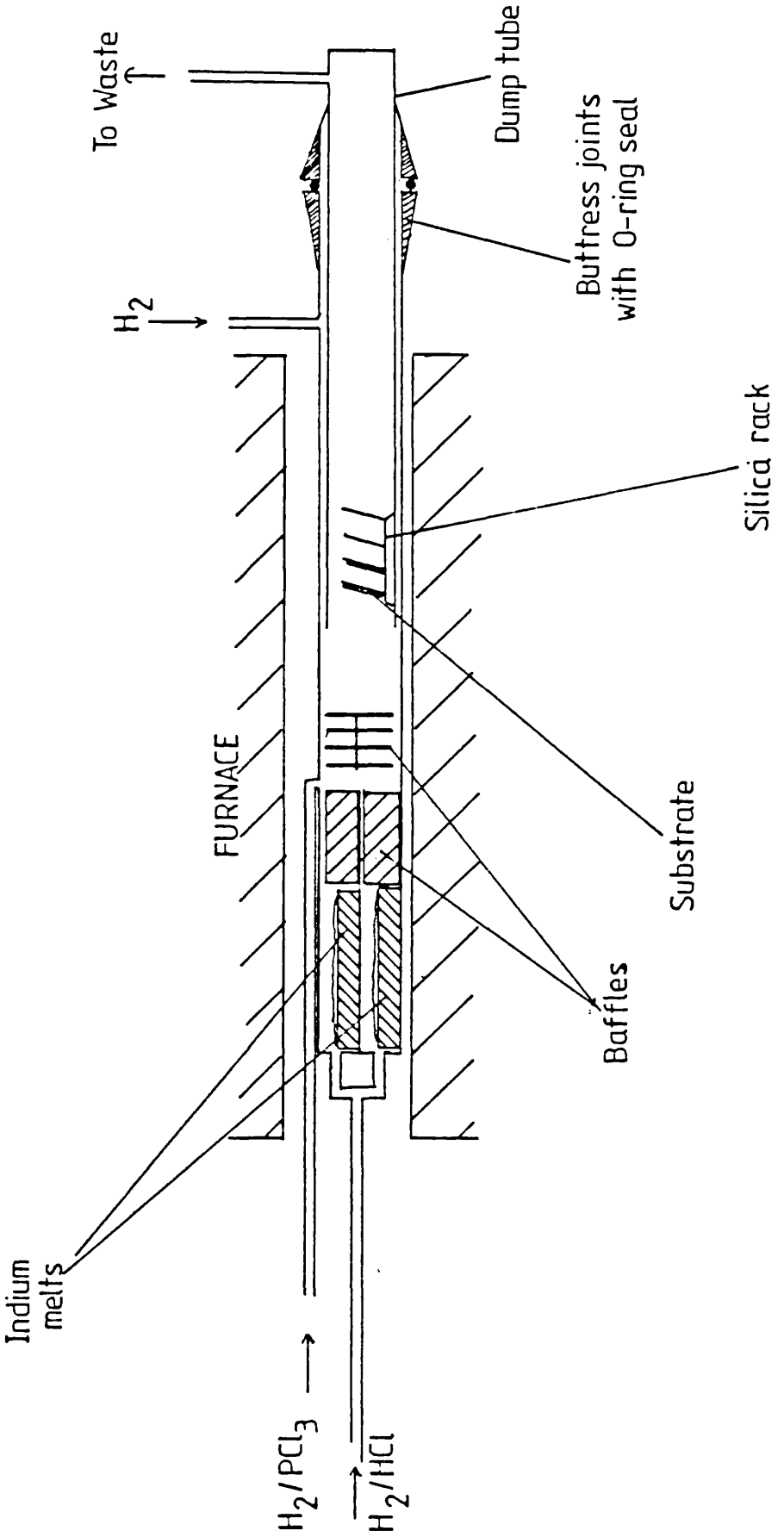

Diagram of growth apparatus

Because there is only a limited range of conditions in which growth can occur in this system, it was important to measure both growth and etch rates. Consequently, all substrates were weighed before and after each experiment.

5.3 Results

The earliest experiments were carried out using a mixture of 10% HCl in hydrogen. After dilution by the PCl_3 and dump-tube purge lines, this gave a maximum InCl pressure of $\sim 3 - 5 \times 10^{-2}$ atm in the growth zone. The calculations described above (section 5.1) indicated that a supersaturation for growth could readily be achieved. In practice the change in weight of a substrate during a 5h experiment at $\sim 650^{o}C$ was either negligible, or showed a very small loss. This result suggested the experimental conditions were close to equilibrium. Failure to achieve supersaturation could have two causes: The first possible cause of error was inaccuracies in the thermodynamic data. For example an error of ~ 4.5 kcal mol^{-1} in the free energy of reaction would represent an order of magnitude error in the equilibrium constant: Secondly, the neglect of other species eg P_2 and $InCl_2$, could also account for the absence of a supersaturation for growth. To overcome this problem, the growth temperature was dropped to $600^{o}C$. The calculation described in section 2 gave a maximum estimated growth rate of ~ 8 μm h^{-1} assuming a transport distance -ℓ- of ~ 1 cm. Even allowing for a reduction in supersaturation, there should still have been a detectable growth rate. In practice, the results were the same as for growth at $650^{o}C$.

In view of these results, a second source of trouble was investigated: the efficiency of the source. The importance of this is demonstrated in fig 6 in which the partial pressure product (K^{*}) is plotted as a function of PCl_3 pressure. Two curves are shown: the upper curve is for an 100% efficient source, and is identical therefore, to fig 1.

Fig 5-6

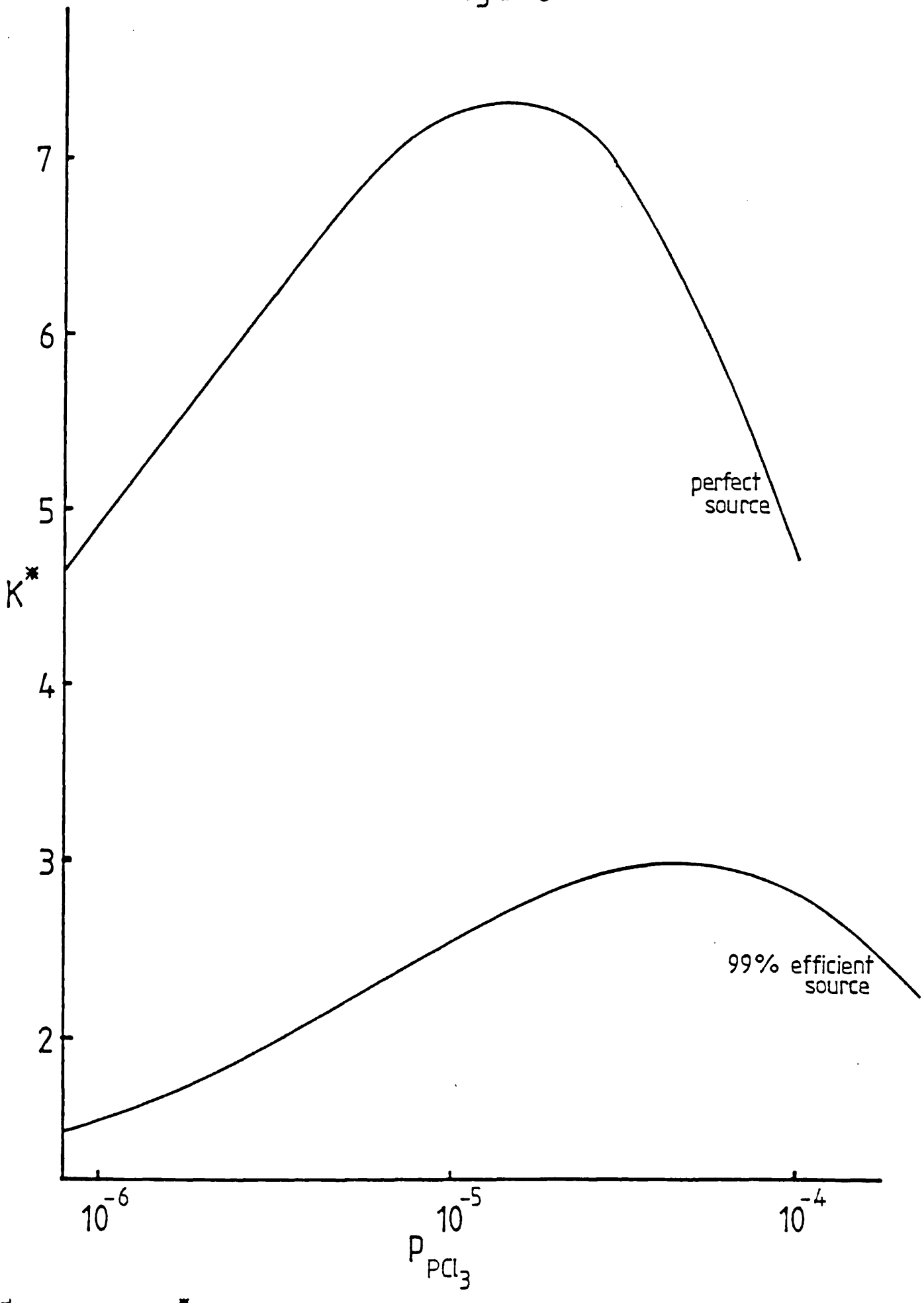

K^* vs. p_{PCl_3} showing effect of inefficient In source

The lower curve was calculated on the assumption that only 99% of the input HCl came to equilibrium with the metal source. It can be seen that this small loss of source efficiency caused a very significant reduction in the value of K^* and hence in the supersaturation. Indeed, in some cases it is clear that source inefficiency can cause a change from growth to etching conditions.

Although no absolute measurement of source efficiency was available, the effect of any change designed to improve efficiency could be readily assessed by weighing the melt before and after each experiment and hence measuring the amount of HCl transported. The changes introduced concentrated on two aspects. The most important factor affecting source efficiency was the residence time - the time the gas was in contact with the melt. It has been reported that for maximum source efficiency, the residence time should be at least 2 sec [23]. Residence time may be increased by reducing the flow rate over the melt, increasing the gas volume above the melt and by increasing the length of the melt. However, all of these methods are limited by practical considerations: thus, the flow rate must be sufficient to maintain the pressure of InCl in the reaction zone. A limit to the volume above the melt is imposed both by the size of the apparatus and by the need to ensure there is no dead space where gas may pass without coming into contact with the melt. Finally, the length of the melt is limited by the length of the high temperature zone ie by the characteristics of the furnace. The final experimental arrangement is shown in fig 5. To ensure a slow flow rate over the source, yet maintain the total flow of InCl into the deposition region, the input

flow of HCl was split and passed over two separate source boats. These were made of vitreous carbon, were 12.5 cm long (the maximum length possible) and had a semi-circular cross-section. The source chambers were made of silica tubing chosen to be a close fit, thus eliminating any dead space at the sides of the boats. A baffle at the down-stream end of the source chamber prevented the other reactants reaching the melts by back-diffusion.

Despite the changes made to the source boats, there was still no significant weight change during an experiment. Occasionally the silica upstream of the substrates had a grey deposit which appeared to be Indium. This suggested that the failure to grow might be due to the absence of sufficient PCl_3. To test this a series of experiments were carried out in which the indium pressure, source and substrate temperatures were kept constant and the PCl_3 pressure varied. The results are shown in fig 7 (table 1), normalised for a substrate weighing 100 mg. Since all the substrates involved were cleaved from the same sample slice, the weight was proportional to the area. At the highest PCl_3 pressure (2.64×10^{-3} atm) the weight loss was very rapid (-27.03 mg h^{-1}). Decreasing the PCl_3 pressure reduced this etch rate and at PCl_3 pressuresbelow $\sim$ $8\text{-}9 \times 10^{-4}$ atm growth occurred. However, the growth rates were very small. Examination of fig 7 showed that the maximum growth rate (at a PCl_3 pressure of about 6×10^{-4}atm) was unlikely to exceed 0.2 mg h^{-1}. It was also possible to estimate the value of K^o from the conditions for zero growth. This gave $K^o = 0.7$.

The very low growth rate was plainly unacceptable. Although the InCl pressure might be raised to some extent by increasing the input flow of HCl, this would lead to a reduction in source efficiency. In order to

TABLE 5.1

Run	P_{PCl_3}	Growth rate (mg h^{-1})
CK8	2.64×10^{-3}	-27.03
CK9	1.35×10^{-3}	-2.01
CK10	8.99×10^{-4}	-0.25
CK11	6.96×10^{-4}	+0.089
CK12	4.36×10^{-4}	+0.045

Experimental growth rates with the corresponding PCl_3 pressures.

Fig 5-7

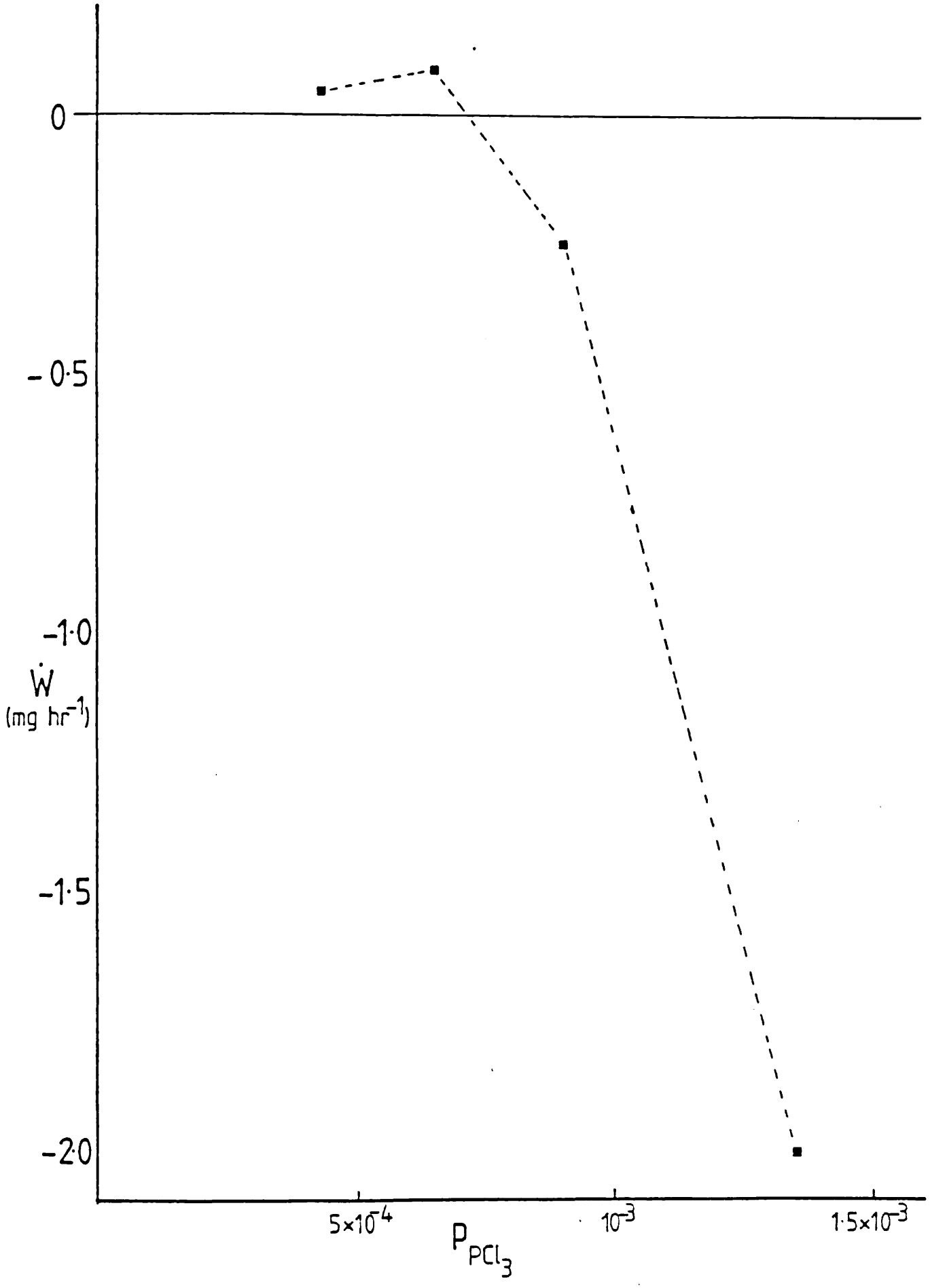

Experimental variation of growth rate vs. p_{PCl_3}

achieve a significant increase in growth rate it was necessary to increase the input pressure of HCl over the indium source. Consequently, the HCl supply was altered. Pure HCl was obtained from a cylinder. This was diluted with hydrogen to give a mixture containing $\sim$ 33% HCl. The results were immediate, with a growth rate of 2-2.5 $\mu m\ h^{-1}$. This was reduced to 1.5 - 2.0 $\mu m\ h^{-1}$ on raising the substrate temperature to 650°C.

Having demonstrated the feasibility of growing InP by CVT, there was no attempt made to achieve the control over morphology and doping-level which is necessary for device applications. The major cause of poor morphology appeared to be loss of phosphorus from the substrate due to incongruent evaporation during the warm-up period. This had been reduced by the delay in rolling the furnace into the position for growth. However, it was found that after moving the furnace into position, overheating occurred so that the substrate was subjected to temperatures as high as 700°C. A change in the position of the control thermocouple reduced this overshoot to $\sim$ 5°C with a corresponding improvement in surface quality. The improvement in morphology is shown in figs 8 and 9, which show, respectively, layers grown before and after the overshoot in temperature was eliminated.

Fig 5-8

Photograph of InP layer before elimination of temperature overshoot

Fig 5-9

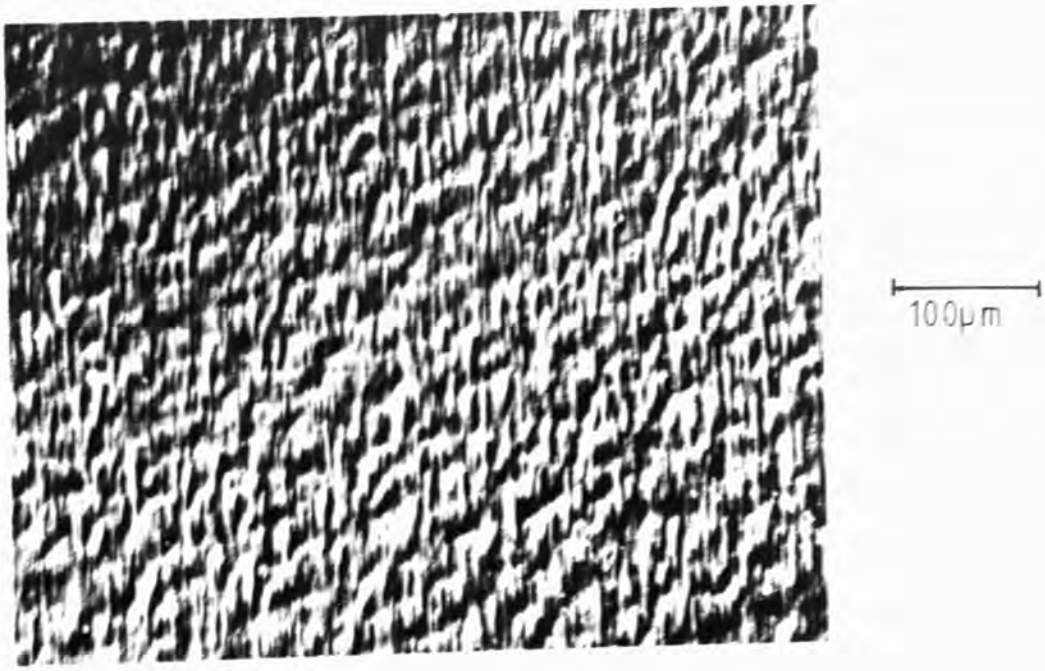

InP layer after elimination of overshoot

5.4 Conclusion

This work demonstrated the ability to grow InP. Although the epitaxial layers produced were not of device quality (in terms of layer morphology and electrical properties), sufficient experiments were performed to indicate that these problems were not insurmountable. Since the ultimate goal was to produce $Ga_xIn_{1-x}As_yP_{1-y}$ layers, attention was now turned to the next stage - the growth of the mixed compound $Ga_xIn_{1-x}As$.

REFERENCES

1 S. Martosudirdjo, J.N. Pratt: Thermochimica Acta, 10, 23, 1974.

2 J.B. Mullin, D.T.J. Hurle: J. Luminescence 7, 176, 1973.

3 D.W. Shaw: J. Phys. Chem. Solids, 36, 111, 1975.

4 JANAF Thermochemical Tables, 2nd Edition: Eds. D.R. Stull, H. Prophet, Nat. Bur. Standards, 1971.

5 M.B. Panish, J.R. Arthur: J. Chem. Thermodynamics 2, 299, 1970.

6 K.J. Bachman, E. Buehler: J. Electrochem. Soc. 121, 835, 1974.

7 R.F.C Farrow: J.Phys. D: Appl. Phys. 7, 2436, 1974.

8 U. Piesbergen: Z. Naturforshung 18a, 141, 1963.

9 R.C. Clarke: Inst. Phys. Conf. Ser. No 45, 19, 1979.

10 H. Seki, M. Kinoshita: Jap. J. Appl. Phys. 8, 500, 1969.

11 J.R. Knight, D.Effer, P.R. Evans: Solid State Electron. 8, 178, 1965.

12 R.C. Clark: J. Cryst. Growth 54, 88, 1981.

13 V.S. Ban: J. Cryst. Growth 17, 19, 1972.

14 See Chapter 3

15 G.M. Rosenblatt, P-K Lee: J. Chem. Phys. 49, 2995, 1968.

16 J.J. Tietjen, R.E. Enstrom, D. Richman: RCA Rev. 31, 635, 1970.

17 G.H. Olsen, T.J. Zamerowski: Prog. Cryst. Growth Charact. 2, 309, 1979

18 V.S. Ban: J. Cryst. Growth 17, 19, 1972.

19 E.J. Tarbox: Ph.D Thesis, London University, 1977

20 D. Battat, M.M. Faktor, I. Garrett, R.H. Moss: J. Chem. Soc. For. Trans I, 70, 2302, 1974.

21 M.M. Faktor, I. Garrett: 'Growth of Crystals from the Vapour', Chapman and Hall, London, 1974.

22 A.K. Chatterjee: Private Communication

23 A.G. Sigai, C.J. Nuese, R.E. Enstrom, T.J. Zamerowski: J. Electrochem. Soc 120, 947, 1973.

CHAPTER SIX: GROWTH OF MIXED III-V COMPOUNDS: THEORY

The mixed III-V compounds, particularly $Ga_xIn_{1-x}As$ and $Ga_xIn_{1-x}As_yP_{1-y}$, are becoming increasingly important for the production of photodetectors and lasers for use in optical communications systems [1,2]. Several techniques have been used to grow epitaxial layers of these materials: LPE [2,3], CVT [4,5], MBE [6] and MOCVD (metal-organic chemical vapour deposition) [7,8]. The most important CVT approach has involved passage of HCl over indium melts with the introduction of arsenic as arsine and phosphorus as phosphine [5]. Both arsine and phosphine decompose slowly, leading to irreproducibility in the gas-phase at the substrate and hence, in the layer. The aim of this work was to develop a growth system which did not involve the hydrides, thus obtaining better control of the composition of the growing layers.

One alternative method for the ternary compound involved passing $AsCl_3$ over separate gallium and indium melts [9] - a derivative of the Effer-Minden process for GaAs [10]. Composition of the layer was controlled by the pressure of $AsCl_3$ over the two melts. Although, in theory, a satisfactory method for the ternary compound, it was less flexible than the (Ga, In)/HCl/AsH_3 system or the system described below and it could not easily be extended to the growth of the quaternary material.

The growth system developed in this work was based on the InP system described in chapter 5. Thus, the group III elements were introduced into the deposition zone as monochlorides produced by the reaction of HCl with the liquid metal. The group V elements were introduced as the trichlorides, which are reduced rapidly to the elements at the growth temperatures.

In this chapter, theoretical models of the growth system are presented. A simple, equilibrium model is discussed first, and is followed by an examination of the driving force for growth. Finally a model based on the gas-transport processes is presented. Equilibrium based models have been produced by various workers [11,12,13] and are included here for completeness, and because they provide a foundation for the more sophisticated models. These models use well-established concepts and equations. However, the application of these equations to the quaternary and ternary growth systems is novel, and the resulting models revealed several features obscured by the equilibrium calculations.

The main problem associated with the growth of ternary and quaternary compounds is control of the layer composition. At typical growth temperatures (650^{o}-$700^{o}C$), all compositions of $Ga_xIn_{1-x}As_yP_{1-y}$ can exist [14] (ie $0 \leq x \leq 1$, $0 \leq y \leq 1$). The factors controlling growth composition are therefore very important and during the discussion of the growth models, particular attention will be paid to this aspect.

6.1 Equilibrium Models

The simplest theoretical model is one in which the solid is assumed to be in equilibrium with the vapour phase. Equations describing the equilibrium condition are then developed. This has been done for both the ternary [11] and quaternary system [12,13]. However, the results are frequently presented in an inconvenient form. The equations shown below were derived independently by the author, in order to obtain the information required for developing the practical growth system.

6.1.1 The Ternary System: $Ga_xIn_{1-x}As$

In all theoretical discussions of the growth of a ternary III-V compound it was assumed that this was a solid solution of two binary compounds. Thus (Ga, In) As was regarded as a solution of GaAs and InAs. For simplicity the solution was assumed to be ideal, although Panish and Ilegem's have shown that the phase diagrams of mixed III-V compounds are best interpreted using a regular solution model [14]. However, as will be shown below, the assumption of ideal behaviour does not affect the qualitative results and quantitative differences are small compared to those arising from other sources (such as inaccuracies in the thermodynamic data, or from the neglect of minority species).

Only one growth reaction was considered for each of the binary compounds:

$$GaAs_{(s)} + HCl_{(g)} \rightleftharpoons GaCl_{(g)} + \tfrac{1}{4}As_{4(g)} + \tfrac{1}{2}H_{2(g)} \quad \ldots\ldots 1$$

$$InAs_{(s)} + HCl_{(g)} \rightleftharpoons InCl_{(g)} + \tfrac{1}{4}As_{4(g)} + \tfrac{1}{2}H_{2(g)} \quad \ldots\ldots 2$$

Thus, as in the case of InP, minority gas-phase species (As_2, the dichlorides etc) were neglected. Although a simplification, this does not alter the qualitative results of the model. Furthermore, the thermodynamic values are not known with sufficient accuracy to justify use of the complex equations necessary if the minority species are to be included.

The equilibrium constants for reactions 1 and 2 are

$$K_{GaAs} = \frac{P_{GaCl}\ P_{As_4}^{\frac{1}{4}}\ P_{H_2}^{\frac{1}{2}}}{a_{GaAs}\ P_{HCl}} \qquad \ldots\ldots\ 3$$

$$K_{InAs} = \frac{P_{InCl}\ P_{As_4}^{\frac{1}{4}}\ P_{H_2}^{\frac{1}{2}}}{a_{InAs}\ P_{HCl}} \qquad \ldots\ldots\ 4$$

where a_i is the activity of solid i. For the pure binary compounds $a_{GaAs} = a_{InAs} = 1$ and for an ideal solid solution the activities denote the composition. Thus, for $Ga_xIn_{1-x}As$, $a_{GaAs} = x$ and $a_{InAs} = 1-x$ and from 3 and 4 is obtained the relation

$$\frac{x}{1-x} = \frac{P_{GaCl}}{P_{InCl}} \cdot \frac{K_{InAs}}{K_{GaAs}} \qquad \ldots\ldots\ 5$$

Equation 5 demonstrates that at equilibrium the solid composition is a function solely of the Ga:In ratio in the gas-phase and the ratio of the equilibrium constants, which is in turn a function of temperature only. The equation is readily extended to deal with non-ideal solutions by the inclusion of activity coefficients (γ_{InAs} and γ_{GaAs});

$$\frac{x}{1-x} = \frac{P_{GaCl}}{P_{InCl}} \cdot \frac{K_{InAs}\ \gamma_{InAs}}{K_{GaAs}\ \gamma_{GaAs}} \qquad \ldots\ldots 6$$

For a regular solution, the activity coefficients are given by [15]:

$$\ell n\ \gamma_{GaAs} = \frac{\Omega}{RT}(1-x)^2 \qquad \ldots\ldots 7$$

and

$$\ell n\ \gamma_{InAs} = \frac{\Omega}{RT} x^2 \qquad \ldots\ldots 8$$

where Ω is termed an interaction parameter which for $Ga_xIn_{1-x}As$ has an estimated value of 3000 cal mol^{-1} [14]. A consequence of the regular solution model is that the full range of solutions ($0 \leqslant x \leqslant 1$) is only possible when $\frac{\Omega}{RT} \leqslant 2$. At typical growth temperatures (630-660°C), this condition is clearly met, and all compositions may be obtained. However, when $\frac{\Omega}{RT} > 2$ a miscibility gap appears in the phase diagram. At room temperature, therefore, the $Ga_{0.47}In_{0.53}As$ layer (lattice-matched to InP) is thermodynamically unstable (metastable).

The effect of assuming ideal behaviour is to produce an apparent error in the equilibrium constants of the deposition reactions and hence, in the free energies. This can be demonstrated by considering just one of the reactions, eg that for GaAs. The equilibrium constant for this reaction may be written

$$K_{GaAs} = \exp - \frac{\Delta G}{RT} = \frac{P_{GaCl}\ P_{As_4}^{\frac{1}{4}}\ P_{H_2}^{\frac{1}{2}}}{x\ \gamma_{GaAs}\ P_{HCl}} \qquad \ldots\ldots 9$$

Substituting for γ_{GaAs} from 8, and rearranging gives:

$$\exp\left[-\frac{(\Delta G - \Omega\,(1-x)^2)}{RT}\right] = \frac{P_{GaCl}\,P_{As_4}^{\frac{1}{4}}\,P_{H_2}^{\frac{1}{2}}}{xP_{HCl}} \qquad \ldots\ldots\ 10$$

Clearly, the assumption of an ideal solution is equivalent to an error of $\Omega\,(1-x)^2$ in the free energy of the reaction. For (Ga,In)As, this has a maximum value of 3 kcal mol^{-1} (as x tends to zero), and for $Ga_{0.47}In_{0.53}As$, the error is less than 1 kcal mol^{-1}. These errors are less than, or of the same order, as the uncertainty in the estimated thermodynamic values for the reactions.

The way in which non-ideal behaviour alters the relationship between the solid and vapour compositions is illustrated in fig 1, in which the mole fraction of gallium arsenide in the solid (γ) is plotted as a function of the ratio P_{GaCl}/p_{InCl}. The solid lines were calculated using equation 6 while the broken lines represent non-ideal behaviour and were calculated using equations 6, 7 and 8:-

$$\frac{x}{1-x}\exp\left[\frac{3000}{RT}\,(1-2x)\right] = \frac{P_{GaCl}}{P_{InCl}} \cdot \frac{K_{InAs}}{K_{GaAs}} \qquad \ldots\ldots\ 11$$

The curves were plotted for three different values of the ratio K_{InAs}/K_{GaAs}. Using literature thermodynamic values [16-21], K_{InAs}/K_{GaAs} was estimated to be $\simeq 35$. Hence, for lattice-matched material ($x = 0.47$) the ratio P_{GaCl}/p_{InCl} was estimated to be $\simeq 0.025$.

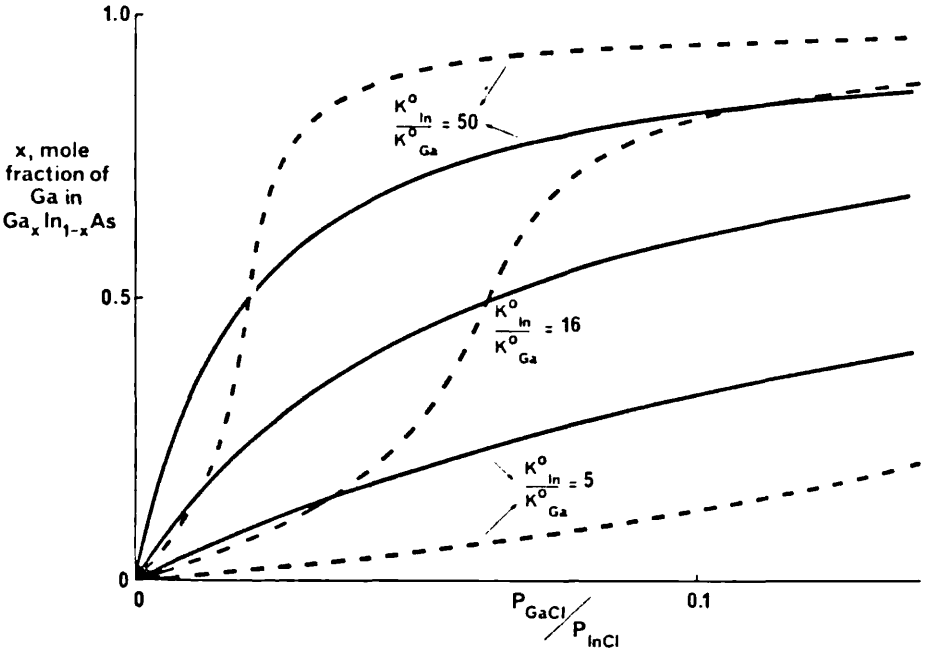

Solid composition vs. gas-phase composition

Calculated for ideal(———) and regular(- - - - -) solid solutions

6.1.2 Quaternary System: $Ga_xIn_{1-x}As_yP_{1-y}$

The procedure was similar to that adopted for the ternary compound: the quaternary material was considered to be a solid solution of the four binary compounds GaAs, InAs, GaP, InP. For each binary compound, the deposition reaction was assumed to be:

$$MX_{(s)} + HCl_{(g)} \rightleftharpoons M\,Cl_{(g)} + \tfrac{1}{4}\,X_{4(g)} + \tfrac{1}{2}\,H_{2(g)} \qquad \ldots\ldots\ 12$$

where M = Ga, In and X = As, P. The corresponding equilibrium constant is then

$$K_{MX} = \frac{P_{MX}\,(P_{X_4})^{\frac{1}{4}}\,P_{H_2}^{\frac{1}{2}}}{\alpha_{MX}\,P_{HCl}} \qquad \ldots\ldots\ 13$$

where α_{MX} is the activity of MX in the solid solution. The main difficulty with this procedure was obtaining values for α_{MX}. As in the case of $Ga_xIn_{1-x}As$, the solid solution was assumed to be ideal. It was then possible to write the identity,

$$Ga_xIn_{1-x}As_yP_{1-y} \equiv (GaAs)_a(InAs)_b(GaP)_c(InP)_d \qquad \ldots\ldots\ 14$$

where a, b, c, d are the mole fractions of the individual binary compounds.

From 14 were obtained the equations

$$a + b + c + d = 1 \qquad \ldots\ldots\ 15$$

$$x = a + c \qquad \ldots\ldots\ 16$$

and $$y = a + b. \qquad \ldots\ldots\ 17$$

Equations 15-17 are not sufficient to define a unique set (a,b,c,d) for particular values of x and y. A self-consistent set of binary activities may be obtained by considering the vapour phase deposition of each, and the conditions for equilibrium. These activities do not have any physical significance, but are a product of the particular mathematical model used.

From 14 therefore the four equilibrium constants are:

$$K_1 = \frac{P_{GaCl}\, P_{As_4}^{\frac{1}{4}}\, P_{H_2}^{\frac{1}{2}}}{a\, P_{HCl}} \qquad \ldots\ldots 18$$

$$K_2 = \frac{P_{InCl}\, P_{As_4}^{\frac{1}{4}}\, P_{H_2}^{\frac{1}{2}}}{b\, P_{HCl}} \qquad \ldots\ldots 19$$

$$K_3 = \frac{P_{GaCl}\, P_{P_4}^{\frac{1}{4}}\, P_{H_2}^{\frac{1}{2}}}{c\, P_{HCl}} \qquad \ldots\ldots 20$$

$$K_4 = \frac{P_{InCl}\, P_{P_4}^{\frac{1}{4}}\, P_{H_2}^{\frac{1}{2}}}{d\, P_{HCl}} \qquad \ldots\ldots 21$$

Equations 18-21 may be combined to give expressions for the ratios P_{GaCl}/P_{InCl} and P_{As_4}/P_{P_4}:

$$\frac{P_{GaCl}}{P_{InCl}} = \frac{K_1}{K_2} \cdot \frac{a}{b} = \frac{K_3}{K_4} \cdot \frac{c}{d} \qquad \ldots\ldots 22$$

and

$$\frac{P_{As_4}}{P_{P_4}} = \frac{K_1\ a}{K_3\ c} = \frac{K_2\ b}{K_4\ d} \qquad \ldots\ldots\ 23$$

An expression for say, d may be obtained from both 21 and 23

$$d = \frac{K_2}{K_4} \cdot b \cdot \frac{K_3}{K_1} \cdot \frac{c}{a} \qquad \ldots\ldots\ 24$$

By combining equations 15, 16 17 and 24, the activities of the binary compounds may be defined. Thus from 15

$$a + b = 1 - (c + d) \qquad \ldots\ldots\ 25$$

and substituting in 17

$$y = 1 - c - d \qquad \ldots\ldots\ 26$$

and on addition of 26 to 16:

$$x + y = 1 + a - d \qquad \ldots\ldots\ 27$$

whence

$$a = x + y + d - 1 \qquad \ldots\ldots\ 28$$

Rearrangement of 26 gives

$$c = 1 - y - d \qquad \ldots\ldots\ 29$$

and from 25

$$b = 1 - d - x \qquad \ldots\ldots\ 30$$

Substituting for a, b and c in 24 yields, on rearrangement

$$(z-1)d^2 + [(z-1)(x+y-1) + 1]d-(1-x)(1-y) = 0 \quad \ldots\ldots 31$$

where

$$z = \frac{K_1K_4}{K_2K_3} \quad \ldots\ldots 32$$

Equation 31 may readily be solved for d. Note that the value of d is a function of z (that is, the value of the equilibrium constants), emphasising the fact that the division of the quaternary compound into a solution of four binary species is an artificial convention to enable a thermodynamic description of the system to be formulated in terms of known parameters.

As in the case of the ternary compounds, the equilibrium relationship between solid and gas composition was investigated.

From 1, it was shown that

$$x = a + c \text{ and } y = a + b$$

Similarly

$$1-x = b + d \quad \ldots\ldots 33$$

and

$$1-y = c + d \quad \ldots\ldots 34$$

Then,

$$\frac{x}{1-x} = \frac{a+c}{b+d} \qquad \ldots\ldots 35$$

But, the activities of the binaries can be obtained from equations 18-21, so equation 35 becomes

$$\frac{x}{1-x} = \frac{\dfrac{P_{GaCl}\, P_{As_4}^{\frac{1}{4}}\, P_{H_2}^{\frac{1}{2}}}{K_1} + \dfrac{P_{GaCl}\, P_{P_4}^{\frac{1}{4}}\, P_{H_2}^{\frac{1}{2}}}{K_3}}{\dfrac{P_{InCl}\, P_{As_4}^{\frac{1}{4}}\, P_{H_2}^{\frac{1}{2}}}{K_2} + \dfrac{P_{InCl}\, P_{P_4}^{\frac{1}{4}}\, P_{H_2}^{\frac{1}{2}}}{K_4}} \qquad \ldots\ldots 36$$

which can be simplified to:

$$\frac{x}{1-x} = \frac{P_{GaCl}}{P_{InCl}} \cdot \frac{\left[\dfrac{P_{As_4}^{\frac{1}{4}}}{K_1} + \dfrac{P_{P_4}^{\frac{1}{4}}}{K_3}\right]}{\left[\dfrac{P_{As_4}^{\frac{1}{4}}}{K_2} + \dfrac{P_{P_4}^{\frac{1}{4}}}{K_4}\right]} \cdot \qquad \ldots\ldots 37$$

A similar equation may be obtained for the solid P:As ratio:

$$\frac{y}{1-y} = \frac{P_{As_4}^{\frac{1}{4}}}{P_{P_4}^{\frac{1}{4}}} \cdot \frac{\left[\dfrac{P_{GaCl}}{K_1} + \dfrac{P_{InCl}}{K_2}\right]}{\left[\dfrac{P_{GaCl}}{K_3} + \dfrac{P_{InCl}}{K_4}\right]} \qquad \ldots\ldots 38$$

Let $r_1 = \dfrac{P_{GaCl}}{P_{InCl}}$ and $r_2 = \dfrac{P_{As_4}^{\frac{1}{4}}}{P_{P_4}^{\frac{1}{4}}}$

then equations 37 and 38 become:

$$\frac{x}{1-x} = r_1 \frac{\left[r_2/K_1 + 1/K_3 \right]}{\left[r_2/K_2 + 1/K_4 \right]} \qquad \ldots\ldots 39$$

and

$$\frac{y}{1-y} = r_2 \frac{\left[r_1/K_1 + 1/K_2 \right]}{\left[r_1/K_3 + 1/K_4 \right]} \qquad \ldots\ldots 40$$

Equations 39 and 40 are the basic equations describing the relationships between solid and vapour composition and show that, for example, the Ga:In ratio in the solid is determined not only by the ratio r_1 (p_{GaCl}/p_{InCl}) but also by r_2 (p_{As_4}/p_{P_4}). Similarly, r_1 and r_2 both have an influence on the As:P ratio. This is seen more clearly in figures 2 and 3 which were calculated using literature data [16-21]. Fig 2 shows x (Ga content) as a function of p_{GaCl}/p_{InCl} for several different values of p_{P_4}/p_{As_4}. The curves are similar in shape to those in fig 1 and all lie within the limiting curves of the two ternary compounds ((Ga,In)P and (Ga,In)As for which $r_2 = 0$ and ∞ respectively). Thus, for $r_2 \to \infty$ ($p_{As_4} >> p_{P_4}$), equation 39 simplifies to

$$\frac{x}{1-x} = r_1 \frac{K_2}{K_1} = \frac{p_{GaCl}}{p_{InCl}} \cdot \frac{K_2}{K_1} \qquad \ldots\ldots 41$$

which is equation 5 (section 6.1.1).

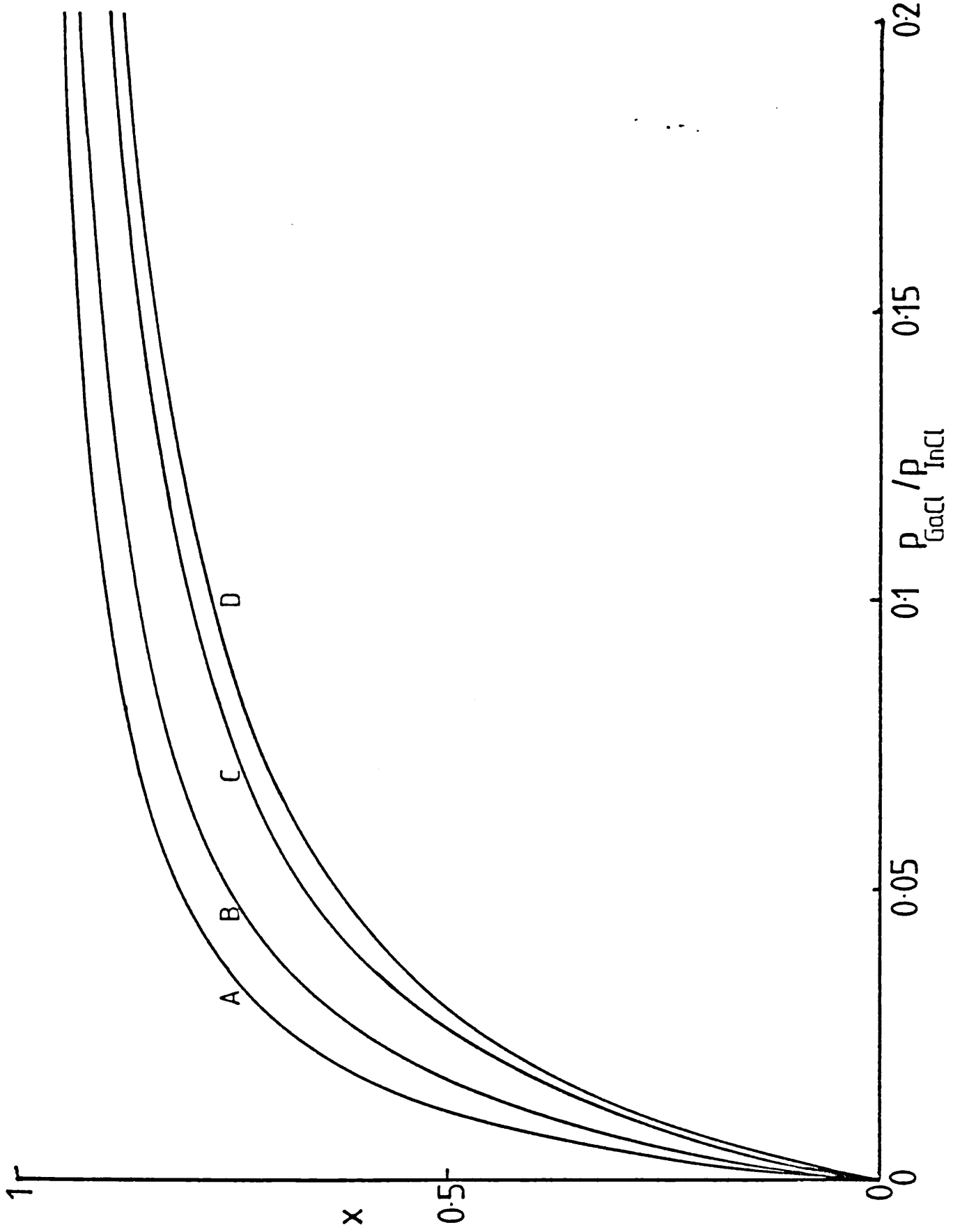

Dependence of gallium content of solid (x) on metal-chloride ratio.

Curves are plotted for the following ratios p_{As_4}/p_{P_4} :- A : 0 ; B : 10^{-4} ; C : 1 ; D : ∞.

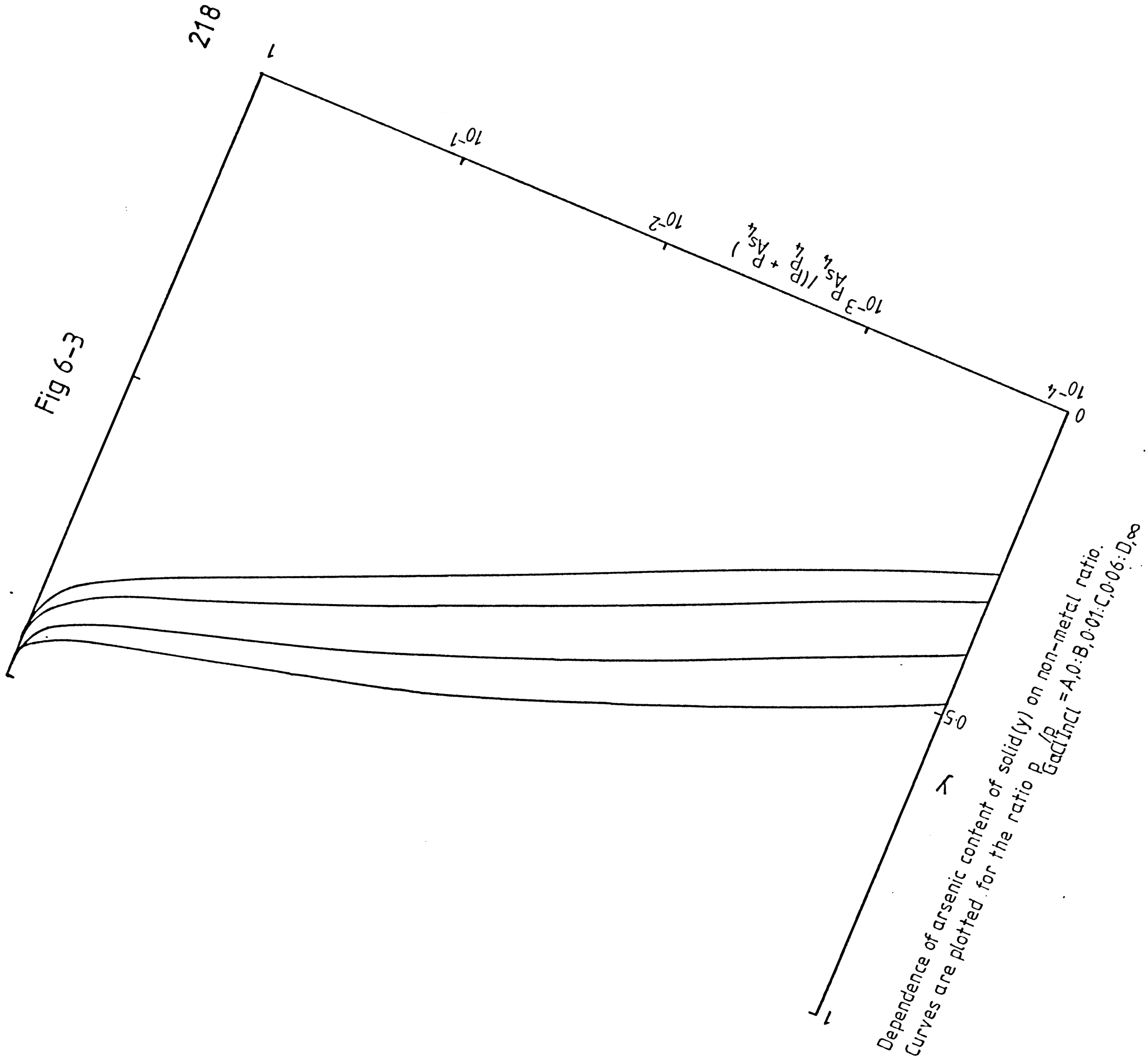
218
1
10⁻¹
10⁻²
10⁻³ P_As4 /(P_P4 + P_As4)
10⁻⁴
0
8
5
0
λ
1
Fig 6-3
Dependence of arsenic content of solid(y) on non-metal ratio.
Curves are plotted for the ratio P_GaCl/P_InCl = A,0:B,0·01:C,0·06:D,∞

Fig 3 shows y (As content) as a function of this ratio p_{As_4}/p_{P_4}. Again the curves lie within the limits set by the ternary compounds (Ga(As,P) and In(As,P)). However, the solid composition is a far less sensitive function of the non-metal pressure ratio and the dependence is best shown by plotting the gas composition on a logarithmic scale covering four orders of magnitude. This is a result of the ¼ power dependence of y or p_{As_4}/p_{P_4}. Comparison of figs 2 and 3 shows that the composition of the solid is more sensitive to the ratio r_1 (p_{GaCl}/p_{InCl}) than to p_{As_4}/p_{P_4}. The calculations emphasised the importance of controlling the composition of the vapour phase. This is even more important than in ternary growth.

Equations 39 and 40 make it possible to calculate r_1 and r_2 without the need to determine the activities a, b, c and d. However, the assumption of an ideal solid solution is implicit in these equations.

If $X = \frac{x}{1-x}$ and $Y = \frac{y}{1-y}$ then from 39

$$r_1 = X \frac{\left[r_2/K_2 + 1/K_4 \right]}{\left[r_2/K_1 + 1/K_3 \right]} \qquad \ldots\ldots 42$$

Similarly, from 40

$$r_2 \left[r_1/K_1 + 1/K_2 \right] = Y \left[r_1/K_3 + 1/K_4 \right] \qquad \ldots\ldots 43$$

$$\therefore \quad \frac{r_2 r_1}{K_1} + \frac{r_2}{K_2} = Y \frac{r_1}{K_3} + Y/K_4$$

$$\text{and} \quad \left[\frac{r_2}{K_1} - \frac{Y}{K_3} \right] r_1 = Y/K_4 - \frac{r_2}{K_2} \qquad \ldots\ldots 44$$

Substituting for r_1 from 42 gives

$$\left[\frac{r_2}{K_1} - \frac{Y}{K_3}\right] \cdot X \cdot \left[\frac{r_2}{K_2} + \frac{1}{K_4}\right] = \left[\frac{Y}{K_4} - \frac{r_2}{K_2}\right] \left[\frac{r_2}{K_1} + \frac{1}{K_3}\right]$$

Multiplying out and rearranging:

$$r_2^2 \left[\frac{1+X}{K_1K_2}\right] + r_2 \left[\frac{(X-Y)}{K_1K_4} + \frac{(1-XY)}{K_2K_3}\right] - Y\frac{(1+X)}{K_3K_4} = 0 \qquad \ldots\ldots 45$$

Equations 42 and 45 may be solved for any particular set (x,y), and enable the relationship between solid and vapour to be expressed in another, more useful plot. Using Vėgards Law the various compositions corresponding to lattice-matching with InP may be found and from 42 and 45, the corresponding values of r_1 and r_2 may be calculated. The result of the calculations is shown in fig 4, in which r_1 is plotted against r_2 and the various curves correspond to solids with a particular lattice-parameter. Each point on a curve represents a different band-gap. The further the point is from the origin, the smaller the band-gap. The advantage of this plot is that the qualitative changes in growth conditions which are necessary to produce a material with a particular lattice-parameter and band-gap are readily apparent. Although errors in the thermodynamic data, and the simplicity of the model give rise to quantitative errors, the qualitative relationships are unaltered.

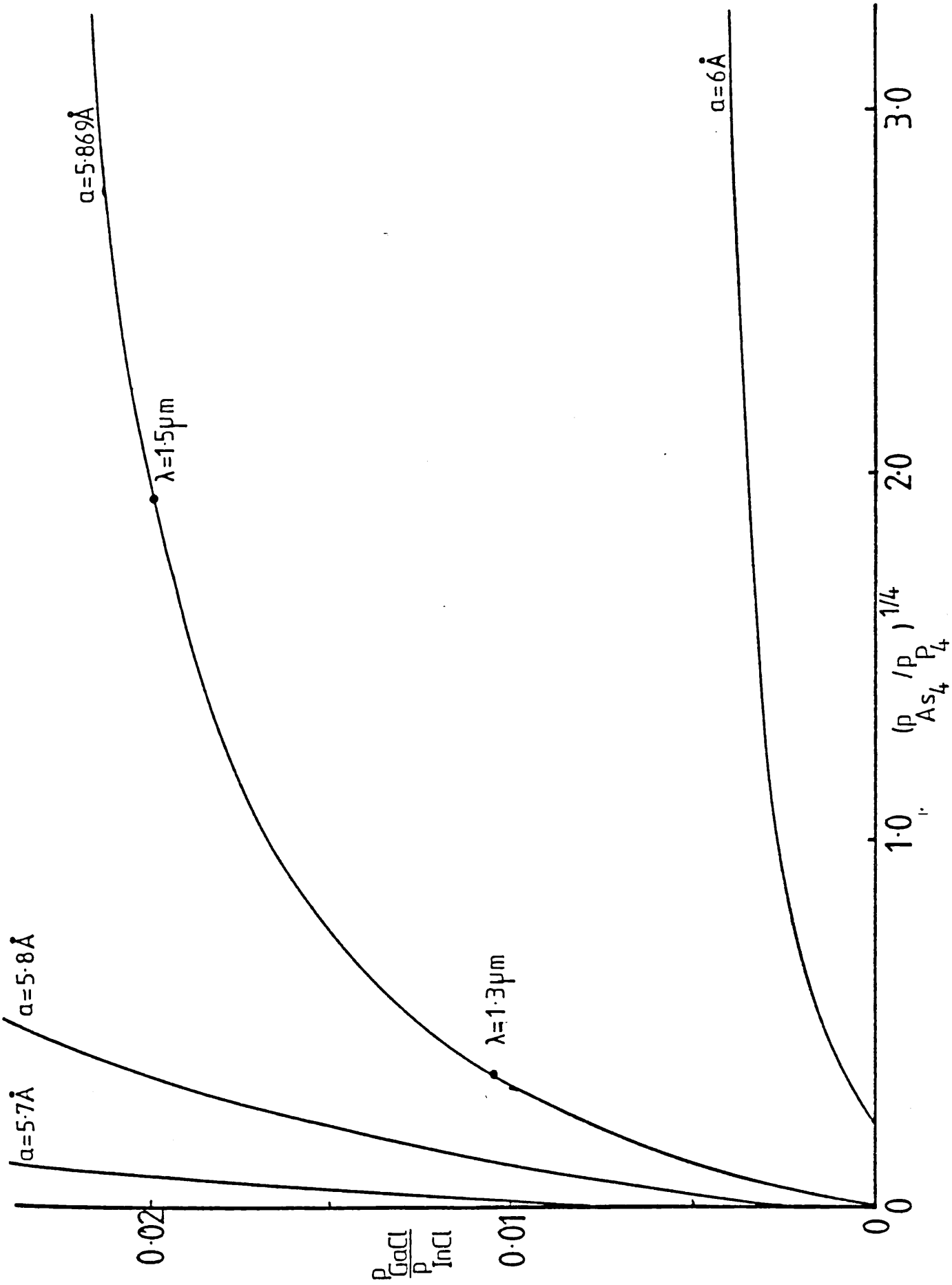

Metal chloride vs. non-metal pressure ratios showing conditions for constant lattice-parameter

Current optical communications systems operate at 1.3 μm wavelength and therefore, the experimental work was aimed to produce material with the corresponding band-gap and lattice-matched to InP. Using the data and formulae of Sugiyama et al [22] the required solid was estimated to be $Ga_{0.33}In_{0.67}As_{0.71}P_{0.29}$. From the data in figs 2, 3 and 4, the required gas ratios for growth at 650°C were calculated to be

$$\frac{P_{InCl}}{P_{GaCl}} = 93.7 \qquad \frac{P_{P_4}}{P_{As_4}} = 62.6$$

However, even quite small errors in the thermodynamic constants could radically change the conditions. For example, a factor of 2 in the value of K_2 (corresponding to an error uncertainty in ΔG of $\pm$ 1.28 kcal mol^{-1}) gave the range

$$59.8 < \frac{P_{InCl}}{P_{GaCl}} < 149.8, \quad 299.4 > \frac{P_{P_4}}{P_{As_4}} > 11.29$$

Plainly then, the thermodynamic calculations gave useful qualitative information, but were an unsatisfactory guide as to precise growth conditions. The values of p_{P_4}/p_{As_4} were particularly misleading as the existence of the dimer species in the vapour (explicitly ignored in deriving equations 39 and 40) would strongly influence the required input pressures of the trichlorides PCl_3 and $AsCl_3$.

6.2 Non-Equilibrium Thermodynamic Models

Equilibrium models provide a valuable insight into the behaviour of the growth systems. However, by only considering equilibrium systems many features of the non-equilibrium (growth) system are hidden. This can be illustrated by examining the thermodynamic driving force (or overpotential) for growth (ω). For a binary growth system such as that for InP, the overpotential is given by (see chapter 2, equation 7)

$$\omega = RT\ell ns \qquad \ldots\ldots 46$$

where $s = K^*/K^o$.

The definition of overpotential in the ternary and quaternary growth systems is less straightforward. In this section, an expression for overpotential is derived and the results discussed. The expression is derived rigorously for the quaternary growth system: the ternary system is then considered as a special case.

6.2.1 Quaternary System

For this calculation, the growth reaction is written as:

$$Ga_xIn_{1-x}As_yP_{1-y} + HCl \rightleftharpoons x\ GaCl + (1-x)\ InCl + \frac{y}{4}\ As_4 + \frac{(1-y)}{4}\ P_4 + \tfrac{1}{2}\ H_2 \qquad \ldots\ldots 47$$

The calculation proceeds by noting that overpotential, as defined by equation 46, is the negative of the affinity of reaction [23], which is defined by the equation:

$$\text{Affinity} = -\left(\frac{\partial G}{\partial \xi}\right)_{T,p} = -\sum_i \nu_i \mu_i \qquad \ldots\ldots 48$$

where ν_i is the stoichiometric coefficient, μ_i the chemical potential and $d\xi$ a measure of the extent of reaction:

$$d\xi = \frac{dn_a}{\nu_a} = \frac{dn_b}{\nu_b} = \ldots \frac{dn_m}{\nu_m}$$

where dn_a is the change in the number of moles of species a in the system.

The problem is then to obtain from 48 an expression analogous to 46, from which the overpotential may be calculated using known thermodynamic data.

The starting point is the identity 14

$$Ga_xIn_{1-x}As_yP_{1-y} \equiv (GaAs)_a\ (InAs)_b\ (GaP)_c\ (InP)_d \qquad \ldots\ldots 14$$

The calculation of numerical values for a, b, c and d will be considered later. For the present, it will be assumed that a unique set of binary mole-fractions can be calculated.

Using equations 16, 17, 33 and 34

$$x = a + c \qquad 16 \qquad\qquad y = a + b \qquad 17$$

$$(1-x) = b + d \qquad 33 \qquad\qquad (1-y) = c + d \qquad 34$$

equation 47 may be rewritten:

$$(GaAs)_a\ (InAs)_b\ (GaP)_c\ (InP)_d + (a + b + c + d)\ HCl \rightleftharpoons$$

$$(a + c)\ GaCl + (b + d)\ InCl + \left(\frac{a + b}{4}\right)\ As_4 + \left(\frac{c + d}{4}\right)\ P_4$$

$$+ \tfrac{1}{2}\ (a + b + c + d)\ H_2 \qquad \ldots\ldots\ 49$$

The overpotential ΔG is given by

$$\omega = \sum_i \nu_i \mu_i \qquad \ldots\ldots\ 50$$

so,

$$\omega = (a + c)\mu_{GaCl} + (b + d)\mu_{InCl} + \left(\frac{a + b}{4}\right)\mu_{As_4} + \left(\frac{c + d}{4}\right)\mu_{P4}$$

$$+ \tfrac{1}{2}\ (a + b + c + d)\mu_{H_2} - a\mu_{GaAs} - b\mu_{InAs} - c\mu_{GaP}$$

$$- d\mu_{InP} - (a + b + c + d)\mu_{HCl} \qquad \ldots\ldots\ 51$$

Equation 51 may be expressed more concisely by extracting terms in a, b, c and d. Collecting together the terms in a (ie the contribution to overpotential arising from the deposition of GaAs) gives

$$\omega_{GaAs} = a\mu_{GaCl} + \frac{a}{4}\mu_{As_4} + \tfrac{1}{2}\ a\mu_{H_2} - a\mu_{GaAs} - a\mu_{HCl}$$

$$= a\left[\mu^{o}_{GaCl} + RT\ell np_{GaCl} + \tfrac{1}{4}\ \mu^{o}_{As_4} + \frac{1}{4}\ RT\ell np_{As_4}\right.$$

$$+ \tfrac{1}{2}\ \mu^{o}_{H_2} + \tfrac{1}{2}\ RT\ell np_{H_2} - \mu^{o}_{GaAs} - RT\ell n\ \gamma_1\ a$$

$$\left. - \mu^{o}_{HCl} - RT\ell np_{HCl}\right] \qquad \ldots\ldots\ 52$$

where μ_i^o is the standard chemical potential of species i, p_i the pressure of species i, γ_1 the activity coefficient and $\gamma_1 a$ the activity of GaAs in the solid solution.

Equation 52 may be further clarified: the deposition reaction for GaAs is

$$GaAs + HCl \rightleftharpoons GaCl + \tfrac{1}{4}As_4 + \tfrac{1}{2}H_2 \qquad \ldots\ldots 53$$

$$\therefore \quad \sum_j \mu_j^o = \Delta G_1^o = -RT\ell n\ K_1^o$$

where the subscript j refers to all species in equation 52 and ΔG_1^o and K_1^o are the standard free energy and equilibrium constant for reaction 53.

The logarithmic terms may also be gathered together as

$$RT\ell n\ K_1^* - RT\ell n\ \gamma_1 a$$

where K_1^* - the partial pressure product, is

$$K_1^* = \frac{P_{GaCl}\ P_{As4}^{\frac{1}{4}}\ P_{H2}^{\frac{1}{2}}}{P_{HCl}}$$

Hence the contribution to overpotential arising from GaAs deposition is

$$\Delta G_{GaAs} = a\ RT\ell n\ s_1 - a\ \ell n\gamma a \qquad \ldots\ldots 54$$

where $s_1 = K_1^*/K_1^o$

A similar treatment may be applied to the deposition of the other binary compounds, so that the total overpotential is defined by

$$\frac{\omega}{RT} = a \ln s_1 + b \ln s_2 + c \ln s_3 + d \ln s_4$$

$$- [a \ln \gamma_1 a + b \ln \gamma_2 b + c \ln \gamma_3 c + d \ln \gamma_4 d] \quad \ldots\ldots 55$$

The overpotential is thus a function of two terms - the first related to the overpotentials of the four binary compounds, the second related to the free energy of mixing.

In order to proceed further, it is necessary to calculate a unique set (a, b, c, d) for each quaternary composition (x,y). In section 6.1.2 this was achieved from equations 15, 16, 17 and 24. Equations 15-17 are the three independent equations obtained from equation 14 and may be used here. However, equation 24 was obtained from the conditions for equilibrium and cannot be assumed to apply in a non-equilibrium system.

In the absence of a fourth condition, it is found that for a given vapour and solid (x,y) composition, the overpotential depends on the choice of the binary activities. This reflects the artificiality of dividing the quaternary into four binary compounds. A fourth condition is obtained by considering the way the overpotential varies with the values of a, b, c and d. This passes through a maximum and the best set is assumed to be that corresponding to the maximum overpotential which is found by

differentiating equation 55 with respect to, say, d. For an ideal solution ($\gamma_1 = \gamma_2 = \gamma_3 = \gamma_4 = 1$):

$$\frac{d(\omega/RT)}{d(d)} = \frac{da}{d(d)} \ln \sigma_1 + \frac{db}{d(d)} \ln \sigma_2 + \frac{dc}{d(d)} \ln \sigma_3 + \ln \sigma_4$$

$$- \frac{da}{d(d)} \cdot \ln a + \frac{da}{d(d)} + \frac{db}{d(d)} \cdot \ln b + \frac{db}{d(d)}$$

$$+ \frac{dc}{d(d)} \cdot \ln c + \frac{dc}{d(d)} + \ln d + 1 \qquad \ldots\ldots 56$$

From equations 15, 33 and 34:

$$b = 1 - x - d \qquad \ldots\ldots 57$$

$$c = 1 - y - d \qquad \ldots\ldots 58$$

$$a = x - y + d - 1 \qquad \ldots\ldots 59$$

for which

$$\frac{da}{d(d)} = 1; \quad \frac{db}{d(d)} = -1; \quad \frac{dc}{d(d)} = -1$$

Substituting in 56 and setting $\frac{d(\omega/RT)}{d(d)} = 0$ gives the condition

$$\ln a - \ln b - \ln c + \ln d = \ln \sigma_1 - \ln \sigma_2 - \ln \sigma_3 + \ln \sigma_4 \qquad \ldots\ldots 60$$

or

$$\frac{ad}{bc} = \frac{\sigma_1 \sigma_4}{\sigma_2 \sigma_3} \qquad \ldots\ldots 61$$

In the chloride - CVD process for $Ga_xIn_{1-x}As_yP_{1-y}$, the supersaturations are not independent of each other and equation 61 can be shown to be equivalent to

$$\frac{ad}{bc} = \frac{K_2 K_3}{K_1 K_4}$$

This is the same condition which applies to the equilibrium system (equation 24). The generalised thermodynamic treatment discussed thus includes the equilibrium system as a special case. Note that the division of the quaternary solid into four binaries simply enables overpotential and equilibrium to be calculated in a self-consistent manner from known thermodynamic data. The mole-fractions a, b, c, d have no physical significance, and can be seen from equation 24 to depend on the particular values of the equilibrium constants used.

For any given composition (x,y) the corresponding binary mole-fractions (a, b, c, d) may be calculated using the equations developed in section 6.1.2 providing the solid solution is assumed to be ideal. It is then possible, using equation 55, to calculate for a given gas-phase composition the overpotential for the whole range of solids $0 < x < 1$, $0 < y < 1$. The result is an overpotential surface. In an equilibrium system this surface will touch the zero plane at one point only. An experimental growth system for $Ga_xIn_{1-x}As_yP_{1-y}$ is described in chapter 7. The overpotential surface for typical growth conditions in this apparatus has been calculated and the results are shown in figs 5 and 6. Each line represents a section through the overpotential

Fig 6-5

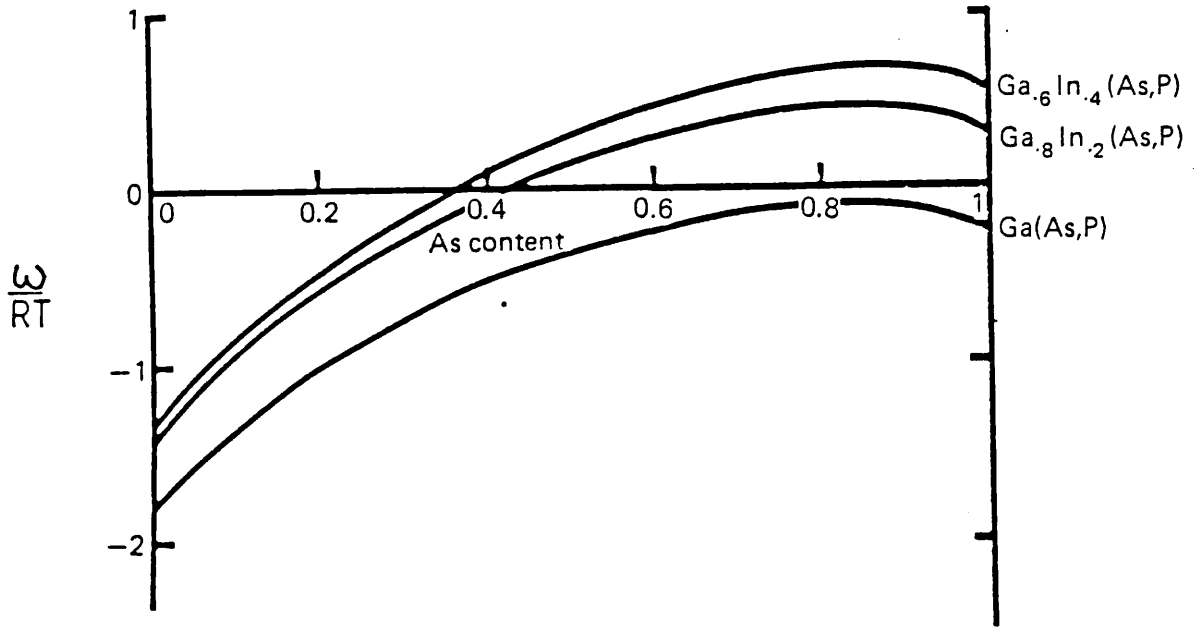

Fig 6-6

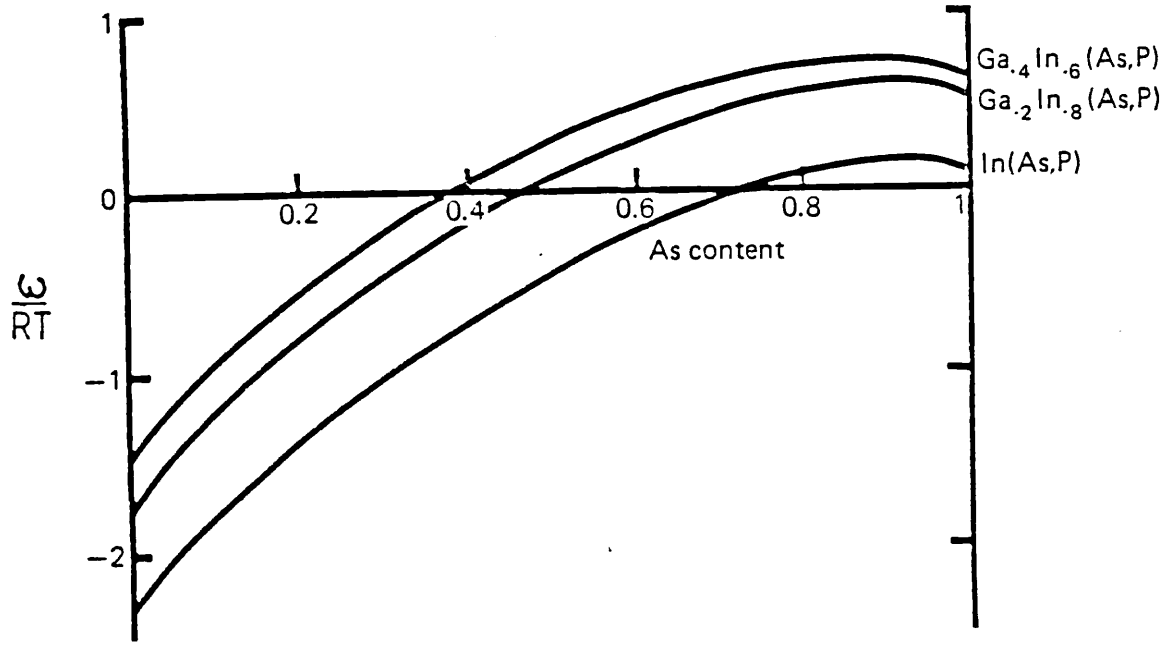

Sections through the Overpot^{l}. Surface corresponding to normal conditions for quaternary growth

surface corresponding to constant x (Ga content in the solid). Overpotential is plotted as a function of y (As content). It is immediately apparent from figs 5 and 6 that there is not a unique solid composition which can be deposited from a given gas-phase. Instead, a range of solid compositions may be grown. In the region of maximum overpotential, the surface resembles a very shallow dome and quite large changes in composition ($\pm$ 10 atomic % in gallium) do not greatly alter the overpotential. In general, growth systems give reproducible material with very narrow composition ranges. The control of layer composition thus depends on the transport in vapour and the surface kinetics and not simply on the thermodynamics of the system. This will be discussed later.

A second feature which is apparent from figs 5 and 6 is that there is a range of compositions which are undersaturated with respect to the vapour, and can be etched. Of particular importance is the fact that the substrate material - InP - is undersaturated and may be attacked by the vapour phase during the early stages of growth before a protective layer of ternary or quaternary material has formed.

6.2.2 Ternary System: The Effect of Non-ideality

The calculations for the quaternary system involved the assumption that the solid was an ideal solution. The qualitative effect of non-ideality may be estimated by examining the limiting case of a ternary system eg $Ga_xIn_{1-x}As$. The overpotential for this system is given by

$$\frac{\omega}{RT} = x \ln s_1 + (1-x) \ln s_2 - x \ln \gamma_{GaAs}\, x - (1-x) \ln \gamma_{InP}\, (1-x)$$

..... 62

Combining this with equations 8 and 9 gives

$$\frac{\omega}{RT} = x \ln s_1 + (1-x) \ln s_2 - \frac{\Omega}{RT} x (1-x) - x \ln x$$

$$- (1-x) \ln (1-x) \qquad \ldots\ldots 63$$

This is plotted in fig 7 for different values of the interaction parameter. It can be seen that the effect of non-ideality is to flatten the overpotential curves, but that their overall shape is unaltered.

Equation 63 may also be differentiated with respect to x:

$$\frac{\partial(\frac{\omega}{RT})}{\partial x} = \ln \frac{s_1}{s_2} + \ln \frac{(1-x)}{x} - \frac{x}{1-x} - \frac{x}{x} + \frac{1}{1-x} - \frac{\Omega}{RT} + \frac{2\Omega}{RT} X$$

$$= \ln \frac{s_1}{s_2} + \ln \frac{(1-x)}{x} + \frac{\Omega}{RT} (2x-1) \qquad \ldots\ldots 64$$

At the maximum of the curve, $\partial (\omega/RT)/\partial x = 0$ is

$$\ln \frac{x}{1-x} + \frac{\Omega}{RT} (1-2x) = \ln \frac{s_1}{s_2}$$

or

$$\frac{x}{1-x} \exp \frac{\Omega}{RT} (1-2x) = \frac{s_1}{s_2} \qquad \ldots\ldots 65$$

Substituting for s_1 and s_2 yields:

$$\frac{x}{1-x} \exp \frac{\Omega}{RT} (1-2x) = \frac{P_{GaCl}}{P_{InCl}} \cdot \frac{K_{InAs}}{K_{GaAs}} \qquad \ldots\ldots 66$$

which is identical to equation 11 obtained for the equilibrium system.

Fig 6-7

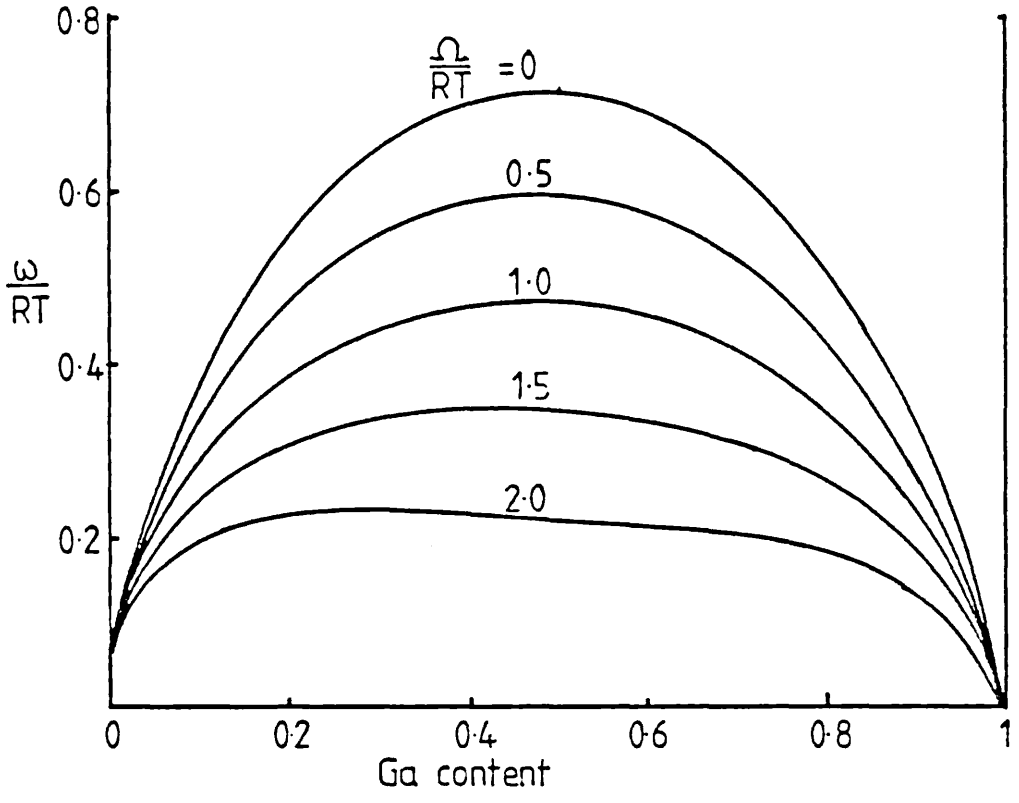

Overpotential curve for GaInAs growth showing effect of non-ideality in the solid

6.3 Non-equilibrium Transport Model

In section 6.2 it was shown that in a non-equilibrium system a wide range of different solid compositions may be grown. This ambiguity is removed by the action of the surface kinetics and transport. In this section the effect of gas transport is discussed in more detail, using the growth of $Ga_xIn_{1-x}As$ as an example. As in the case of InP growth, it is possible to obtain transport equations relating the bulk and interfacial pressures and the growth rate, without making any assumptions concerning the presence (or absence) of an equilibrium gas-phase at the interface.

The growth equation is written formally as

$$Ga_xIn_{1-x}As + HCl \rightleftharpoons x\ GaCl + (1-x)\ InCl + \tfrac{1}{4}\ As_4 + \tfrac{1}{2}\ H_2 \quad \ldots\ldots\ 67$$

Clearly the transport equations for HCl and As_4 will be the same as for a binary compound (see equations 20 and 21 of chapter 5), as will the calculation of the velocity of the Stefan flow (equation 18 of Chapter 5). Only the equations for the metal halides differ. Thus, for GaCl, the transport equation is

$$J_{GaCl} = x\ J = \tfrac{1}{4}\ J\ \frac{P_{GaCl}}{P} - \frac{D}{RT}\ \frac{dp_{GaCl}}{dx} \quad \ldots\ldots\ 68$$

where J is the transport flux of the solid $Ga_xIn_{1-x}As$.

Similarly,

$$J_{InCl} = (1-x)J = \tfrac{1}{4}\ \frac{P_{InCl}}{P} - \frac{D}{RT}\ \frac{dp_{InCl}}{dx} \quad \ldots\ldots\ 69$$

On rearrangement and integration, equation 68 becomes

$$P_{GaCl}(o) = \frac{4}{3} \times P - (\frac{4}{3} \times P - P_{GaCl}(\ell))\exp - \xi \qquad \ldots\ldots 70$$

where $\xi = \frac{3}{4} \frac{JRT\ell}{DP}$

Let $P_{GaCl}(\ell) + P_{InCl}(\ell) = \varepsilon$ and $P_{GaCl}(\ell) = y\varepsilon$

Then, on simplifying for the case when $\xi << 1$, equation 70 becomes

$$P_{GaCl}(o) = y\varepsilon + \frac{4}{3} x\xi \qquad \ldots\ldots 71$$

Similarly, from equation 67

$$P_{InCl}(o) = (1-y)\ \varepsilon + \frac{4}{3}\ (1-x)\ \xi \qquad \ldots\ldots 72$$

By analogy with the InP system, the interfacial pressures of As_4 and HCl are given by

$$P_{As_4}(o) = [\eta/4 + \xi/3] \qquad \ldots\ldots 73$$

and

$$P_{HCl}(o) = [3\eta - \frac{4}{3}\ \xi] \qquad \ldots\ldots 74$$

where η is now the input pressure of $AsCl_3$.

It is not possible to proceed beyond equations 71-74 without some knowledge of the surface kinetics. However, the way in which transport considerations can affect the growth of the ternary can be demonstrated by examining a system in which the surface processes are rapid compared to the growth rate, and are non-specific (that is, the incorporation of one of the metals is not kinetically favoured). For this system the ternary solid will be in equilibrium with the interfacial species and the equilibrium conditions for the two binary solids must be satisfied:

$$K^{o}_{GaAs} = \frac{(y\varepsilon + \frac{4}{3} x \xi)(\eta/4 + \xi/3)^{\frac{1}{4}}}{a_{GaAs}\ (3\eta - \frac{4}{3}\xi)} \qquad \ldots\ldots\ 75$$

and

$$K^{o}_{InAs} = \frac{[(1-y)\varepsilon + \frac{4}{3}(1-x)\xi](\eta/4 + \xi/3)^{\frac{1}{4}}}{a_{InAs}\ (3\eta - \frac{4}{3}\xi)} \qquad \ldots\ldots\ 76$$

For an ideal solid solution $a_{GaAs} = x$ and $a_{InAs} = (1-x)$.

Equations 75 and 76 may then be solved simultaneously to give x and ξ. Note that for this system, only one steady state composition is formed for a given set of input pressures. Dividing 75 by 76 gives

$$\frac{K^{o}_{GaAs}}{K^{o}_{InAs}} = \frac{(1-x)}{x} \cdot \frac{(\frac{4}{3} x + y\ \varepsilon)}{(\frac{4}{3}(1-x)\xi + (1-y)\varepsilon)} \qquad \ldots\ldots\ 77$$

For computation it is more satisfactory to introduce a new variable $\alpha = \frac{x}{1-x}$ which has a physical meaning for any positive value. Then, $x = \frac{\alpha}{1+2}$ and $1-x = \frac{1}{1+\alpha}$ and equation 77 may be rewritten as a quadratic in α

$$\alpha^2 \left[\frac{K^{o}_{GaAs}}{K^{o}_{InAs}}(1-y)\ \varepsilon\right] + \left[\frac{K^{o}_{GaAs}}{K^{o}_{InAs}}(\frac{4}{3}\xi + (1-y)\ \varepsilon) - \frac{4}{3}\xi - y\varepsilon\right]\alpha$$

$$-y\varepsilon = 0 \qquad \ldots\ldots\ 78$$

It is clear from 78 that the composition of the grown layer will be a function of growth rate, as well as the input pressures of gallium and indium chlorides.

Figs 8 and 9 illustrate the main features of a transport limited growth system. These were calculated using (where relevant) typical input pressures of the practical growth system, and literature values of K^{o}_{GaAs} and K^{o}_{InAs}. Fig 8 shows the variation of growth rate (ξ) with arsenic trichloride pressure (η). Several curves are shown. These were all calculated with the same total metal chloride pressure (constant ε) but different values of the ratio p_{GaCl}/p_{InCl} (ie different values of y). The general shape of the curves is the same as that for InP (fig 2 of chapter 5), and may be explained in the same terms. Except where the growth rate is limited by arsenic transport (low value of η), the growth rate increases with increasing GaCl content in the vapour. This reflects an increase in supersaturation. Fig 9 also shows the variation of growth rate with $AsCl_3$ pressure, but in addition shows the corresponding variation of solid composition. At the positions of zero growth, the composition is defined by equation 5. However, as growth rate increases, the gallium content in the growing layer decreases. Note that from equation 75 it is clear that this compositional variation is a consequence of the change in growth rate, rather than a direct effect of arsenic trichloride pressure. The physical explanation for this behaviour is illustrated in fig 10. This shows the bulk gas composition and the interfacial pressures of InCl and GaCl for two growth rates. The rates at which these species are transported to the interface are proportional to their partial pressure gradients, which in turn are experimentally determinable from the composition of the grown solid.

Fig 6-8

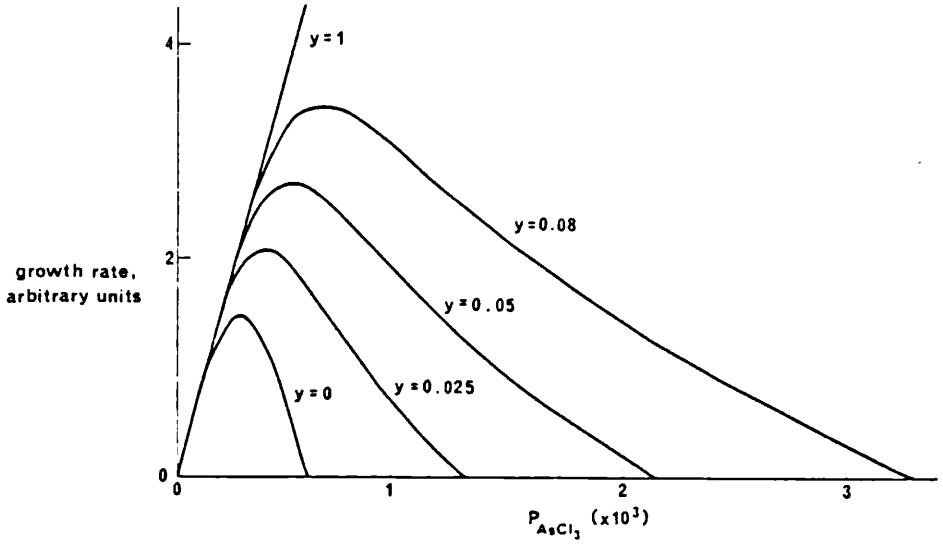

Growth rate of GaInAs vs. $AsCl_3$ pressure.

[$p_{GaCl} + p_{InCl}$ = constant; $y = p_{GaCl}/(p_{GaCl} + p_{InCl})$]

Fig 6-9

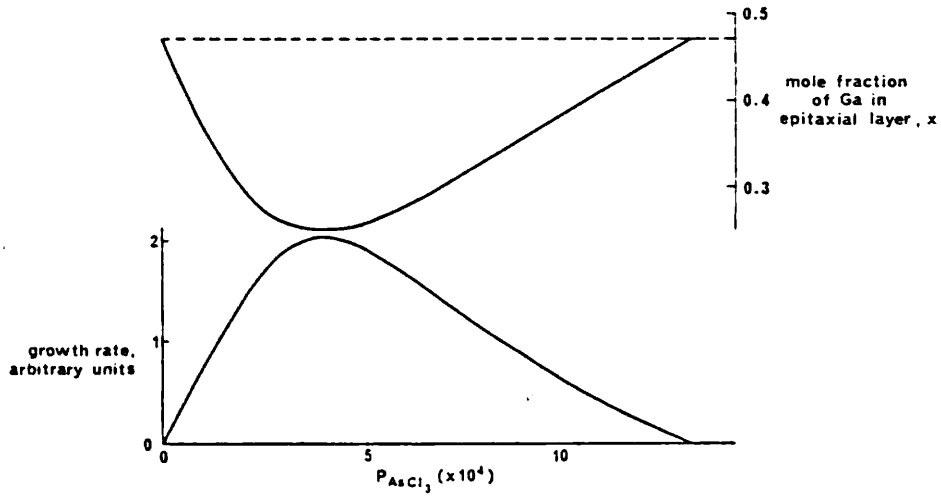

Growth rate vs. $AsCl_3$ pressure with corresponding variation in solid composition

Fig 6-10

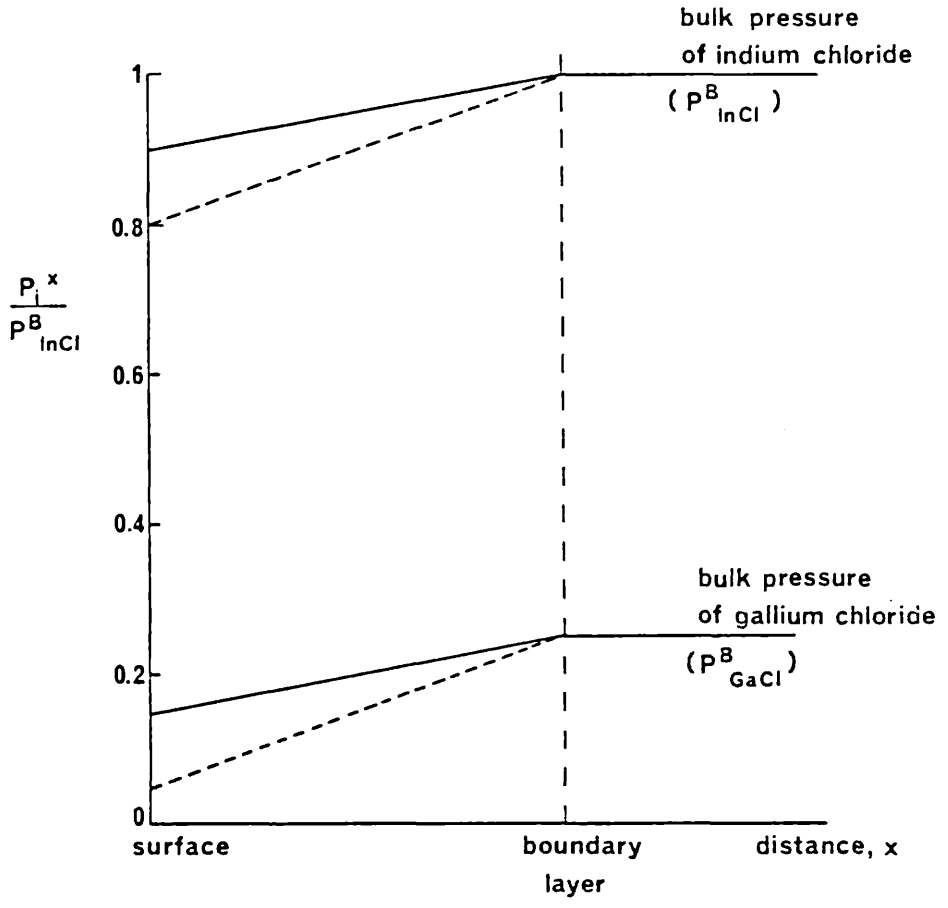

Schematic diagram of partial pressure profile at interface.

Bulk pressure ratio=0·25. At interface, ratio=0·17 and is reduced to 0·063 on doubling the growth rate (broken lines)

The increase in growth rate will reduce the interfacial pressure of both species. However, the effect is proportionately greater for the minority species (in this case GaCl), and the increased growth rate results in a reduction in the gallium content of the grown layer. Any factor which changes growth rate will also alter the interfacial gas composition. Even if the system is not transport limited the effect may still be observed although the magnitude of the changes will be less.

6.4 Summary

In this chapter the growth of ternary and quaternary compounds was examined. Simple equilibrium models demonstrated the connection between solid composition and that of the vapour. By extending the thermodynamic treatment to non-equilibrium systems it was shown that under typical growth conditions a wide range of solid compositions could be grown. In practice, surface kinetic and transport factors will result in only one composition and this was demonstrated using a transport-limited growth model. The model showed that solid composition was function of both gas composition and growth rate. It is clear that the nature of the substrate, the orientation and the number and type of surface defects will all influence the composition of the growing layer.

REFERENCES

1 R.L. Moon, A.G. Antypas, L.W. James: J. Electron. Mat. 3, 635, 1974.

2 Y. Takeda, A. Sasaki: J. Cryst. Growth 45, 257, 1978.

3 T.Y. Wu, G.L. Pearson: J. Phys. Chem. Solids 33, 409, 1972.

4 J.J. Tietjen, J.A. Amick: J. Electrochem. Soc. 113, 724, 1966.

5 G.H. Olsen, T.Z. Zamerowski: Prog. Cryst. Growth Charact. 2, 309, 1979.

6 B.I. Miller, J.H. McFee: J. Electrochem. Soc. 125, 1310, 1978.

7 B.J. Baliga, S.K. Ghandi: J. Electrochem. Soc. 122, 683, 1975.

8 J.P. Duchemin, J.P. Hirtz, M. Razeghi, M. Bonnet, S.D. Hersee: J. Cryst. Growth 55, 64, 1981.

9 S.B. Hyder: J. Electrochem. Soc. 123, 1503, 1976.

10 J.R. Knight, D. Effer, P.R. Evans: Solid State Electron. 8, 178, 1965.

11 K. Kajiyama: J. Electrochem. Soc. 123, 423, 1976.

12 A. Koukitu, H. Seki: J. Cryst. Growth 49, 325, 1980.

13 H Nagai: J. Cryst. Growth 48, 359, 1980.

14 M.B. Panish, M. Ilegems: 'Progress in Solid State Chemistry' 7, 39, Pergamon Press, Oxford, 1972.

15 E.A. Guggenheim: 'Mixtures', Oxford, 1952.

16 See references 1-8 of chapter 5.

17 E.J. Tarbox: PhD Thesis, London 1977.

18 D.R. Stull, G.C. Sinke: 'Thermodynamic Properties of the Elements' American Chemical Society 1956.

19 D. Battat, M.M. Faktor, I. Garrett, R.H. Moss: J. Chem. Soc. Far. Trans I, 70, 2302, 1974.

20 J.J. Murray, C. Pupp, R.F. Pottie: J. Chem. Phys. 58, 2569, 1973.

21 A.N. Krestovnikov, V.B. Ufimtsev, V.V. Egorkin: Russ. J. Phys. Chem. 47, 308, 1973.

22 K. Sugiyama, H. Kojima, H. Enda, M. Shibata: Jap. J. Appl. Phys. 16, 2197, 1977.

23 K. Denbigh: 'The Principles of Chemical Equilibrium' Cambridge 1971.

CHAPTER 7: GROWTH OF MIXED III-V COMPOUNDS: EXPERIMENTAL

Whereas the previous chapter concentrated on theoretical aspects of the growth of ternary and quaternary compounds, this chapter is concerned with the development of the growth systems and the results obtained. The (Ga,In)As layers were used to fabricate avalanche photodiodes operating at wavelengths up to 1.67 μm. The reactants were described in chapter 6.

7.1 Material and Apparatus

7.1.1 Materials

The materials used in the work were identical to those used in the InP growth (section 5.2.1), with the addition of gallium and $AsCl_3$. Both of these were supplied by Mining and Chemical Products Ltd (MCP) and were the same grade as In and PCl_3 respectively.

$AsCl_3$ was introduced into the reaction zone by a bubbler arrangement similar to that used for PCl_3.

7.1.2 Apparatus

The $Ga_xIn_{1-x}As$ growth was carried out using the apparatus shown schematically in fig 1. This system will be discussed in detail, after which the modifications necessary for growth of the quaternary will be described.

The gas inlet system allowed hydrogen/hydrogen chloride mixtures to be passed over a vitreous carbon boat containing a gallium/indium melt. $AsCl_3$ was introduced through a separate inlet, as was hydrogen sulphide - the n-type dopant which was produced in

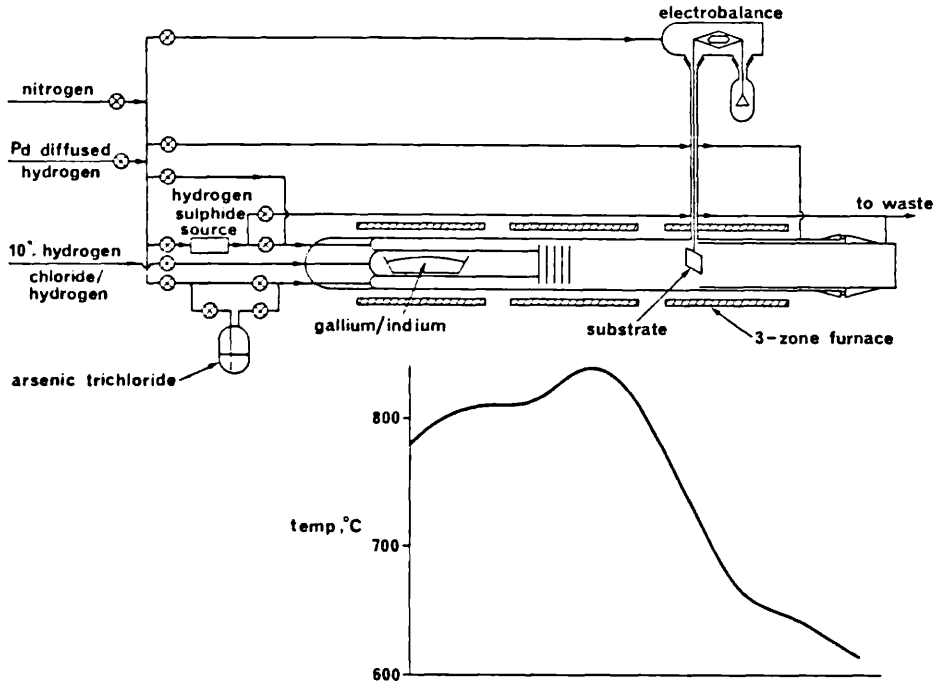

Diagram of growth system for GaInAs

situ by the reduction of sulphur vapour in the hydrogen gas-stream. The gas streams were mixed in a central zone; baffles ensured good mixing and minimised back-diffusion. Waste products were collected in a removeable linear tube. The annular space round this tube was purged with hydrogen. A recording electrobalance was included in the system design to enable the weight of the substrate to be monitored continuously. Although not essential for the routine growth of ternary layers for device fabrication, the weighing facility offered three advantages. Firstly, the time taken to optimise growth conditions was greatly reduced as the effects of a change in growth conditions could be observed immediately, allowing the exploration of several sets of conditions in a single experiment. Secondly, by changing the growth conditions in a systematic manner, investigations into the dependence of growth rate on the various input parameters could be made. Finally it allowed the growth of layers of predetermined thickness. The balance head was purged with hydrogen continuously, to prevent attack by the corrosive reactant gases. A constriction at the lower end of the balance side-arm prevented back-diffusion by increasing the gas-velocity at this point. The substrate was supported vertically on a slica cradle which was suspended from the balance. A silica dome attached to this cradle prevented the flow from the balance purge line disturbing the gas-composition adjacent to the substrate.

The whole system was heated by a three zone resistance furnace; a slot in the third zone allowed the furnace to be rolled on and off the substrate zone. Typical temperature settings were: metal source zone 800°C, gas mixing zone 850°C and substrate zone 650°C. In order to minimise incongruent evaporation of the substrates, the furnace was heated to temperature in a rolled off position, then moved to its final position immediately prior to growth.

To grow the quaternary material an additional bubbler, containing PCl_3, was incorporated into the system. The bubbler was identical to that described in chapter five. The system was also modified to provide separate sources for Ga and In (fig 2). To obtain the required ratio of GaCl:InCl in the vapour, a 10% HCl supply was connected to the Ga line, and a pure HCl supply to the In line. Both HCl supplies were diluted with hydrogen prior to passing over the metal sources.

7.1.3 Analysis of the Epitaxial Layers

A variety of techniques were used to determine layer composition. The difference between the lattice parameter of the layer and that of the InP substrate was obtained using X-ray diffraction techniques: especially double crystal X-ray diffraction. The plots obtained (rocking curves) gave information about the mean composition and the uniformity of the layer. A typical plot of a $Ga_xIn_{1-x}As$ layer is shown in fig 3. Compositional inhomogeneities and curvature due to mismatch were indicated by a broadening of the layer peak (fig 4).

Fig 7-2

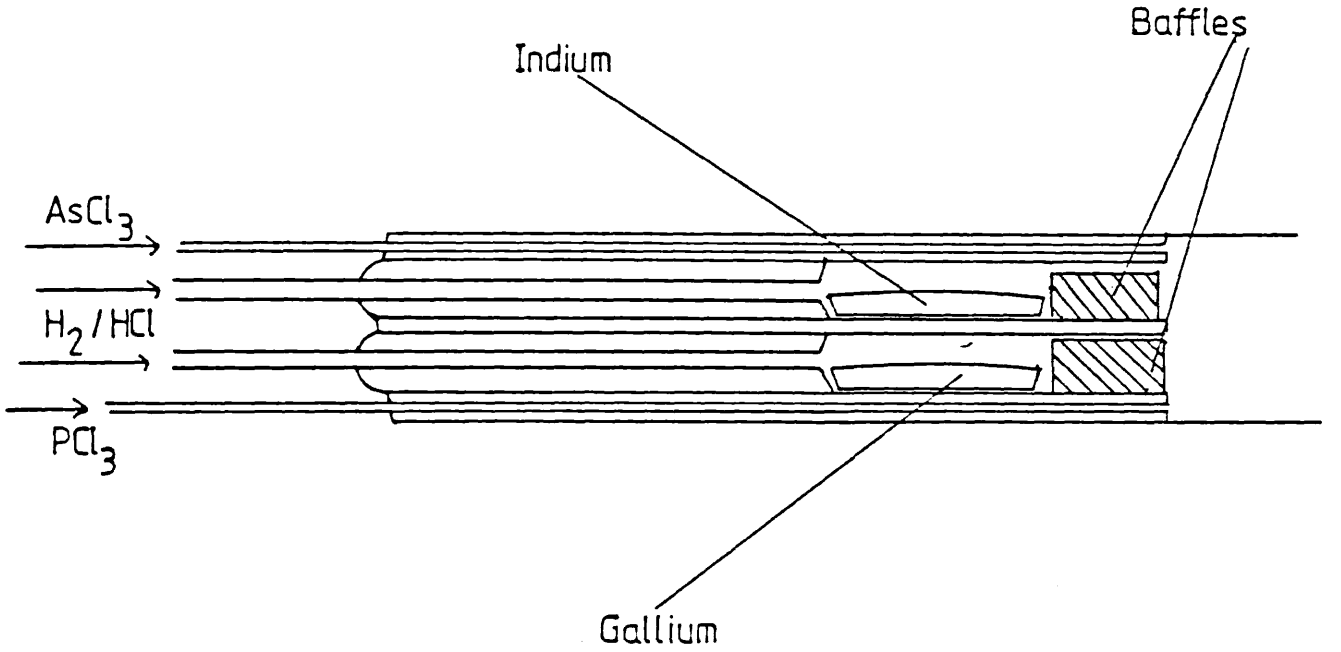

Diagram of source arrangement for quaternary growth

Fig 7-3

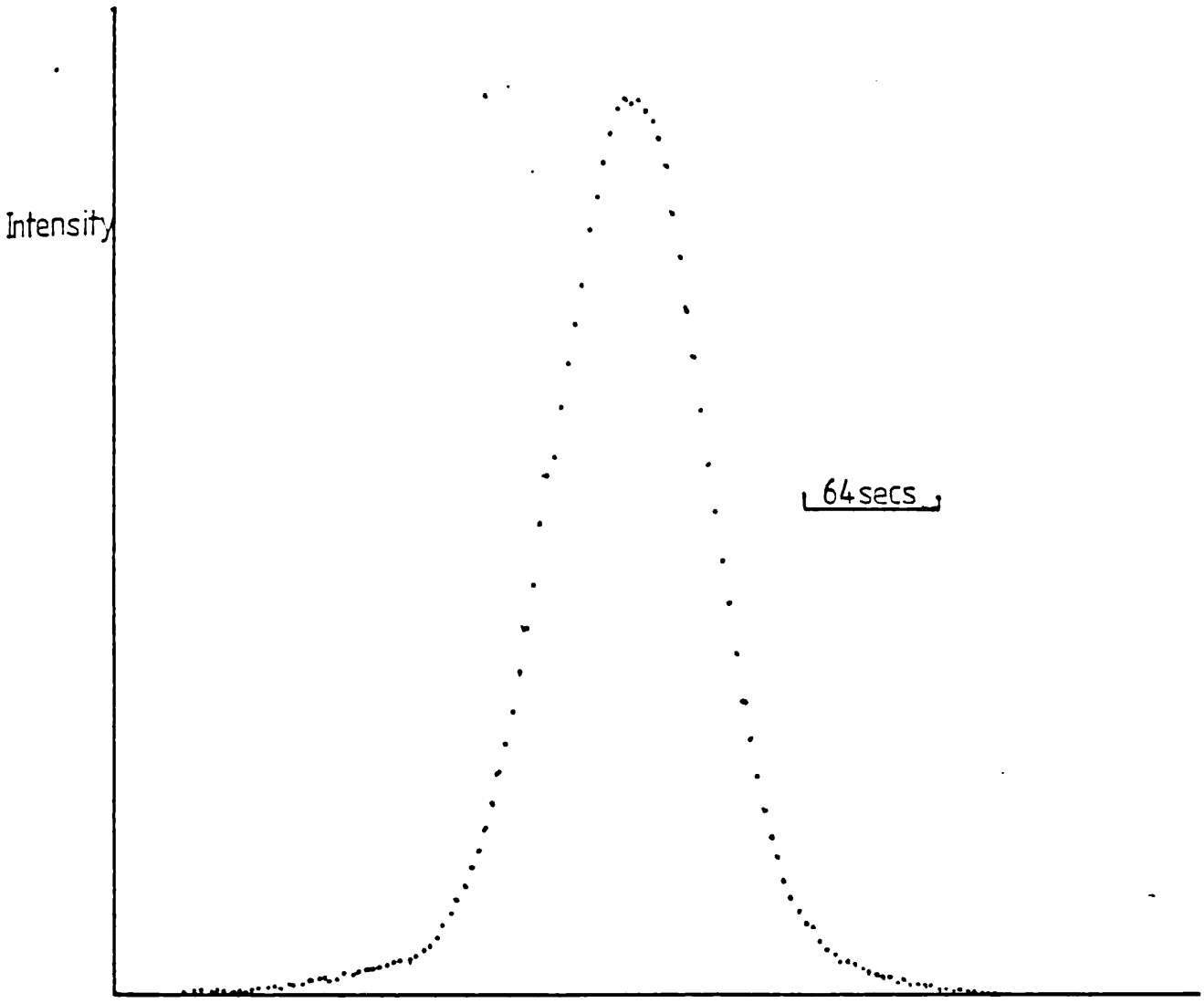

X-ray rocking curve for lattice-matched GaInAs

Fig 7-4

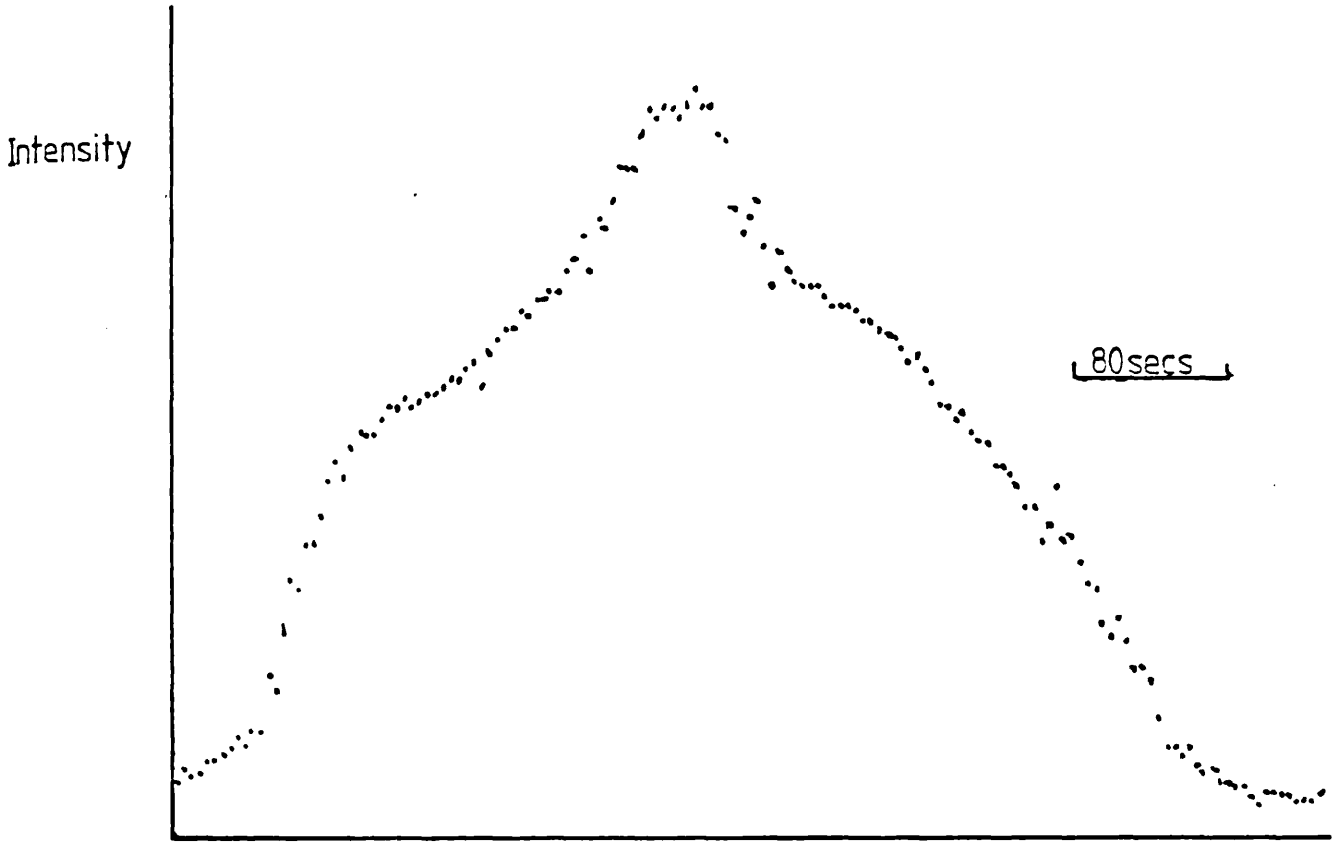

X-ray rocking curve for inhomogeneous GaInAs layer

Measurement of the lattice parameter was sufficient to determine the layer composition of a ternary using Vegards law, and estimation of the band-gap from the IR absorption spectrum, or from cathodoluminescence measurements could be used to confirm the results. However, for a quaternary layer both composition and band-gap were necessary before a unique composition could be assigned to the layer, using the equations and data Sugiyama et al [1].

Other analytical methods used were differential pulse polarography (DPP) and energy dispersive X-ray spectroscopy (EDAX). Both techniques gave a direct measure of the amount of the various chemical elements in the samples. EDAX was mainly used when layers were very poor and X-ray diffraction techniques and band-gap measurements either could not be made, or were inconclusive. However the technique was of low accuracy ($\pm$ 5-10 at %) unless a standard of known composition was available. It was not used when the other methods could be used. DPP allowed the gallium and indium content to be measured with a nominal accuracy of $\pm$ 2%. Good quality layers of $Ga_xIn_{1-x}As$ were close to lattice-matched and showed close agreement between X-ray, band-gap and DPP measurements (often within $\pm$ 0.5%). Poor quality material showed broad X-ray peaks, low and broad cathodoluminescence peaks and sloping band edges in the IR plot. Agreement between the various techniques was much poorer with differences of 4 at % or more between the results.

7.2 Growth of $Ga_xIn_{1-x}As$

7.2.1 Mixed-Metal Sources

It was shown in chapter 6 that control of the gas-phase is essential if the growth composition is to be reproducible. The metal chloride source was a melt containing a solution of Ga and In, over which HCl passed. The vapour composition was determined by the melt composition. This system avoided the need for complex gas control systems, and meant that the gas-phase ratio would not be affected by variations in the source efficiency.

The simple thermodynamic calculations shown in section 6.1.2 suggested a trial composition of around 2.5 at % Ga. However, lattice-matched layers were eventually obtained using a melt containing 3.2 at % Ga. This error may have reflected the inaccuracies of the equilibrium constants or the non-ideality of the solid solutions. An additional error was caused by differences in the equilibrium constants for the reactions of Ga and In with HCl so that the vapour composition was not the same as that of the melt; the difference in equilibrium constants caused Ga to be transported preferentially. Thus, in a series of experiments, successive grown layers became enriched in In. The effect was minimised by the use of large melts.

The changing composition of the melt with time was studied by taking two small samples ($\sim$ 1mg) from opposite ends of the melt ($\sim$ 200 g). The melt was stirred prior to sampling to reduce the effects of any melt inhomogeneities. The results are shown in

Fig 7-5

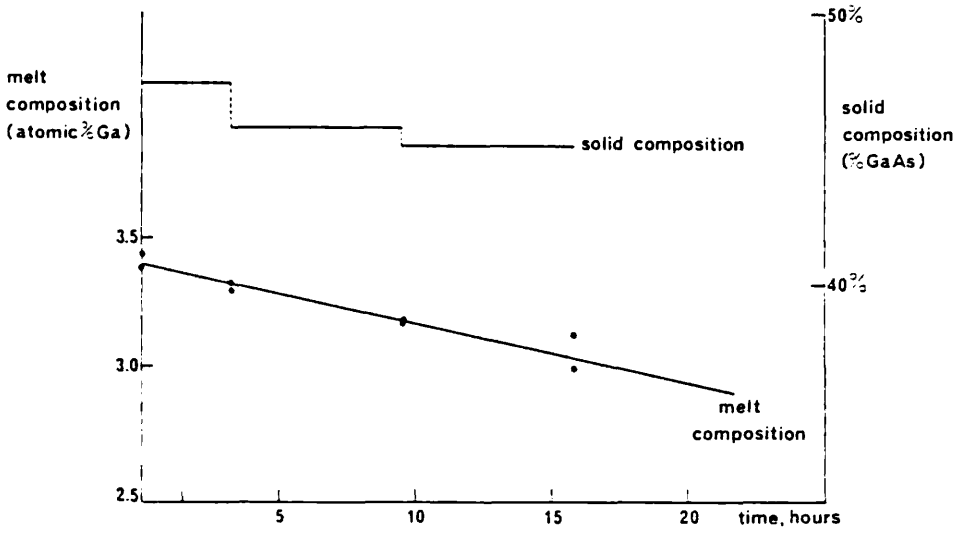

Experimental variation of melt composition with time

Corresponding layer compositions for each growth run shown as horizontal lines.

fig 5, together with the corresponding changes observed in the growing layer. Each sample result is a combination of 20 determinations with a mean square deviation of approx 1%. The two samples taken at 0 hrs showed a significant difference in composition, as did those at 15.75 hrs. Since the differences were far larger than the experimental errors in the AAS determinations, it was concluded that these results reflected the inhomogeneity of the melt at the time of sampling.

It was clear from fig 5 that the composition variation in the grown layers was small over the period of a normal growth experiment ($\sim$ 2 hrs). Furthermore, using the data from fig 5, it was possible to calculate the amount of alloy required to restore the melt to the required composition after each growth run. Using this procedure routinely, the compositional reproducibility from run to run (over 350 runs) was within 1 at % of the required composition. The rate of depletion of the melt was modelled (see appendix : section 7.5). The model showed the rate of depletion to be a function of the ratio K^o_{Ga}/K^o_{In} where K^o_i is the equilibrium constant of the reaction of metal with HCl. Combining the experimental results with the depletion model (fig 6) enabled K^o_{Ga}/K^o_{In} to be estimated - a value of 2 was obtained for a melt at 800°C. The ratio of metal chlorides over the substrate was then calculated to be

$$\frac{P_{InCl}}{P_{GaCl}} \simeq 15 \qquad \ldots\ldots$$

Fig 7-6

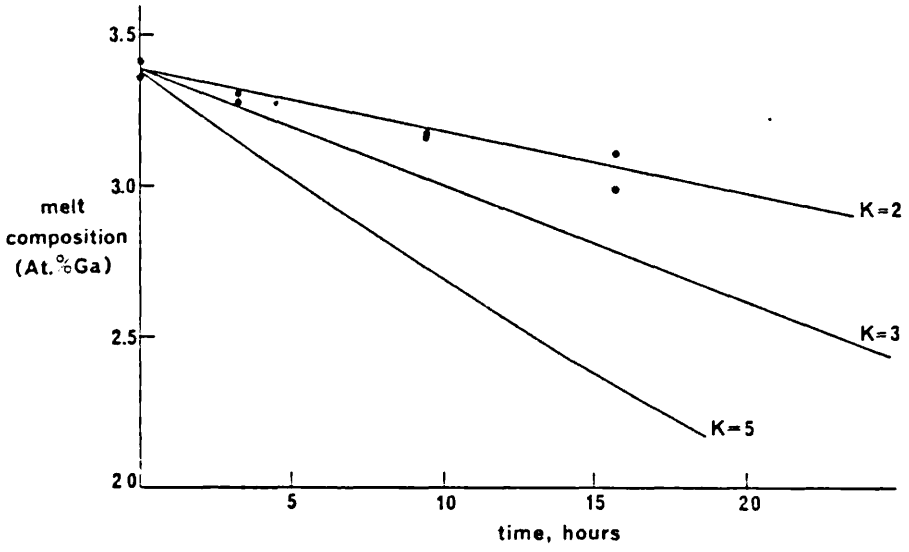

Calculated variation of melt composition with time, for three values of $K = K_{Ga}/K_{In}$. Experimental points lie close to line K=2

The pressure ratio over the substrate was also found directly by growing $Ga_xIn_{1-x}As$ with the system containing two separate sources. For this system, lattice-matched material was obtained when

$$\frac{P_{InCl}}{P_{GaCl}} = 17.4$$

which is in reasonable agreement with the estimated value found above.

7.2.2 Growth Experiments

Compositional control was good - within $\pm$ 1 at % from run to run. The layers usually gave narrow cathodoluminescence and rocking curve peaks (figs 3 and 7). Morphology, similarly, was good. The layer were mirror like to the naked eye and in general showed a uniform surface structure under the microscope (fig 8). The most common surface feature was a large shallow mound with a tail and, sometimes, a square or line in the centre (fig 9). These features, known as 'parachutes', did not affect the suitability of the material for device purposes: the layers were used in the fabrication of photodiodes [2].

Although most experiments were aimed to produce material for devices, it was possible to carry out some more fundamental studies. The variation of growth rate with $AsCl_3$ pressure was examined by growing with the $AsCl_3$ bubbler at several different temperatures during one experiment. The growth rate was measured using the electrobalance and the results are shown in fig 10. It can be seen that the general shape of the curve is similar to the theoretical curves

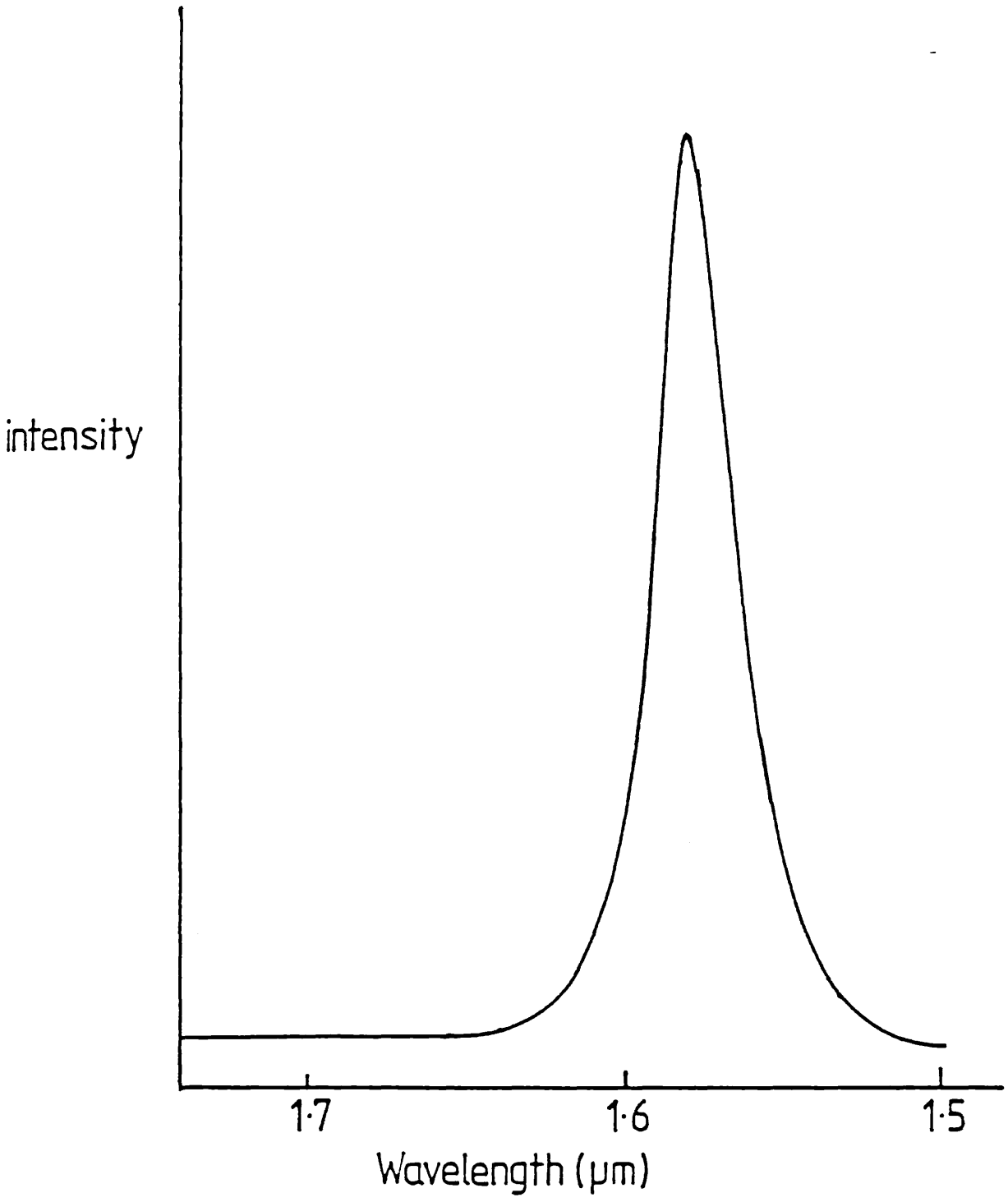

Cathodoluminescence spectrum of GaInAs layer at 100K

Fig 7-8

Photograph of GaInAs layer -

Fig 7-9

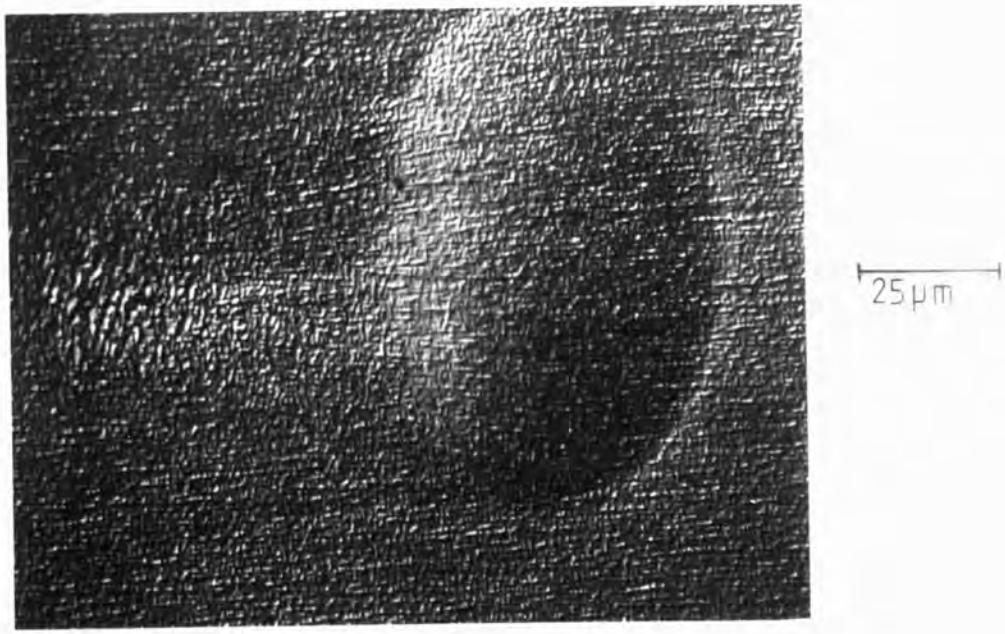

Photograph of a 'parachute'.

Fig 7-10

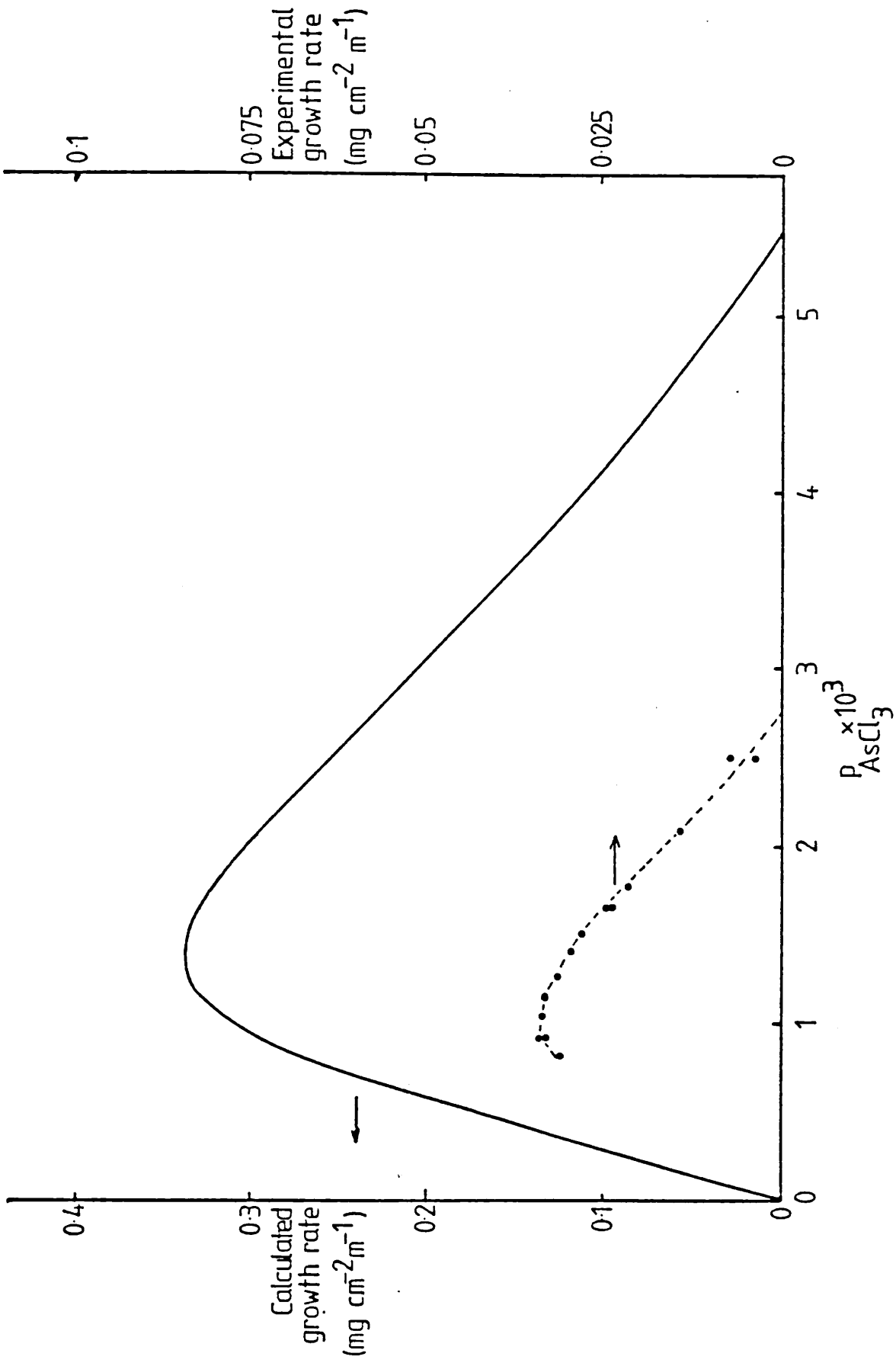

Experimental growth rate vs p_{AsCl_3} compared with transport model.

(figs 8 and 9 of chapter 6). Certain differences are immediately apparent: thus, the maximum growth rate, and the point where the experimental curve changes from growth to etching, occur at different pressures from those found in the theoretical curves. Also, when the calculated transport function was converted to an experimental growth rate using a value of 1 cm for the transport distances (ℓ) (see section 5.1.2), the maximum theoretical growth rate was approximately ten times the observed maximum rate. This is an indication of kinetic factors influencing growth rate, but could also arise from errors in the estimation ℓ and those arising from the assumption of a single diffusion constant for all species.

The pressure of $AsCl_3$ which gives a zero growth rate corresponds to the equilibrium situation. This point is unaffected by kinetics; hence, the discrepancy between the experimental and theoretical $AsCl_3$ pressure for equilibrium is the result of errors in the thermodynamic data used in the theoretical calculations. These errors would also affect the calculated growth rate.

Clear evidence for the existence of kinetic barriers was demonstrated by examining the growth on different substrate orientations. It was shown in section 4.1 that the kinetic barriers to the growth of III-V compounds vary with orientation. A similar variation was expected for the growth of the mixed III-V compounds: if the growth were transport limited then there would be no differences in the growth rate on different substrate orientations. To test this, the ternary material was grown on (100) and (111A) substrates simultaneously. The growth rate on the (111A) surface was found

to be approximately double that on the (100) surface. This is clear evidence that surface kinetics are important in the growth of the ternary. The possibility that this result might simply be due to the different positions of the slices in the reactor was eliminated by repeating the experiment with two substrates of (100) orientation. There was no significant difference in the growth rates on the two substrates. Growth conditions in the experiment were chosen to give lattice-matched layers on the (100) surface. The expectation of good lattice-matching on the (100) substrate was borne out in the experiment ($Ga_{0.472}In_{0.528}As$). In contrast, the mismatch between the epitaxial layer and substrate on the (111A) surface was so large that in some places it peeled off from the substrate (fig 11). The composition of this layer was significantly higher in In ($Ga_{0.43}In_{0.57}As$). The relationship between growth rate and composition was consistent with the transport model of section 6.3: thus, the faster growth rate produced material with a lower Ga content (see fig 9 of chapter 6).

Further evidence that composition was a function of growth orientation was obtained from the growth which occurred on the edges of the substrate (fig 12). In many cases the edge growth was found to peel off or even induce cleavage in the substrate - a clear indication of mismatch between the substrate and the epitaxial growth.

Fig 7-11

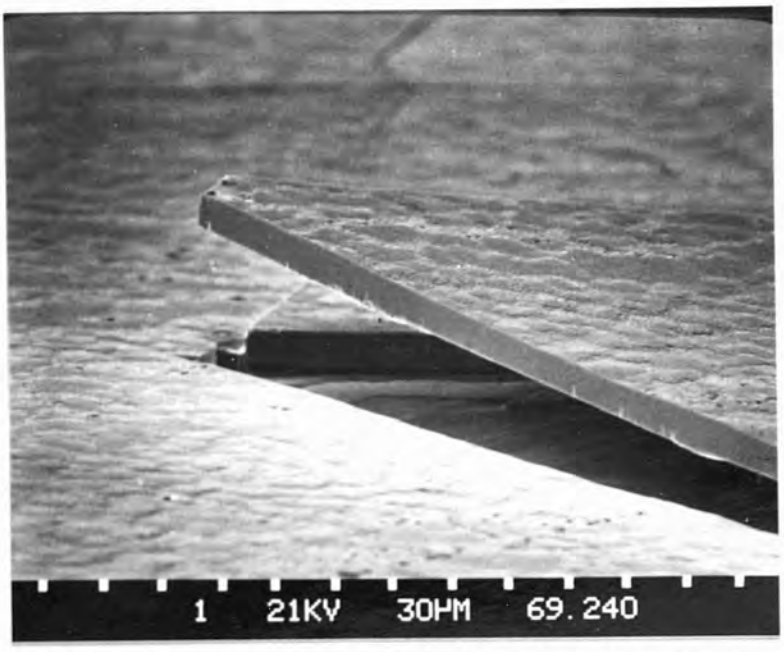

SEM Photograph of mismatched and peeling layer on (111) substrate.

Fig 7-12

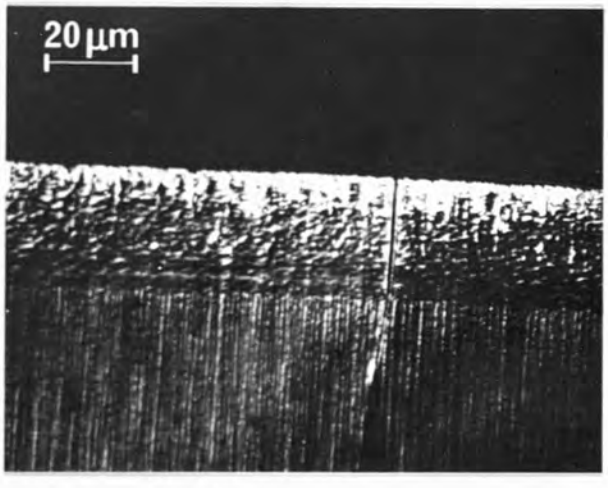

Photograph of edge growth.

7.3 Growth of Quaternary Compounds

In a ternary system, the choice of a particular lattice-parameter also fixes the band-gap of the material. The addition of a fourth component allows the band-gap and lattice parameter of a quaternary compound to be varied independently. As with (Ga,In)As, the lattice-parameter was chosen to give lattice-matching to InP and the band-gap was determined by the use to which the material could be put. The most important use of the quaternary material is in the fabrication of LED's and lasers for optical communications systems. Current interest is in systems operating at 1.3 μm or 1.5 μm and the band-gaps were chosen to correspond to these wavelengths. Initially, work was concentrated on obtaining material with a band-gap corresponding to about 1.3 μm, lattice-matched to InP ie material with a composition around $Ga_{0.33}In_{0.67}As_{0.71}P_{0.29}$ [1].

7.3.1 Metal Sources

Initial experiments were carried out with a single mixed-metal source, as with the work on (Ga,In)As. However, this was later replaced by two separate metal sources allowing the gallium and indium chloride input pressures to be altered independently. The reasons for this are discussed below; here the discussion concentrates on the properties of the pure sources.

The standard procedure to start growth was to open the HCl lines to the indium and gallium lines first, and to open the line to trichloride bubblers after a delay of 0 to $\sim$ 5 minutes. The weight changes during the early stages of growth were followed using the electrobalance and always showed the same features; there was a rapid loss of weight immediately on opening the trichloride

lines, followed by a period of 4-5 minutes when there was little change in weight before, finally, growth started (fig 13). It was found that by increasing the delay between opening the HCl lines and the trichloride lines the period of rapid weight loss could be reduced. If the delay exceeded about 5 minutes, then no rapid weight loss was observed. The results were interpreted as arising from an induction period of about 4-5 minutes associated with the metal melts. A possible cause of this induction period was that when HCl reacted with the metals to form the chlorides, the metal chlorides did not, initially, pass into the reaction zone, but dissolved in the melts. This process continued until the melt was saturated.

Further information was obtained by growing layers of GaAs and InP on their respective substrates. Qualitative results were similar to those obtained with ternary and quaternary growth. The weight vs time plots are shown in fig 14. The plot for InP is similar to that observed in quaternary growth - giving an induction period for the In source of 4-5 minutes. The GaAs plot is somewhat different - the initial rate of weight loss is slower than that observed with InP. Since the weight loss is due to the attack of the substrate by HCl formed by reduction of trichlorides, this suggests that the exchange current for the GaAs/HCl reaction is smaller than that for InP/HCl. The fact that GaAs is normally grown at much higher temperatures (750^{o}C) than InP (650^{o}C) also supports this view [3]. The induction period for the Ga melt was much longer than that for In - about 8-9 mins.

Fig 7-13

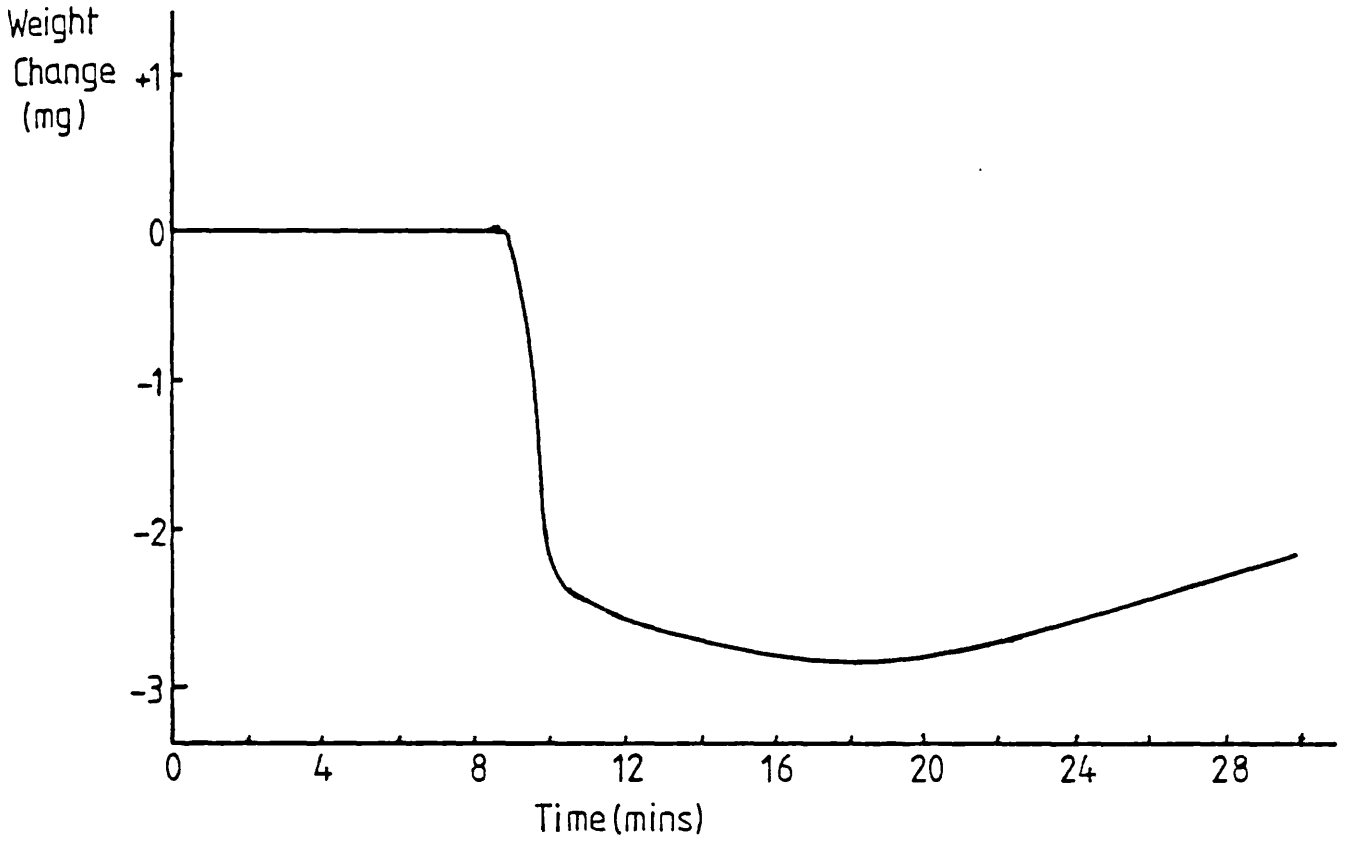

Weight change vs. time for quaternary growth showing initial weight loss

Fig 7-14

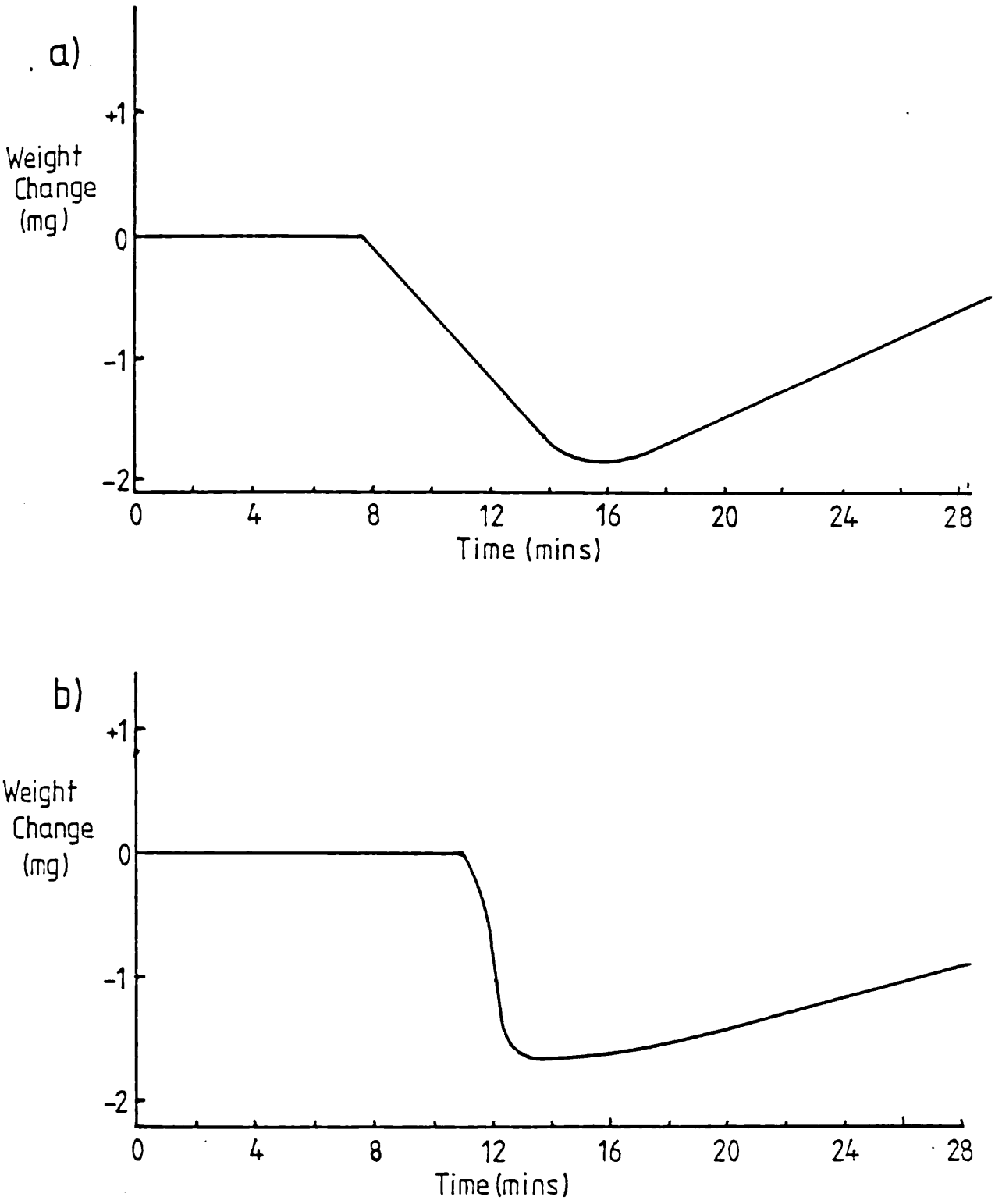

Weight change vs. time for a)GaAs & b)InP growth showing initial weight loss.

No induction period was detected when using a mixed-metal source. This means that any induction period was shorter than the delay between opening the $AsCl_3$ bubbler, and the $AsCl_3$ vapour reaching the substrate zone. It was suggested above that the melt induction period was caused by the need to form a saturated solution of the metal chloride in the melt. If the solubility of the chloride is reduced, then the induction period will also be reduced. This may explain the difference between the pure metal sources and the mixed metal source since the addition of a third component to a solution is known to reduce the solubility of the solute [4].

7.3.2 Composition

Thermodynamic calculations based on equations 37 and 38 of chapter 6 suggested that for the solid $Ga_{0.33}In_{0.67}As_{0.71}P_{0.29}$ the gas ratios should be:

$$\frac{P_{InCl}}{P_{GaCl}} = 93.71 \qquad \frac{P_{P_4}}{P_{As_4}} = 62.63$$

Because there was a limit to the total pressure of PCl_3 and $AsCl_3$ which could be introduced in the system without giving rise to an etching vapour, the achievement of the very high non-metal ratio would have required the $AsCl_3$ temperature to be very low ($\sim -30^{\circ}C$), necessitating the purchase of special low temperature coolers. However, the solid composition depended on the quater power of the non-metal pressures ($p_{P_4}^{\frac{1}{4}}$ and $p_{As_4}^{\frac{1}{4}}$), and quite small errors in the thermodynamic data could alter the estimated ratio by several orders of magnitude as was shown in section 6.1.2. Furthermore, workers using phosphine and arsine had not reported the need for

such extreme ratios [5]. As a first step, then, it was decided to carry out some trial experiments using pressure ratios close to unity. These trial runs were carried out using a mixed-metal source.

The results are shown in table 1. Compositions were determined by combining double crystal X-ray diffraction results with IR band-edge determinations using the equations and data of Sugiyama et al [1]. The results in table 1 indicate clearly that layers of the required composition could be grown using a value of p_{As_4}/p_{P_4} close to 1. However, reproducibility was apparently poor. This reflects the poor quality of the layers. The X-ray peaks were very broad (cf fig4) and the layers gave very sloping IR spectra, (fig 15). As predicted in section 6.1.2 the As:P ratio in the solid was strongly influenced by the ratio p_{GaCl}/p_{InCl}. However, whereas section 6.1.2 predicts a steady change of solid As content with increasing InCl content the results in table 1 show that solid containing the highest As content was obtained with the intermediate values of p_{InCl}/p_{GaCl}. No attempt was made to investigate the phenomenum further in view of the poor quality of the layers and the consequent uncertainty in the results. It was clear that control of gas composition was more critical in quaternary growth than for ternary growth and that the steady variation of melt composition with time was a serious problem. Consequently, the apparatus was altered to allow separate gallium and indium sources to be used. An additional advantage of this new system was that it allowed multi-layer growth to be carried out.

TABLE 1

SAMPLE	P_{InCl}/P_{GaCl}	P_{As_4}/P_{P_4}	COMPOSITION (nominal)
CK36	16	1.02	$Ga_{0.78}In_{0.22}As_{0.35}P_{0.65}$
CK38	102	1.02	$Ga_{0.14}In_{0.86}As_{0.60}P_{0.40}$
CK40.1	39	1.02	$Ga_{0.39}In_{0.61}As_{0.76}P_{0.24}$
CK40.2	39	1.02	$Ga_{0.43}In_{0.57}As_{0.76}P_{0.24}$
CK41.1	39	1.02	$Ga_{0.31}In_{0.89}As_{0.72}P_{0.28}$
CK41.2	39	1.02	$Ga_{0.39}In_{0.61}As_{0.84}P_{0.16}$

Results of early experiments using mixed-metal source.

Fig 7-15

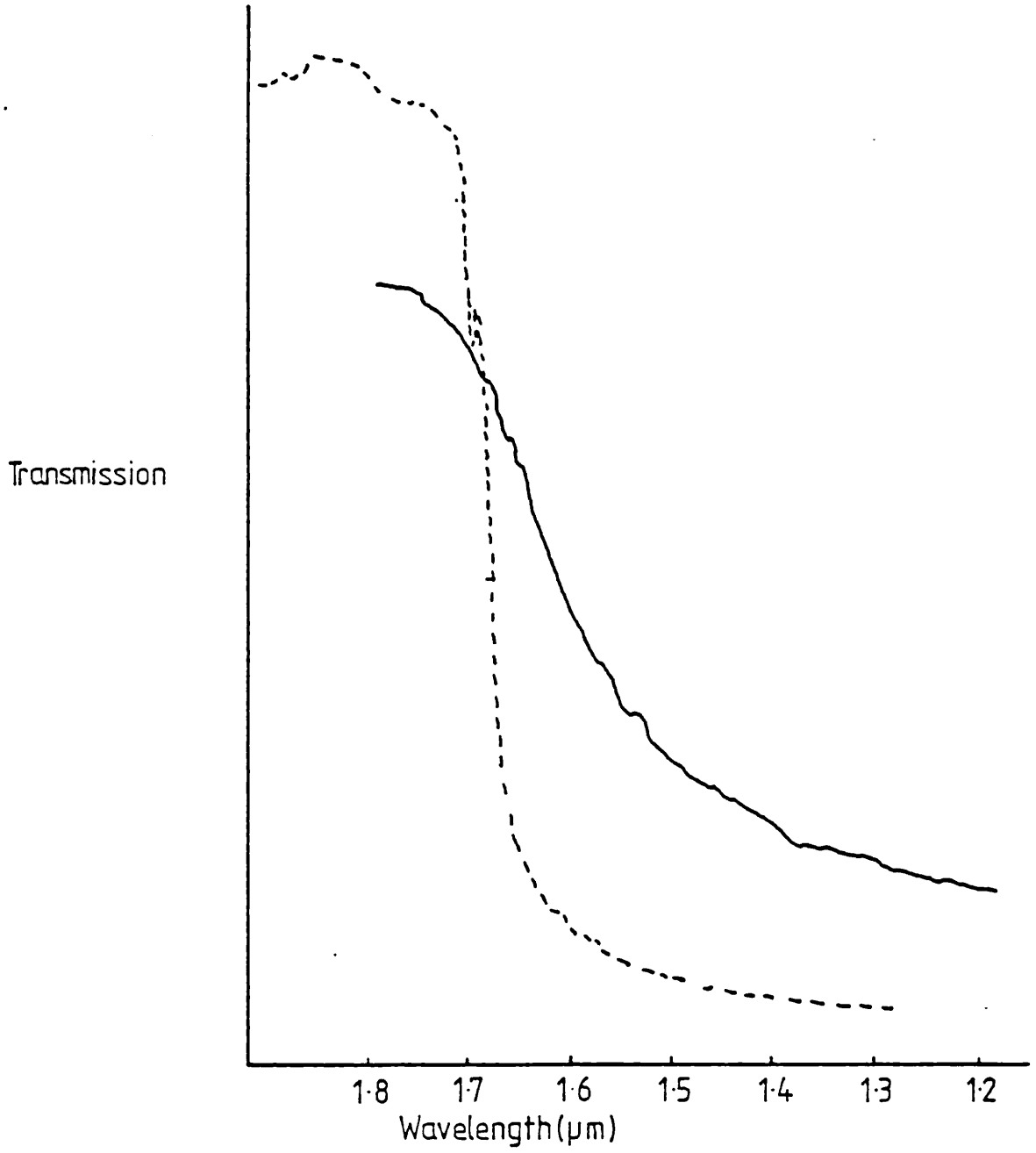

IR spectrum of poor (solid line) and good (broken line) GaInAs layers

Several trial experiments were carried out before layers close to the required composition were obtained. The results are shown in table 2. It will be seen that the final growth conditions differed somewhat from those indicated in table 1. This may reflect errors in the estimation of the InCl and GaCl pressures when using the mixed-metal melt. Despite the change in sources the quality of the layers was not greatly improved. Indeed, some of the initial layers were so poor that layer composition could only be measured with EDAX. However, the general crystal quality and the layer morphology are discussed in more detail below. In general, the double-crystal diffraction peaks were broad, and cathodoluminescence intensity was low.

Because of changes in growth temperature, it is not immediately apparent from table 2 what effect a change in the ratio p_{As_4}/p_{P_4} had on layer composition. However examination of the results for CL21 and 22 (and to a lesser extent CL10 and 11) suggest that the composition obeys a law of the form

$$\frac{y}{1-y} \alpha \frac{p_{As_4}}{p_{P_4}}$$

rather than the predicted variation from equation 38 of chapter 6:

$$\frac{y}{1-y} \alpha \left(\frac{p_{As_4}}{p_{P_4}} \right)^{\frac{1}{2}}$$

Even more significant is the fact that the value of p_{AsCl_3}/p_{PCl_3} is very close to unity. This is in contrast to the metal chloride ratio which shows reasonable agreement (within a factor of 2)

TABLE 2

SAMPLE	P_{InCl}/P_{GaCl}	P_{AsCl_3}/P_{PCl_3}	Growth Temp (°C)	COMPOSITION
CL9	33	0.98	680	$Ga_{0.74}In_{0.26}As_{0.27}P_{0.73}$*
CL10	50	0.88	680	$Ga_{0.34}In_{0.66}As_{0.58}P_{0.42}$
CL11	50	1.16	680	$Ga_{0.77}In_{0.23}As_{0.65}P_{0.35}$*
CL19	50	1.56	680	$Ga_{0.36}In_{0.64}As_{0.76}P_{0.24}$
CL20	50	1.56	680	$Ga_{0.37}In_{0.63}As_{0.76}P_{0.24}$†
CL21	50	1.55	660	$Ga_{0.33}In_{0.67}As_{0.63}P_{0.35}$
CL22	50	1.82	660	$Ga_{0.37}In_{0.63}As_{0.76}P_{0.24}$
CL24	50	1.82	660	$Ga_{0.37}In_{0.63}As_{0.77}P_{0.23}$

Results of Experiments using separate metal sources

*EDAX results

†Surface Layer Present

with the thermodynamic calculations. Similar results have been obtained by other workers. Thus, Olsen and Zamerowski [5] grew $GaAs_yP_{1-y}$ in the range $0.1 < y < 0.5$, using ratios of PH_3/AsH_3 within the range $0.1 < p_{PH_3}/p_{AsH_3} < 10$- indeed, unless the solid P:As ratio is very extreme, the gas phase ratios are close to unity. There are several reasons for this lack of agreement between the calculated and observed ratios of the group V vapour species. Firstly, the existence of dimeric species (which were neglected in the thermodynamic calculation of section 6.1.2) means that solid composition will be more sensitive to changes in the group V ratio in the vapour than was predicted. Secondly, the ratios in the hydride systems will be distorted by the fact that PH_3 and AsH_3 decompose slowly in the vapour, so that the systems contain significant amounts of unreacted hydride. Both these factors suggest modifications to the thermodynamic model. However, growth is a non-equilibrium situation and it was shown in section 6.3 that gas transport can also influence composition. In a steady-state system, the relative rates of transport of P and As must reflect the composition of the solid. For a typical growth system, in which p_{PCl_3} and $p_{AsCl_3} \ll 1$, this can be expressed by the relation

$$\frac{J_{As}}{J_P} = \frac{p_{As}^B - p_{As}^S}{p_P^B - p_P^S} = \frac{y}{1-y} \qquad \ldots\ldots 1$$

where J_i is the transport rate of species i, and p_i^B and p_i^S the bulk and surface pressures respectively. Note that equation 1 does not assume equilibrium at the surface; also the pressures are always first order terms in the transport equations. Two limiting cases may be considered:

1. $p_{As}^B >> p_{As}^S$, $p_P^B >> p_P^S$

This case is trivial and represents the situation in a system which is far from equilibrium. Equation 1 simplifies to

$$\frac{p_{As}^B}{p_P^B} = \frac{y}{1-y}$$

2. p_{As}^B , p_P^B << other reactants.

In section 6.3 it was shown that when the pressure of the arsenic species was small, the growth rate of (Ga,In)As was directly proportional to the pressure of $AsCl_3$ (fig 8 of chapter 6). This was because at low $AsCl_3$ pressures, the growth rate was controlled by the rate at which As reached the surface. A similar situation will occur in the growth of (Ga,In)P at low PCl_3 pressures (cf chapter 5). Clearly, when the P and As species are only present at low pressures,

$$J_{As} \alpha p_{As}^B \text{ and } J_P \alpha p_P^B$$

Hence,

$$\frac{J_{As}}{J_P} = \frac{y}{1-y} \alpha \frac{P^B_{As}}{P^B_P}$$

The effect of transport, then is to moderate the relationship so that there is a linear dependence between solid and vapour compositions.

In section 6.2 the thermodynamic aspects of the non-equilibrium system were considered and it was shown that under the experimental growth conditions, a wide range of different solids could be deposited. For example, it is clear from figs 5 and 6 of chapter 6 that changes of $\pm$ 10% in, say, Ga content did not significantly reduce the supersaturation for growth. Although the layers grown in this system were not of the highest quality, the analytical results indicated a relatively small compositional variation in the layers (within 2% in any component). Similarly, the results in tables 1 and 2, although showing some irreproducibility, do not show the wide range of compositions which might be expected on the basis of the overpotential curves. This is another demonstration of the importance of transport and surface kinetics in determining the composition of growing layers. However, results were obtained which showed that a given vapour phase could, on occasions, produce more than one solid composition. For example, some layers were found to have two distinct compositions. Polarograph measurements showed the top 0.7 μm or so to have 20-30 at % more Ga, than the bulk of the layer. By removing the top 0.7 μm, the bulk of the layer was found to have a composition similar to those in table 2:

$Ga_{0.35}In_{0.65}As_{0.72}P_{0.28}$. Similar results were obtained using EDAX, which also showed that lumps visible on the surface of some samples (fig 16) were Ga-rich. No explanation of these results has been found, although the lumps are clearly regions of abnormal growth where the conbination of surface kinetics and transport is likely to lead to a different composition from the rest of the surface. Nevertheless, the overpotential curves do show that these composition changes are possible, and show the limits of what may be grown.

7.3.3 Morphology

Once material which was close to lattice-matched with InP had been obtained, the main effort was put into improving the homogeneity and reducing the compositional variation of the material. Important criteria for distinguishing good and bad material were the width of the X-ray rocking curves and the cathodoluminescence peaks. It was found that the general appearance of the layers was a good guide to the overall quality.

Several factors were found to affect the morphology of the layers. A serious problem during the early experiments was the nucleation which occurred on the silica-ware. Growth was only possible in a very narrow range of gas compositions: if the supersaturation was too high, nucleation on the silica occurred leading to loss of control of the vapour composition over the solid and a corresponding loss of control of the solid composition (as exemplified by cathodoluminescence results - fig 17).

Fig 7-16

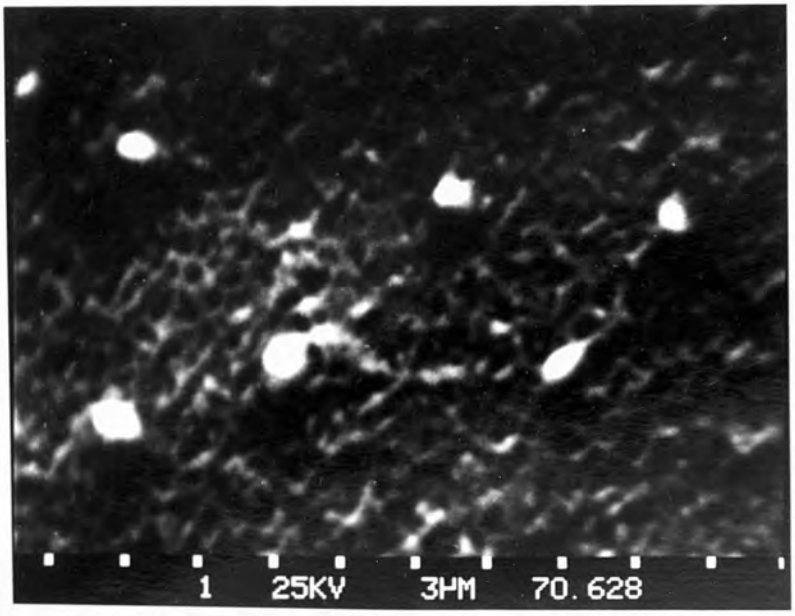

SEM photograph of Ga-rich lumps on surface

Fig 7-17

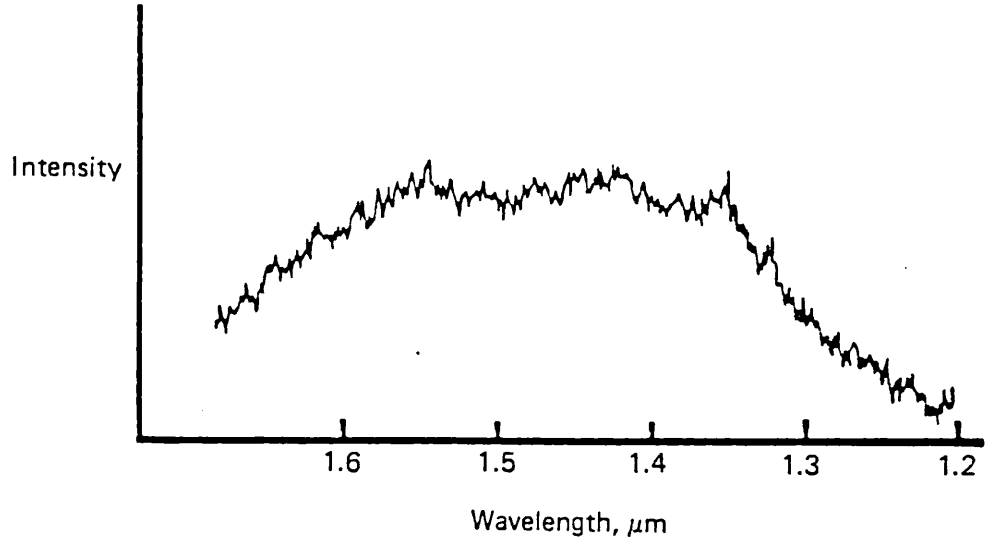

Cathodoluminescence spectrum of inhomogeneous quaternary layer

Elimination of nucleation produced an improvement in layer quality, but the cathodoluminescence peaks and rocking curves were still relatively broad. A second problem was the deterioration of the substrate prior to growth. To investigate this, layers of the ternary $Ga_{0.47}In_{0.53}As$ were grown. The epitaxial layers were then selectively etched with 1:1:8 $H_2SO_4:H_2O:H_2O_2$, which does not attack InP. This revealed a severely pitted surface (fig 18).

Substrate damage may be caused by several processes:

1. loss of phosphorus by incongruent vapourisation

2. attack by excess PCl_3 and $AsCl_3$ during the early stages of growth, before the metal sources had reached full efficiency (section 7.3.1).

3. attack by the steady-state gas composition which, although supersaturated with respect to the quaternary, many still attack the substrate material (section 6.2.1).

Incongruent evaporation was minimised by the arrangement of a rolling furnace (section 7.1.2) which minimised the time the substrate was at a high temperature in the absence of reactants. This procedure had been found to give good results when growing (Ga,In)As using the mixed-metal source.

The difference in induction period between the pure metal sources and the mixed-metal source was discussed in section 7.3.1. The rapid losses in weight immediately upon opening the PCl_3 and $AsCl_3$ lines were clear evidence that there was attack of the substrate

Fig 7-18

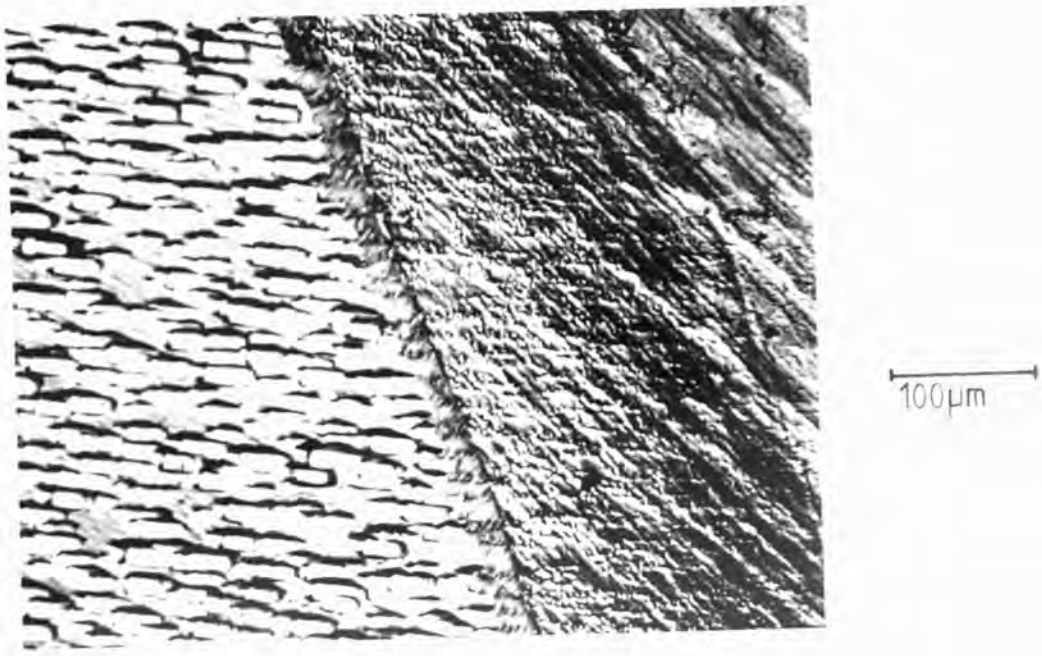

Photograph of substrate after removal of epitaxial layer by etching.
(Surface of substrate visible in top r.h. corner.)

during the early stages of an experiment. Some attempts were made to eliminate the problem by delaying the opening of the chloride lines. Various start-up procedures were tried, but none were satisfactory. The best results were obtained by opening the group V lines about two minutes after the HCl line. Longer delays reduced the measured weight loss, but also gave rise to poorer morphology - possibly due to the deposition of metallic Ga or In on the substrate.

The solution to this problem was to enclose the sample in a box to protect it from the gas-phase (fig 19). This approach had been used successfully by Susa et al [6]. Preliminary results for (Ga,In)As growth are encouraging (fig 20), and etching to the surface shows damage is far less severe (fig 21 - cf fig 18).

The third source of substrate damage is the attack of the substrate by the steady-state gas-phase. It was shown in figs 5 and 6 of chapter 6 that phosphorus-rich solid compositions were unstable with respect to the vapour. This was of particular importance in the early stages of growth since the substrate material in all experiments was InP. Until the substrate had been completely covered by a layer of quaternary compound, it could be etched by the vapour phase. Similar conditions in LPE gave rise to 'melt-back' phenomena [7].

During the early stages of growth both etching and growth could occur simultaneously at different points on the substrate. Although it was not possible to determine the importance of this process under normal growth conditions, the existence of this phenomenon was demonstrated by altering the growth conditions so that the

Fig 7-19

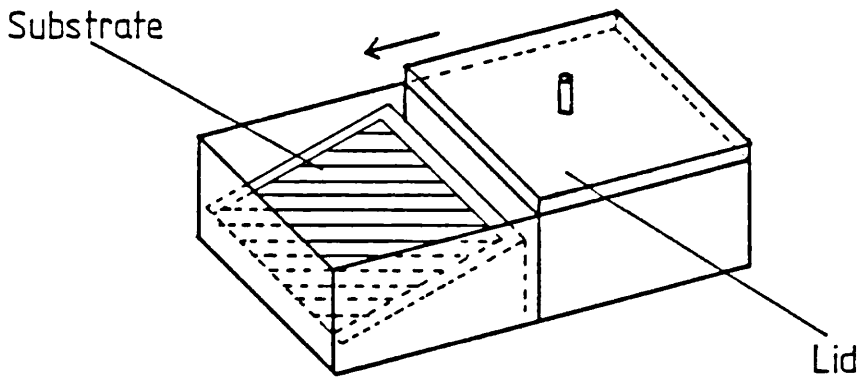

Box with sliding lid to protect substrate

Fig 7-20

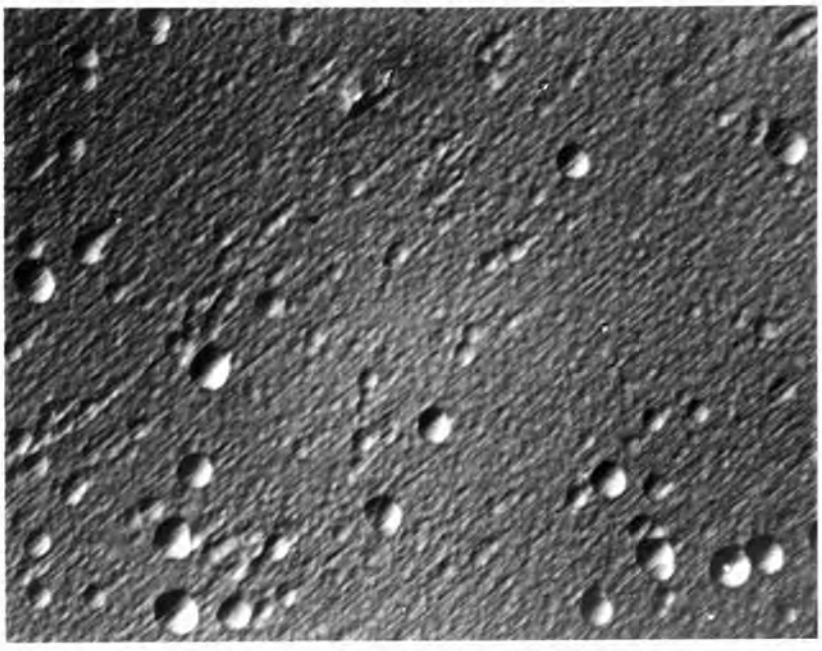

100μm

Photograph of GaInAs layer grown on a substrate which was protected from the gas-phase prior to growth

Fig 7-21

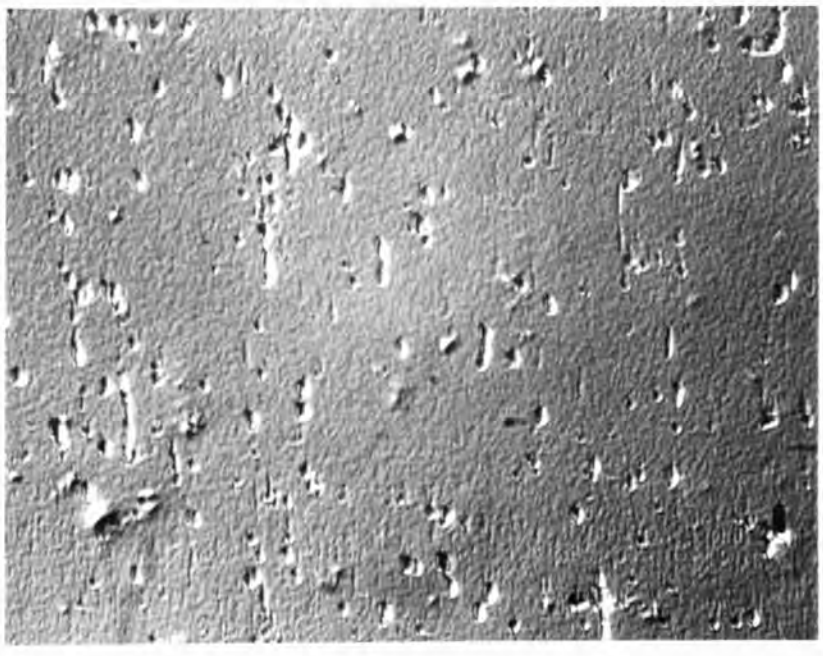

100μm

Photograph of sample in fig 20 after removal of epitaxial layer. Damage to substrate is far less severe than that shown in fig 18

InCl pressure in the reaction zone was approximately two orders of magnitude lower than in a normal growth experiment. The corresponding overpotential surface is shown in fig 22 and it can be seen that the highest overpotentials correspond to $GaAs_yP_{1-y}$ and that the overpotential decreases rapidly as the indium content of the solid increases. The vapour is highly unsaturated with respect to the InP.

During the experiment, the output from the balance showed a continuous and rapid loss of weight indicating that the vapour was etching the substrate. Using an external balance it was confirmed that $\sim$ 80 mg of material had been lost from the substrate. However, on all of the surrounding silica surfaces there was a heavy deposit, even on parts of the apparatus at temperatures some 20-30^{o}C higher than the substrate. The orange-red colour of this deposit indicated a high GaP content. Examination of the substrate showed that despite the high rate of weight loss observed, there had been significant deposition on the substrate itself. The bulk of this deposit was in the form of a continuous matt film apparently covering the whole of the surface. This could be readily removed from the underlying substrate (a consequence of the high mismatch between layer and substrate) thus enabling the total amount of deposit to be weighed. The weight of the deposit was approximately 40 mg. As well as the continuous matt layer of deposit, some fragments of a thin, shiny layer were observed peeling off from the surface (fig 23); in addition, underneath the main layer a patchy layer resembling polycrystalline material was observed (fig 24). The irregular distribution of this layer created a network of channels underneath the continuous layer.

Fig 7-22

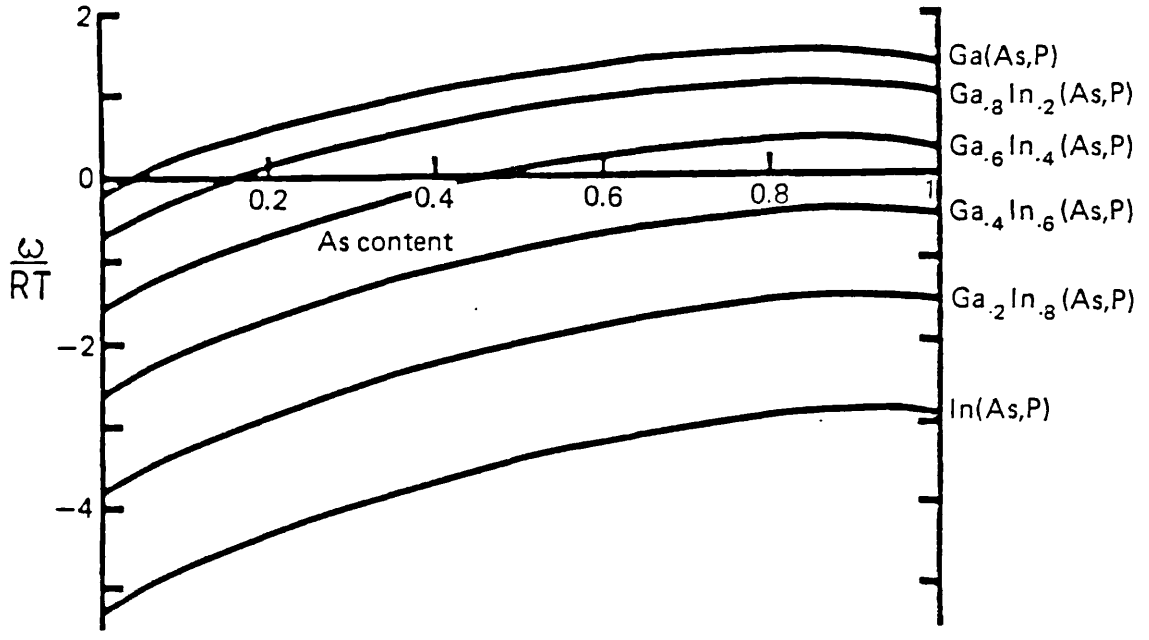

Sections through the overpotential surface corresponding to a vapour-phase with a very low InCl content:

$$p_{InCl}/p_{GaCl}=0{\cdot}5$$

Fig 7-23

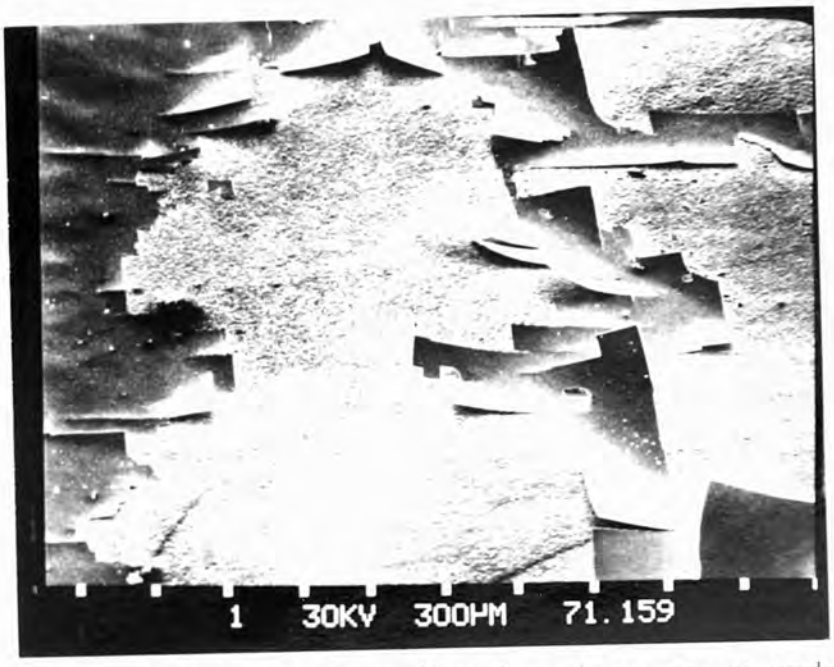

SEM Photograph of thin layer peeling from layer grown under conditions of fig 22

Fig 7-24

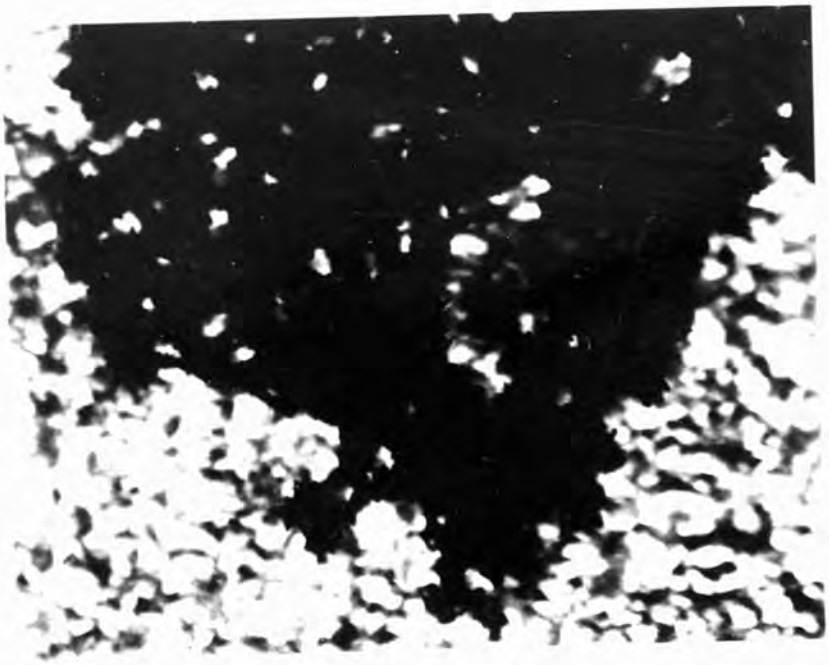

Photograph of the irregular polycrystalline layer.

Analysis of the layers using energy dispersive x-ray spectroscopy (EDAX) showed all three layers to have the same composition (within the accuracy of the technique). In all three cases the material consisted mainly of gallium and phosphorus, with only small amounts of indium (< 5% of metal content) and arsenic (< 10% of non-metal content). The main difference between the layers appears to have been textural rather than compositional and will not, therefore, be discussed further here.

These results confirmed the major prediction of fig 22 that although there was a supersaturation for the growth of a gallium rich material, the substrate was undersaturated with respect to the vapour and could be etched. Furthermore, it was clear that both processes could occur simultaneously. Note, however, that the overpotential curves showed a maximum for arsenic-rich solids. The fact that the actual layer contained over 90% phosphorus may have reflected a kinetic barrier to arsenic incorporation but was more probably due to errors in the thermodynamic data of the GaP/HCl reaction leading to an underestimate of the supersaturation of GaP.

The same processes of simultaneous growth and etching can occur under the normal growth conditions. This may provide a source of irreproducibility - attack of the substrate will alter the reactant pressures immediately above the surface; consequently the early stages of growth cannot be accurately controlled by the input pressures.

7.4 Conclusion

The ability to grow both $Ga_xIn_{1-x}As$ and $Ga_xIn_{1-x}As_yP_{1-y}$ was clearly demonstrated. Good control of the material properties of $Ga_xIn_{1-x}As$ was obtained using a mixed metal source. The balance enabled the predicted variation of growth rate with $AsCl_3$ pressure (section 6.3) to be confirmed. Experiments involving differently oriented substrates showed that surface kinetics influenced both growth rate and composition.

Growth of the quaternary is less well-developed. Nevertheless, layers showed only a small range of properties and evidence was presented suggesting that the major limitation was attack of the substrate prior to growth. This problem was less important in the (Ga,In)As growth because of the difference in behaviour between pure metal sources and a mixed-metal source.

7.5 Appendix: The Gallium-Indium Source

Initially, the melt is assumed to be an ideal solution and the reaction with hydrogen chloride is examined. If Z is the mole fraction of Ga in the melt, then the equilibrium constants for the reactions to form the monohalides can be written:

$$K_1 = \frac{P_{GaCl}\, P_{H_2}^{\frac{1}{2}}}{Z\, P_{HCl}} \qquad \ldots\ldots 1$$

$$K_2 = \frac{P_{InCl}\, P_{H_2}^{\frac{1}{2}}}{(1-Z)\, P_{HCl}} \qquad \ldots\ldots 2$$

eliminating $P_{H_2}^{\frac{1}{2}}/P_{HCl}$ from (1) and (2) gives

$$\frac{P_{GaCl}}{P_{InCl}} = \frac{z}{1-z} \cdot \frac{K_1}{K_2} \qquad \ldots\ldots 3$$

Clearly the gas composition is determined by the melt composition and temperature only. Unless $K_1 = K_2$, the composition of the source will change with time. We are interested in minimising and quantifying the change.

The model adopted is very simple: a known amount of the melt is placed in a closed container of volume V. Hydrogen, containing a partial pressure - ε - of HCl enters the container and the system is allowed to reach equilibrium. It is a simple matter to calculate the equilibrium concentrations or pressures of the various species. To simulate flow conditions the whole of the vapour phase is assumed to be swept away rapidly without any further alteration of melt. This is replaced with a fresh gas sample and the system again allowed to reach equilibrium. By choosing a sufficiently small value of V (and a correspondingly large number of cycles) the depletion of the melt can be reproduced as a function

of total volume of gas flowed, and hence as a function of time.

Let N_1 be the initial number of moles of Ga in the melt, N_2 the initial number of moles of In in the melt and $k = \frac{\varepsilon V}{RT}$, the number of moles of HCl introduced into gas-phase during one cycle of the calculation.

After equilibrium there will be in the gas phase n_1 moles of GaCl, n_2 moles of InCl and $(k-n_1-n_2)$ moles of HCl.

In the melt there are (N_1-n_1) moles of Ga and (N_2-n_2) moles of In.

The mole fractions of Ga and In in the melt are given by

$$Z = \frac{N_1 - n_1}{(N_1 + N_2) - (N_1 + n_2)} \qquad 1 - Z = \frac{N_2 - n_2}{(N_1 + N_2) - (n_1 + n_2)}$$

and the gas-phase pressures are

$$p_{GaCl} = n_1 \frac{RT}{V} \qquad p_{InCl} = n_2 \frac{RT}{V}$$

$$p_{HCl} = \varepsilon - (n_1 + n_2) \frac{RT}{V}$$

(Assuming the total pressure to be 1 atm and take $p_{H_2}^{\frac{1}{2}} \simeq 1$ - a simplification valid for the growth system).

Substituting in 1 and 2:

$$K_1 = \frac{n_1}{[k - (n_1 + n_2)]} \cdot \frac{[N_1 + N_2 - (n_1 + n_2)]}{[N_1 - n_1]} \qquad \ldots\ldots 4$$

$$K_2 = \frac{n_2}{[k - (n_1 + n_2)]} \cdot \frac{[N_1 + N_2 - (n_1 + n_2)]}{[N_2 - n_2]} \qquad \ldots\ldots 5$$

These equations may be solved simultaneously for n_1 and n_2. Flow conditions are simulated by repeating the calculation using the new values of N_1 and N_2. The accuracy with which the calculation reproduces the flowing system will depend on the volume increment chosen (ie k). The smaller k is, the greater the accuracy; but the number of calculations required will also increase.

Equations (4) and (5) may be simplified if the following conditions hold true:

i. There is a large excess of one component of the melt (ie $N_1 \ll N_2$).

ii. The equilibrium constant for the reaction of the minority species is less than or close to the value of the constant for the majority species, (ie $K_1/K_2 \leqslant 1$). This ensures $n_1 \ll n_2$.

iii. The equilibrium constant for the reaction of the majority species is much greater than unity (ie $K_2 \gg 1$).

Conditions (i) and (iii) are known to apply to the experimental system and the thermodynamic data for reactions of the metals with HCl suggest condition (ii) could apply. Then if a new variable - α - is defined by $\alpha = \frac{k}{N_2}(K-1)$ (where $K = {}^{K_1}/K_2$), and it is assumed that the volume increments are small, so that $\alpha \ll 1$, it can be shown that the composition is approximated by

$$Z = \frac{N_1}{N_2}(1 - \alpha) = Z_o (1 - \alpha) \qquad \ldots\ldots 6$$

where Z_o is the initial mole fraction of gallium in the melt.

If the calculation is carried out m times, then after the m^{th} cycle the composition is given by

$$Z_m = Z_o [1-a]^m \qquad \ldots\ldots 7$$

But, it was assumed $\alpha << 1$, so (7) may also be approximated:

$$Z_m \simeq Z_o [1-\alpha m] \qquad \ldots\ldots 8$$

(8) may also be expressed as a time dependence:

$$\alpha m = \frac{km}{N_2} (K-1) = \frac{\varepsilon Vm}{RT} \cdot \frac{(K-1)}{N_2}$$

but $Vm = Ft$, where F is flow rate and t is time and so,

$$\alpha m = \frac{\varepsilon Ft}{RT} \frac{(K-1)}{N_2} = \beta t \qquad \ldots\ldots 9$$

where $\beta = \frac{\varepsilon T}{RT} \frac{(K-1)}{N_2}$ $\qquad \ldots\ldots 10$

and (8) becomes

$$\underline{\underline{Z_t \simeq Z_o(1-\beta t)}} \qquad \ldots\ldots 11$$

Equations (10) and (11) indicate that small values of ε and F and a large source will minimise the incongruency. This is quantified for a specimen source and shown in figure 6 (section 7.2.1) based on the full expression (equations 4 and 5).

The rate of depletion of the melt can be seen to be a sensitive function of K - the ratio of the equilibrium constants - although absolute values of K_1 and K_2 are unimportant when both are extreme. The rate of depletion is approximately constant for small values of K_1 but some curvature is apparent in the curve where K = 5. It is clear from fig 6 that the experimental melt compositions (from fig 5) lie close to the line for K = 2. Thus the equilibrium constant for the Ga/HCl reaction is approximately double that for the In/HCl reaction at 800°C. At this stage it is possible to relax the assumption that the melt is an ideal solution. Equation 3 becomes

$$\frac{P_{GaCl}}{P_{InCl}} \frac{(1-Z)}{Z} = \frac{K_1}{K_2} \frac{\gamma_{Ga}}{\gamma_{In}} = K$$

where γ_i is the activity coefficient of species i. The activity coefficients at 800°C over the composition range of interest, give [8]

$$\frac{\gamma_{Ga}}{\gamma_{In}} \simeq 1.6$$

Hence, the ratio K_1/K_2 (where 1 refers to Ga/HCl, and 2 to In/HCl) is approximately 1.3 at 800°C.

REFERENCES

1 K. Sugiyama, H. Kojima, H. Enda, M. Shibata: Jap. J. Appl. Phys. 16, 2197, 1977.

2 A.K. Chatterjee, M.M. Faktor, M.H. Lyons, R.H. Moss: J. Cryst. Growth - accepted for publication.

3 L. Hollan, J.P. Hallais, J.C. Brice: Chapter 1 in 'Current Topics in Materials Science' 5, Ed. E. Kaldis, North-Holland, Amsterdam, 1980.

4 E.A. Moelwyn - Hughes: 'Physical Chemistry', Pergamon, Oxford 1961.

5 G.H. Olsen, T.Z. Zamerowski: Prog. Cryst. Growth Charact. 2, 309, 1979.

6 N. Susa, Y. Yamauchi, H. Kanbe: Jap. J. Appl. Phys. 20, L253, 1981.

7 P. Kordos, G.L. Pearson, M.B. Panish: J. Appl. Phys. 50, 1902, 1979.

8 M.B. Panish, M. Ilegems: 'Progress in Solid-State Chemistry', 7, 39, Pergamon Press, 1972.

CHAPTER 8: CONCLUSION

A crystal growth system may be studied at many different levels. A convenient division is thermodynamics, gas-transport processes and surface-kinetics and in this thesis aspects of all three fields of study have been considered. Thermodynamics and gas-transport theory were both used to model the vapour-phase growth of the mixed III-V compounds ($Ga_xIn_{1-x}As$ and $Ga_xIn_{1-x}As_yP_{1-y}$) and examination of the equilibrium systems for growth of ternary and quaternary III-V compounds enabled the most important factors governing composition to be identified. However, equilibrium thermodynamics did not provide a complete description of the non-equilibrium growth system. This was shown, in the case of the ternary and quaternary growth, to obscure important features of the system - particularly the possibility of a range of compositions in the growing layer.

Although thermodynamics was used to estimate possible growth conditions, it gave no information about growth rates. Estimates of growth rates were obtained using models based on the gas-transport equations; but although the equations were quite general, they could only be solved if equilibrium was assumed at the solid-vapour interface ie any effects of surface kinetics were assumed to be negligible. Despite this limitation, these calculations were shown to give a useful description of the growth systems and revealed features of mixed III-V compound growth which were hidden by the thermodynamic models. Thus, it was found that although a range of compositions of $Ga_xIn_{1-x}As$ could, on the basis of the thermodynamic driving force, be grown from the vapour, a layer grown under transport-limited conditions had a single composition. Furthermore, this composition was shown to be a function of the growth rate. This finding provided a mechanism by which

surface kinetics could affect composition of the growing layer, without the need to invoke any specificity in the reaction.

The thermodynamic and transport models provided enough information to enable a growth system to be developed, and gave a qualitative explanation for most of the results obtained. However, it was apparent that certain morphological features of the grown layer and the quantitative aspects of the work, required a much more detailed knowledge of the surface reactions. Little work has been carried out in this field for III-V compound growth. A first step is the study of the variation of growth rate with the various reaction parameters (temperature and reactant pressures). To correlate the results, the kinetic terms were gathered together in a single function called the exchange current, which eliminated those changes due solely to differences in supersaturation. The dependence of exchange current on reactant pressures was then a reflection of the various reactions occurring at the surface. Although the pressures of the reactants at the interface differed from the bulk pressures; it was shown that when gas-transport was confined to a region of known geometry the interfacial pressures could be calculated from the growth rate. The modified entrainment method (MEM) exploits this principle and the uncoupling of transport and surface kinetic processes by this technique was demonstrated for the sublimation of red phosphorus and the GaAs/HCl reaction. However, the requirements of British Telecom did not allow extensive investigation of these systems and clearly the work could be continued by making a detailed study of the factors which affect the rate of the GaAs/HCl reaction. Similar studies on the growth systems for InAs, InP and GaP could also be made.

At all levels there is scope for further work. Thus, more accurate thermodynamic information for the reactant species is still required,

particularly for species such as As_2P_2 and AsP etc. Similarly, only a very simple transport model was considered: bulk gas movements caused by convection were not considered, nor was the model extended to transport in more than one dimension. Such calculations have been carried out by Rosenberger and others [1] for the simple physical vapour transport systems, but the complex geometries which are found in practical CVT systems make it difficult to carry out the same calculations for these systems. In any event, the calculations are unlikely to significantly alter the qualitative picture obtained using the simple one-dimensional model.

Perhaps the most rewarding field of study is the investigation of the various processes occurring on the surface. One line of approach is the examination of the dependences of exchange current with the input conditions. However, this exchange current is an aggregate of many different surface processes (adsorption, surface diffusion, surface reactions) and a full understanding of the system would require identification of the individual reaction steps. To learn about these requires far more specific tools for examining the surface during the reaction. Some progress has been made in this direction by the use of ellipsometry to study the growth of GaAs/HCl in situ [2]. Unfortunately interpretation of the results is neither easy nor unambiguous. Low energy electron diffraction (LEED), reflection high energy electron diffraction (RHEED) and Auger electron spectroscopy (AES) have been used to aid the interpretation of the ellipsometry results, but all three techniques are carried out in high vacuum necessitating the removal of the sample from the growth environment, with inevitable perturbation of the surface. Clearly, the study of the exchange currents would be required both to aid the interpretation and to support the conclusions of these more detailed surface investigations.

On a more practical level, reproducible growth of high quality quaternary layers has still to be achieved. The effect of growth conditions (temperatures and reactant pressures) on the morphology and the electrical properties has yet to be investigated in a systematic manner since the demands of device production mean that once satisfactory conditions have been found, there is little incentive to investigate further. Similarly, methods of substrate preparation and the relationship between substrate morphology and the quality of the epitaxial layers are not well understood.

Clearly, to obtain a complete description of the growth of III-V compounds requires much further experimentation. Nevertheless, a necessary precursor to this work is the development of thermodynamic and transport models of growth which provide a framework in which to interpret the more detailed experiments. This has now been done for the ternary and quaternary III-V compounds and it was shown that a successful growth system could be constructed on the basis of these models. Studies of the exchange current have yet to be performed, but the effectiveness of MEM as a kinetic probe has been demonstrated.

REFERENCES

[1] F. Rosenberger: 'Fundamentals of Crystal Growth I' Springer-Verlag, Berlin 1979.

[2] J.B. Theeten, F. Hottier: Surface Science 58, 583, 1976.

Journal of Crystal Growth 46 (1979) 21–30

THE MODIFIED ENTRAINMENT METHOD AND ITS APPLICATION TO THE STUDY OF HETEROGENEOUS REACTIONS

M.M. FAKTOR, I. GARRETT and M.H. LYONS
Post Office Research Centre, Martlesham Heath, Ipswich IP5 7RE, England

Received 8 July 1977; manuscript received in final form 20 June 1978

The modified entrainment method is a simple and revealing means of investigating potential chemical vapour transport systems, and in favourable cases may provide thermochemical data for the reactions. In this paper we extend the theory underlying the method showing how we may, by altering the experimental conditions, study the surface kinetics. A simple expression is obtained relating a measured rate of weight loss with a single kinetic parameter – the exchange current. In the light of this discussion some experimental results obtained from the GaAs/HBr system are analysed.

1. Introduction

In a recent paper [1], we described a modified entrainment method for exploring potential chemical vapour transport systems in a way that is rapid, revealing, and quantitative. The method may be used simply to establish the best range of experimental conditions for chemical vapour transport, or one may go further and obtain accurate thermochemical data for the transport reactions concerned [2]. In this paper we consider the implications of so designing the experimental system that the reaction is driven significantly away from equilibrium. We show that the modified entrainment method then provides a useful way of investigating the reaction kinetics of transport reactions. We develop the theory in a general form, referring to a quite general reaction and without restricting ourselves to particular atomistic mechanisms.

In section 2 we consider first of all the sublimation of a single component solid to develop the ideas from the simplest system. In section 3, we consider a general reaction and establish quite general kinetic expressions and results. Some specific examples of transport reactions are considered in section 4, and some experimental results discussed.

2. Sublimation of a single component solid

In the development of the theory of the modified entrainment method (MEM), we had a constraint that the resistance of the channel to gas flow should be large [3] and the sample should have a large surface area, so that the partial pressures of all components within the reaction cell are maintained close to their equilibrium values in spite of a small leakage through the channel which provides the experimentally observable parameter, namely the rate of loss of weight r^0. If we relax this constraint, the partial pressures inside the reaction cell are determined by the relative kinetics of surface reaction and gas transport along the channel and no longer approximate to equilibrium values.

Consider the sublimation of a single component solid:

$$\mathrm{A(solid)} \rightleftharpoons \mathrm{A(gas)}$$

the rate of weight loss r^* under non-equilibrium conditions may be expressed in terms of forward and reverse rate constants k_f and k_r (in mol s^{-1} cm^{-2}) as:

$$r^* = (k_f S - k_r S p_A^*) M , \qquad (1)$$

where S is the sample surface area, p_A^* the non-equi-

librium partial pressure of A, and M the formula weight.

The rate constants k_f and k_r are functions of temperature and of the crystallographic orientation of the sample surface, state of contamination, defects or damage, etc. Eq. (1) assumes that forward and reverse rates are independent, which is reasonable for this simple system. In section 3 we remove this assumption.

At equilibrium, forward and reverse rates are equal. From eq. (1) we find

$$r^* = k_r MS(p_A^0 - p_A^*) , \tag{2}$$

where p_A^0 is the equilibrium partial pressure (saturated vapour pressure) of A. Now we can express p_A^* in terms of r^* from gas transport theory [1,2]. We find:

$$p_A^* = P(1 - e^{-\xi^*}) , \tag{3}$$

where P is the total pressure, including the inert carrier gas, and ξ^* is the transport function defined for this system by:

$$\xi^* = RTlr^*/DPCM . \tag{4}$$

C and l are the cross-sectional area and length of the channel, D is the diffusion coefficient of A in the carrier gas, and R and T are the gas constant and absolute temperature.

Eliminating p_A^* from eqs. (2) and (3) we find:

$$r^* = k_r MS[p_A^0 - P(1 - e^{-\xi})] ,$$

and if $\xi \ll 1$ as is usually the case, this reduces to:

$$k_r S = \frac{r^*}{p_A^0 M - RTlr^*/DC} , \tag{5}$$

which relates the rate constant k_r to the experimentally measured quantity r^*. Alternatively, we can remove r^* between eqs. (2) and (3) to obtain:

$$\left(\frac{DPC}{RTl}\right)\frac{1}{k_r S p_A^0}\ln\left(\frac{P}{P - p_A^*}\right) = 1 - \frac{p_A^*}{p_A^0} . \tag{6}$$

We can represent k_r in terms of a sticking coefficient α_L [4,5]:

$$k_r = \alpha_L/(2\pi MRT)^{1/2} = \alpha_L Z ,$$

where Z is the Zeldovitch factor from the kinetic theory of gases, and $0 \leqslant \alpha_L \leqslant 1$. If $p_A^* \ll P$, eq. (6) takes the form:

$$\left[\left(\frac{D}{RTlZ}\right)\left(\frac{C}{\alpha_L S}\right) + 1\right]\frac{p_A^*}{p_A^0} = 1 . \tag{7}$$

Note that $\alpha_L S$ is the effective surface area of the

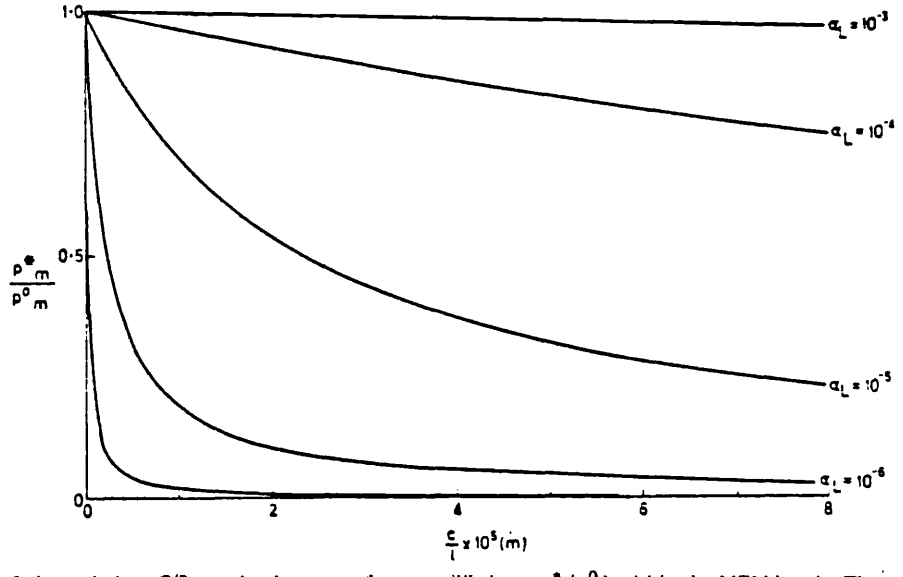

Fig. 1. The effect of channel size (C/l) on the departure from equilibrium (p_A^*/p_A^0) within the MEM bottle. The curves have been calculated for several values of the sticking coefficient (α_L), assuming $p^0 = 10^{-7}$ atm and a total pressure $P = 10^{-4}$ atm.

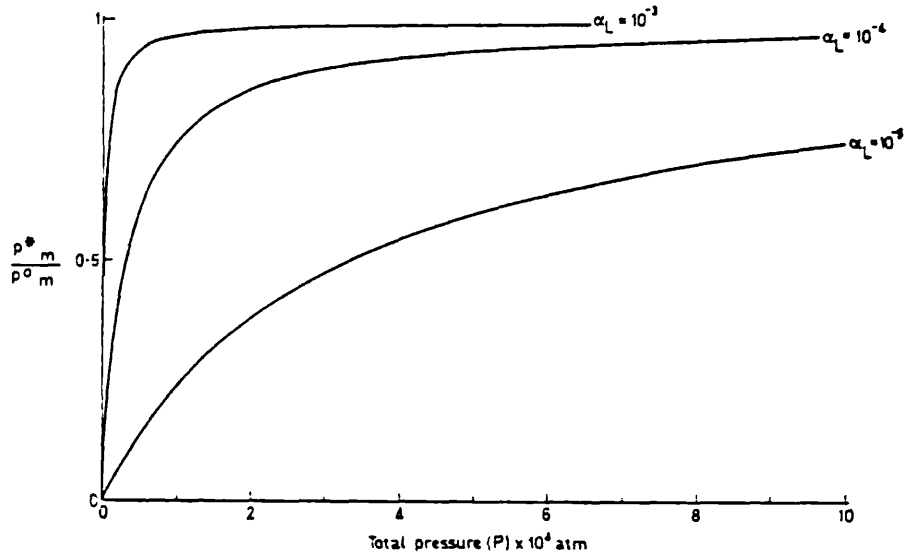

Fig. 2. The effect of total pressure on departure from equilibrium.

sample and C is the area of the channel. The quantity p^*_A/p^0_A is the departure from equilibrium brought about by $C/\alpha_L S$ not being zero. The relationship is part of a rectangular hyperbola (fig. 1). The effect of total pressure (P) is implicit in eq. (7), as it affects D in inverse proportion (fig. 2).

3. Kinetic description of a general transport reaction

We consider a quite general reaction to transport a solid compound M:

$$M + aA + bB + \ldots \rightleftharpoons qQ + rR + \ldots , \tag{8}$$

where all species except M are gaseous. The equilibrium constant for this reaction may be written:

$$K^0 = \prod_i p_i^{\nu_i} , \tag{9}$$

where the stoichiometric coefficients ν_i are taken to be negative for reactants and positive for products. We consider the general kinetic expressions for the forward and reverse reaction rates, taking "forward" as being from left to right in the reaction as written:

$$J_f = k_f S \prod_i p_i^{x_i} , \tag{10}$$

$$J_r = k_r S \prod_i p_i^{y_i} . \tag{11}$$

Consider the equilibrium situation: $J_f = J_r$. Hence:

$$K^0 = k_f/k_r = \prod_i p_i^{y_i - x_i} .$$

Thus $y_i = x_i + \nu_i$. Now consider a net reaction rate J (mol s^{-1}):

$$J = r^*/M = J_f - J_r = J_{ex}[K^0/K^* - 1] , \tag{12}$$

where:

$J_{ex} = J_r$ is the "exchange flux" ,

$K^* = \prod_i p_i^{\nu_i}$ for non-equilibrium p_i .

The term in square brackets in eq. (12) is a measure of the Gibbs free energy available to drive the heterogeneous reaction. The exchange current J_{ex} is a purely kinetic quantity which is a useful indication of how hard the transport reaction may be driven without gross departure from equilibrium.

The crystal grower normally wants to grow single-crystal material, avoiding grain boundaries, stacking faults, twinning and so on. All these phase defects are the result of atoms becoming accommodated in incorrect crystallographic sites, and thus having slightly more potential energy than they would have in their correct sites. The business of the crystal grower, if he wants single-crystal material, is to maximise the

chances of each atom finding a correct lattice site. The average number of sites explored by each atom should thus be as large as possible. This exploration may take place by exchange between the vapour phase and the surface of the sample, or by fast diffusion of adsorbed species on the sample surface. Some information about surface mobility may be deduced from the pre-exponential factor in the kinetic rate constant [6]. The modified entrainment method provides a direct method of measuring the exchange flux between vapour and surface, and the average number of sites explored by each atom is simply the ratio of exchange flux J_{ex} to net growth rate J. A high exchange flux permits one to drive the reaction at a high rate without a large departure from equilibrium. In the modified entrainment method, the reaction may be driven hard by reducing the gas transport resistance of the channel, or by reducing the surface area of the sample. Either action pursued far enough will reduce the observed rate of weight loss r^* below the value r^0 predicted for the equilibrium situation.

To develop eq. (12) further, we need relations between the p_i^* and r^*, from gas transport theory. Developing a general gas transport theory along the lines of refs. [3,7,8], we can relate the partial pressures $p_i(0)$ in the reaction cell to the pressure $p_i(l)$ at the channel outlet:

$$\frac{p_i(0)}{P} - \frac{\nu_i}{N} = \left[\frac{p_i(l)}{P} - \frac{\nu_i}{N}\right] e^{-\xi}, \tag{13}$$

where $N = \Sigma_i \nu_i$.

This equation applies to equilibrium and non-equilibrium cases alike. Also

$$\xi = RTlNJ/DP = RTlNr/DPMC. \tag{14}$$

We consider the case of a reaction which is not extreme (case 1 in ref. [3]), and divide the reacting gaseous species into three groups:
(I) All reactants.
(II) All products which are not also included in the gas stream through the furnace.
(III) All other products.
For group II, let $\Sigma_{II}\nu_i = N'$. For all species, let $p_i(l)/P = \epsilon_i$ ($\epsilon_i = 0$ for all group II species). Then since the reaction is not extreme, $\xi \ll \epsilon_i$ for all non-zero ϵ_i; in other words, none of the reactants is used up completely or nearly so. We can now write the equilibrium constant of K^* in terms of the partial pressures:

$$K = \prod_i p_i^{\nu_i} = P^N \prod_i \{\nu_i/N\xi + \epsilon_i\}^{\nu_i}.$$

Thus

$$\frac{K}{P^N} = \prod_{\mathrm{I}} \epsilon_i^{\nu_i} \prod_{\mathrm{II}} \left\{\frac{\nu_i}{N}\xi\right\}^{\nu_i} \prod_{\mathrm{III}} \epsilon_i^{\nu_i}$$

$$= (\xi^{N'})\Big(\prod_{\mathrm{I,III}} \epsilon_i^{\nu_i}\Big)\Big(\prod_{\mathrm{II}} \left\{\frac{\nu_i}{N}\right\}^{\nu_i}\Big). \tag{15}$$

The third term is a pure number; the second contains the dependence on the feed components, and the first is the dependence on ξ or r. We write eq. (15) simply as:

$$K = P^N \xi^{N'} a(\epsilon_i). \tag{16}$$

Now eq. (12) becomes:

$$r^* = r_{ex}[(r^0/r^*)^{N'} - 1], \tag{17}$$

in which $r_{ex} = MJ_{ex}$.

This general kinetic relationship expresses the dependence of the observed effect r^* on the equilibrium situation represented by r^0 and the fundamental kinetic parameter r_{ex}. Eq. (17) can be used to predict values of r^* from any proposed atomistic kinetic mechanism, via eqs. (10) and (11).

4. Some specific reaction systems

As the first example, we consider a dissociative sublimation reaction, such as encountered in the vapourisation of II–VI compounds:

$$\mathrm{BC(s)} \rightleftharpoons \mathrm{B(g)} + \frac{1}{m}\mathrm{C}_m\mathrm{(g)}, \tag{18}$$

$$K = p_{\mathrm{B}} p_{\mathrm{C}_m}^{1/m}. \tag{19}$$

For this reaction, $N = 1 + 1/m$, $N' = N$, and if the experiment is conducted in a stream in inert gas, $\epsilon_i = 0$ for all components. Then, from eq. (13) with $\xi \ll 1$:

$$p_i(0)/P \simeq \nu_i \xi/N. \tag{20}$$

Thus

$$p_B = \frac{P}{N}\xi\,, \quad p_{C_m} = \frac{P}{Nm}\xi\,,$$

$$r_{ex} = k_r SM\left(\frac{P}{N}\right)\xi^{x_B}\left(\frac{P}{Nm}\xi\right)^{x_C}.$$

Thus

$$r^* = \frac{k_r SM}{m^{x_C-1/m}}\left(\frac{P}{N}\xi\right)^{x_B+x_C-N} \times\left[K^0 - \left(\frac{P}{N}\xi\right)^N\left(\frac{1}{m}\right)^{1/m}\right]. \qquad (21)$$

This equation may be compared with eq. (12). The comments following eq. (12) are equally applicable here.

In fact, an experiment conducted in inert gas only ($\epsilon_B = \epsilon_C = 0$) yields information about $x_B + x_C$ only, not about x_B and x_C independently. If we make, say, ϵ_c non-zero, then eq. (21) becomes:

$$r^* = k_r SM\left(\frac{P}{N}\xi\right)^{x_B}\left(\frac{P}{Nm}\xi + \epsilon_C\right)^{x_C} \times\left[K^0\left(\frac{P}{N}\right)^{-1}\left(\frac{P}{Nm}\xi + \epsilon_C\right)^{-1/m} - 1\right]. \qquad (22)$$

We now have a term which depends on ϵ_C; variations in the value of this term as ϵ_C is changed yield x_C.

As a second example, we consider the reaction of a III–V compound with a hydrogen halide transporting agent [9]. Such a transport goes by several reactions in the temperature range 600–1100°C [2,10,11]. We consider only one of these reactions for the purposes of illustration:

$$GaAs + HBr \rightleftharpoons GaBr + \tfrac{1}{2}As_2 + \tfrac{1}{2}H_2\,.$$

For this system, $N = 1$. Group I contains HBr, group II contains GaBr and As_2, so $N' = 3/2$, and group III contains H_2. Thus, from eqs. (12) and (17):

$$r^* = r_{ex}\left[\frac{K^0}{K^*} - 1\right] = r_{ex}\left[\left(\frac{r^0}{r^*}\right)^{3/2} - 1\right],$$

and

$$r_{ex} = k_r SM\, p_{GaBr}^{x_1+1}\, p_{As_2}^{x_2+1/2}\, p_{H_2}^{x_3+1/2}\, p_{HCl}^{x_4-1}\,.$$

The partial pressures may be found from eq. (13), and again we take $\xi \ll 1$:

$$p_{GaBr} = P\xi\,, \quad p_{As_2} = P\xi/2\,,$$

$$p_{HCl} = (\epsilon - \xi)P\,, \quad p_{H_2} = (1 - \epsilon + \xi/2)P\,.$$

Measurement of r^* allows us to calculate ξ and hence all the partial pressures and K^*. Then from eq. (12) we find r_{ex} and hence k_r, if we know the area of the sample. By making use of the experimental variables P, T, and the ϵ_i it may be possible to establish empirical values for the x_i. These values may then suggest an atomistic mechanism.

5. Discussion

Experiments using the modified entrainment technique have so far been aimed at obtaining thermodynamic data. For this reason, experimental data which can be fitted to eq. (17) are limited. Nevertheless in some cases the results of an experiment using MEM have given clear indication of surface kinetic effects influencing the measured rate of weight loss. As an example of how we can use eq. (17) to obtain kinetic information, we have examined the results of Miss E.J. Tarbox [12] which were obtained with the GaAs–HBr system.

It should be stressed that the use of crushed, polycrystalline material in this work limits the usefulness of the kinetic results. The values of activation energy etc found below represent average values which could differ considerably from those applicable to a single surface orientation. In addition, changes in the exposed surfaces of the sample as the reaction proceeds will be reflected in the overall exchange rate, and it is likely that the rates calculated below do not represent steady-state values accurately. Clearly, future experiments designed to reveal kinetic information must involve the use of samples which may be considered to have only one exposed face of known orientation.

Bearing in mind these problems, we now consider the presently available results for the GaAs/HBr system in more detail. These are shown in fig. 3 and fig. 4 (for pressures of HBr, ϵ, of 0.0354 and 0.0591 respectively). Three different channel sizes were used; all nominally the same length but with diameter of 1 mm, 2 mm and 3 mm. If equilibrium in the bottle

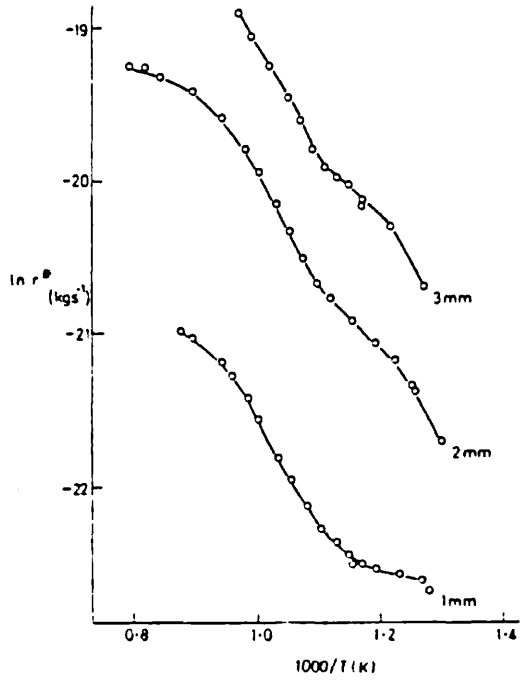

Fig. 3. Experimental plots of rate of weight loss versus reciprocal temperature for the GaAs/HBr system. The three curves were obtained using channels of 1 mm, 2 mm and 3 mm diameter. The pressure of HBr (ϵ) was 0.0354 atm.

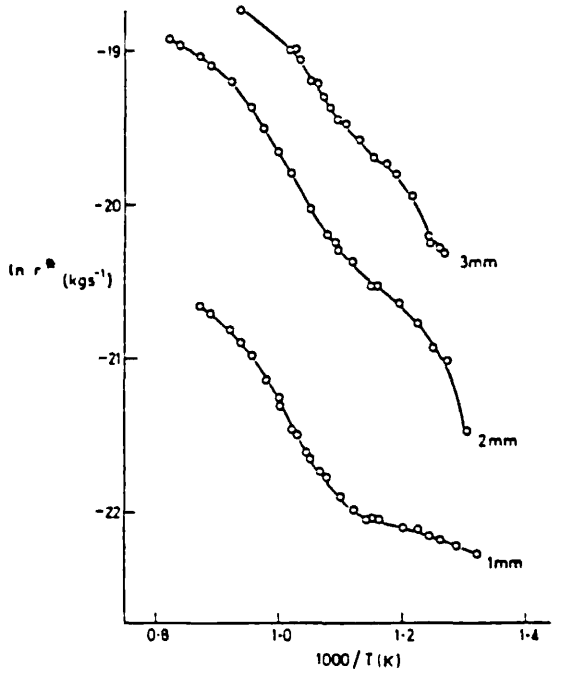

Fig. 4. Experimental plots of rate of weight loss versus reciprocal temperature for GaAs/HBr system. ϵ = 0.0591.

was attained for all three channel sizes, then the shapes of the curves would be identical. The curves for the 2 and 3 mm channels would simply be vertical transpositions of the 1 mm curve, the vertical difference between the curves being the logarithm of the ratio of the channel resistances.

Since the curves obtained for the larger channels clearly differ in shape from that obtained with a 1 mm channel, it is clear that surface kinetics do play an important part in determining the overall rate of weight loss, i.e. we are in a situation where we may apply eq. (17). This view is further strengthened by the results shown in fig. 5 in which two samples were studied under the same conditions (3 mm channel, ϵ = 0.0354). The only difference between the two samples was the surface area: one sample was finely ground whereas the other was more coarsely ground and therefore had a smaller surface area. Exact calculations are not possible, but a ratio of about 4 : 1 in the areas is reasonable. It can be seen in fig. 5 that at temperatures below about 1000 K the coarse ground

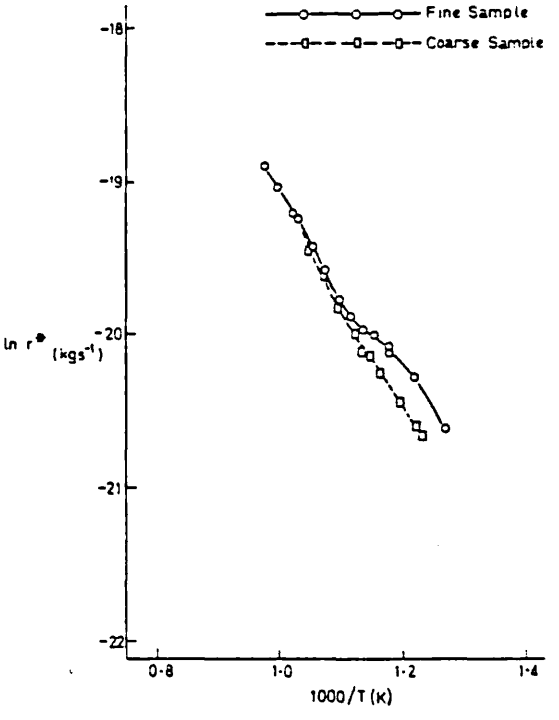

Fig. 5. Experimental results for Ga/As/HBr system showing effect of altering sample area. Channel was 3 mm diameter, ϵ = 0.0354.

sample gave a lower rate of weight loss, the difference increasing at lower temperatures.

Our experimental weight loss curves enable us to obtain r^* at any temperature. However, if we are to obtain any quantitative kinetic information we must also know r^0 (the rate of weight loss when equilibrium is attained in the sample bottle). In our kinetic analysis of these results we have assumed that the experiments carried out using a 1 mm channel do correspond to equilibrium conditions inside the bottle. Whilst it is true that the conditions inside the bottle are closer to equilibrium with a 1 mm channel than with a 2 or 3 mm channel, we cannot be absolutely certain that equilibrium is achieved. However, the results given in figs. 3 and 4 show very clearly that the slope of the plots increases very markedly with decreasing temperature in the low temperature positions of the curves when channels of 2 mm and 3 mm diameter are used. This sudden increase in slope (which corresponds to a change from gas-transport and equilibrium limitations on rate of weight loss to surface kinetic limits) is not observed with a 1 mm channel. This would suggest that in the experimental surface temperature range, kinetics have only a small effect (if any) on overall rate of weight loss with a 1 mm channel.

To estimate the equilibrium curves for the 2 and 3 mm channels, the results from the 1 mm channel was transposed vertically until the high temperature parts of the curve coincided. The lower temperature portions of the 2 and 3 mm curves were found to lie beneath the theoretical plot, indicating the effect of surface kinetics.

The extent by which the 1 mm curve is shifted vertically should reflect the ratios of the channel resistance. Table 1 shows the theoretical resistance ratios calculated from the channel dimensions, and the experimental values indicated by the distance needed to shift the 1 mm channel as described above.

It will be seen that the experimental ratios obtained for two different HBr pressures are similar, although they are somewhat higher than those calculated from the channel dimensions.

The exchange currents may be calculated using eq. (17) in the form

$$r_{ex} = \frac{r^*}{[(r^0/r^*)^{\mathcal{N}} - 1]}$$

Table 1
Table showing the relative sizes of the transport conductances of the channels; theoretical values obtained from the channel dimensions; for experimental values, see text

	Channel size (mm)		
	1	2	3
Ratio of channel conductance (R)			
Theoretical	1	4.25	10.20
Experimental			
$\epsilon = 0.0354$	1	4.95	12.18
$\epsilon = 0.0591$	1	5.16	11.47
$\ln R$			
Theoretical	0	1.45	2.32
Experimental			
$\epsilon = 0.0354$	0	1.60	2.50
$\epsilon = 0.0591$	0	1.64	2.44

To use this equation we need to assume what the transport reaction is (so that $\mathcal{N}'$ may be determined). The surface kinetic effects become apparent at temperatures below about 850 K. By comparison with the GaAs/HCl [5] system, it seems likely that the predominant reaction at these temperatures is

$$GaAs + 2\,HBr \rightleftharpoons GaBr_2 + \tfrac{1}{2}\,As_2 + H_2 .$$

For this reaction $\mathcal{N}' = 3/2$.

The exchange currents in the temperature range 909–769 K were calculated for both channel sizes and two HBr pressures (ϵ). The results are shown in figs. 6 and 7 in the form of $\ln r_{ex}$ versus reciprocal temperature plots. The results may be seen to lie approximately along straight lines from which we could estimate the activation energy of the reaction. Table 2 lists the activation energy found from each plot. The arithmetical mean value of these results is 205 kJ mol^{-1}. The spread in values reflects inaccuracies in the data used, and may also be due in part to the pressure dependence of the exchange rate which is given by

$$r_{ex} = k_r S M p_{GaBr_2}^{x_1+1} p_{As_2}^{x_2+1/2} p_{H_2}^{x_3+1} p_{HBr}^{x_4-2} . \qquad (23)$$

In order to obtain values of the activation energy (included in the Arrhenius rate constant k_r) we have assumed that the exchange current has only a small dependence on the pressures of the various species

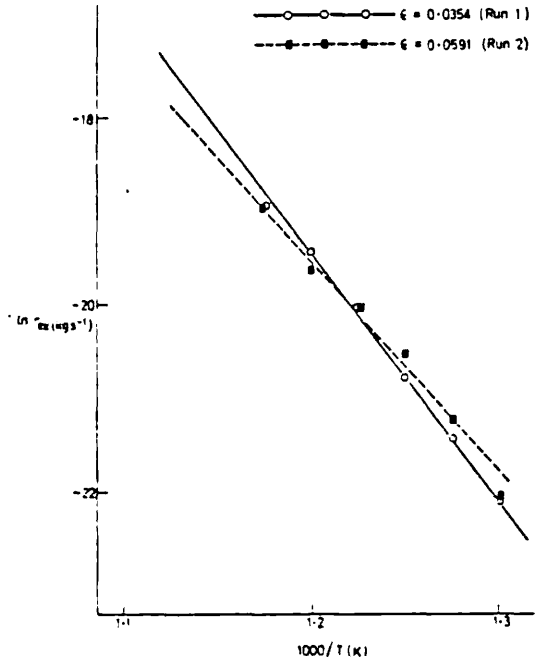

Fig. 6. Exchange current versus reciprocal temperature, calculated from results obtained with the 2 mm channel.

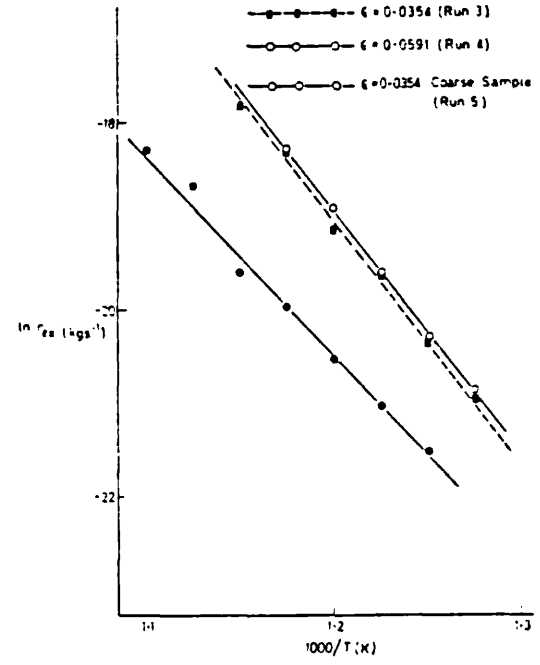

Fig. 7. Exchange current versus reciprocal temperature, calculated from results obtained with 3 mm channel.

Table 2
Experimental values of the activation energy, calculated from figs. 6 and 7

Run	Channel size (mm)	ϵ	E (kJ mol^{-1})
1	2	0.0354	223
2	2	0.0591	190
3	3	0.0354	222
4	3	0.0591	215
5	3 a)	0.0354	180

a) Coarse sample.

when compared with the changes brought about by the temperature dependence of k_r. Although this is an assumption, some idea of the effect of pressure changes on the exchange rates can be gauged by comparing the results of runs (1) and (2) (2 mm channel) and runs (3) and (4) (3 mm channel). In both sets of results the only difference between the two runs is in the pressure of HBr used, and hence the pressures of all the other gas-phase species. Examination of figs. 6 and 7 shows that for the 3 mm channel the results for the lower HBr pressure lie on a line below that obtained for the higher pressure. With the 2 mm channel the results for $\epsilon = 0.0591$ are scattered about the line for $\epsilon = 0.0354$. These results could easily arise from experimental scatter and it is clear that the overall dependence of the exchange current on the pressures of the gas-phase species is small when compared with the temperature dependence.

The fact that there is only a low dependence of the exchange rate on pressure of the reacting species imposes certain constraints on the values of x_1, x_2, x_3 and x_4. If we define the exchange current by

$$r_{ex} = \beta\, e^{-E/RT}, \tag{24}$$

then by comparison with (23),

$$\beta = \kappa S M\, p_{GaBr_2}^{x_1+1}\, p_{As_2}^{x_2+1/2}\, p_{H_2}^{x_3+1}\, p_{HBr}^{x_4-2}, \tag{25}$$

where k is the Arrhenius constant (temperature independent part of k_r), S is the sample area, and M is the gram formula weight of GaAs.

Since the pressures of all the species are small compared to p_{H_2}, we may take this as constant.

Under normal experimental conditions $p_{H_2} = 1$.

We may simplify further by expressing p_{As_2} and p_{HBr} in terms of ϵ and P_{GaBr} using the stoichiometry of the reaction

$$GaAs + 2\,HBr \rightleftharpoons GaBr_2 + \tfrac{1}{2}\,As_2 + H_2 \,. \tag{26}$$

Let

$$p_{GaBr_2} = p \,. \tag{27}$$

Then

$$p_{As_2} = p/2 \,, \tag{28}$$

$$p_{HBr} = (\epsilon - p) \,. \tag{29}$$

Substituting in (25) we obtain

$$\beta = \frac{\kappa SM}{2^{x_2+1/2}} P^{x_1+x_2+3/2} (\epsilon - p)^{x_4-2} \,. \tag{30}$$

Now supposing we measure the exchange current at two different HBr pressures – ϵ_1 and ϵ_2 – but at constant temperature. We denote the corresponding exchange currents as r_1 and r_2.

The ratio of these exchange currents is given by

$$\frac{r_1}{r_2} = \frac{\beta_1}{\beta_2} \frac{e^{-E/RT}}{e^{-E/RT}} = \left(\frac{p_1}{p_2}\right)^{x_1+x_2+3/2} \left(\frac{\epsilon_1 - p_1}{\epsilon_2 - p_2}\right)^{x_4-2} \,. \tag{31}$$

Eq. (31) enables us formally to define the conditions under which $r_1 = r_2$. These are given by the equation

$$\left(\frac{p_1}{p_2}\right)^{x_1+x_2+3/2} = \left(\frac{\epsilon_2 - p_2}{\epsilon_1 - p_1}\right) \,. \tag{32}$$

Eq. (32) simply expresses the fact that the change in rate brought about by, the change in $GaBr_2$ pressure is exactly compensated by the dependence of the rate on the corresponding change in HBr pressure. Obviously, whatever the values of p_1, p_2, ϵ_1 and ϵ_2, we can always find a suitable set of values of x_1, x_2 and x_4 which will satisfy eq. (32). However, without knowing the functional dependence of p and ϵ (which will depend on the equilibrium constant, the channel size in the MEM bottle and the magnitude of the exchange current) it is not clear whether or not equation (32) could be satisfied by the same set of values x_1, x_2 and x_4 over a range of values of ϵ_1 and ϵ_2. An exception to this is when $x_1 + x_2 = -3/2$ and $x_4 = 2$ so that the indices are zero. Eq. (32) will then be satisfied whatever values of ϵ_1 etc we have, and we can also simplify eq. (30) so that we have

$$\beta = \kappa SM/2^{x_2+1/2} \,. \tag{33}$$

Clearly there is much scope for further experimentation. Although there is no significant change in rate with ϵ over the very limited range studied, it is possible that gross changes in ϵ (perhaps an order of magnitude or more) will be reflected in the value of the exchange current. There is also the possibility that changes of the Ga : As ratio in the gas-phase (at present fixed by the stoichiometry of the solid) could also affect the exchange current.

By assuming the exchange current has the form

$$r_{ex} = \beta\, e^{-E/RT} \,,$$

where β is a constant, we were able to calculate values of β for each of the experiments listed in table 2. These values are shown in table 3, and were calculated using the value of 205 kJ mol^{-1} (found above) for the activation energy.

It is clear that the values of β are very similar. The differences between the values of β from different samples are due to the samples having different areas. This is most clearly seen in comparing runs (5) (coarse sample) and (3) (fine sample) in table 3. The value of β for the fine ground sample is approximately four times that of the coarse sample.

It should be noted that although table 3 gives a good indication of the relative sizes of β, there may be considerable error in the absolute values. The value of the activation energy could be in error by ±20 kJ mol^{-1} and the corresponding range of values of β covers two orders of magnitude in the experimental temperature range.

Despite these uncertainties, the absolute values of

Table 3
Experimental values of the pre-exponential factor (β)

Run	Channel size (mm)	ϵ	β (kg s^{-1})
1	2	0.0354	2.64×10^4
2	2	0.0591	2.79×10^4
3	3	0.0354	4.24×10^4
4	3	0.0591	4.62×10^4
5	3 [a]	0.0354	0.98×10^4

[a] Coarse sample.

β do enable us to draw the tentative conclusion that the whole of the GaAs surface is involved in the reaction, rather than just at active centres associated with defects. We can see this if we assume a value of 10 cm^2 for the area of the coarse sample (run 5). On converting the results shown in table 3 to units of atoms cm^{-2} s^{-1}, we find:

$$\kappa = p_{GaBr}^{x_1+1} p_{As_2}^{x_2+2} p_{H_2}^{x_3+1} p_{HBr}^{x_4-2}$$
$$= 4 \times 10^{27} \text{ atom cm}^{-2} \text{ s}^{-2} .$$

This value is close to the maximum value of the reaction rate

$$\nu C_s \sim 10^{28} ,$$

where ν is the frequency of the surface vibrations ($\sim 10^{13}$ s^{-1}) and C_s is the number of surface atoms per unit area ($\sim 10^{15}$ cm^{-2}).

6. Conclusions

The effect of kinetically hindered reactions on the theory of the modified entrainment method has been analysed and general kinetic relationships found. The rate of weight loss under non-equilibrium conditions is related to its hypothetical value under equilibrium conditions via a general kinetic parameter, the exchange rate. This experimentally measurable parameter has a direct conceptual meaning; it can also be expressed in terms of a rate constant and concentration or partial pressure terms, and so forms a link between experiment and modelling.

The theory was applied to some results from the GaAs/HBr system. The limited results available showed no significant dependence of the exchange rate on the gas pressures and we were able to obtain a value of 205 ± 20 kJ mol^{-1} for the activation energy. Using an estimated value for the area of the samples, we calculated the pre-exponential factor β as

$$\beta \simeq 4 \times 10^{27} \text{ atoms cm}^{-2} \text{ s}^{-1} .$$

At a typical growth temperature of 1000 K, these figures given a value for the exchange current r_{ex}, of 1.9×10^{-8} kg s^{-1} or 69 mg h^{-1}. This figure may be compared with typical growth rates of 1–11 mg h^{-1}. It is clear that under normal growth conditions, growth rates are significant compared with the rate of surface processes.

The discussion of results for the GaAs/HBr system indicated the need for further experimentation. Nevertheless, the calculations serve to show the sort of information which can be obtained when the modified entrainment method is applied to kinetic problems.

Acknowledgements

We wish to thank A. Finch, P. Gardner and Miss E.J. Tarbox of Royal Holloway College, London, for their assistance in the preparation of this paper. Acknowledgement is also made to the Director of Research of the British Post Office for permission to publish this work.

References

[1] M.M. Faktor and I. Garrett, J. Crystal Growth 38 (1977) 213.
[2] D. Battat, M.M. Faktor, I. Garrett and R.H. Moss, J. Chem. Soc. Faraday Trans I, 70 (1974) 2302.
[3] D. Battat, M.M. Faktor, I. Garrett and R.H. Moss, J. Chem. Soc. Faraday Trans. I, 70 (1974) 2267.
[4] I. Langmuir, Phys. Rev. 2 (1913) 329.
[5] I. Langmuir and C.M. Mackay, Phys. Rev. 4 (1914) 377.
[6] D.O. Hayward and B.M.W. Trapnell, Chemisorption (Butterworths, London, 1964).
[7] M.M. Faktor, R. Heckingbottom and I. Garrett, J. Chem. Soc. A (1970) 2657.
[8] M.M. Faktor, R. Heckingbottom and I. Garrett, J. Chem. Soc. A (1971) 1.
[9] J.R. Knight, D. Effer and P.R. Evans, Solid State Electron. 8 (1965) 178.
[10] M.M. Faktor, I. Garrett, M.H. Lyons and R.H. Moss, J. Chem. Soc. Faraday Trans. I, 73 (1977) 1446.
[11] Y. Kuniya and M. Hosaka, J. Crystal Growth 28 (1975) 385.
[12] E.J. Tarbox, Ph.D. Thesis, Royal Holloway College, London University (1977).